NUREG/CR–4219
ORNL/TM–9593/V11&N2
Vol. 11, No. 2

Heavy-Section Steel Technology Program

Semiannual Progress Report for April – September 1994

Prepared by
W. E. Pennell

Oak Ridge National Laboratory

Prepared for
U.S. Nuclear Regulatory Commission

AVAILABILITY NOTICE

Availability of Reference Materials Cited in NRC Publications

Most documents cited in NRC publications will be available from one of the following sources:

1. The NRC Public Document Room, 2120 L Street, NW., Lower Level, Washington, DC 20555-0001

2. The Superintendent of Documents, U.S. Government Printing Office, P. O. Box 37082, Washington, DC 20402-9328

3. The National Technical Information Service, Springfield, VA 22161-0002

Although the listing that follows represents the majority of documents cited in NRC publications, it is not intended to be exhaustive.

Referenced documents available for inspection and copying for a fee from the NRC Public Document Room include NRC correspondence and internal NRC memoranda; NRC bulletins, circulars, information notices, inspection and investigation notices; licensee event reports; vendor reports and correspondence; Commission papers; and applicant and licensee documents and correspondence.

The following documents in the NUREG series are available for purchase from the Government Printing Office: formal NRC staff and contractor reports, NRC-sponsored conference proceedings, international agreement reports, grantee reports, and NRC booklets and brochures. Also available are regulatory guides, NRC regulations in the *Code of Federal Regulations*, and *Nuclear Regulatory Commission Issuances*.

Documents available from the National Technical Information Service include NUREG-series reports and technical reports prepared by other Federal agencies and reports prepared by the Atomic Energy Commission, forerunner agency to the Nuclear Regulatory Commission.

Documents available from public and special technical libraries include all open literature items, such as books, journal articles, and transactions. *Federal Register* notices, Federal and State legislation, and congressional reports can usually be obtained from these libraries.

Documents such as theses, dissertations, foreign reports and translations, and non-NRC conference proceedings are available for purchase from the organization sponsoring the publication cited.

Single copies of NRC draft reports are available free, to the extent of supply, upon written request to the Office of Administration, Distribution and Mail Services Section, U.S. Nuclear Regulatory Commission, Washington, DC 20555-0001.

Copies of industry codes and standards used in a substantive manner in the NRC regulatory process are maintained at the NRC Library, Two White Flint North, 11545 Rockville Pike, Rockville, MD 20852-2738, for use by the public. Codes and standards are usually copyrighted and may be purchased from the originating organization or, if they are American National Standards, from the American National Standards Institute, 1430 Broadway, New York, NY 10018-3308.

DISCLAIMER NOTICE

NUREG/CR-4219
ORNL/TM-9593/V11&N2
Vol. 11, No. 2

Heavy-Section Steel Technology Program

Semiannual Progress Report for April – September 1994

Manuscript Completed: January 1996
Date Published: April 1996

Prepared by
W. E. Pennell

Oak Ridge National Laboratory
Managed by Martin Marietta Energy Systems, Inc.

Oak Ridge National Laboratory
Oak Ridge, TN 37831-6285

S. N. Malik, NRC Project Manager

Prepared for
Division of Engineering Technology
Office of Nuclear Regulatory Research
U.S. Nuclear Regulatory Commission
Washington, DC 20555-0001
NRC Job Code B0119

Abstract

The Heavy-Section Steel Technology (HSST) Program is conducted for the Nuclear Regulatory Commission (NRC) by Oak Ridge National Laboratory (ORNL). The program focus is on the development and validation of technology for the assessment of fracture-prevention margins in commercial nuclear reactor pressure vessels. The HSST Program is organized in seven tasks: (1) program management, (2) constraint effects analytical development and validation, (3) evaluation of cladding effects, (4) ductile-to-cleavage fracture-mode conversion, (5) fracture analysis methods development and applications, (6) material property data and test methods, and (7) integration of results.

The program tasks have been structured to place emphasis on the resolution fracture issues with near-term licensing significance. Resources to execute the research tasks are drawn from ORNL with subcontract support from universities and other research laboratories. Close contact is maintained with the sister Heavy-Section Steel Irradiation (HSSI) Program at ORNL and with related research programs both in the United States and abroad. This report provides an overview of principal developments in each of the seven program tasks from April 1994 to September 1994.

Contents

List of Figures

List of Tables

Preface

The Heavy-Section Steel Technology (HSST) Program, which is sponsored by the Nuclear Regulatory Commission, is an engineering research activity devoted to extending and developing the technology for assessing the margin of safety against fracture of the thick-walled steel pressure vessels used in light-water-cooled nuclear power reactors. The program is being carried out in close cooperation with the nuclear power industry. This report covers HSST work performed in April–September 1994. The work performed by the Oak Ridge National Laboratory (ORNL) and by subcontractors is managed by the Engineering Technology Division (ETD) of ORNL. Major tasks at ORNL are carried out by the ETD and the Metals and Ceramics Division. The following is a list of previous progress reports on this program:

ORNL-4176
ORNL-4315
ORNL-4377
ORNL-4463
ORNL-4512
ORNL-4590
ORNL-4653
ORNL-4681
ORNL-4764
ORNL-4816
ORNL-4855
ORNL-4918
ORNL-4971
ORNL/TM-4655 (Vol. II)
ORNL/TM-4729 (Vol. II)
ORNL/TM-4805 (Vol. II)
ORNL/TM-4914 (Vol. II)
ORNL/TM-5021 (Vol. II)
ORNL/TM-5170
ORNL/NUREG/TM-3
ORNL/NUREG/TM-28
ORNL/NUREG/TM-49
ORNL/NUREG/TM-64
ORNL/NUREG/TM-94
ORNL/NUREG/TM-120
ORNL/NUREG/TM-147
ORNL/NUREG/TM-166
ORNL/NUREG/TM-194
ORNL/NUREG/TM-209
ORNL/NUREG/TM-239
NUREG/CR-0476 (ORNL/NUREG/TM-275)
NUREG/CR-0656 (ORNL/NUREG/TM-298)
NUREG/CR-0818 (ORNL/NUREG/TM-324)
NUREG/CR-0980 (ORNL/NUREG/TM-347)
NUREG/CR-1197 (ORNL/NUREG/TM-370)
NUREG/CR-1305 (ORNL/NUREG/TM-380)
NUREG/CR-1477 (ORNL/NUREG/TM-393)
NUREG/CR-1627 (ORNL/NUREG/TM-401)
NUREG/CR-1806 (ORNL/NUREG/TM-419)
NUREG/CR-1941 (ORNL/NUREG/TM-437)
NUREG/CR-2141, Vol. 1 (ORNL/TM-7822)
NUREG/CR-2141, Vol. 2 (ORNL/TM-7955)
NUREG/CR-2141, Vol. 3 (ORNL/TM-8145)
NUREG/CR-2141, Vol. 4 (ORNL/TM-8252)
NUREG/CR-2751, Vol. 1 (ORNL/TM-8369/V1)
NUREG/CR-2751, Vol. 2 (ORNL/TM-8369/V2)
NUREG/CR-2751, Vol. 3 (ORNL/TM-8369/V3)
NUREG/CR-2751, Vol. 4 (ORNL/TM-8369/V4)
NUREG/CR-3334, Vol. 1 (ORNL/TM-8787/V1)
NUREG/CR-3334, Vol. 2 (ORNL/TM-8787/V2)
NUREG/CR-3334, Vol. 3 (ORNL/TM-8787/V3)
NUREG/CR-3744, Vol. 1 (ORNL/TM-9154/V1)
NUREG/CR-3744, Vol. 2 (ORNL/TM-9154/V2)
NUREG/CR-4219, Vol. 1 (ORNL/TM-9593/V1)
NUREG/CR-4219, Vol. 2 (ORNL/TM-9593/V2)
NUREG/CR-4219, Vol. 3, No. 1 (ORNL/TM-9593/V3&N1)
NUREG/CR-4219, Vol. 3, No. 2 (ORNL/TM-9593/V3&N2)
NUREG/CR-4219, Vol. 4, No. 1 (ORNL/TM-9593/V4&N1)
NUREG/CR-4219, Vol. 4, No. 2 (ORNL/TM-9593/V4&N2)
NUREG/CR-4219, Vol. 5, No. 1 (ORNL/TM-9593/V5&N1)
NUREG/CR-4219, Vol. 5, No. 2 (ORNL/TM-9593/V5&N2)
NUREG/CR-4219, Vol. 6, No. 1 (ORNL/TM-9593/V6&N1)
NUREG/CR-4219, Vol. 6, No. 2 (ORNL/TM-9593/V6&N2)
NUREG/CR-4219, Vol. 7, No. 1 (ORNL/TM-9593/V7&N1)
NUREG/CR-4219, Vol. 7, No. 2 (ORNL/TM-9593/V7&N2)
NUREG/CR-4219, Vol. 8, No. 1 (ORNL/TM-9593/V8&N1)
NUREG/CR-4219, Vol. 8, No. 2 (ORNL/TM-9593/V8&N2)
NUREG/CR-4219, Vol. 9, No. 1 (ORNL/TM-9593/V9&N1)
NUREG/CR-4219, Vol. 9, No. 2 (ORNL/TM-9593/V9&N2)
NUREG/CR-4219, Vol. 10, No. 1 (ORNL/TM-9593/V10&N1)
NUREG/CR-4219, Vol. 10, No. 2 (ORNL/TM-9593/V10&N2)
NUREG/CR-4219, Vol. 11, No. 1 (ORNL/TM-9593/V11&N1)

Executive Summary

W. E. Pennell

The Heavy-Section Steel Technology (HSST) Program is conducted for the Nuclear Regulatory Commission (NRC) by Oak Ridge National Laboratory (ORNL). The program focus is on the development, validation, and application of technology for the assessment of fracture-prevention margins in commercial nuclear reactor pressure vessels (RPVs). The scope of the project includes development and experimental validation of analysis methods, development of testing techniques and the generation of materials property data, integration of analysis methods and materials data into a comprehensive RPV integrity assessment methodology, technology transfer through participation in national and international codes and standards activities, and support to NRC in the area of RPV integrity assessment. Program activities are structured to provide support to NRC for the resolution of specific RPV licensing issues. Licensing issues directly influenced by this technology include the definition of RPV pressure-temperature (P-T) curves and low-temperature overpressure protection relief valve set points, evaluation of RPV integrity under pressurized-thermal-shock (PTS) transient loading, safety evaluations of RPVs containing material with low-upper-shelf Charpy energy, and data transfer from small-scale surveillance specimens for application in RPV structural integrity assessments.

1 Program Management

A revision to the HSST Program Brief for the FY 1994 performance period was received from NRC. Preparation of a revision to the HSST Program 189 for FY 1994 was completed. Program modifications that resolved problems encountered in the biaxial and finite-length shallow-flaw fracture toughness testing programs were incorporated into the revised 189, which was approved by NRC. Preparation and review of the HSST Program semiannual progress report for the period October 1992 to March 1993 was completed. Resource expenditure estimating spreadsheets were prepared and issued to the HSST Program task leaders for use in preparing their input to the FY 1995 189. These spreadsheets will provide information on the resource expenditure for each of the program deliverables and will provide a basis for the negotiation phase of the 189 preparation procedure, which is required by the recently issued NRC Directive 11.7. Preparation of the FY 1994 procurement package was completed for the consulting subcontract with Professor S. Rolfe, of the University of Kansas, and an interagency agreement with the Carderock Division of the Naval Surface Warfare Center (CDNSWC) for performance of dynamic fracture toughness tests.

Papers and/or presentations summarizing recent research results from the HSST Program were presented to the British Nuclear Energy Society Conference on Thermal Reactor Safety Assessment, the ORNL Engineering Technology Division Advisory Committee, AEA Technology Risley and Harwell laboratories, at The Welding Institute (TWI) in the United Kingdom, and at the American Society of Mechanical Engineers (ASME) Pressure Vessel and Piping Division Conference. Results from the recent analysis and testing activities in the biaxial testing program were reviewed and evaluated. Shallow-flaw fracture toughness test data for A 533 B material at a test temperature ($T - RT_{NDT}$) of –10°C were generated using biaxial loading ratios of 1:0, 1:0.6, and 1:1 (see Task 2). The test data were found to correlate well with relatively simple function of ln(R), where R is the width of the plastic zone along the direction of crack propagation, as determined from nonlinear finite-element analysis. This relationship suggests that crack-tip strains may be a controlling influence on cleavage crack initiation in the transition temperature range. In subsequent discussions held at the University of Maryland, Professor Irwin emphasized that consideration of strain-rate effects was essential to understanding the process of fracture initiating in brittle carbide particles and propagating through the adjacent ferrite grain material.

The HSST Program Manager visited the AEA Technology Risley and Harwell laboratories and TWI to exchange information on research program results and discuss their interpretation. Discussions at the AEA Technology Risley Laboratory focused on a comparison of results from the biaxial fracture toughness testing at the host laboratory and the HSST Program tests. The AEA Technology team did not detect any biaxial effects on fracture toughness and concluded that plastic straining of the test specimen ligament may have occurred in their tests. The Harwell Laboratory is developing miniature fracture toughness test specimens. The miniature fracture toughness specimens are sized such that they can be fabricated from the broken halves of Charpy surveillance specimens. The Harwell research team showed considerable interest in evidence from the recent HSST biaxial testing program; it suggests that, in the transition temperature region, crack-tip strains may have a controlling influence on the fracture process. The Harwell team plans to revisit the miniature specimen analysis and investigate the crack-tip strain field behavior. TWI raised concerns relating to locally intensified strain-aging of material at the tips of preexisting cracks, which are located adjacent to areas where further welding operations have been performed. Examples are cracks adjacent

to weld repairs and cracks in areas influenced by the cladding process. A foreign travel report covering these visits was prepared and issued.

The HSST Program Manager is a voting member of the ASME Section XI Task Group on Operability (TGO) and the Working Group on Operating Plant Criteria (WGOPC). The WGOPC has identified a need for development of procedures for calculating P-T limits for reduced postulated defect sizes; an initiative has been launched to meet this need. Action items relating to this initiative include (1) compiling a list of variables that affect fracture toughness of pressure vessel materials and (2) collecting materials data reflecting the effect of these variables. During the current reporting period the HSST Program Manager completed one of the actions required for item (2). A shallow-flaw fracture toughness data base was assembled for A 533 B plate material and submerged-arc RPV welds. The data were presented to the WGOPC at the May 3, 1994, meeting. A joint meeting of the ASME Section XI Working Groups on Flaw Evaluation and the WGOPC was held to review the selection of stress-intensity-factor equations for semielliptical surface flaws for inclusion in ASME Sect. XI, Appendix G. The chairmen of the working groups requested copies of the HSST Program reports on stress-intensity-factor influence coefficients (SIFICs) for semi-elliptical inner-surface flaws. The requested reports were forwarded to them.

During the current reporting period, HSST Program personnel published four NRC reports, four letter reports, one foreign trip report, one publication in a refereed journal, two papers in technical society publications, and gave ten presentations at program reviews and technical society and NRC-sponsored national and international meetings.

2 Constraint Effects Analytical Development and Validation

The focus of this task is on the development and validation of dual-parameter correlations to reflect the effect of crack-tip constraint on the fracture toughness of RPV steels. Crack-tip constraint conditions of particular concern in RPV structural integrity evaluations are those associated with shallow flaws and biaxial loading. Work continued during this performance period on development of a heat-treating procedure for application to HSST plate 14 that would yield properties comparable to those of radiation-sensitive RPV steel irradiated to a fluence of 1.5×10^{19} neutrons/cm^2 (E > 1 MeV). Promising results had been obtained previously using a 1010°C (1850°F) normalizing treatment followed by a rapid air quench. Application of this heat-treating procedure to the test materials, however, resulted in a stress-strain curve uncharacteristic of irradiated A 533 steel. Arrangements are being made for a commercial vendor to perform a more standard heat treatment of plate 14.

Testing of a pilot series of cruciform beams with finite-length surface flaws was completed during this period. It was discovered that the specimens appeared to have been overheated during electron-beam (EB) welding of the beam arms with the result that the basic material properties had been altered. Additional material from the CE-01 plate was used to fabricate four new specimens. A design change was made to simplify the EB weld joint between the test section and beam arms and move the joint further from the test section. Replacement specimens were fabricated and tested. Posttest investigation of the fracture surface revealed that fracture initiation occurred near the center of the specimen, indicating that the specimen design was acceptable for use in the clad-material finite-length-flaw test program. Testing of the initial series of cruciform specimens with uniform-depth flaws was also completed. Results from these tests indicate that biaxial loading can produce a significant reduction in the shallow-flaw fracture toughness of RPV steel.

Prior analyses of the cruciform specimen have predicted "stiffer" deformation behavior that was obtained in the experiments. The stress-strain curve used as input for the analyses was developed using plate material with some prior history (the material was first used in the wide-plate tests and then as beam specimen material in the shallow-flaw test program). Stress-strain characterization results have now been produced using virgin plate material. The new stress-strain curve analyses exhibit an earlier departure from linearity, lower yield stress, lower ultimate stress, a higher uniform elongation, and slightly less strain hardening than the stress-strain curve used in prior analyses. Prediction of deformation response for the cruciform specimens was improved by use of this new curve. Fracture toughness values from the shallow-flaw biaxial tests are currently being updated using the new stress-strain curve.

Application of the stress-based, Dodds-Anderson (D-A), stressed-volume constraint correction procedure did not predict the effects of biaxial loading on shallow-flaw fracture toughness observed in the cruciform specimen tests. It was concluded that a fracture criterion based only on opening-mode stresses was not an adequate basis for a constraint-effects methodology for application to biaxial loading conditions. An alternate strain-based approach was evaluated. Based on the limited amount of data currently available, it was found that a dual-parameter correlation, using plastic zone radius along the direction of crack

propagation as the second parameter, was capable of representing the observed effects of biaxial loading on fracture toughness.

3 Evaluation of Cladding Effects

Stainless steel cladding can act to inhibit the initiation and propagation of cracks from finite-length surface flaws. This property is not reflected in existing RPV structural integrity analysis methods. Objectives for this task are to (1) experimentally determine the influence of cladding on crack initiation from finite-length surface flaws in a prototypical RPV biaxial stress field, and (2) develop and validate the technology required for incorporation of those effects into RPV structural-integrity assessment methods.

Work continued on developing a quantitative description of the effects of cladding on the fracture behavior of shallow surface cracks in RPVs. Fracture toughness tests were performed on three full-thickness clad beam specimens taken from the RPV of a canceled nuclear plant. The RPV material was A 533 B with a stainless steel clad overlay on the inner surface. The shell segment included two circumferential welds and one longitudinal weld. The welds were submerged-arc welds with A 533 B class 1 filler metal. The plate material, clad overlay, and weldment were completely prototypic of a production-quality RPV. The shell had a nominal inner radius of 2210 mm and a thickness of 232 mm. In previously reported work, Irwin and Zhang of the University of Maryland performed material gradient studies on a large weld section, joining two forged A 508 shells from a stainless-steel-clad RPV. They found hardness elevations in the region of A 508 material near the clad/base interface, an area of the vessel that was affected by the reheat cycle of the cladding process. Irwin and Zhang indicated that these hardness elevations would probably translate into a reduction of cleavage initiation toughness. Flaw depths tested in this series were selected to position the crack tips in this region. Cracks with depth (a) to thickness (W) ratios (a/W) of 0.5, 0.1, and 0.05 were tested. All of the crack tips were located in the longitudinal weld portion of the RPV shell material. Fracture toughness (K_{Jc}) values obtained for the 0.5, 0.1, and 0.05 a/W cracks were 173.5, 393.3, and 225.4 MPa$\sqrt{m}$, respectively. These results indicate that the mean value of fracture toughness increases as a/W decreases in prototype full-thickness test specimens, but the differences in lower-bound deep- and shallow-flaw fracture toughness are relatively small. These trends are consistent with trends observed in previously reported data from shallow- and deep-flaw tests on 100-mm-thick single-edge-notched beam (SENB) specimens fabricated from A 533 B plate material.

Characterization tests were performed on RPV weld material, including Charpy V-notch tests, nil-ductility temperature (NDT) tests, and tensile tests. The impact and tensile data were used to develop a consistent set of material properties needed for the clad beam test data evaluation and finite-element analyses. The automated-ball-indentation technique was used to determine the yield stress for the base and clad material. The yield stress for the weld material was found to be 36% higher than the yield stress for the base material. Measurements of the slot width were made after machining of the flaws. The slot width at the surface was found to be 0.14 m larger that the slot width at the deepest point in the a/W = 0.5 deep flaw, indicating that significant tensile stresses existed in the material that had been cut. Analysis to determine the magnitude of these residual stresses is in progress. During August 1994, testing was completed on the fourth (CB-1.4) and fifth (CB-1.5) full-thickness clad beams at the National Institute of Standards and Technology in Gaithersburg, Maryland. Analysis of data from these tests will be completed in the next reporting period.

The influence of crack depth on crack-tip constraint was investigated using both the J-Q methodology of O'Dowd and Shih and the D-A scaling model. Both shallow-crack clad beam specimens were found to have Q values of about –0.78 at failure (for r = 2), which represents a significant loss of constraint. The Q value for the shallow-crack clad beam specimens was very similar to the value for the shallow-crack SENB specimens previously tested at ORNL. The D-A scaling model appeared to be effective in adjusting the test data to account for in-plane loss of constraint.

The HSST Program is participating in Project FALSIRE, an international program to assess various fracture methodologies through interpretive analyses of selected large-scale fracture experiments. Analyses were performed for that portion of the Project FALSIRE II devoted to the French clad beam experiments, DSR3 and DD2. These clad beams containing subclad cracks were tested in four-point bending. The central part of each beam was fabricated from A 508 class 3 steel with an RT_{NDT} of –40°C. Specimen DSR3 had dimensions of 120 × 145 × 1700 mm, with a 4.5-mm layer of cladding on the top surface. Specimen DD2 had dimensions of 119.2 × 145 × 1700 mm with a 6.0-mm layer of cladding. Each beam contained a small subclad crack (approximately semielliptical) with a depth of 13 mm and length of 40 mm for DSR3 and a depth of 4.5 mm and length of 48 mm for DD2. The cladding layer had relatively low yield stresses and high toughness. Data collected during the tests included load, load-point

displacement, strains, and temperatures. In the DSR3 test, cleavage fracture initiated in the ferritic base material, with no crack arrest. In the DD2 test, the point of cleavage initiation was located about 1.5 to 2 mm from the clad-base interface; the corresponding location in the DSR3 test was about 2.5 mm from the interface. Calculated crack-mouth-opening displacements (CMODs) and strains for both DSR3 and DD2 show that the largest values were located near the clad/base interface, where the cladding layer stretched and allowed the crack to open more. The calculated K_I values for the initiation locations fall below the lower-bound fracture toughness of the base-metal small-scale specimens at the test temperature. Localized strain-aging, which occurs at the tips of preexisting cracks that are located adjacent to areas where further welding operations are in progress (i.e., cracks in areas influenced by the cladding process), may have influenced these test results.

Efforts to develop a cladding material with the properties required for the HSST Program investigation of cladding effects on fracture initiation from finite-length surface flaws have not yet produced the required material. Because of difficulties associated with achieving the target toughness properties using heat treatment, deterministic analyses were performed to determine whether the tearing toughness of irradiated cladding should be considered an issue in meeting the goals of the clad testing program. Results showed that the stainless steel cladding was not predicted to experience tearing during the experiment. It was concluded, therefore, that a relatively high tearing toughness of the cladding should not be an issue in achieving the objectives of the clad cruciform testing program. It was further concluded that use of available RPV shell material would be the most desirable approach to an evaluation of cladding effects on fracture toughness of shallow flaws. The clad cruciform specimens will therefore be fabricated from clad plate material taken from the RPV from a canceled nuclear plant.

Studies were undertaken to explain the discrepancies between measured and calculated structural response of certain ORNL biaxial bend tests in which the calculated stiffness of the test specimen was higher than the measured stiffness. Three-dimensional (3-D) mesh refinement studies indicated that the finite-element model used in the ORNL analyses was a converged model and that additional mesh refinement did not improve the predicted structural response. Efforts to determine the cause of the observed differences between the measured and calculated stiffness of the test specimen will now concentrate on boundary conditions and material property representation.

4 Ductile-to-Cleavage Fracture-Mode Conversion

This task investigates the effect of prior ductile tearing on cleavage-fracture-initiation toughness. Ductile tearing prior to cleavage fracture initiation is frequently observed in tests performed at temperatures corresponding with the lower transition region of the fracture toughness curve. Evidence exists that ductile tearing may act to increase crack-tip constraint and thereby influence fracture toughness.

During this report period, work continued on the characterization of precleavage tearing behavior and development of a fracture-mode conversion model to take into account any precleavage ductile tearing in fracture predictions. Metallurgical investigations were carried out to determine the fracture-surface characteristics associated with precleavage ductile tearing and mode conversion to cleavage. A number of shallow-flaw beam fracture surfaces were examined to identify the amount of precleavage ductile tearing and the location of the cleavage origin. Scanning-electron-microscope photographs were examined to determine void size and spacing on the fracture surfaces. Preliminary experiments conducted at the University of California, Santa Barbara, demonstrated the feasibility of fracture surface reconstruction using replicas of fracture toughness specimens. Potential applications for this technique in the development of a tearing-cleavage mode conversion model are under review.

A fracture prediction model applicable to the transition toughness region of the fracture toughness curve is being developed. Recent studies have indicated that the onset of stable ductile tearing produces stress fields ahead of the growing crack and crack-tip profiles that differ from those of a stationary crack. A logic diagram has been produced that combines the five areas of research involved in this task: fracture and tearing toughness data collection and evaluation, cleavage-initiation model development, ductile-tearing model development, fractography and micromechanical features investigation, and fracture-mode conversion model development and validation. Dual-parameter methodologies, including stress-based and stress-strain-based characterizations of cleavage fracture, are included in the logic diagram. The ductile tearing model provides output that represents essential input to the selected cleavage model for predicting fracture initiation. Initial evaluations will focus on constitutive formulations that describe progressive damage and material softening of the local crack-tip region. Performance assessments of the candidate

cleavage and ductile-tearing models will provide necessary input for defining the tearing-to-cleavage mode conversion model.

Development and verification of the WARP-3D finite-element code continues during this report period. This research code analyzes very large 3-D solid models encountered in fracture mechanics studies of crack-tip fields and ductile crack growth. WARP-3D has extensive nonlinear material modeling capabilities. Nonlinear constitutive material models include rate-independent and rate-dependent von Mises plasticity with various isotropic/kinematic hardening rules and a Gurson hole growth model. The WARP-3D computer program is being developed by Professor R. Dodds at the University of Illinois, with support from an HSST Program subcontract. Discussions were held with Professor Dodds regarding the material parameters needed for the WARP-3D finite-element program. The specified parameters for the model include the flow properties of the material, the initial void volume fraction (porosity) f_o, and a porosity at microscopic rupture f_c. These material parameters will be obtained from fractography and micromechanical investigation elements of this task.

5 Fracture Analysis Methods Development and Application

Development of the Fracture Analysis of Vessels, Oak Ridge (FAVOR) computer program continued. FAVOR is an advanced program for the analysis of RPV failure rates under PTS transient loading. The program is being developed in a manner that will make an executable version of FAVOR available to users without making the source deck available to them. This feature makes configuration control of the program possible.

During the current reporting period, a letter report was completed that presents a data base of SIFICs for circumferentially oriented finite-length semielliptical inner-surface flaws. SIFICs were generated for circumferentially oriented finite-length semielliptical inner-surface flaws with aspect ratios [total crack length (2c) to crack depth (a)] of 2, 6, and 10. The SIFICs were computed for flaw depths in the range of $0.01 < a/t < 0.5$ with particular emphasis on shallow flaws ($a/t < 0.1$). SIFICs were also computed for two cladding thicknesses [$t_{clad} = 3.96$ mm (0.156 in.) and $t_{clad} = 6.35$ mm (0.25 in.)]. All of the SIFICs generated thus far have been implemented in the FAVOR computer program.

Two documents were completed to satisfy quality assurance (QA) requirements of the FAVOR computer code. These documents satisfy requirements specified in the ASME NQA-2a-1990 Addenda to ASME NQA-2-1989 Edition, "Quality Assurance Requirements for Nuclear Facility Applications." The ORNL Computing Applications Division conducted a QA surveillance of FAVOR. The findings of the QA surveillance were satisfactory in 24 out of 25 categories examined. Remedial action has been taken to correct the noted deficiency. Probabilistic fracture-mechanics (PFM) sensitivity analyses were performed to determine the potential impact of various modifications to the fracture-mechanics model currently specified in Regulatory Guide 1.154. Specific fracture-mechanics model assumptions examined included flaw geometry, the effect of stainless steel cladding, flaw density, and fracture initiation and arrest toughness. The current development version of FAVOR was used to perform these sensitivity analyses. A report summarizing results from theses analyses was prepared and submitted to the NRC. This information will be factored into the NRC plans for the revision to Regulatory Guide 1.154.

6 Material Property Data and Test Methods

This task provides support to the other fracture technology development tasks and performs evaluations of specific RPV materials issues. An experimental investigation of the ductile tearing toughness of A 302 B pressure vessel steel was completed. Information from this investigation was compiled in a letter report, "Presentation of Preliminary J-R Curve Fracture Toughness Data on Modified A 302 Grade B Steel." The test results showed that the ductile-tearing toughness of modified A 302 grade B is somewhat inferior to the tearing toughness of more recently produced grades of pressure vessel steel.

A project was initiated to determine why J-R curves generated in isothermal tests on the 2.25 Cr-1 Mo steel used for the PTSE-2 experiment did not correctly characterize the ductile tearing observed in the PTSE-2 test vessel. The experimental plan was developed to generate J-R curves in a simulation of the thermal gradient experienced by the PTSE-2 test vessel. Work was also performed in support of a program of dynamic fracture toughness testing of A 533 B pressure vessel steel. Recommendations regarding material characterization testing were prepared for inclusion in the test specification, and a subcontract for performance of the dynamic fracture toughness testing was placed with the Carderock Division of the Naval Surface Warfare Center.

7 Integration of Results Into a State-of-the-Art Methodology

The primary objective for this task is to extract and interpret fracture technology advances generated in the HSST Program research tasks, and in the HSSI Program and other fracture technology research programs, and assemble them into a validated state-of-the-art methodology for assessing the structural integrity of irradiation-embrittled RPVs containing flaws. In addition, this task is responsible for the rapid transfer of fracture technology advances to national consensus codes and standards. Task seven also provides special technical assistance to NRC for the evaluation and resolution of RPV structural integrity issues.

In the current reporting period, this task provided a response to a request from the NRC for a technical review of a translated Russian report and accompanying documents concerning a proposed warm prestressing (WPS) procedure for increasing the effective fracture toughness of embrittled materials in Russian and East European pressurized-water reactor vessels. The Russian approach to RPV integrity is similar in concept to that of the United States. Their reference temperature, T_k, is based on Charpy impact energy data and room temperature yield stress. Their reference flaw has a depth-to-length ratio of one-third. Russian reactor vessels were designed to have less water between the core and the vessel wall than U.S. vessels; consequently, their fluences are as much as ten times those of U.S. vessels. Because of the phosphorous and copper contents of the Russian vessel materials, annealing is only partially effective in reducing embrittlement. These factors have prompted the Russians to consider a combination of annealing and WPS as a means of recovering lost safety margins.

The Russian WPS procedure for reactor vessels has been patented and is not described in any of the documents reviewed. Application of a thermal shock to the inner surface of the vessel following the high-temperature-soak portion of the annealing cycle appears to be a logical choice for inducing the WPS effect because this could be done without unacceptable permanent deformation of the vessel. From small- and medium-scale specimen test results, the Russians concluded that WPS effects are governed mainly by crack-tip blunting and are almost unaffected by the degree of intermediate unloading and residual stresses. They postulate that the crack-tip-opening displacement is the relevant fracture criterion. They judge that residual stress effects are significant under small-scale yielding conditions, but not for fully plastic conditions. HSST Program experimental data for Intermediate Test Vessels ITV-7A and ITV-8 support this assessment.

Strain aging constitutes a possible limitation on WPS reliability. The Russians recognized this possible material-dependent limitation on WPS and have conducted hold time tests on warm-prestressed specimens to 10,000 h, demonstrating no significant effects for the materials tested. It should be noted, however, that the weld heat-affected zones (HAZs) of A 533 B steel used in U.S. vessels may be much more sensitive to thermal embrittlement than the base metal. Confirmatory tests on A 533 B specimens containing weld HAZ material would be required to determine if the results obtained by the Russians are applicable to U.S. reactors. Ductile crack growth during the WPS cycle is a further potential concern that has not yet been resolved.

Heavy-Section Steel Technology Program Semiannual Progress Report for April–September 1994

1 Program Management*

W. E. Pennell

The Heavy-Section Steel Technology (HSST) Program is conducted for the Nuclear Regulatory Commission (NRC) by Oak Ridge National Laboratory (ORNL). The program focus is on development and validation of technology for the assessment of fracture-prevention margins in commercial nuclear reactor pressure vessels (RPVs).

RPV structural integrity issues of current concern to NRC are defined in the FY 1994 Statement of Work (SOW) for the HSST Program. Six technical issues are identified in the SOW: (1) crack-tip constraint effects on fracture toughness of RPV materials, (2) effects of stainless steel cladding on the initiation and propagation of shallow surface cracks, (3) ductile-to-cleavage fracture-mode conversion, (4) fracture-analysis methods development, (5) materials property data and test methods development, and (6) integration of results from the research programs into a state-of-the-art methodology for RPV structural integrity assessments. The HSST Program is structured to provide the research results required for resolution of these issues. Management direction and control of the program are implemented using a seven-element Level 1 work breakdown structure (WBS) and a linked cost-schedule performance monitoring system. The current HSST Program Level 1 WBS is shown in Fig. 1.1. Each element of the Level 1 WBS represents a separate research or management task with a designated task leader. Within each of the Level 1 WBS elements, a Level 2 WBS defines research subtasks, and a Level 3 WBS defines the individual milestones within a subtask.

Staffing for the research tasks is drawn from the Engineering Technology, Metals and Ceramics, and Computing Applications Divisions at ORNL. Subcontracts with consultants, universities, and other research laboratories are used to gain access to special expertise and capabilities required for certain research tasks. A summary of resources applied to the HSST research tasks during this report period is given in Fig. 1.2.

A revision to the HSST Program Brief for the FY 1994 performance period was received from NRC. The

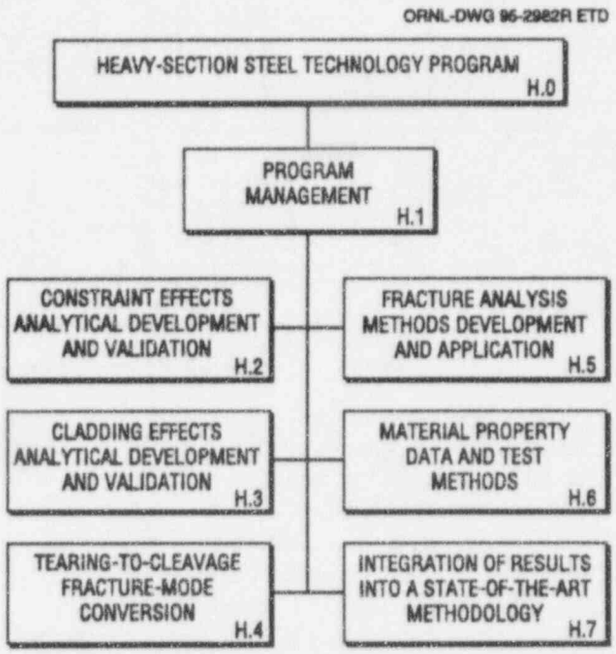

Figure 1.1 Level 1 breakdown structure for HSST Program

modification implements previously recommended changes to test programs scheduled for the FY 1994 performance period. Preparation of a revision to the HSST Program 189 for FY 1994 was completed.

Recommendations for the programmatic response to problems encountered in the biaxial and finite-length shallow-flaw fracture-toughness testing programs were forwarded to the NRC HSST Program Monitor. The recommendations were for (1) replacement of the defective biaxial test specimens and (2) reduction of the test temperature for the finite-length-flaw biaxial test specimens. Direction was received from the NRC HSST Program Monitor for implementation of the recommended changes.

Preparation and review of the HSST Program semiannual progress report for the period October 1992 to March 1993 was completed, and the camera-ready copy was forwarded to NRC for publication.

*This report is written in metric units. Conversions from English units for all SI quantities are listed on p. 85 of this report.

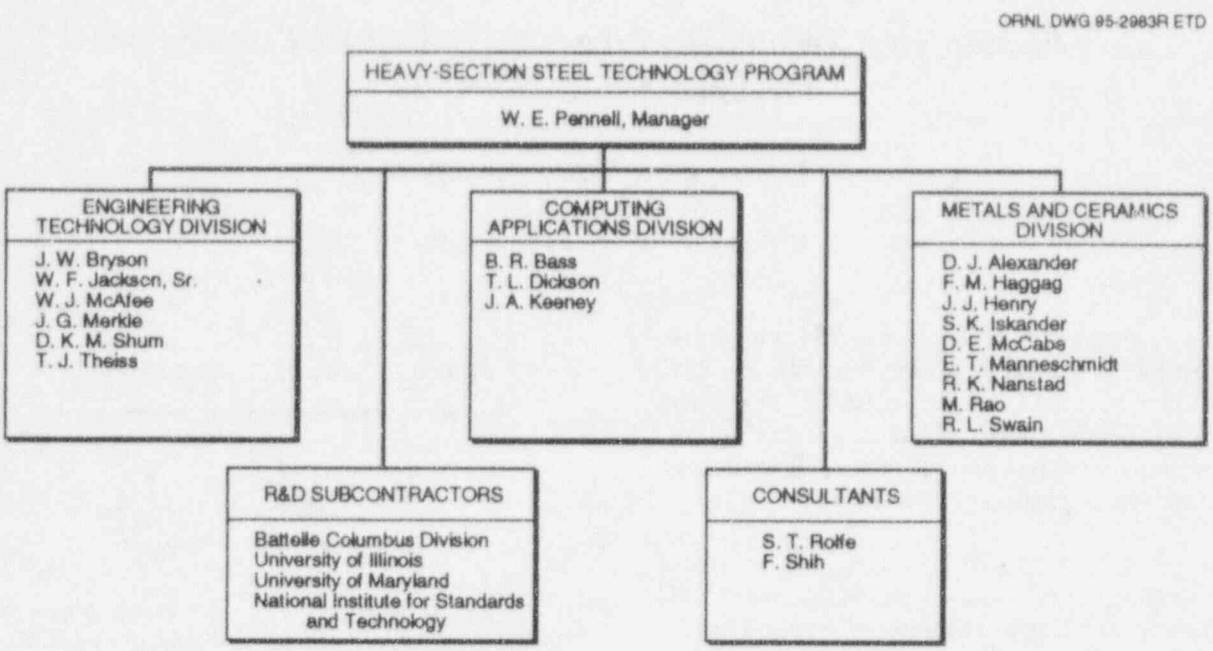

Figure 1.2 Resources applied to HSST Program R&D tasks

A meeting of NRC contractors involved in the Regulatory Guide 1.154 update project took place at the NRC White Flint, Rockville, offices on June 27, 1994. T. Dickson and the HSST Program Manager attended the meeting. The meeting objective was to coordinate the contractor activities so as to assure that the project objectives would be achieved. Contractor interface relationships and information flow paths were defined.

The HSST Program manager attended a briefing on NRC Directive 11.7, given by the ORNL NRC Programs Office. NRC Handbook 11.7 defines a three-step process for preparation and approval of a 189, one of which is a negotiation between the NRC Project Manager and the ORNL Project Manager. Resource expenditure estimating spreadsheets were prepared and issued to the HSST Program task leaders for use in preparing their input to the FY 1995 189. These spreadsheets will provide information on the resource expenditure for each of the program deliverables and will provide a basis for the negotiation phase of the 189 preparation procedure.

Preparation of the FY 1994 procurement package for the consulting subcontract with Prof. S. Rolfe, of the University of Kansas, was completed. Technical evaluations of the proposal subsequently received from Prof. Rolfe and a proposal from the University of Illinois (Prof. R. Dodds) were also completed.

Notification was received from R. Link of the Carderock Division of the Naval Surface Warfare Center (CDNSWC) that checkout testing of their 220-kip high-rate testing machine had been successfully completed. Documentation required for placement of an interagency agreement (IAG) with CDNSWC for performance of dynamic fracture toughness tests was completed and forwarded to the Department of Energy (DOE) Oak Ridge Operations Office for establishment of the required IAG. Data from these tests are required for the evaluation of dynamic effects on crack propagation during a pressurized-thermal-shock (PTS) event.

A paper by W. E. Pennell and W. R. Corwin entitled "Reactor Pressure Vessel Structural Integrity Research in the U.S. Nuclear Regulatory Commission HSST and HSSI Programs" was presented at the British Nuclear Energy Society (BNES) Conference on Thermal Reactor Safety Assessment. W. E. Pennell presented (1) "HSST Program Research into Constraint Effects in Fracture" to Dr. David Ward of the ORNL Engineering Technology Division Advisory Committee on April 19, 1994; (2) "An Interim Report on Shallow-Flaw Fracture Technology Development" at AEA Technology-Risley and Harwell Laboratories and at The Welding Institute (TWI) in the United Kingdom on August 8, 10, and 11, respectively; and (3) "Biaxial Loading and Shallow Flaw Effects on Crack-Tip Constraint and Fracture Toughness" at the American Society of Mechanical Engineers (ASME) Pressure Vessel and Piping Division Conference in Minneapolis, Minnesota, on June 23, 1994. A paper with the same title (item 3), authored by W. E. Pennell, B. R. Bass, J. W. Bryson, W. J. McAfee, T. J. Theiss, and M. C. Rao, was published in the volume of conference proceedings entitled "Changing Priorities of Codes and Standards: Failure,

Fatigue, and Creep," ASME PVP-Vol. 286, June 1994. A presentation entitled "Shallow Flaw and Biaxial Loading Effects on the Fracture Toughness of Reactor Pressure Vessel Material" was prepared. The HSST Program manager is scheduled to present this material to the Pressure Vessel Research Council (PVRC) in New York on October 12, 1994. The presentation incorporates the latest updates of data from the biaxial and large-scale shallow-flaw fracture toughness testing programs. Direction was also received for HSST Program participation in the 1995 ASME Pressure Vessel and Piping Division Conference. Abstracts for papers by B. R. Bass, J. A. Keeney, and W. J. McAfee, "Assessment of the Fracture Behavior of Weld Material in Full-Thickness Clad Beams;" and W. E. Pennell, B. R. Bass, J. W. Bryson, and W. J. McAfee, "An Interim Report on Shallow Flaw Fracture Technology Development," were prepared and forwarded to the conference organizers.

Results from the recent analysis and testing activities in the biaxial testing program were reviewed and evaluated. Shallow-flaw fracture toughness test data for A 533 B material at a test temperature ($T - RT_{NDT}$) of –10°C were generated using biaxial loading ratios of 1:0, 1:0.6, and 1:1 (see Task 2). The test data were found to correlate well with relatively simple functions of ln(R), where R is the width of the plastic zone along the direction of crack propagation, as determined from nonlinear finite-element analysis. While these simple relationships were derived from a very small data base and may not perform as well when additional biaxial fracture toughness data become available, their close correlation with the test data does suggest some interesting possible links between biaxial loading and fracture toughness. The crack-tip displacement, and therefore the root radius (r) of the blunted crack, can be directly related to the width (R) of the plastic zone. Strains in the plastic zone, adjacent to the blunted crack tip, increase as the root radius of the blunted crack decreases. The correlation of fracture toughness under biaxial loading with the plastic zone width (R) may therefore be due to the effect of biaxial loading in restricting the growth of the root radius of the blunted crack such that either (1) strains in the near-tip region increase to the plane-strain fracture ductility of the material or (2) strain hardening of the near-tip material increases to the point where the yield-limited opening-mode stresses increase to the fracture stress of the material. Information on the currently available test data and the interim evaluation results was communicated to the HSST Program consultants, Profs. R. Dodds, S. Rolfe, and F. Shih.

The HSST Program Manager, together with members of the HSST Program research team, attended the NRC-sponsored "Workshop on Constraint Effects in Fracture—No. 2." The workshop was held at the U.S. Naval Academy in Annapolis, Maryland, on April 20 and 21, 1994. The meeting participants discussed a number of constraint modeling and application issues raised by the HSST Program participants. These included (1) the J-Q trajectories calculated for the biaxial test specimens and (2) the treatment of data scatter in the RPV surveillance application of small-scale, low-constraint, fracture toughness specimens. The discussions resulted in a general understanding of the issues but did not result in their resolution.

An HSST Program team visited the University of Maryland (UM) on April 22, 1994, for discussions with Profs. G. R. Irwin, C. W. Schwartz, and X. J. Zhang. The discussions centered on observations from fractographic examinations conducted at UM and their implications for constraint effects models. Prof. Irwin emphasized that consideration of strain-rate effects was essential to understanding the process of fracture initiating in brittle carbide particles and propagating through the adjacent ferrite grain material. The HSST Program Manager provided the UM team with a review of the data scatter that had been observed in fracture toughness tests on specimens with low crack-tip constraint.

A request was received from Dr. Marc C. Burstow of the University of Sheffield, England, for a copy of the paper by W. E. Pennell et al., "Biaxial Loading and Shallow-Flaw Effects on Crack-Tip Constraint and Fracture Toughness." Dr. Burstow is investigating constraint effects of mismatched welded joints on fracture toughness. A copy of the paper was sent to him.

The HSST Program manager visited the AEA Technology Risley and Harwell Laboratories and TWI in the United Kingdom. The purpose of these visits was to exchange information on research program results and discuss their interpretation. Discussions at the AEA Technology Risley laboratory focused on a comparison of results from the biaxial fracture toughness testing at the host laboratory and the HSST Program tests at ORNL. The AEA tests have been performed using a plate specimen of the type developed by Prof. D. Aurich at Bundesanstalt für Materialprüfung in Berlin, Germany. Tests were run in the temperature range $-11°C < (T - T_{ref}) < +7°C$. Results obtained showed essentially no effect of biaxial loading on fracture toughness. Surface strains measured on the crack plane, but ~30 mm from the end of the crack, were in the range $0.95\% < \varepsilon_f < 1.05\%$ at the fracture load in the uniaxial tests and $0.45\% < \varepsilon_f < 0.72\%$ at fracture in the biaxial tests of the a/W = 0.1 specimens. The AEA Technology team concluded that plastic straining of the test specimen ligament may have occurred in their tests. Arrangements were completed for Dr. Andrew Sherry of AEA

Technology to visit ORNL on November 11, 1994, for a tour of the ORNL biaxial testing facility and discussions of the biaxial testing program analysis and test results.

The Harwell Laboratory is developing miniature fracture toughness test specimens. The miniature fracture toughness specimens are sized such that they can be fabricated from the broken halves of Charpy surveillance specimens. Two different specimen designs have evolved. The smaller of the specimens has an outside diameter of 4 mm, and the other specimen is 8 mm in diameter. The Harwell research team considers the synergistic effects of thermal aging (interface segregation) and irradiation embrittlement (microstructural changes) to occur to their maximum extent in very small segments of the RPV structure, particularly at the interface between the vessel structural material and the cladding. The miniature specimens have the potential capability of measuring the fracture toughness of materials taken from the clad/base-material interface region. The Harwell research team showed considerable interest in evidence from the recent HSST biaxial testing program, which suggests that, in the transition temperature region, crack-tip strains may have a controlling influence on the fracture process. The Harwell team plans to revisit the miniature specimen analysis and investigate the crack-tip strain field behavior.

The U.K. Health and Safety Executive–Nuclear Installations Inspectorate (HSE–NII) requires that the Magnox reactor RPVs operate at temperatures corresponding to the upper shelf of the Charpy energy curve. Data from the Charpy surveillance specimens has shown an upward shift in the 40-J Charpy impact energy temperature (T_{cv}), which is incompatible with this requirement. NII is using both AEA Technology and TWI to perform analyses and tests to provide an independent assessment of the integrity of the Magnox RPVs. Discussions at TWI focused on the potential impact of a strain-controlled failure mode on the TWI biaxial fracture toughness test results and their conclusions on biaxial loading effects. In other discussions during this visit, TWI raised concerns relating locally intensified strain aging of material at the tips of preexisting cracks, which are located adjacent to areas where further welding operations have been performed. Examples are cracks adjacent to weld repairs and cracks in areas influenced by the cladding process. The net effect of locally intensified strain aging is to restrict further plastic deformation of the crack-tip material and, thereby, reduce the transition-range fracture toughness of material at the crack tip by reducing its ability to yield and produce blunting. In the context of RPV integrity research, this effect could impact the material fracture toughness associated with preexisting subclad flaws. A foreign travel report (ORNL/FTR-5102) covering these visits was prepared and issued.

A request was received from Dr. F. Simenon of Battelle Pacific Northwest Laboratory (PNL) for photographs that show the geometry of the weld passes in a typical pressurized-water reactor (PWR) RPV weld. Photographs were sent of weld material taken from a longitudinal beltline weld from the RPV for a canceled PWR plant. The photographs showed a transverse section through the weld and fracture surfaces from three full-scale single-edge-notched-beam fracture toughness specimens made from the same material. Demarcation lines between the weld beads were visible on the fracture surfaces. The photographs are to be used in a PNL subcontract with V. Oliver of Rolls-Royce and Associates in the United Kingdom for the generation of a flaw distribution for use in RPV PTS analysis.

The HSST Program Manager is a voting member of the ASME Section XI Task Group on Operability (TGO) and the Working Group on Operating Plant Criteria (WGOPC). The objective for the TGO is to prepare a draft of a proposed Code Case on the operability of nuclear plants in which nonconforming pipe support conditions have been discovered during operation, or an event, not included in the design basis loading, has occurred. The TGOPC focus is on the continuing development and refinement of criteria used to evaluate the integrity of operating nuclear plants, with special emphasis on the structural integrity of the RPV.

The TGOPC has identified a need for development of procedures for calculating P-T limits for reduced postulated defect sizes; an initiative has been launched to meet this need. An action item resulting from this initiative, which directly involves the HSST Program, calls for (1) compiling a list of variables that affect fracture toughness of pressure vessel materials, (2) compiling the available materials data reflecting the effect of these variables, and (3) preparing a recommendation, based on a statistical evaluation of the data, for a fracture toughness curve for Appendix G of Sect. XI of the Code.

During the current reporting period the HSST Program Manager completed one of the actions required for item (2). A shallow-flaw fracture toughness data base was assembled for A 533 B plate material and submerged-arc RPV welds. The data were presented to the WGOPC at the May 3, 1994, meeting. The interim assessment provided to the Working Group was that the lower bound to the shallow-flaw fracture toughness scatter band appeared to be similar to the lower bound to the deep-flaw fracture toughness data. Data scatter and mean fracture toughness values are, however, higher for shallow flaws than for deep flaws. Attention was drawn to the significant influence of

the normalizing parameter (RT_{NDT} or NDT) used to characterize the shallow-flaw fracture toughness data sets.

A joint meeting of the ASME Section XI Working Groups on Flaw Evaluation and the WGOPC was held to review the selection of stress intensity factor equations for semielliptical surface flaws for inclusion in Sect. XI, Appendix G. The chairmen of the working groups each requested that copies of the HSST Program reports on stress-intensity-factor influence coefficients (SIFICs) for semielliptical inner-surface flaws be forwarded to them. The requested reports, together with disks containing the SIFIC data, were forwarded to each of the working group chairmen on August 25, 1994.

During the current reporting period, HSST Program personnel published four NRC reports,[1–4] four letter reports,[5–8] one foreign trip report,[9] one publication in a refereed journal,[10] two papers in technical society publications,[11–12] and gave ten presentations at program reviews and technical society and NRC-sponsored national and international meetings.[13–22]

References

1. R. H. Dodds, Jr., University of Illinois, for Martin Marietta Energy Systems, Inc., "Constraint Effects on Fracture Initiation Loads in HSST Wide-Plate Tests," USNRC Report NUREG/CR-6259 (ORNL/TM-12796), July 1994.*

2. W. E. Pennell et al., Martin Marietta Energy Systems, Inc., Oak Ridge Natl. Lab., "HSST Semiannual Progress Report for October 1992–March 1993," USNRC Report NUREG/CR-4219 (ORNL/TM-9493/V9&N2), July 1994.*

3. C. W. Schwartz, University of Maryland, for Martin Marietta Energy Systems, Inc., Oak Ridge Natl. Lab., "Crack-Speed Relations Inferred from Large Single-Edge-Notched Specimens of A 533 B Steel," USNRC Report NUREG/CR-5861 (ORNL/Sub/79-7778/9), May 1994.*

4. J. A. Keeney et al., Martin Marietta Energy Systems, Inc., Oak Ridge Natl. Lab., "Preliminary Assessment of the Fracture Behavior of Weld Material in Full-Thickness Clad Beams," USNRC Report NUREG/CR-6228 (ORNL/TM-12735), May 1994.*

5. J. A. Keeney, Martin Marietta Energy Systems, Inc., Oak Ridge Natl. Lab., "Cleavage Fracture Analyses of the French Clad Beam Experiments—DSR3 and DD2," ORNL/NRC/LTR-94/24, August 1994.

6. G. R. Irwin, X. J. Zhang, and C. W. Schwartz, University of Maryland, for Martin Marietta Energy Systems, Inc., Oak Ridge Natl. Lab., "Small Scale Non-Uniformities Related to Cleavage Initiation and their Implications for Constraint Modeling," ORNL/NRC/LTR-94/18, June 1994.

7. C. W. Schwartz, University of Maryland, for Martin Marietta Energy Systems, Inc., Oak Ridge Natl. Lab., "Crack-Tip Loading Rates Preceding Cleavage Reinitiation," ORNL/NRC/LTR-94/10, June 1994.

8. T. L. Dickson, Martin Marietta Energy Systems, Inc., Oak Ridge Natl. Lab., "Impact of Dynamic Crack Arrest on Fracture Analyses of Reactor Pressure Vessels Subjected to Pressurized-Thermal-Shock," ORNL/NRC/LTR-94/35, May 1994.

9. W. E. Pennell, Martin Marietta Energy Systems, Inc., Oak Ridge Natl. Lab., "Foreign Trip Report of W. E. Pennell," ORNL/FTR-1502, August 1994.

10. J. A. Keeney, "An Evaluation of Analysis Methodologies for Predicting Cleavage Arrest of a Deep Crack in an RPV subjected to PTS Loading Conditions," *ASME-PVP* 116, 128 (June 1994).

11. W. E. Pennell and W. R. Corwin, Martin Marietta Energy Systems, Inc., Oak Ridge Natl. Lab., "Reactor Pressure Vessel Structural Integrity Research in the U.S. Nuclear Regulatory Commission HSST and HSSI Programs" (Thomas Telford Services Inc., April 1994).

12. W. E. Pennell et al., "Biaxial Loading and Shallow Flaw Effects on Crack-Tip Constraint and Fracture Toughness," *Changing Priorities of Codes and Standards: Failure, Fatigue, and Creep, ASME-PVP* 186 (June 1994).

13. W. E. Pennell and W. R. Corwin, Martin Marietta Energy Systems, Inc., Oak Ridge Natl. Lab., "Reactor Pressure Vessel Structural Integrity Research in the U.S./NRC HSST and HSSI Programs," presented at the BNES/ENS International Conference, United Kingdom, April 1994.

14. W. E. Pennell, Martin Marietta Energy Systems, Inc., Oak Ridge Natl. Lab., "HSST Program Research into Constraint Effects in Fracture," presented to Dr. D. Ward of the ORNL Engineering Technology Division Advisory Committee, April 1994.

15. W. E. Pennell, Martin Marietta Energy Systems, Inc., Oak Ridge Natl. Lab., "Interim Report: Shallow-Flaw Fracture Toughness Data for Reactor Pressure Vessel Plate and Weld Material," presented to the ASME Section XI Working Group on Operating Plant Criteria, Atlanta, Georgia, May 1994.

16. W. J. McAfee, Martin Marietta Energy Systems, Inc., Oak Ridge Natl. Lab., "ORNL Uniaxial and Biaxial Shallow Flaw Fracture Toughness Test Results," presented at the NRC Workshop on Constraint Effects, May 1994.

17. B. R. Bass, Martin Marietta Energy Systems, Inc., Oak Ridge Natl. Lab., "Constraint Model Validation Using Fracture Toughness Data and Fractographic Results from Uniaxial and Biaxial Testing Programs," presented at the NRC Workshop on Constraint Effects in Fracture, May 1994.

18. W. E. Pennell et al., Martin Marietta Energy Systems, Inc., Oak Ridge Natl. Lab., "Biaxial Loading and Shallow-Flaw Effects on Crack-Tip Constraint and Fracture Toughness," presented at the ASME-PVP Conference, Minneapolis, Minnesota, June 1994.

19. J. A. Keeney, Martin Marietta Energy Systems, Inc., Oak Ridge Natl. Lab., "Stress-Intensity-Factor Influence Coefficients for Semi-Elliptical Inner-Surface Flaws in Clad Pressure Vessels," presented at the 26th National Symposium on Fracture Mechanics, June 1994.

20. D. E. McCabe, Martin Marietta Energy Systems, Inc., Oak Ridge Natl. Lab., "Preliminary Review of the Bases for K_{Ic} and K_{Ia} Curved in the ASME Code," presented at the 1994 PVP Conference, Minneapolis, Minnesota, June 1994.

21. D. E. McCabe, Martin Marietta Energy Systems, Inc., Oak Ridge Natl. Lab., "Report on Proposed ASTM Test Practice," presented at the ASTM Committee E08.8 Meeting, June 1994.

22. W. E. Pennell et al., "An Interim Report on Shallow-Flaw Fracture Technology Development," presented to the Fracture Technology Research Centers in the United Kingdom, August 1994.

---

*Available from National Technical Information Service, Springfield, VA 22161.

2 Constraint Effects Analytical Development and Validation

W. J. McAfee

The purpose of this task is to investigate and quantify the effects of constraint on the cleavage initiation toughness of RPV steels. The work is comprised of both analytical and experimental facets. Currently, Task 2 is divided into three subtasks: 2.1 Biaxial Loading Effects Validation Testing, (i) Verification Phase Testing and (ii) Analytical Support; 2.2 Constraint Effects Correlation; and 2.3 Unclad Finite-Length Flaw Development. Progress in the different phases of these subtasks is discussed below.

2.1 Biaxial Loading Effects Validation Testing

2.1.1 Development of Heat Treat Specification for Surrogate Irradiated Base Material (W. J. McAfee, S. K. Iskander, W. F. Jackson, J. J. Henry, Jr., and E. T. Manneschmidt)

Transfer of constraint methodologies and data bases developed under Task 2 to the evaluation of RPV behavior require demonstration of the developed methodologies for materials whose relevant properties simulate "prototypical" irradiated RPV base metal properties. A desirable goal for the base metal is a temperature at the 68-J Charpy V-notch (CVN) impact energy level (T_{68-J}) greater than 50°C (≈120°F) and a room temperature yield strength YS_{RT} in the range of 620 to 690 MPa (90 to 100 ksi). These values are typical for radiation-sensitive RPV steel irradiated to a fluence of 1.5×10^{19} neutrons/cm^2 (>1 MeV). Work was continued during this performance period toward development of a heat-treating procedure for application to HSST plate 14 that would yield properties comparable to those specified above. The effect of procedures developed for other A 533 materials being used in both Task 2 and Task 3 has also been investigated although the thrust of the heat-treating effort has been directed toward plate 14 because it is to be used as the base material for a large matrix of cruciform tests currently planned.

Promising results had been obtained previously using a 1010°C (1850°F) normalizing treatment followed by a rapid air quench. This heat treatment was applied to the three materials that are being used in this task and in Task H3: (1) the Combustion Engineering (CE) wide plate (development matrix of cruciform beams), (2) the plate 14 (to be used in verification matrix tests), and (3) the Standardized Nuclear Unit Power Plant System (SNUPPS) shell (to be used in the clad, cruciform beam tests, Task H3). Blocks approximately 230 by 230-mm (9 by 9-in.) square and 100-mm-thick (4-in.) were cut from plate 14 and the SNUPPS shell. A $91 \times 152 \times 230$-mm ($3.6 \times 6 \times 9$-in.) drop-off left from machining one of the development cruciform beams was used for the CE material. Two thermocouple wells were machined in each block; one 25-mm-deep (1-in.) in the center of the block top face and one 6-mm-deep (1/4-in.) approximately half way between the center and the block edge. These thermocouples were recorded continuously during heat treatment to monitor the response of the bulk material.

The blocks were put into the furnace at room temperature, heated to 1010°C (1850°F), held at 1010°C for 4 h, and then rapid air quenched. The quench rates were in the range of 25°C/min from 1010 to 260°C. Tensile and CVN specimens next were machined from each of these blocks. The Charpy specimens were all taken from a single layer 25 mm below the top surface of the block and were oriented in the L-S direction. The tensile specimens were taken from different depths through the full thickness of the block with their longitudinal axis in the L-direction. The Charpy curves are shown in Fig. 2.1. The transition temperature from the Charpy curve (68-J CVN energy level) for each material was plate 14 (T_{CV} = 85°C), SNUPPS shell material (T_{CV} = 95°C), and CE plate (T_{CV} = 90°C). This was an increase in the transition temperature for all materials as compared to the as-received material as is shown in Fig. 2.2 for the CE material. The CE material as-received characterization results were obtained from the CE wide-plate material and were performed by ORNL[1] and by CE for the Electric Power Research Institute.[2]

A matrix of tensile tests was performed for each material to evaluate the variation in tensile properties through the block thickness and with temperature. The matrices were designed to have the midpoint temperature near the nil-ductility-temperature (NDT) for the material. Since drop-weight tests have not been performed on the heat-treated materials, NDT was estimated as being the 27-J temperature from the respective CVN curves. The response of tensile properties to the heat treating procedure for these materials is summarized in Table 2.1. For comparison, the properties of the CE plate material in the as-received condition are also given. The through-thickness variation in tensile yield was observed to be essentially uniform at all

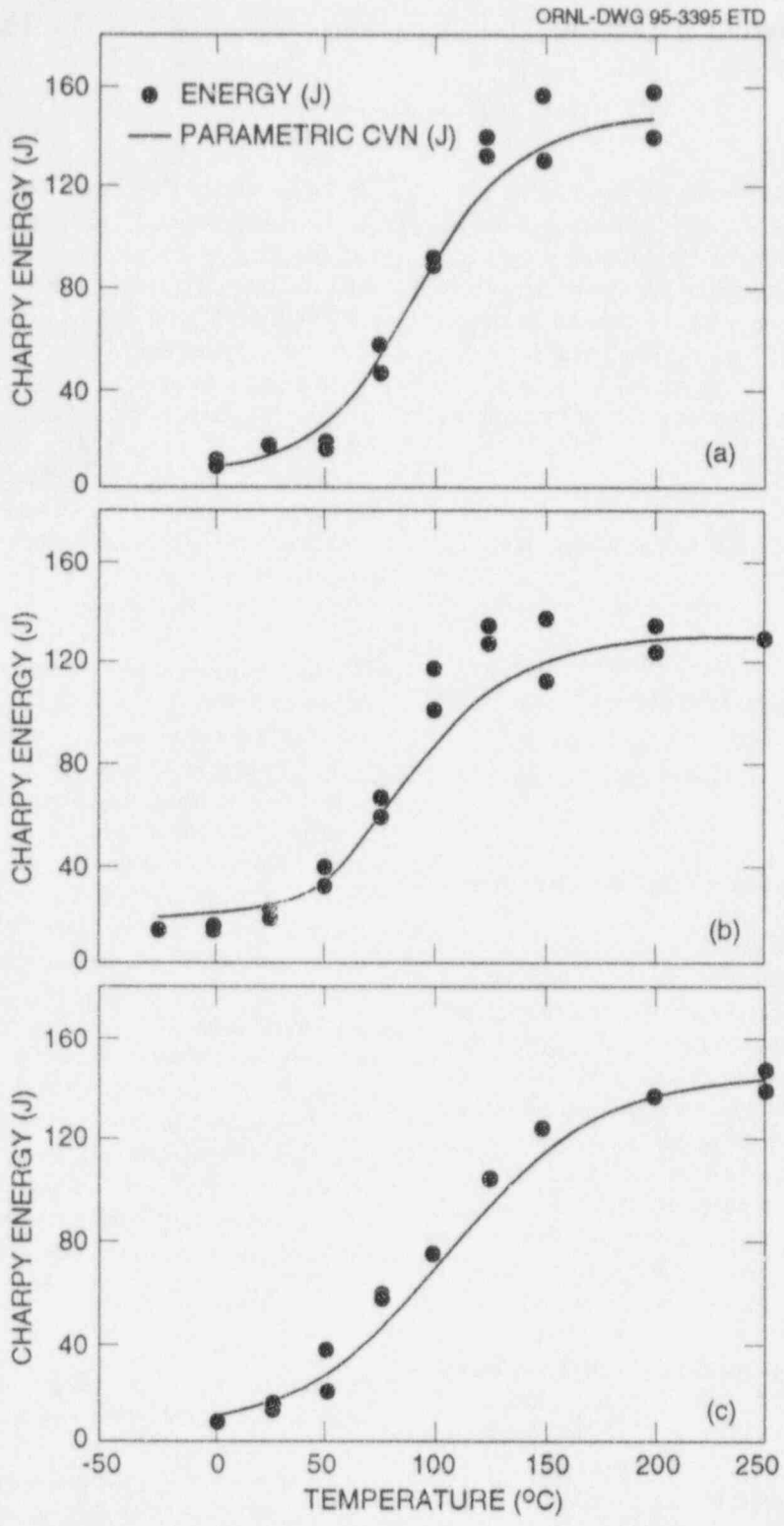

Figure 2.1 Results of testing CVN specimens for heat-treated test materials: (*a*) plate 14, (*b*) SNUPPS material, and (*c*) CE plate. All specimens were taken from a single layer of material

temperatures as is illustrated in Fig. 2.3 for plate 14. Characteristically, ultimate strength showed only a slight increase with decreasing test temperature. These characteristics are good from the standpoint of testing since the tensile properties remain nearly constant over the range of temperatures for which biaxial tests are to be performed. The average ductility, as measured by total elongation, is reduced to near 20% for the heat-treated materials, which represents a reduction of ~35% from the materials in the as-received condition.

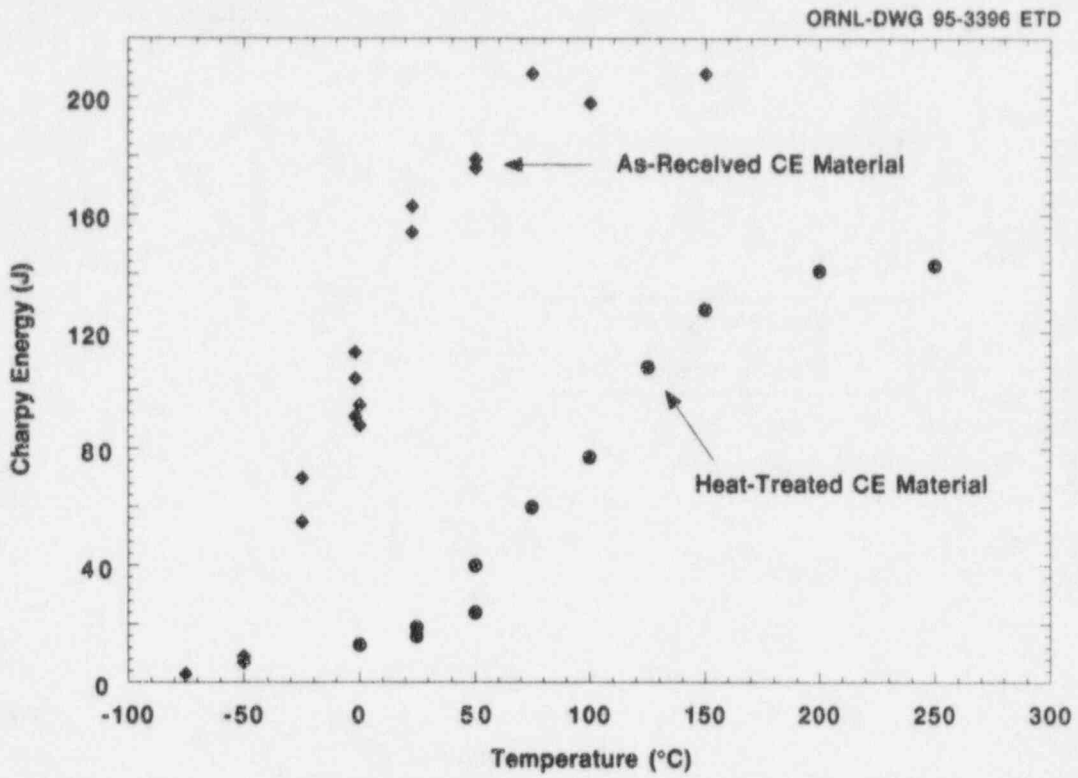

Figure 2.2 Comparison of Charpy results for CE plate material in as-received condition and after normalizing 4 h at 1010°C followed by rapid air quench, showing shift in transition temperature region due to heat treating

Table 2.1 Comparison of heat-treating effects on tensile properties for different HSST test materials (comparisons made at/near NDT for each material)

HSST material	Temperature [°C(°F)]	T_{Cv} [°C(°F)]	NDT [°C(°F)]	Yield stress [MPa (ksi)]	Ultimate stress [MPa (ksi)]	Total elongation (%)
Plate 14 normalized, air cooled	60 (140)	87 (188)[a]	60 (140)[b]	616 (89.3)	772 (112.0)	19
Plate 14 (as-received)	–10 (14)	25 (77)[a]	–10 (14)[b]	438 (63.5)	610 (88.5)	30
SNUPPS normalized, air cooled	57 (135)	88 (190)[a]	57 (135)[b]	525 (76.1)	720 (104.4)	18
CE plate normalized, air cooled	66 (150)	90 (195)[a]	66 (150)[b]	556 (80.6)	761 (110.4)	18
CE plate (as-received)	–45 (–50)[c]	–17 (1)	–35 (–31)[c]	420 (60.9)	621 (90.1)	31

[a] T_{Cv} determined from the lower bound (higher temperature) limit to the CVN curve.
[b] NDT was estimated to be the 27-J temperature from the CVN curve.
[c] Test temperature = NDT – 10°C.

Application of this heat-treating procedure to the candidate materials resulted in a stress-strain curve not characteristic of irradiated A 533 steel. A stress-strain curve for heat-treated plate 14 material at 60°C (140°F) is compared to a stress-strain curve for the same material in the as-received condition in Fig. 2.4. The curve for the heat-treated material has a 0.2% off-set yield stress of 538 MPa (78 ksi) although the onset of nonlinear response occurs at a stress of ~275 MPa (40 ksi). This stress-strain behavior is sufficiently different in character from that of irradiated pressure vessel steels to render it unsuitable for the biaxial testing program. The stress-strain response for heat-treated material exhibits a "power law" type of behavior, achieving 1% strain at a stress in excess of 620 MPa (90 ksi). By contrast, the stress-strain response for an irradiated A 533 B steel at 72°F (Fig. 2.5) retains the characteristic Lüder's band effect at the yield point for fluences ranging from 0.4×10^{19} to 5.5×10^{19} neutrons/cm^2 (E > 1 MeV); Fig. 2.5 was taken from HSST Technical Report No. 32.[3] In addition to an abrupt departure from linearity at the onset of yielding (Lüder's band effect), the irradiated material is characterized by a much-reduced rate of

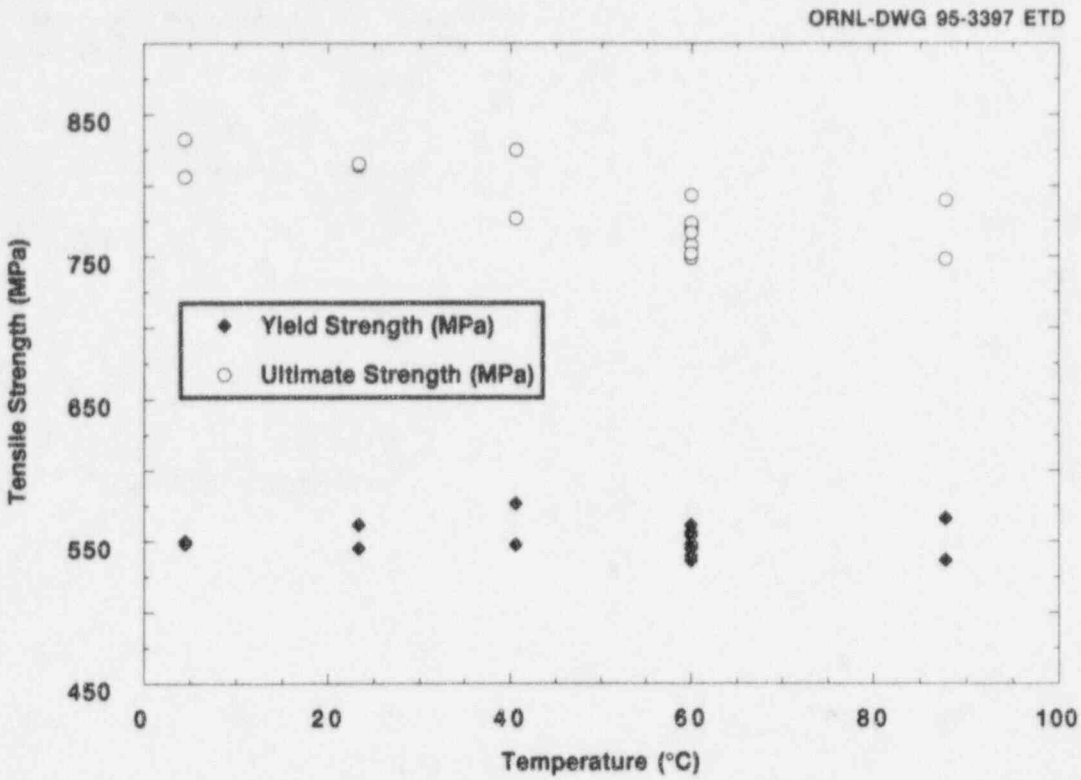

Figure 2.3 Yield and ultimate strength of heat-treated plate 14 not strongly dependent on temperature through the transition temperature region

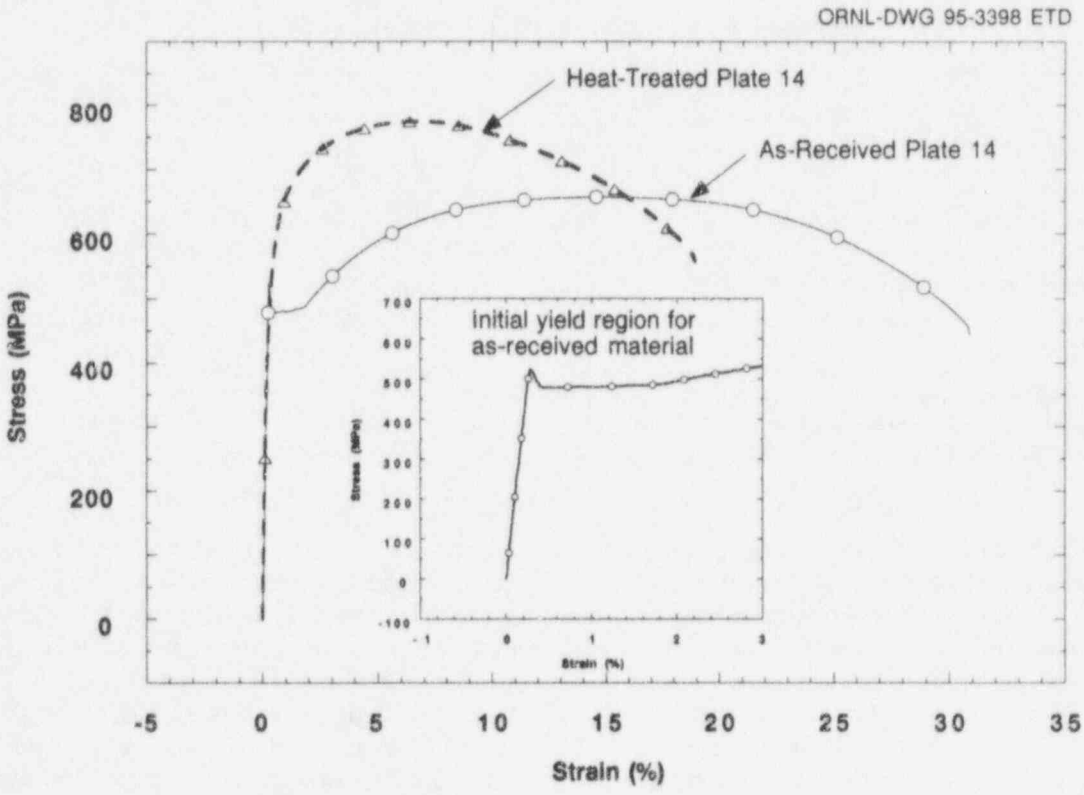

Figure 2.4 Comparison of stress-strain curves for plate 14 in as-received and heat-treated condition showing difference in shape of curve through initial yield region

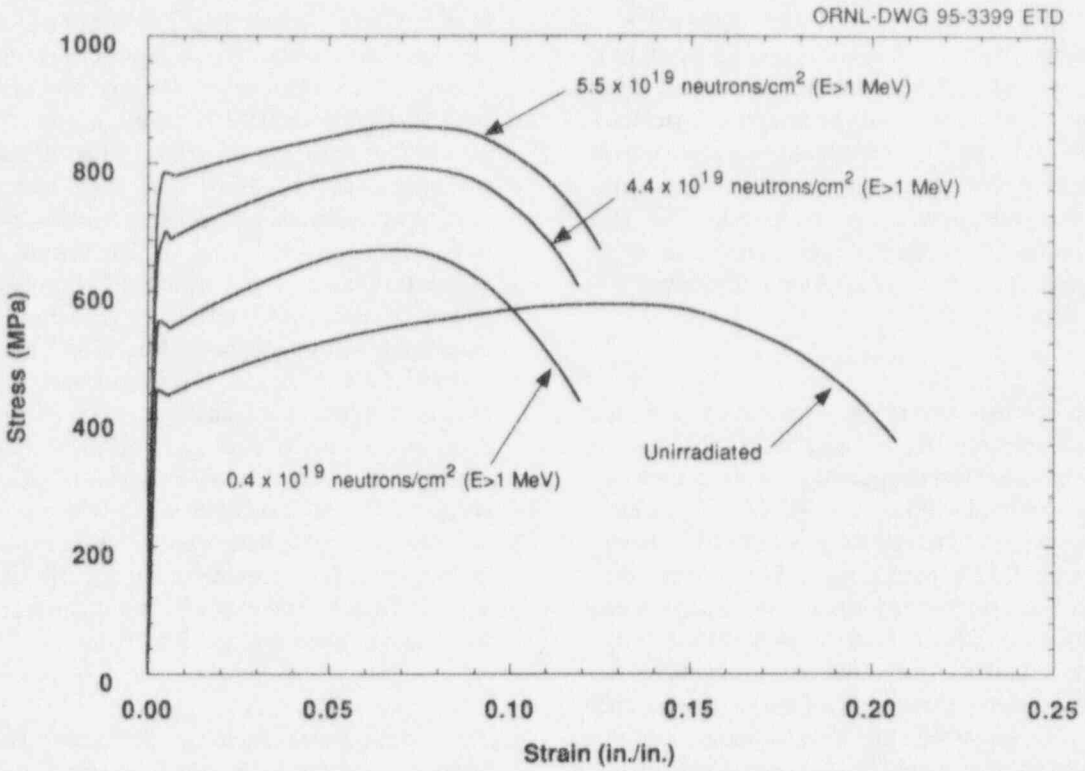

Figure 2.5 Stress-strain behavior of irradiated ASTM A 533 steel at 22°C (72°F) and loading rate of 1.3 × 10^{-4} in./in./s

strain-hardening as compared to the heat-treated material in Fig. 2.4. The absence of the Lüder's band effect and the substantial strain-hardening accompanying the departure from linearity imply development of very limited plasticity in the cruciform specimen under both uniaxial and biaxial loading conditions. Applications of the ORNL plastic zone width model to the cruciform specimen under uniaxial and biaxial loading conditions have confirmed the importance of incorporating certain characteristic features into the constitutive relations. In the context of the irradiated material of Fig. 2.5, the principal features were determined to be the Lüder's band effect and relatively low rate of strain-hardening occurring in the domain of small plastic strains. The HSST experience with the cruciform specimen is that this level of detail is required in the constitutive relations to adequately evaluate biaxial loading effects on crack-tip models. Clearly, these characteristics cannot be represented in a power-law stress-strain curve, such as the popular Ramburg-Osgood relation employed in many applications of constraint methodologies. Thus, any conclusions concerning biaxial effects on fracture toughness derived from Ramburg-Osgood or similar power-law relations should be reevaluated. Furthermore, these inferences should not be limited just to out-of-plane biaxial effects but should be viewed as equally applicable to crack-tip models influenced only by in-plane fields. It has thus been concluded that the heat-treating procedure developed is not acceptable for the intended application. Discussions are currently under way with a commercial vendor to perform a more standard heat treatment of plate 14, which would consist of normalizing at 900°C (≈1650°F) followed by a water quench and temper to achieve the desired tensile properties. The transition temperature would not be controlled in this case.

2.1.2 Tests of Load-Ratio Matrix Cruciform Specimens (W. J. McAfee, B. R. Bass, J. W. Bryson, and W. F. Jackson, Jr.)

The two-dimensional (2-D) flaw, load-ratio test matrix of cruciform beams was completed during this period. Four test specimens had been prepared during the previous reporting period, and testing had begun. It was discovered that the specimens appeared to have been overheated during EB welding of the beam arms with the result that the basic material properties had been altered. With NRC approval, additional material from the CE-01 plate was used to fabricate four new specimens. Note that the CE-01 plate was the source material for the first five specimens in the test series. A clearly identified segment of the 41-cm wide, 107-cm-long, and 25-cm-thick (16- × 42- × 9 3/4-in.) original plate was located in the HSST storage yard and was sufficient to provided the required stock material for these additional specimens. Based on experience in fabricating and testing of the initial five cruciform specimens, a specimen design change was made to alleviate the complexity of the EB weld joint between the test section and

beam arms. Specifically, a 23-cm (9-in.) square blank was used as compared to the original design of 15 cm (6 in.). The blank provided sufficient material so that load diffusion control slots (LDCSs) could be integrally machined into the specimen. The EB weld joining test section with beam arm is now located entirely within homogeneous material as compared to welding across the LDCSs. This has the additional advantage that specimen machining is simpler because it removes some of the intermediate machining steps.

The specimens were tested in the order and under the test conditions (temperature, biaxial load ratio) shown in Table 2.1. The target test temperature for all specimens was –43°C (–46°F) [T – RT_{NDT} of –8°C (–15°F)]. The fracture toughness determined for specimen BB-10 was 109.2 MPa$\sqrt{m}$ (99.4 ksi$\sqrt{in.}$), which is approximately 50% of the value determined from the uniaxially loaded cruciform specimen BB-02. Posttest investigation of the fracture surface indicated initiation near the center of the specimen. A careful evaluation of all test parameters did not indicate any reason why this test should not be considered as a valid fracture toughness test for use in evaluating the effect of constraint on toughness.

Because specimen BB-10 was the first specimen tested under full 1:1 biaxial loading and with the low toughness obtained from this test (Fig. 2.6), it was concluded that the next specimen would be tested under uniaxial loading (0:1). This result would provide a direct comparison with previous data (specimen BB-02), permitting development of conclusions regarding the effect of biaxial loading on toughness. Specimen BB-11 was tested under uniaxial loading at a nominal test temperature of –42°C (–44°F) [T – RT_{NDT} of –7°C (–13°F)]. The test parameters and failure results are given in Table 2.2. Crack-mouth opening displacement (CMOD) results are shown in Fig. 2.7. The calculated fracture toughness from CMOD measurements was 195.4 MPa$\sqrt{m}$ (177.8 ksi$\sqrt{in.}$), which compares well with the toughness obtained from uniaxially loaded cruciform specimen BB-02 [i.e., 214 MPa$\sqrt{m}$ (195 ksi$\sqrt{in.}$)]. In conjunction with the lower toughness measured for specimen BB-10, the failure ductility was reduced by a half as compared to that measured for specimen BB-11. Based on the results from specimens BB-02, BB-10, and BB-11, it appeared that biaxial loading has a dramatic effect on the toughness properties of this material.

The two remaining cruciform specimens were used in an attempt to validate the results from specimen BB-10. Specimens BB-07 and BB-09 were tested under biaxial loading (load ratio of 1:1) at a nominal test temperature of –42°C (–43°F) [T – RT_{NDT} of –7°C (–12°F)]. The results for these tests are summarized in Table 2.2. The CMOD behavior is shown in Figs. 2.8 and 2.9, respectively. The

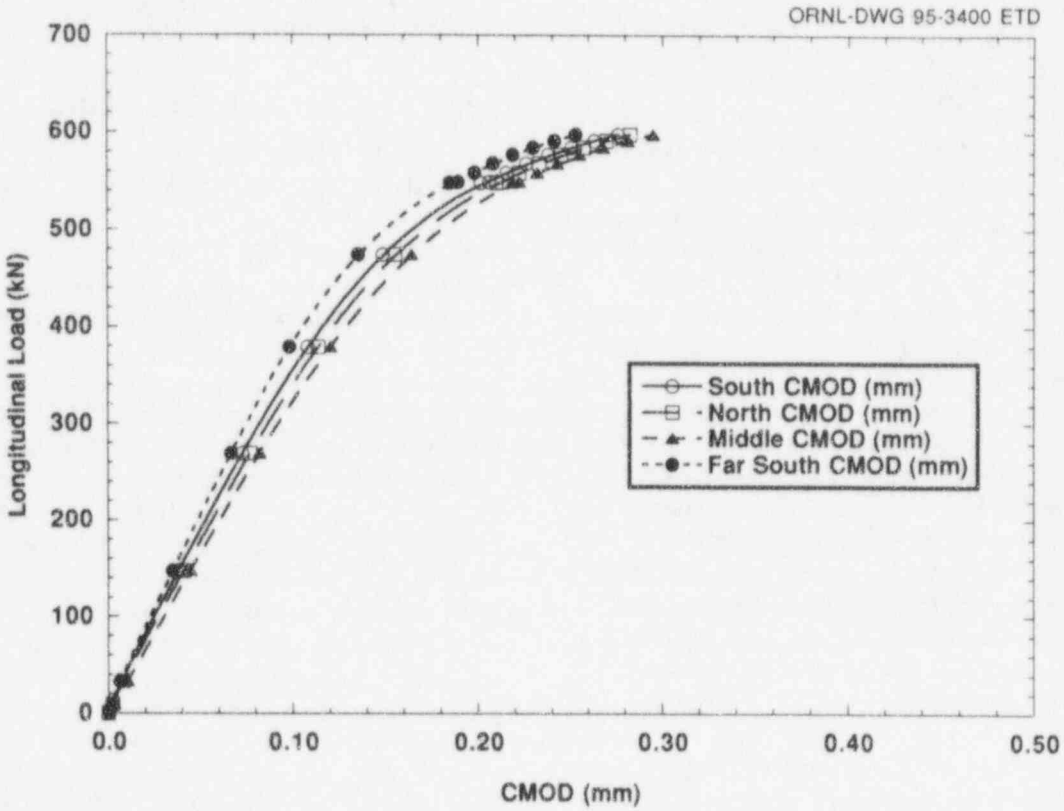

Figure 2.6 CMOD results measured for cruciform specimen BB-10 tested under biaxial (1:1) loading

Table 2.2 Summary of test results for new cruciform specimens in load ratio matrix

Specimen	BB-10	BB-11	BB-07	BB-09
Load ratio	1:1	0:1	1:1	1:1
Failure temperature, °C (°F)	–43 (–46)	–42 (–44)	–42 (–43)	–42 (–43)
Maximum load, kN (kips)	1198 (268.8)	700 (157.3)	1422 (319.7)	1460 (328.2)
Longitudinal load, kN (kips)	598 (134.4)	700 (157.3)	711 (159.9)	729 (163.9)
CMOD, mm (in.)	0.29 (0.0116)	0.70 (0.0275)	0.75 (0.0295)	0.508 (0.0300)
LLD (longitudinal), mm (in.)	2.76 (0.1087)	7.00 (0.2756)	5.70 (0.2244)	6.104 (0.2403)
LLD (transverse), mm (in.)	2.33 (0.0917)	NA	4.51 (0.1777)	5.380 (0.2118)
K_{Jc} from CMOD, MPa$\sqrt{m}$ (ksi$\sqrt{in.}$)	109.2 (99.4)	195.4 (177.8)	219.0 (199.3)	224.5 (204.3)
K_{Jc} from LLD, MPa$\sqrt{m}$ (ksi$\sqrt{in.}$)	103.0 (93.8)	189.4 (172.4)	205.3 (186.9)	207.1 (188.4)

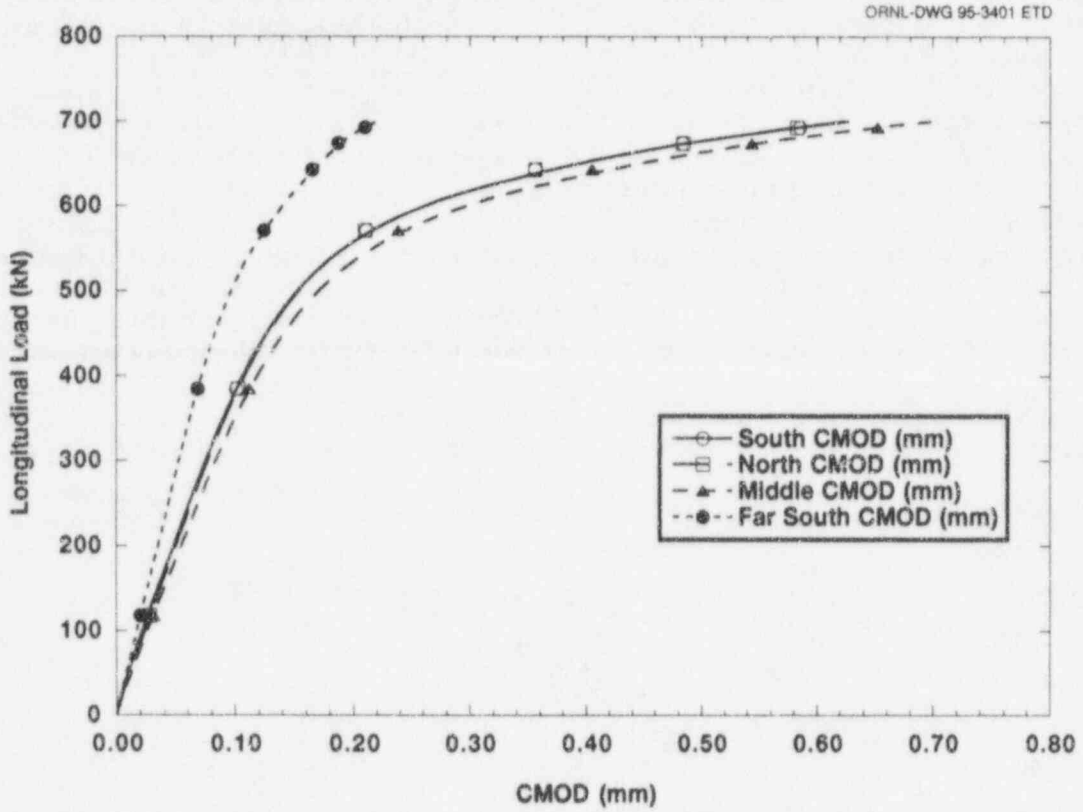

Figure 2.7 CMOD results measured for cruciform specimen BB-11 tested under uniaxial (0:1) loading

calculated fracture toughnesses from these CMOD measurements were 219.0 MPa$\sqrt{m}$ (199.3 ksi$\sqrt{in.}$) and 224.5 MPa$\sqrt{m}$ (204.3 ksi$\sqrt{in.}$). Posttest investigation of the fracture surfaces for all tests indicated initiation near the center of the specimen. This further substantiates the validity of the specimen for obtaining valid fracture toughness results for use in evaluating the effect of constraint on toughness.

A comparison of the measured CMOD at the specimen centerline is shown in Fig. 2.10. It should be noted that the results for specimens BB-01 and BB-02 are not shown because these specimens had a slightly different test section geometry (different LDCSs), which would result in different deformation response. By closely evaluating Fig. 2.10, it can be seen that the 0.6:1 biaxial load cases clearly represent a different set of results so far as deformation is concerned. The 0:1 and 1:1 tend to agree more closely relative to stiffness and, with the exception of specimen BB-10, failure CMOD.

The effect of biaxial loading can be readily seen by comparing all of the cruciform data as shown in Fig. 2.11. Here, the toughness determined from each test is plotted as a function of the biaxial load ratio. Deep-flaw data at the same normalized test temperature are also shown. Finally,

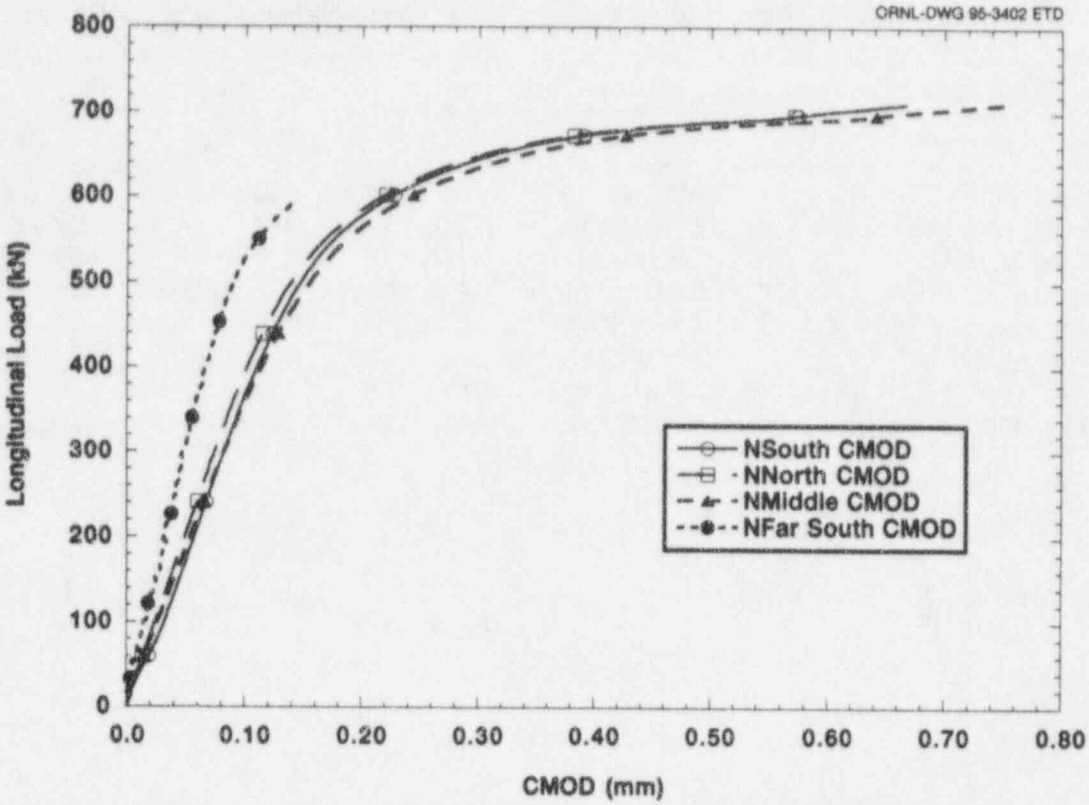

Figure 2.8 CMOD results measured for cruciform specimen BB-07 tested under biaxial (1:1) loading

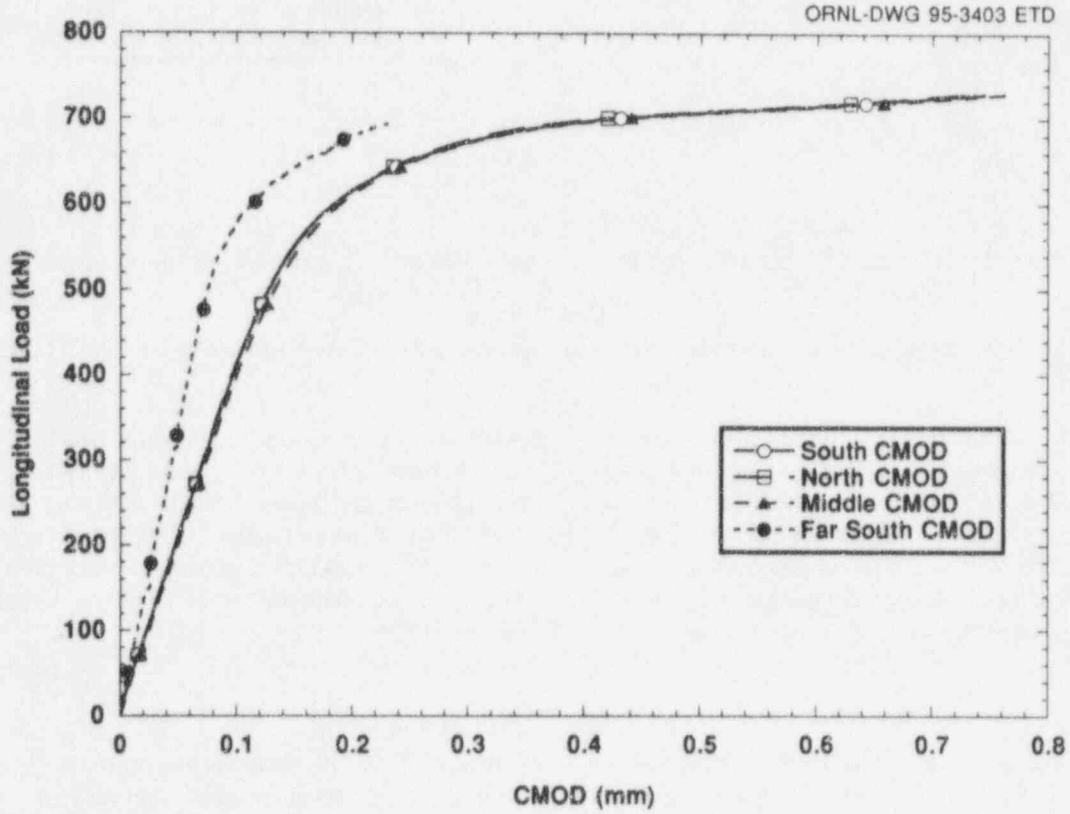

Figure 2.9 CMOD results measured for cruciform specimen BB-09 tested under biaxial (1:1) loading

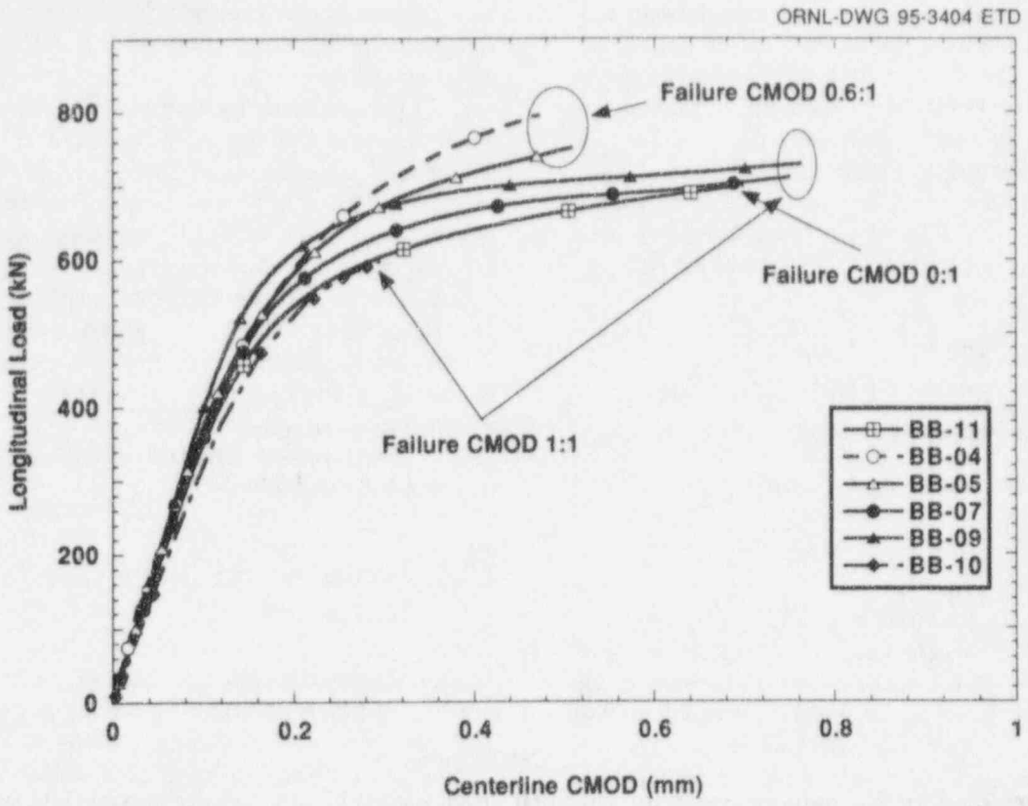

Figure 2.10 Demonstration of effect of biaxial loading on ductility as measured by centerline CMOD in cruciform specimens

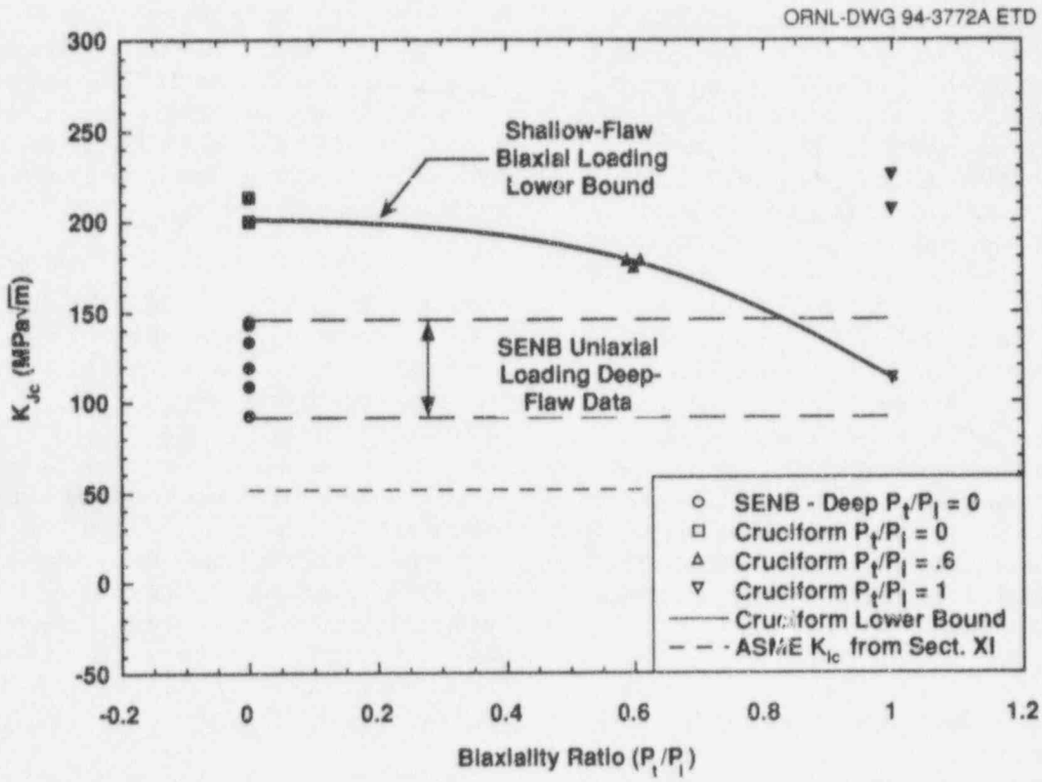

Figure 2.11 Effect of biaxial loading on lower bound toughness for CE plate material tested at T – NDT = –10°C

the ASME Sect. XI K_{Ic} value is shown. A shallow-flaw effect is evident when the biaxial data are compared to the deep-flaw data. The effect of increasing biaxiality reduces the shallow-flaw effect but does not completely eliminate it, at least when the lower bound curves for these data sets are used for comparison. It should also be noted that both the cruciform and deep-flaw data lower bounds are above the ASME Sect. XI K_{Ic} curve. A postulated cause for the high and low toughness results for the biaxial 1:1 data is given in Sect. 2.2.

2.2 Analyses of 2-D Flaw Cruciform Specimens (W. J. McAfee, W. E. Pennell, B. R. Bass, and J. W. Bryson,)

2.2.1 Test and Specimen Modeling

Analyses of the cruciform test results have consistently shown the finite-element model to yield "stiffer" results of deformation behavior than are seen in the experiments. The stress-strain curve being used as input for the analyses was developed using CE wide plate with some prior history; the material was first used in the wide-plate tests and then as beam specimen material in the shallow-flaw test program. The stress-strain characterization results were developed using material with no prior test history; test specimens were taken from virgin plate material. Scoping analyses have demonstrated that prediction of the deformation and, ultimately, the toughness for these specimens depends in no small measure on the constitutive model used, particularly the response through the initial yield region. As a check on the validity of the stress-strain curve being used, additional testing was performed to investigate both temperature and through-thickness dependency of the tensile behavior. The material used was taken from the remaining part of the block used to machine specimen BB-07. Tensile specimens were machined and tested at room temperature and –46°C (–50°F). Little through-thickness variation in tensile behavior was found at either temperature. Also, the temperature dependence closely matched the existing data. The new stress-strain data curve shown in Fig. 2.12 is compared to the original curve used in prior analyses. The new data exhibit an earlier departure from linearity, lower yield, lower ultimate, a higher uniform elongation, and slightly less strain hardening than the stress-strain data that have been used in all analyses to date. For the analyses, the material representation beyond ultimate stress was modeled using perfect plasticity.

Prediction of deformation response for the cruciform specimens was improved by use of this new curve. Figure 2.13 shows a comparison of experimental and finite-element analysis longitudinal surface strain at a point on the specimen symmetry plane located 31.75 mm (1.25 in.) from the flaw plane for the case of uniaxial loading. Excellent agreement between experiment and analysis was obtained, whereas previous analyses tended to under-predict the amount of strain measured. Comparison of experimental and finite-element calculated CMOD and load line displacement (LLD) for the specimens analyzed showed improved agreement between analysis and experiment. The new calculations will also result in a change in the η-factors used to determine fracture toughness. The toughness values are currently being updated based on this new stress-strain curve. These findings demonstrate the necessity for using the proper material model in these types of analyses. Use of a "generic" curve may be sufficient to identify trends but is not appropriate to calculate detailed structural response and toughness.

2.2.2 Evaluation of Existing Constraint Models

The low toughness result obtained from specimen BB-10 gave impetus for reevaluation of existing constraint methodologies. In prior evaluations of the effect of biaxial loading on constraint, the cruciform specimen was investgated using the originally proposed Dodds-Anderson (D-A) stressed-volume constraint correction procedure.[4] A "modified" D-A scaling procedure was used which assumed self-similar shaped stressed areas ahead of the crack and also drew upon a J-Q description of the crack-tip fields. According to Ref. 4, the J_{FB}/J_0 ratio for biaxial 0.6:1 loading was ~25% greater than that for uniaxial loading, which implies greater constraint loss for biaxial 0.6:1 loading than for the uniaxial case, a result inconsistent with the biaxial test results. To resolve this discrepancy, the originally proposed constraint correction model using contour areas was applied to the cruciform specimen.

Maximum principal stress contours in the range $2.5\sigma_0$ to $2.8\sigma_0$ (σ_0 = yield stress) represent critical distances ahead of the crack tip, that is, where cleavage fractures initiate. Maximum principal stress contours $\sigma_1/\sigma_0 = 2.5$ were obtained at several positions along the crack front for a number of load steps (up to 190 kips longitudinal load) using ABAQUS-POST. The contour areas were then determined and plotted against the ABAQUS computed J-values for the respective crack front location and load value. From these curves, J-values for uniaxial and biaxial loading that give the same stressed areas can be determined, and plots of J_B vs J_U can then be constructed (J_B is J for the biaxially loaded specimen, and J_U is J for the uniaxially loaded specimen).

The following results were obtained: (1) self-similar principal stress areas were obtained with increasing load for

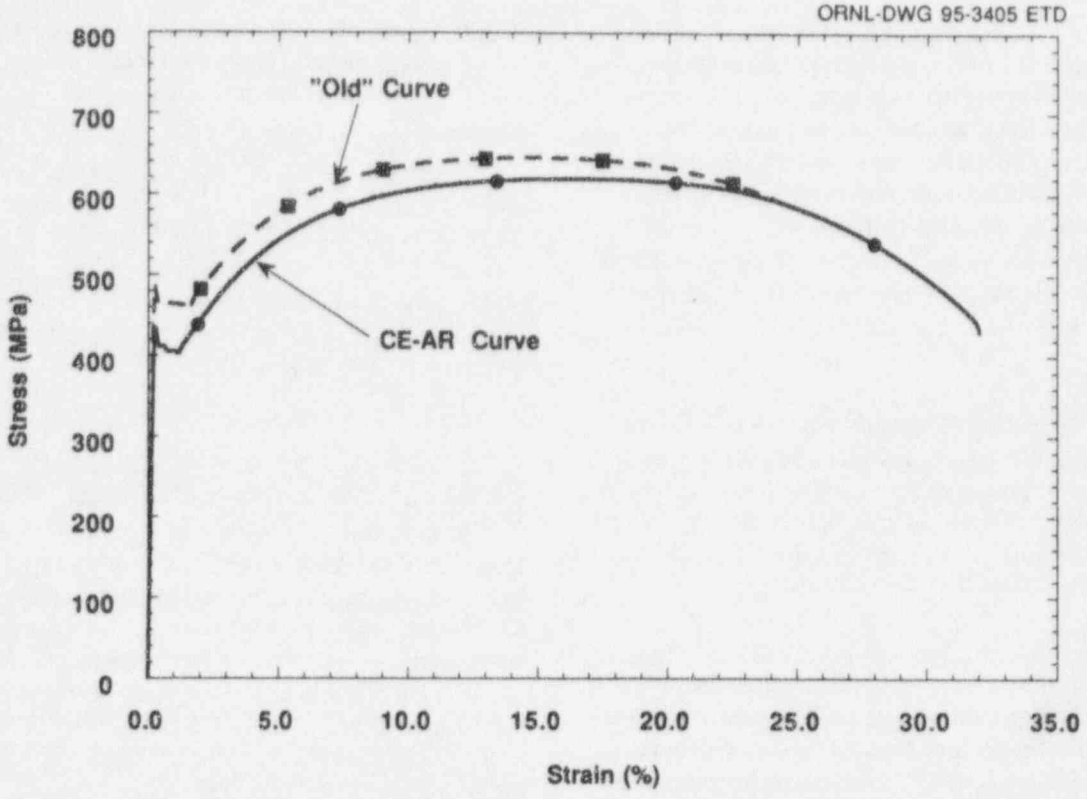

Figure 2.12 Comparison of updated stress-strain curve for CE material (cruciform specimen material) with the curve used in previous analyses

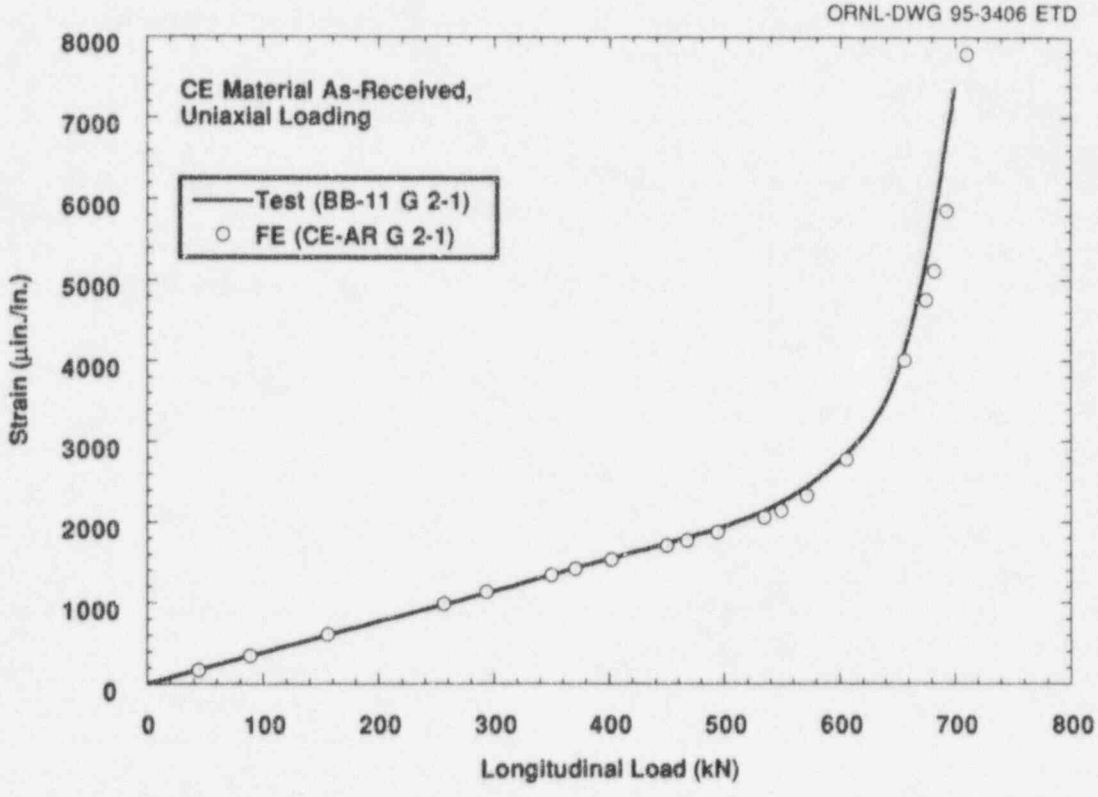

Figure 2.13 Comparison of analysis results using updated stress-strain curve for CE material with experimentally measured longitudinal surface strain at center of bottom surface for uniaxially loaded cruciform specimen BB-11

both uniaxial and biaxial loading; (2) both maximum principal stress area and J were essentially constant for the center 38 mm (1.5 in.) of the specimen, and then both area and J decreased rapidly as the crack-slot juncture was approached; (3) J_B on average was somewhat greater than J_U, which agrees with the "modified" procedure employed in Ref. 5 and implies greater constraint loss for biaxial 0.6:1 loading than for uniaxial loading, a result contrary to the experiments to date. A comparison of the results for $J_{B\ 0.6:1}$ vs J_U is shown in Fig. 2.14.

The D-A scaling procedure was also applied to the biaxial 1:1 loading case. The results indicated little if any biaxial effect and again appeared to be at odds with the experimental result (specimen BB-10). A comparison of D-A scaling procedure for the full biaxial case, $J_{B\ 1:1}$ vs J_U, is shown in Fig. 2.15.

While these are preliminary results, the implication is that the D-A procedure and the J-Q methodology do not adequately describe the effect of biaxial loading on fracture toughness. It is currently felt that the use of a stress-based constraint criterion alone is not sufficient. An alternate strain-based approach has been proposed as is discussed in the next section.

2.2.3 Preliminary Evaluation of an Alternate Dual-Parameter Constraint Model

An investigation of plastic strain accumulation ahead of the crack tip in the cruciform specimens has led to the development of a preliminary dual-parameter constraint model based on plastic strain. Based on the limited amount of data currently available, it was found that an expression using plastic zone radius along the direction of crack propagation provides a good parameter model for the effect of constraint on fracture toughness.

Finite-element analyses were performed on the cruciform specimen to clarify the relationship between biaxiality loading ratio and development of the plastic zone width in the plane of the crack. Note that the stress-strain curve used in the analysis results reported here was developed using the "old" curve for the CE material. The referenced stress components are calculated at the nodal location (N-5006) identified in Fig. 2.16; the coordinate system is given in the same figure. Figure 2.17 indicates that node N-5006 experiences yielding at different load levels, depending on the out-of-plane loading ratio. This behavior appears to be the consequence of the three-dimensional (3-D) stress state and the yield surface model.

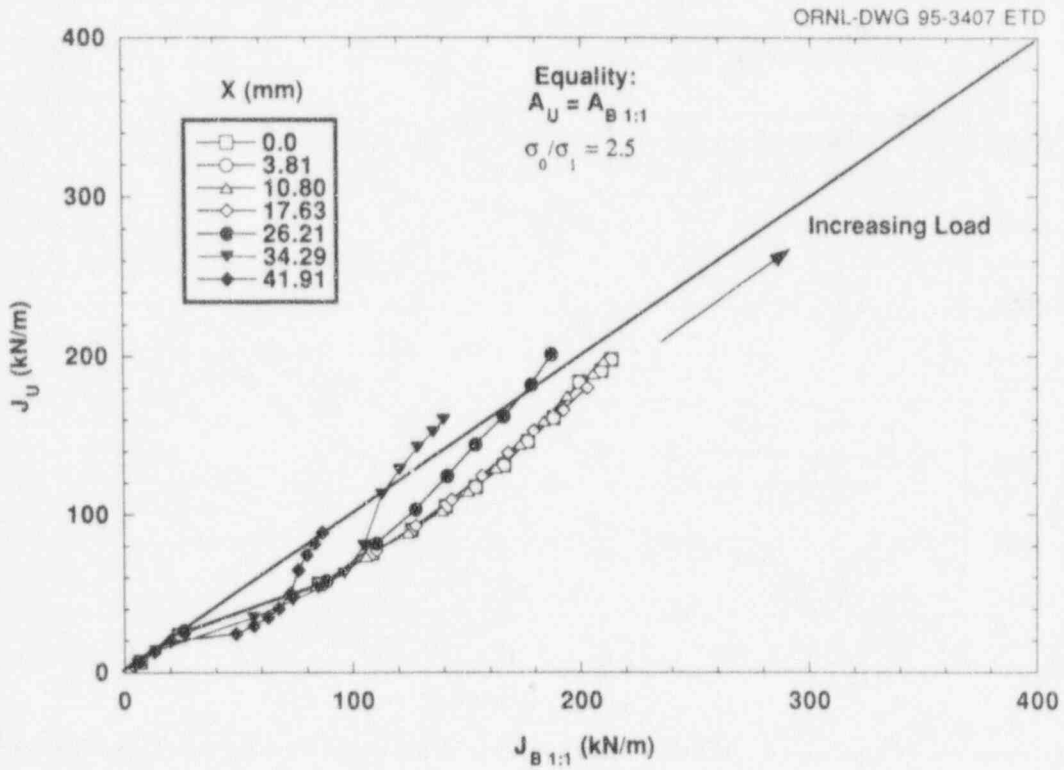

Figure 2.14 Validation check on D-A constraint correction for biaxially loaded (0.6:1) cruciform specimen

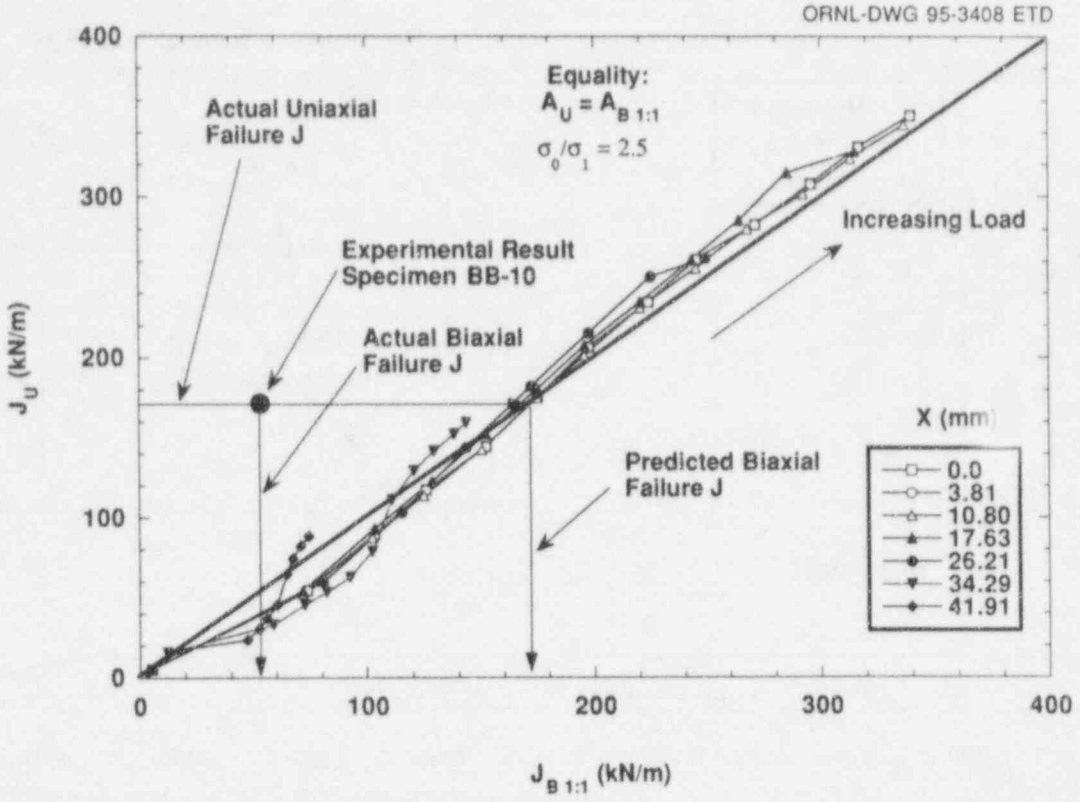

Figure 2.15 Validation check on D-A constraint correction for biaxially loaded (1:1) cruciform specimen

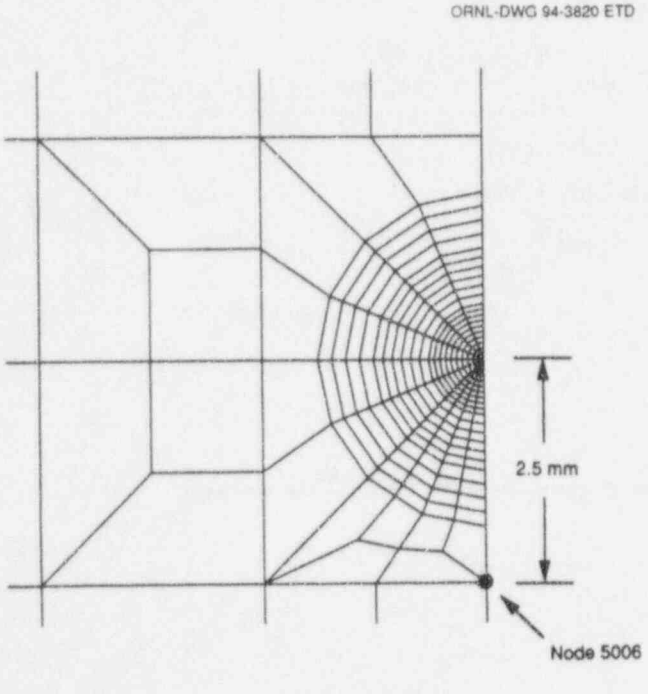

Figure 2.16 Stress components were examined at material point (Node 5006 in FEA model) 2.54 mm (0.100 in.) ahead of crack tip

Using the von Mises yield criterion, yielding occurs when the second deviatoric stress invariant J_2 reaches a critical value; that is, when

$$\sqrt{J_2} = K \ ,$$

where K is a material parameter, and

$$J_2 = (1/6)[(P_1 - P_2)^2 + (P_2 - P_3)^2 + (P_3 - P_1)^2] \ .$$

Here, P_1, P_2, and P_3 are the principal stresses. The above yield criterion can be written in terms of the effective stress s_{eff} according to

$$s_{eff} = \sqrt{(3 \cdot J_2)} = \sqrt{3} \cdot K \ .$$

The Mises effective stress and, consequently, the yield criterion are governed by the differences in the principal stresses.

As shown in Fig. 2.17, for the 1:1 load case, development of the plastic zone width is abrupt at an approximate load level of 1034 MPa (150 kips). For the other two biaxial load cases (0:1 and 0.6:1), the development of the plastic zone with increasing load is more gradual (and appears to be delayed for the 0.6:1 case). The stress components (Cartesian normal stresses, hydrostatic stress, and Mises effective stress) are plotted in Figs. 2.18–2.20 to provide a better understanding of plastic zone development in the cruciform specimen.

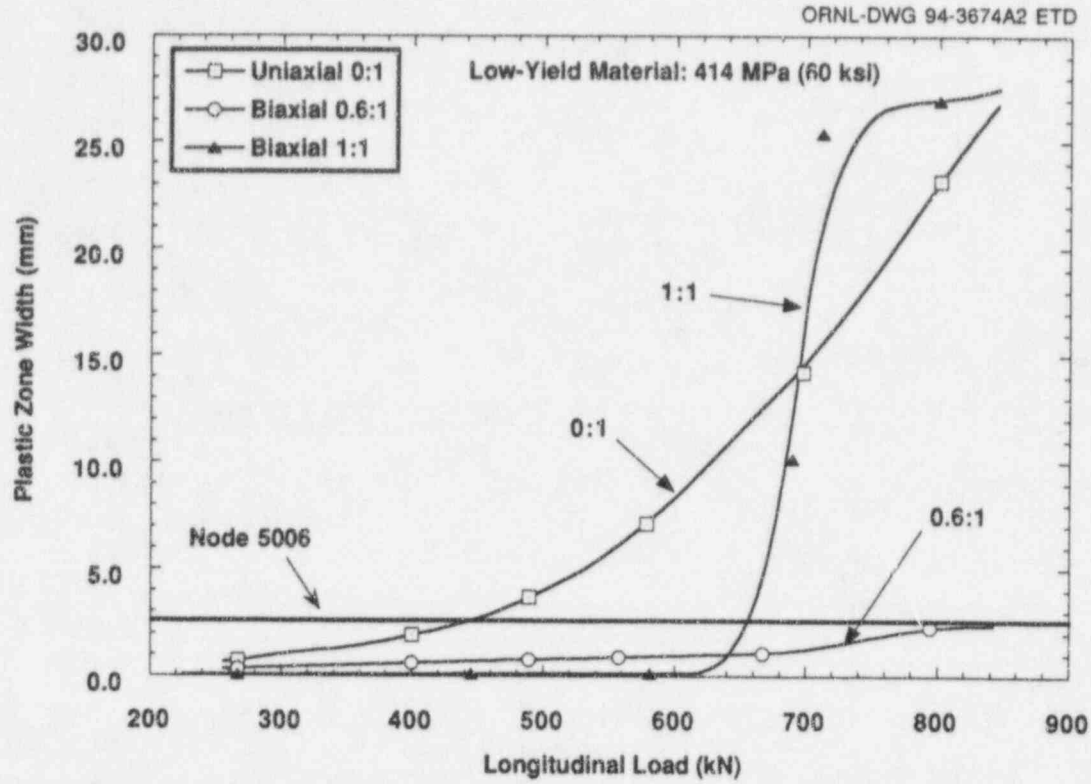

Figure 2.17 Material point (Node 5006) 2.54 mm (0.100 in.) ahead of the crack tip that experiences yielding at different load levels, depending on out-of-plane loading ratio

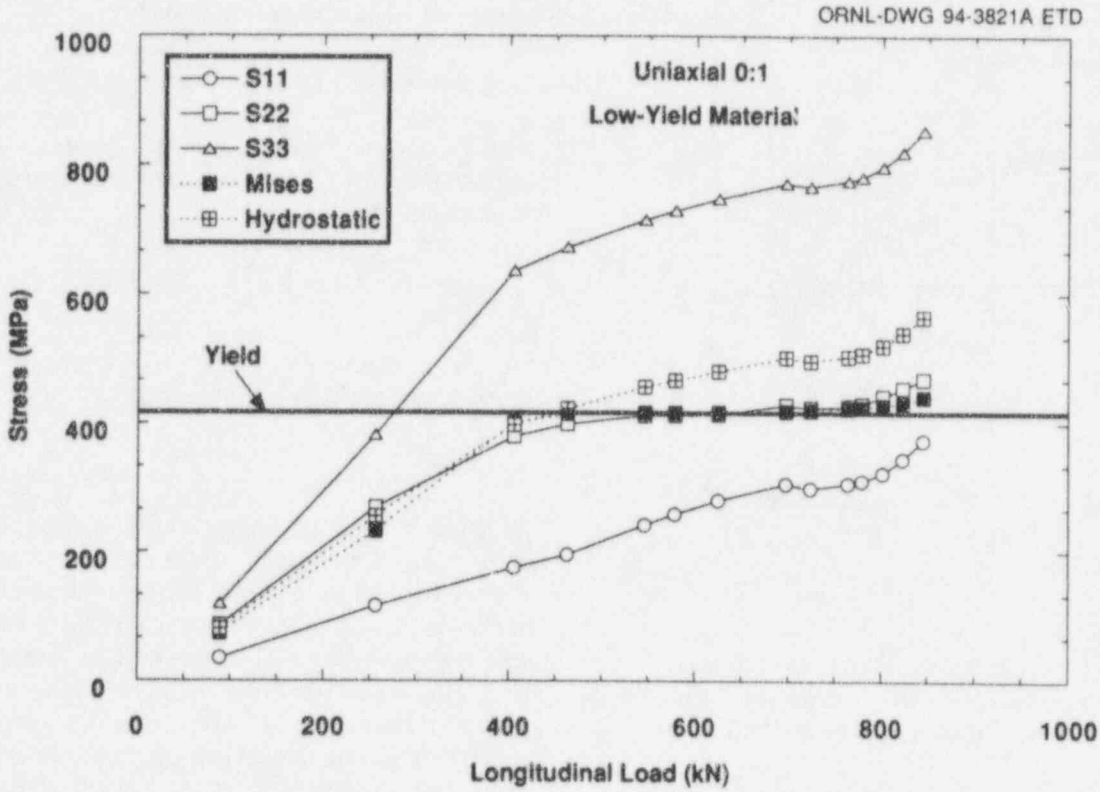

Figure 2.18 Stress components at material point (Node 5006 in FEA model) 2.54 mm (0.100 in.) ahead of crack tip for uniaxial (0:1) loading

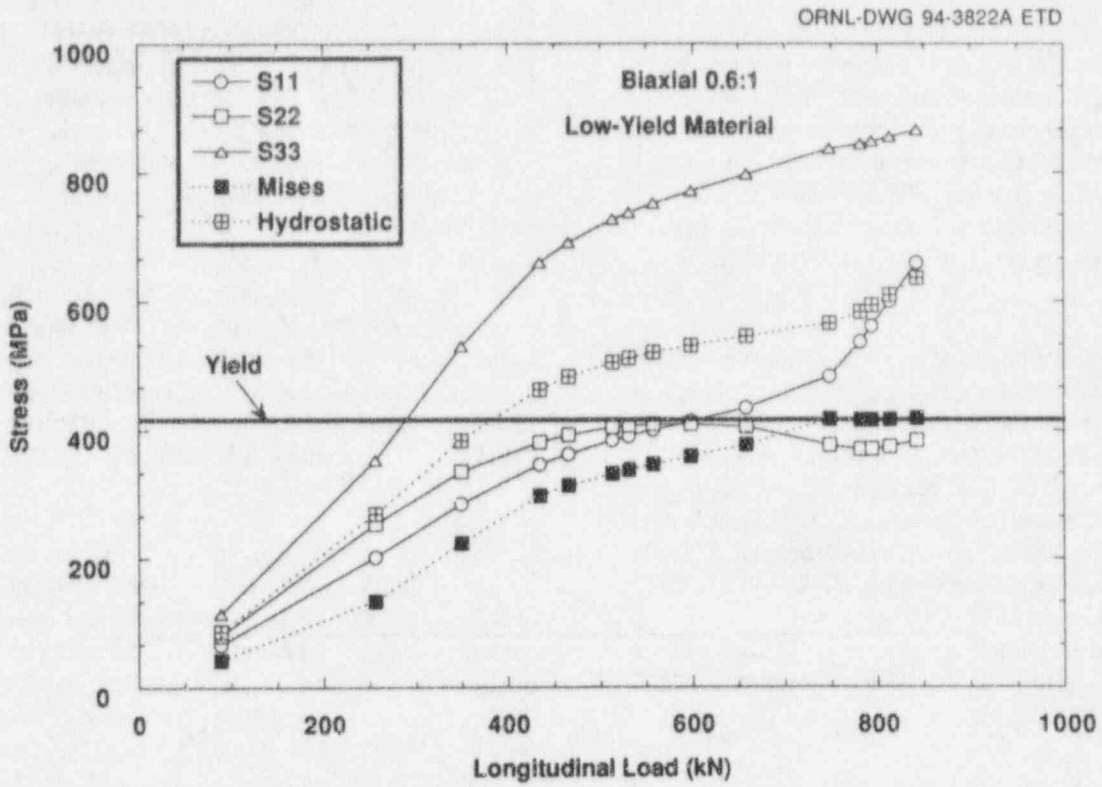

Figure 2.19 Stress components at material point (Node 5006 in FEA model) 2.54 mm (0.100 in.) ahead of crack tip for biaxial (0.6:1) loading

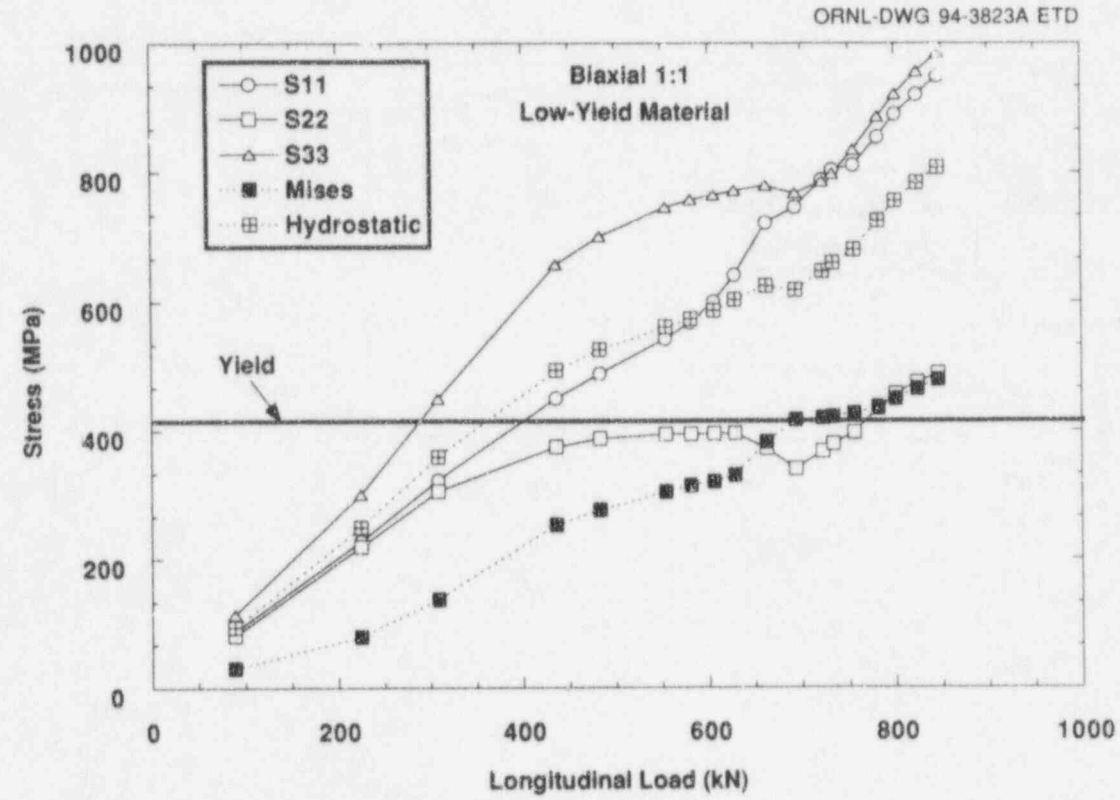

Figure 2.20 Stress components at material point (Node 5006 in FEA model) 2.54 mm (0.100 in.) ahead of crack tip for biaxial (1:1) loading

In Figs. 2.18–2.20, the Cartesian normal stress components (s_{11}, s_{22}, s_{33}) represent good approximations to the magnitude of the principal stress values (the shear stress components are small). Applications of increasing ratios for out-of-plane to in-plane loading are accompanied by substantial elevations of the hydrostatic stress and the out-of-plane normal stress (s_{11}). In contrast, the in-plane normal stress components (s_{22}, s_{33}) do not change a great deal as a function of load ratio, except at the highest load levels.

The behavior of the plastic zone width can be correlated with the applied biaxial loading ratio and resultant out-of-plane normal stress component (s_{11}). For the 0:1 (uniaxial) loading case (Fig. 2.18), the out-of-plane component is well below the two in-plane components, and the onset of yielding occurs at a relatively low applied load. When the out-of-plane load is increased to a 0.6:1 ratio (Fig. 2.19), the out-of-plane component roughly tracks the lower in-plane component up to 1034 MPa (150 ksi) and then begins to increase at a substantially higher rate. The effect of the 0.6:1 load ratio is to delay the onset of yielding to a much higher load than was observed in the 0:1 load case.

For the 1:1 load case (Fig. 2.20), the out-of-plane component (s_{11}) turns up and essentially tracks the opening-mode (maximum) stress component (s_{33}) beyond the 1034-MPa (150-ksi) load level. Also, the normal stress components (s_{22}, s_{33}) and the hydrostatic stress are observed to increase at a greater rate beyond 1034 MPa (150 ksi). (In this load range, observe that the hydrostatic and the out-of-plane stresses for the 1:1 load case are substantially elevated above those of the 0.6:1 case.) Near the 1034-MPa (150-ksi) load level, the plastic zone width progresses abruptly through N-5006, and the node exhibits significant strain hardening. An increase in differences between principal stress components is reflected in the increasing Mises effective stress. This indicates a distinct advantage of the cruciform specimen as compared to other, more conventional types of fracture specimens. That is, the cruciform specimen has the capability for independently controlling the out-of-plane stress component in the test section. Thus, the effects of biaxiality can be studied in detail.

Bases for the use of plastic zone width to correlate fracture toughness data have been presented in the literature.[5] ORNL development of a strain-based correlation is in the formative stages at this time. The effort has been focused on use of simple functions of plastic zone width ahead of the crack tip. A description of plastic zone development with increasing load and biaxial loading is performed using 3-D finite-element analyses (see Fig. 2.17). Preliminary use of the ORNL/HSST strain-based constraint model to predict the effect of biaxial loading on fracture toughness is shown in Fig. 2.21. The biaxial fracture toughness data are plotted as a function of the plastic zone width. For the data

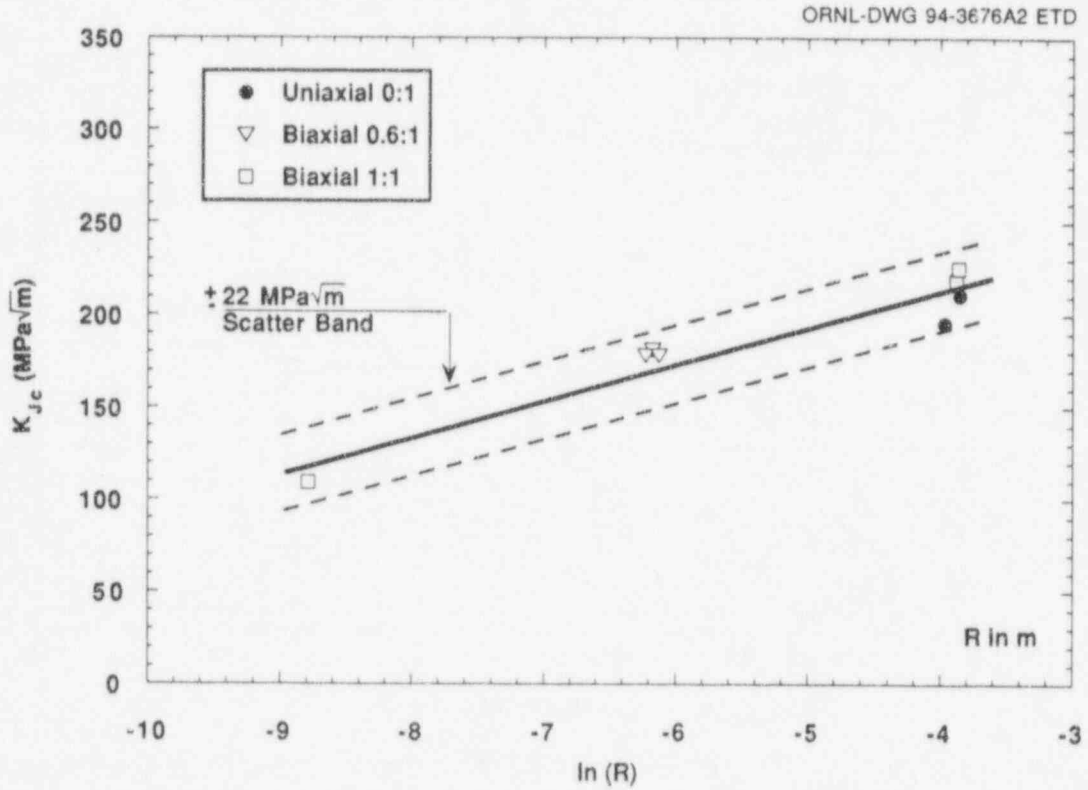

Figure 2.21 Shallow-flaw fracture toughness locus for cruciform tests

set size available, this turns out to be a straight line if ln(R) is used as the independent parameter, R being the plastic zone width. When statistical analyses are performed on the data, a scatter band width of ±22 MPa$\sqrt{m}$ (±20 ksi$\sqrt{in.}$) was determined. While, as noted, the data set being used is small (only 8 biaxial data points) and care must be employed in interpretation, the trend shown in Fig. 2.21 is compelling evidence for use of a plastic strain parameter at the crack tip as a second parameter in a dual-parameter constraint correlation.

Figure 2.22 shows K_J vs ln(R) loading trajectories superimposed on the fracture toughness results shown in Fig. 2.21. The range of fracture toughness values possible for each loading condition is defined by the intersection of the K_J vs ln(R) locus with the fracture toughness locus. As can be seen, the uniaxial (0:1) and biaxial (0.6:1) loading cases have unique intersection regions, and one would expect unique values of toughness for these cases. However, the biaxial (1:1) loading case has a distinct shape that causes the K_J vs ln(R) locus to intersect the toughness locus at two places. That is, there should be two distinct sets of toughness values for the biaxial (1:1) loading case. One set should agree with the results from the uniaxial tests, while the second should have a much lower toughness value. This is exactly the trend observed in the biaxial data set. While this is a preliminary interpretation of the effect of biaxial loading on toughness, the correlation appears very promising because it is consistent with the observed experimental results. Work is continuing to further develop and refine this strain-based model.

2.3 Test and Analysis of Unclad Finite-Length Flaw Cruciform Specimens

(W. J. McAfee, B. R. Bass, J. W. Bryson, and W. F. Jackson, Jr.)

The overall objective of these tests is to investigate the influence of finite-length flaw profiles, out-of-plane loading, and material condition on the effective fracture toughness of RPV plate material. The specific objectives for the subtask are to develop and qualify a viable test specimen, to develop appropriate fabrication procedures, to develop appropriate test procedures, and to generate a limited set of data to examine the influence of flaw geometry and biaxial loading on fracture toughness. An important consideration in the development of a test specimen and appropriate test procedures is establishing a specimen size that permits investigation of the desired range of test parameters yet does not exceed the test capacity of the biaxial fixture. The test results to date indicate that all these objectives have been attained.

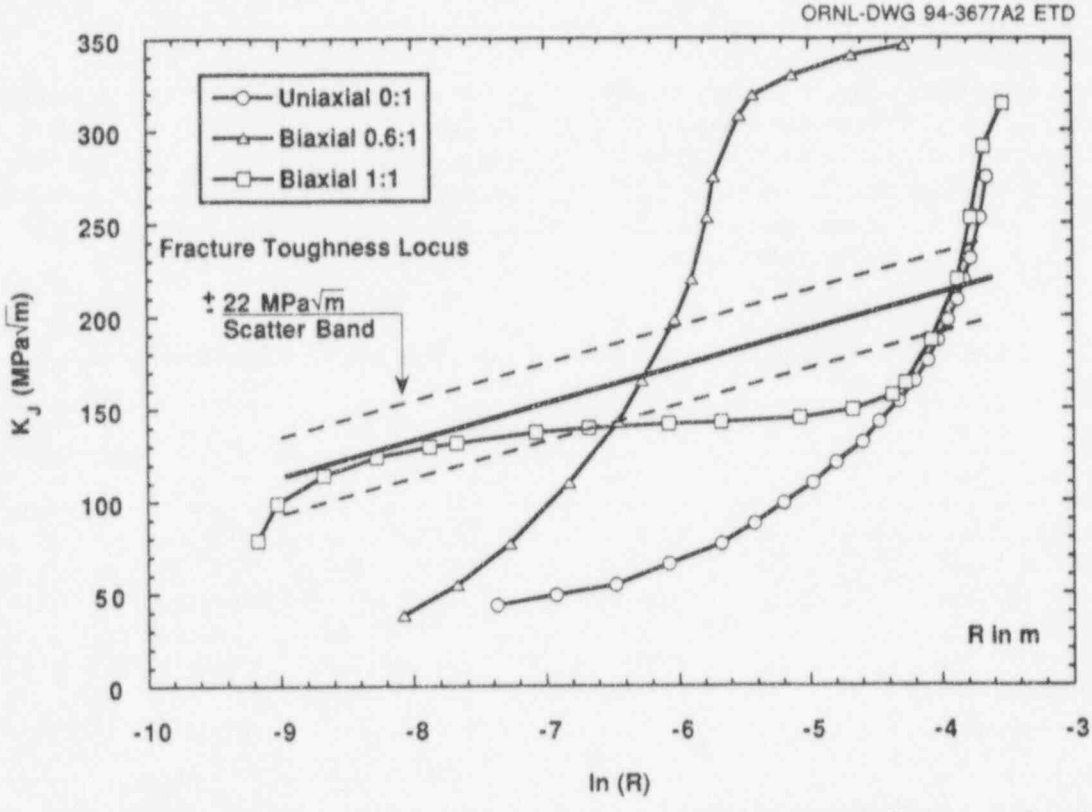

Figure 2.22 Comparison of fracture toughness locus for cruciform tests with K_J–ln(R) trajectories, showing possibility for both low- and high-toughness values for biaxial (1:1) loading

Constraint

The biaxial, finite-length flaw test specimen design has been described in detail in a previous HSST semiannual.[6] The initial flaw geometry selected was a 1.52-cm-deep by 3.81-cm-long (0.6-in. by 1.5-in.) semiellipse. This geometry was developed based on criteria that were established for the general specimen behavior and was to be treated as a reference flaw for future tests in this series. The through-surface finite-length flaw was ram-electrodischarge machined (EDM) into the top surface of the test section, while the overall test section plan form, including the LDCSs, was cut from the parent plate segment using the wire EDM process. The resulting flaw width at the specimen surface was ~0.5 mm (0.020 in.) at the widest point (center) tapering to a tip radius of ~0.08 mm (0.003 in.). These dimensions were determined by machining several development flaws that were then sectioned to measure the final flaw configuration.

Six specimens were fabricated for testing. As determined from the first two tests in this series, the flaw size was too small for the combination of material properties and test temperature. The remaining four specimens were then remachined to a semielliptic flaw 17.8 by 50.8 mm (0.7 by 2.0 in.). This flaw was fatigue precracked to both sharpen the tip and uniformly extend the depth ~1.25 mm (0.050 in.).

In support of establishing test conditions for these four finite-length flaw development specimens, eight drop-weight specimens were machined, and tests were performed to determine the drop-weight nil-ductility transition temperature (NDT) of plate 14 in the as-received condition. NDT was determined to be –20°C (–4°F). The specimens were oriented in the L-S orientation. ASTM E 208-91 states that NDT is independent of specimen orientation, but that orientation should be reported. Note that this temperature corresponds to a CVN impact energy of 26.7 J (20 ft-lb) as calculated from a nonlinear regression hyperbolic tangent fit to data obtained in the L-S orientation.

The finite-length flaw cruciform specimens test results are summarized in Table 2.3. Two of the specimens (CF-2 and CF-5) were tested under uniaxial (0:1) loading and two (CF-3 and CF-6) were tested under full biaxial (1:1) loading. The CMOD values measured for each specimen are shown in Figs. 2.23 through Fig. 2.26. As can be seen, the failure loads are very similar for each test. The CMOD for specimens CF-3 (0:1) and CF-5 (1:1) seem to form one set of values, while those for CF-2 (0:1) and CF-6 (1:1) form another. This could be caused by a difference in the crack depth for each specimen. The fracture surfaces for specimens CF-3 and CF-5 have been removed and examined to make a preliminary determination of the failure initiation location. Specimen CF-3 failed at a point ~30° below the surface (angular measurement from surface with coordinate system located geometric center of semielliptical flaw), which is in the region where finite-element analyses would predict the maximum stress-intensity factor for biaxial (1:1) loading. Specimen CF-5 failed at the deepest point (90° below the surface), which is the point where finite-element analyses would predict the maximum stress intensity factor for 0:1 uniaxial (0:1) loading. Thus, the failure locations are consistent with the predicted flaw behavior. The fracture surfaces for specimens CF-2 and CF-6 have not been removed as yet.

To determine the appropriate fracture toughness values associated with each test, detailed finite-element analyses will be performed using actual flaw depths based on measurements of the fracture surface. These analyses are being set up, and data reduction for these tests should be completed during the next reporting period.

Table 2.3 Summary of test parameters for finite-length flaw cruciform specimens

Specimen	CF-3	CF-5	CF-2	CF-6
Load ratio	1:1	0:1	0:1	1:1
Failure temperature, °C (°F)	–58 (–72)	–58 (–73)	–57 (–70)	–57 (–71)
Maximum load, kN (kips)	1932 (434.4)	983 (220.9)	941 (211.6)	1952 (438.9)
Longitudinal load, kN (kips)	966 (217.1)	982 (220.9)	941 (211.6)	975 (219.3)
Centerline CMOD, mm (in.)	0.503 (0.0198)	0.554 (0.0218)	0.333 (0.0131)	0.386 (0.0152)
LLD (longitudinal), mm (in.)	3.752 (0.1477)	4.488 (0.1767)	3.320 (0.1307)	3.741 (0.1473)
LLD (transverse), mm (in.)	2.908 (0.1145)	NA[a]	NA[a]	3.051 (0.1201)
Failure location (measured from free surface)	30°	90°	TBD[b]	TBD[b]

[a] Not applicable—uniaxial loading.
[b] Specimens have not been cut apart for fracture surface examination.

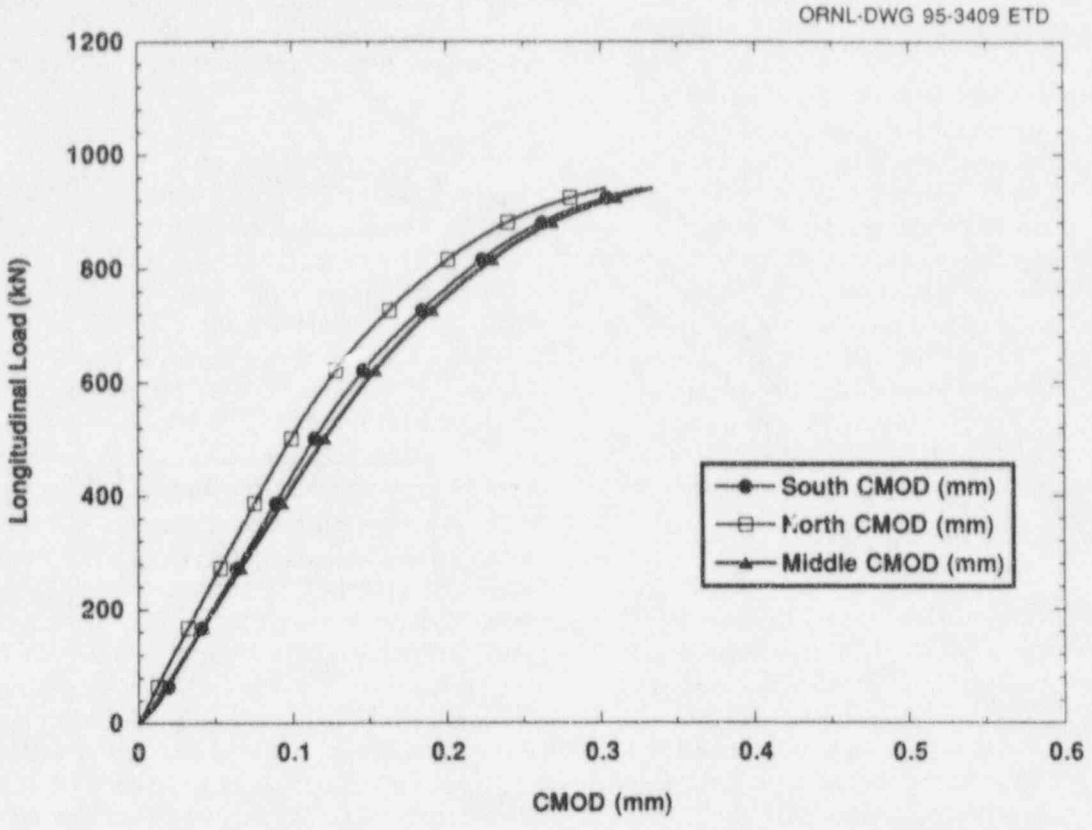

Figure 2.23 CMOD measured for failure test of finite-length flaw cruciform specimen CF-5: load ratio = 0:1

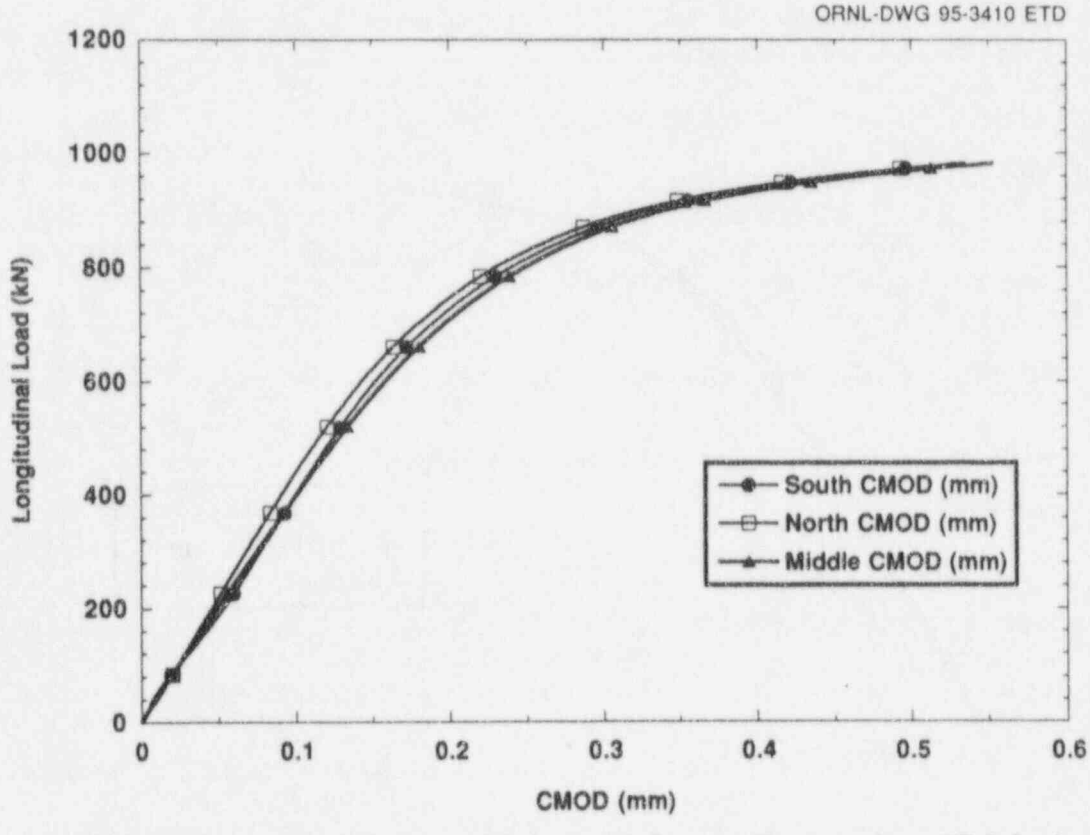

Figure 2.24 CMOD measured for failure test of finite-length flaw cruciform specimen CF-2: load ratio = 1:1

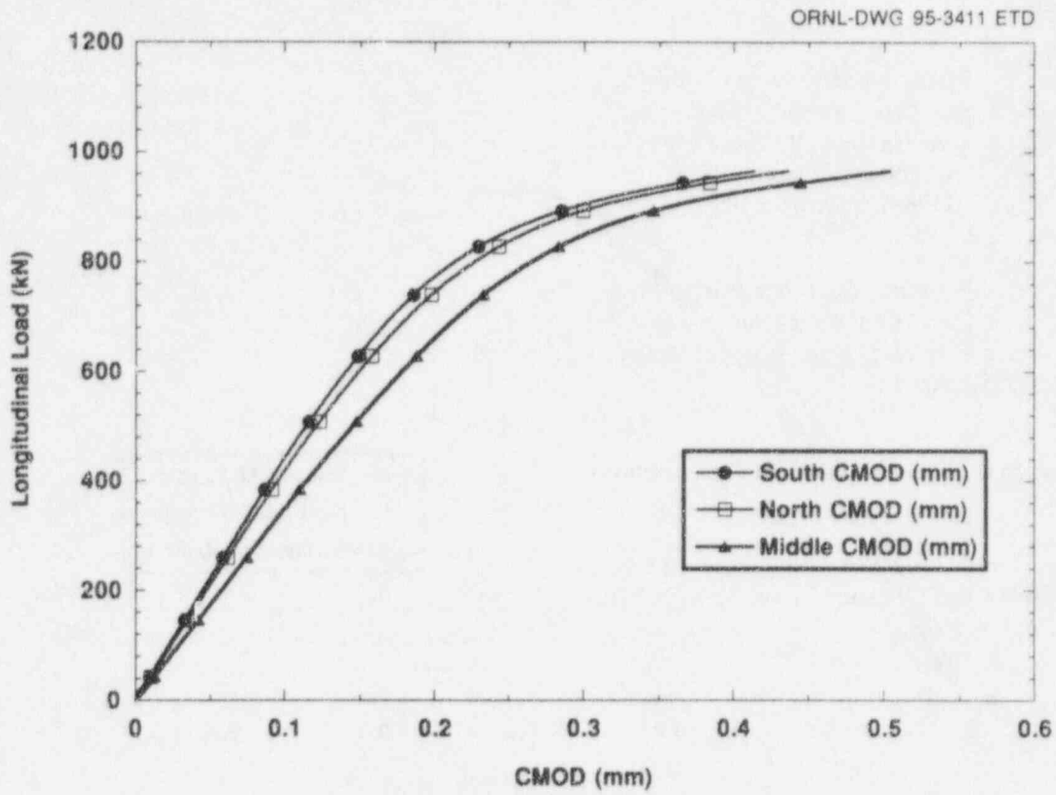

Figure 2.25 CMOD measured for failure test of finite-length flaw cruciform specimen CF-3: load ratio = 0:1

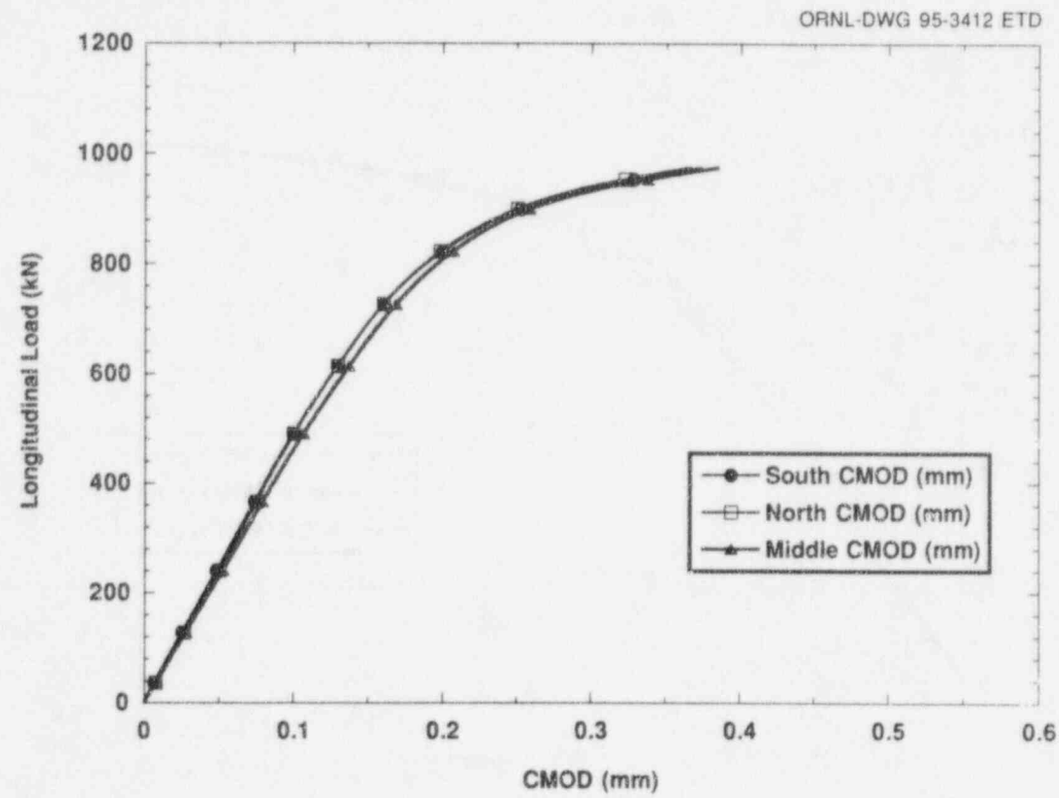

Figure 2.26 CMOD measured for failure test of finite-length flaw cruciform specimen CF-6: load ratio = 1:1

References

1. D. J. Naus et al., Martin Marietta Energy Systems, Inc., Oak Ridge Natl. Lab., "SEN Wide-Plate Crack-Arrest Tests Using A 533 Grade B Class 1 Material: WP-CE Test Series," USNRC Report NUREG/CR-5408 (ORNL/TM-11269), November 1989.*

2. D. J. Ayres et al., Electric Power Research Institute, "Appendix G, Material Characterization," in *Tests and Analyses of Crack-Arrest in Reactor Vessel Materials*, EPRI NP-5125SP, April 1987.

3. J. M. Steichen and J. A. Williams, Hanford Engineering Development Laboratory, "Heavy Section Steel Technology Program Technical Report No. 32, High Strain Rate Tensile Properties of Irradiated ASTM A533 Grade B Class I Pressure Vessel Steel," HEDL-TME-73-74, July 1973.

4. B. R. Bass et al., Martin Marietta Energy Systems, Inc., Oak Ridge Natl. Lab., "Biaxial Loading and Shallow-Flaw Effects on Crack-Tip Constraint and Fracture Toughness," USNRC Report NUREG/CR-6132 (ORNL/TM-12498), January 1994.*

5. V. Weiss, "Material Ductility and Fracture Toughness of Metals," *Proceedings of the International Conference on Mechanical Behavior of Materials, Hyoto, Japan, August 15–20, 1971*, The Society of Materials Science, Japan, 1971.

6. W. E. Pennell et al., Martin Marietta Energy Systems, Inc., Oak Ridge Nat. Lab., "Heavy-Section Steel Technology Semiannual Progress Report for April 1993–October 1993," USNRC Report NUREG/CR-4219 (ORNL/TM-9593, V10&N2), May 1995.*

*Available from National Technical Information Service, Springfield, VA 22161.

3 Evaluation of Cladding Effects

B. R. Bass

3.1 Introduction

During this reporting period, work continued on developing a quantitative description of the effects of cladding on the fracture behavior of shallow surface cracks in RPVs and a methodology for including cladding effects in current RPV integrity assessment procedures.

3.2 Fracture Analysis of Full-Thickness Clad Beam Specimens (J. A. Keeney and B. R. Bass)

3.2.1 Introduction

Maximum tensile thermal stresses induced in an RPV by a PTS transient event occur near the inner surface of the vessel. Maximum irradiation-induced embrittlement also occurs in material adjacent to the inner surface of the RPV. Flaws located in this region of the RPV are, therefore, particularly susceptible to crack initiation during a PTS transient. Evaluations of RPV integrity under PTS loading are based on the Marshall flaw distribution,[1] NRC Regulatory Guide 1.154,[2] and data from deep-crack fracture toughness specimens. The Marshall flaw distribution predicts more small than large flaws, while NRC Regulatory Guide 1.154 requires that all flaws be considered as surface flaws. Probabilistic fracture-mechanics (PFM) analyses of RPVs indicate that a high percentage of the cracks that initiate in cleavage will initiate from shallow flaws.[3] Because the postulated existence of shallow flaws has a dominant influence on the results of PFM analyses and, ultimately, the conditional probability of vessel failure in a PTS evaluation, the shallow surface crack is of major importance in RPV structural integrity assessments.

The HSST shallow-crack fracture toughness testing program[4] has provided data from shallow-crack specimens (cut from homogeneous plate material) that exhibit a fracture toughness significantly higher than that obtained from conventional deep-crack specimens tested in the transition temperature region. The shallow-crack program has tested A 533 Grade B (A 533 B) Class 1 steel, single-edge notch bend (SENB) specimens with an approximate 100-mm beam depth and beam thicknesses of 51, 102, and 152 mm. The shallow-crack data exhibit an elevation in mean fracture toughness and an increase in data scatter relative to the deep-crack toughness data in the transition temperature region. Shallow cracks experience a loss of constraint in the transition region because of the interaction of the crack-tip plastic zone with the free surface of the test specimen.

In addition to the shallow-crack effect, other differences in material conditions exist between conventional deep-crack laboratory specimens and RPVs that could significantly affect fracture toughness. First, shallow cracks in an RPV are located in the near-surface region of the vessel plate or weld material where metallurgical gradients or inhomogeneities exist as a result of application of the stainless steel cladding. Irwin and Zhang[5] performed material gradient studies on a large weld section joining two forged A 508 shells from a stainless-steel-clad RPV. They found hardness elevations in the region of A 508 material near the clad/base interface, an area of the vessel that was affected by the reheat cycle of the cladding process. Irwin and Zhang indicate that these hardness elevations probably translate into a reduction of cleavage initiation toughness. Second, fracture toughness curves used in RPV assessments are based on data from deep-crack L-T oriented fracture toughness specimens taken from the 1/4-thickness, homogeneous region of source plates. Axial cracks in plate material of an RPV are oriented in the L-S material direction rather than the L-T orientation. Third, reheating due to multiple passes in the welding process leads to inhomogeneities of microstructure and hardness within the weld metal.[5] Finally, any residual stresses that remain after the usual postweld stress relief heat-treatment cycle could affect fracture behavior.

The HSST Program is investigating effects of these conditions on fracture toughness through testing of full-thickness clad beam specimens taken from the RPV of a canceled nuclear plant. The specimens are fabricated at ORNL and tested at the National Institute of Standards and Technology (NIST), Gaithersburg, Maryland. Fracture toughness data are generated from three-point arc-bend specimens (229- by 226-mm cross section and ~1300-mm chord length) fabricated from full-thickness RPV clad, weld, and plate material. A summary of the HSST full-thickness clad beam testing program, material characterization, and testing procedures was given in a previous report.[6]

Cracks in the initial series of three beams (CB-1.1, -1.2, and -1.3) were located in weld material. Analyses of the test data from specimens CB-1.1, -1.2, and -1.3 are described herein, including comparisons of test data with finite-element analysis results and applications of

toughness estimation techniques. Applications of the stress-based constraint characterizations developed by O'Dowd and Shih[7–9] and by Dodds and Anderson[10–12] to the clad beam data are also included. Finally, a summary and some preliminary conclusions, together with a review of future plans for the clad beam testing program, are given.

3.2.2 Details of Test Specimen

The full-thickness clad beam specimens were fabricated from the SNUPPS shell segment that was available from a canceled PWR plant (the plant was canceled during construction, and the vessel was never in service). The RPV material is A 533 B with a stainless-steel-clad overlay on the inner surface. The shell segment includes two circumferential welds and one longitudinal weld. The welds are submerged-arc welds with A 533 B Class 1 filler metal. The plate material, clad overlay, and weldment are completely prototypic of a production-quality RPV. The shell has a nominal inner radius of 2210 mm and a thickness of 232 mm.

Because the initial series of three specimens was intended to investigate the fracture behavior of the longitudinal weld material, the test beams were cut in the circumferential direction of the shell. A longitudinal master blank with a length sufficient to fabricate three test beams was first flame-cut from the shell. The three required blanks were then saw-cut from the master blank and machined to final dimensions incorporating handling, load contact, and flaw details. A sketch of the specimen geometry is shown in Fig. 3.1.

The specimen was designed to be tested in three-point bending with a load span (S) of 1219.2 mm. Flat, parallel load contact points were machined on the top and bottom surfaces of the beam (see Fig. 3.1) to remove surface irregularities and to ensure uniform load application across the width of the beam. The flaw was machined in the beam using the wire EDM process and extended from the shell inner surface, that is, the clad surface, to predetermined depths into the beam. The final dimensions for each clad beam specimen are shown in Table 3.1. Note that the flaw in each beam was machined to a different depth. One deep-flaw specimen (CB-1.1) and two shallow-flaw specimens (CB-1.2 and -1.3) were produced. The crack depth (a) listed for each beam is the final depth after fatigue precracking.

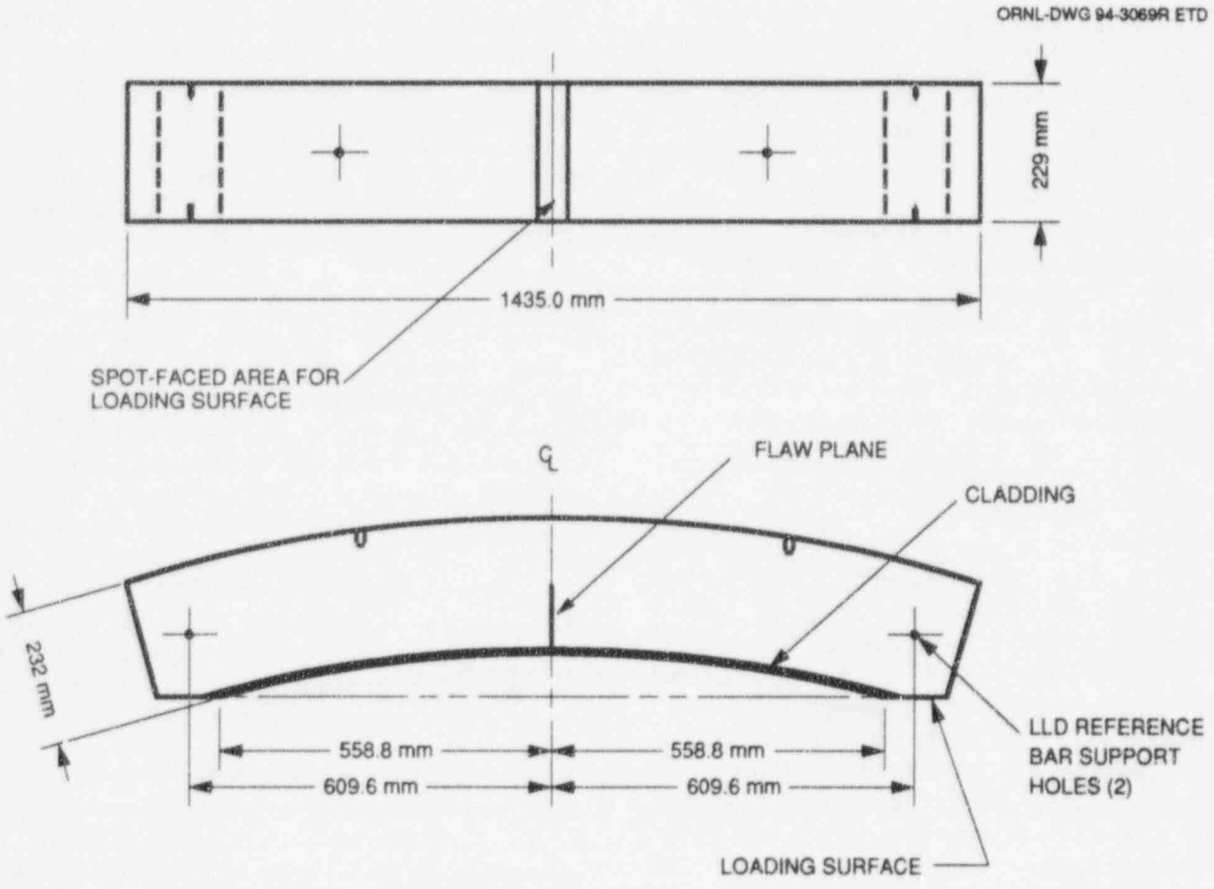

Figure 3.1 Sketch of full-thickness clad beam specimen

Table 3.1 Parameters defining specimen geometry of full-thickness clad beam specimens

	CB-1.1[a]	CB-1.2	CB-1.3
Load span (S), mm	1219.2	1219.2	1219.2
Thickness (B), mm	230.2	230.2	229.6
Width (W), mm	225.7	224.3	224.3
Crack depth (a), mm	117.5	10.8	23.7
Ratio (a/W)	0.50	0.05	0.10

[a]Used as development beam.

The shell contained both axial and circumferential welds, and in the course of cutting the beam blanks, the upper circumferential weld was made available for the characterizations. Tests using the Automated Ball Indentation (ABI) technique indicate that the tensile properties of the axial and circumferential weld are similar. The characterization of the circumferential weld included CVN tests, reference nil-ductility temperature (RT_{NDT}) determinations,[13] and tensile tests. The impact and tensile data were used to develop a consistent set of material properties needed for the clad beam test data evaluation and the finite-element analyses. These properties are listed in Table 3.2. The ABI technique was used to determine the yield stress for the base and clad material. The tabulated yield stress for the weld material is 36% higher than the yield stress for the base material. The weld material exhibits a significant overmatch in yield stress as compared to the yield stress for the base material.

Table 3.2 Material properties at test temperature of –25°C

	Base metal	Weld metal	Cladding
Modulus of elasticity (E), MPa	200,000	200,000	152,000[a]
Poisson's ratio (ν)	0.3	0.3	0.3
Yield stress (σ_0), MPa	440[b]	599[c]	367[b]
Ultimate stress (σ_u), MPa	660[d]	704[e]	659
RT_{NDT}, °C		–23	
NDT, °C		–50	

[a]Measured E value from Ref. 13.
[b]σ_0 measured by ABI technique.
[c]Evaluated from $\sigma_0 = 390 + 51{,}650/(T + 273)$, where T is the material temperature.
[d]σ_u measured by Rockwell B indentation technique.
[e]Evaluated from $\sigma_u = 488 + 52{,}830/(T + 273)$.

The full-thickness clad beam tests were performed at NIST using the 53.4-MN servo-hydraulic test machine with a three-point bend fixture. This fixture was designed for a load capacity of at least 15 MN, which was calculated to be in excess of that required for these tests. Special large-range crack-opening-displacement gages and associated electronics were obtained specifically for these tests. Because the tests were performed at a low temperature, an environmental chamber was fabricated to completely enclose the test article and load-contact points to facilitate control of both time- and spatial-dependent specimen temperature variations.

Cooling was achieved by a spray of liquid nitrogen (LN_2) onto the beam surface. A procedure was developed whereby the desired test temperature would be negatively exceeded by ~5°C, the LN_2 spray would be stopped, and the beam would be allowed to thermally equilibrate and warm to the test temperature. This was acceptable because the rate of change in temperature was much less than the time interval required to perform the fracture tests.

The load P vs displacement curves for each of the three beams (CD-1.1, -1.2, and -1.3) are shown in Fig. 3.2(*a*) for LLD and in Fig. 3.2(*b*) for CMOD, respectively. These curves depict the inelastic behavior in the shallow-crack specimens as fracture conditions are approached. The conditions of each specimen at failure are listed in Table 3.3 The plastic component of the area under each P vs displacements curve (defined as U_{pl} for LLD and A_{pl} for CMOD) and the corresponding η-factors, η_{pl}^{ℓ} and η_{pl}^{c}, are also included in Table 3.3. Toughness data for the clad beam specimens were calculated using the techniques described in Ref. 14. The P vs CMOD method,[15] considered the more accurate of the techniques examined for determining fracture toughness of shallow-crack specimens, is the primary method used for the clad beam analyses. The critical J-integral values were converted to critical elastic-plastic, stress-intensity factors (K_{Jc}), using the plane-strain formulation. The toughness values determined for the tests, along with the parameters used to estimate the toughness, are included in Table 3.3.

3.2.3 Clad Beam Posttest Analyses

3.2.3.1 Finite-Element Analysis

The 2-D analyses were performed on the clad beam specimen depicted in Fig. 3.1 using the ABAQUS finite-element program.[16] The plane-strain analyses were carried out using an incremental elastic-plastic constitutive model and small-strain theory. Local crack-tip fields obtained from these analyses are used in the application of stress-based constraint characterization models. A one-half section of the complete clad beam specimen illustrated in Fig. 3.1 is represented in the 2-D finite-element model of Fig. 3.3.

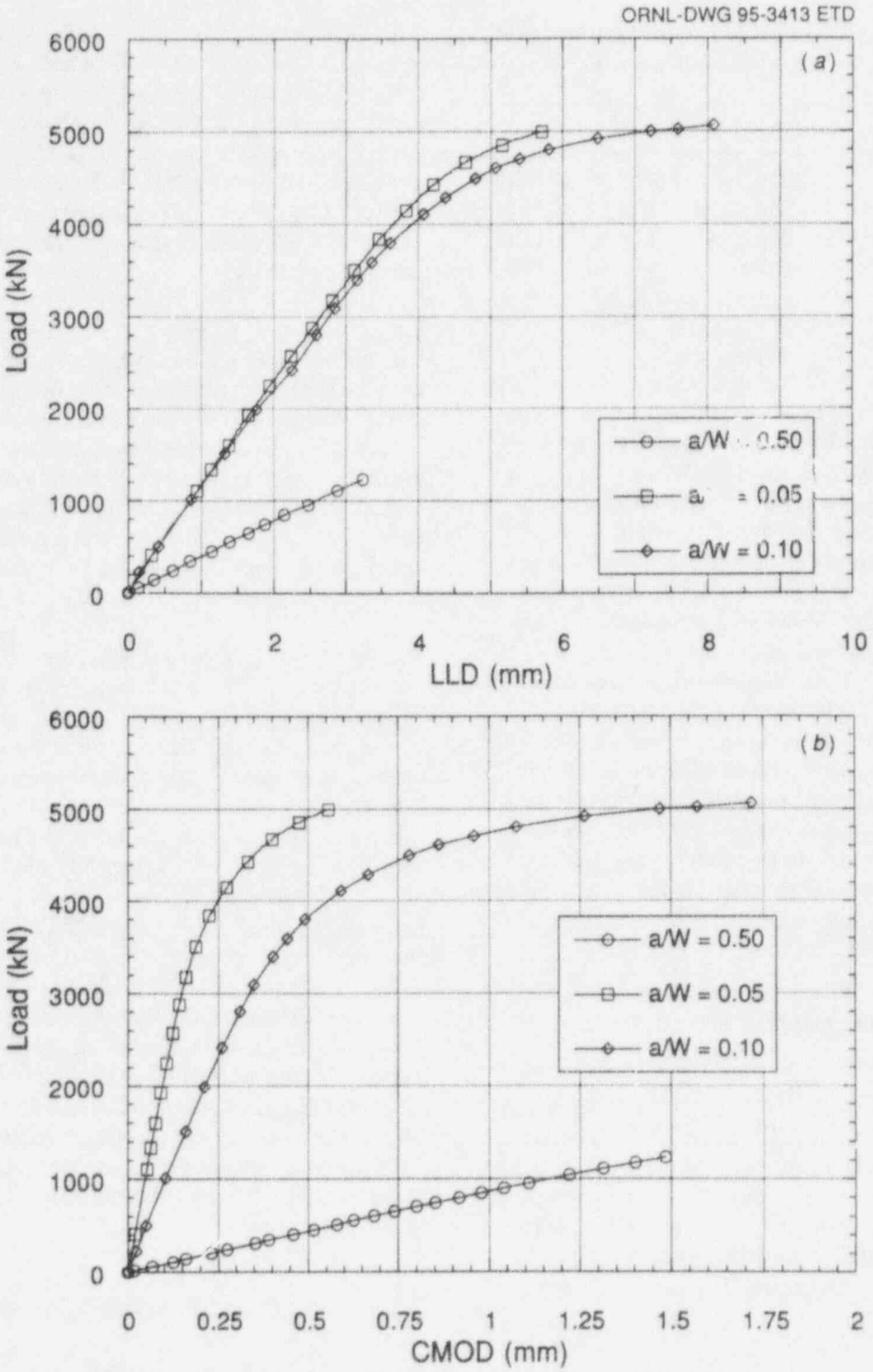

Figure 3.2 Load vs displacement response for clad beam specimens: (*a*) LLD and (*b*) CMOD

The model of the clad beam specimen with a/W = 0.05 in Fig. 3.3 incorporates the curvature of the plate and the flat cut-out where the specimen is supported during loading. The model has a highly refined mesh in the crack-tip region [Fig. 3.3(*c*)] to provide resolution of stress fields over the normalized distance $2 \le r\sigma_0/J \le 10$ in front of the crack; r is the distance from the crack tip, and σ_0 is the yield stress. The outermost semicircular ring of nodes in the mesh, shown in Fig. 3.3(*c*), has a radius of 3.6 mm. The model consists of 3712 nodes and 1155 eight-node isoparametric elements. Collapsed-prism elements arranged in a focused fan configuration at the crack tip are used to produce a 1/r strain singularity appropriate for inelastic analysis. Reduced integration was used for all the elements except for the inner ring of elements at the crack tip in the shallow-crack models. The use of full integration for the

Table 3.3 Summary of results from the full-thickness clad beam testing program

	CB-1.1	CB-1.2	CB-1.3
a/W	0.50	0.05	0.10
Temperature, °C	−25.5 ± 1.0	−25.0 ± 1.0	−25.0 ± 1.0
Stroke rate, mm/min	2.49	8.38	6.89
Time to failure, s	230	366	440
Failure conditions			
P, kN	1232.5	5002.3	5060
LLD, mm	3.236	5.767	8.083
CMOD, mm	1.485	0.567	1.718
U_{pl}, kN-mm	135	6,427	16,879
A_{pl}, kN-mm	88	1,473	5,486
η-factors			
η^{ℓ}_{pl}	1.37	0.79	1.05
η^{c}_{pl}	2.26	4.16	4.08
Fracture toughness			
Elastic component			
J_{el}, kN/m	131.3	110.6	230.5
K_I, MPa$\sqrt{m}$	173.0	154.5	223.1
P vs CMOD			
J_{pl}, kN/m	8.1	124.7	486.0
Total J, kN/m	139.4	235.3	716.5
K_{Jc}, MPa$\sqrt{m}$	173.5	225.4	393.3
P vs LLD			
J_{pl}, kN/m	7.4	103.8	384.8
Total J, kN/m	138.7	214.4	615.3
K_{Jc}, MPa$\sqrt{m}$	173.1	215.2	364.5

innermost ring helps in the convergence of the model at high loads.

Material properties used for both pretest and posttest analyses of the clad beam specimens were taken from Table 3.2 and from the multilinear true stress vs true plastic-strain curves given in Fig. 3.4. For the posttest analyses, Young's modulus (E) and σ_0 for the weld metal were reduced from the pretest values by ~2 and 10%, respectively, to produce better agreement with P vs CMOD data from the tests. The hardening portion of the stress-strain curve was kept consistent with the pretest estimation of material hardening. The technique of lowering E and σ_0 to achieve better agreement with the measured P vs CMOD data has been used in previous analytical studies of bend specimens.[4] This technique was used because the 2-D plane-strain model is too stiff for an exact comparison between measured and calculated P vs CMOD. Analytical evaluations of an uncracked, 2-D, plane-strain model, using an elastic-perfectly plastic material model, have shown that the limit load is overestimated by ~12% due to the plane-strain effect. The overestimation of the plane-strain effect can be compensated for by lowering the yield stress. The effective modulus (E_m) was calculated for each clad beam specimen based on American Society for Testing and Materials (ASTM) Test Method for J_{Ic}, A Measure for Fracture Toughness (E 813), which accounts for various uncertainties in testing. Should E_m deviate from E by more than 10%, then the test is not considered valid. The percent deviations for CB-1.1, -1.2, and -1.3 were 4.7, 2.8, and 0.5%, respectively.

Results from the posttest analyses of tests CB-1.1, -1.2, and -1.3 are summarized in Fig. 3.5(*a*) and (*b*). Comparison of the measured and calculated P vs displacement responses provides a way to interpret the accuracy of the analysis results and to establish confidence in the calculated fracture-mechanics parameters. The calculated P vs LLD curves are compared with measured data for each test in Fig. 3.5(*a*). For the shallow-crack specimens, calculated LLD values at a given load were greater than measured values for the full range of loading. In contrast, comparisons of calculated and measured P vs CMOD in Fig. 3.5(*b*) show good agreement. The difficulties in analytically modeling the measured responses of P vs LLD *and* P vs CMOD simultaneously have been described in Refs. 4, 14, and 15.

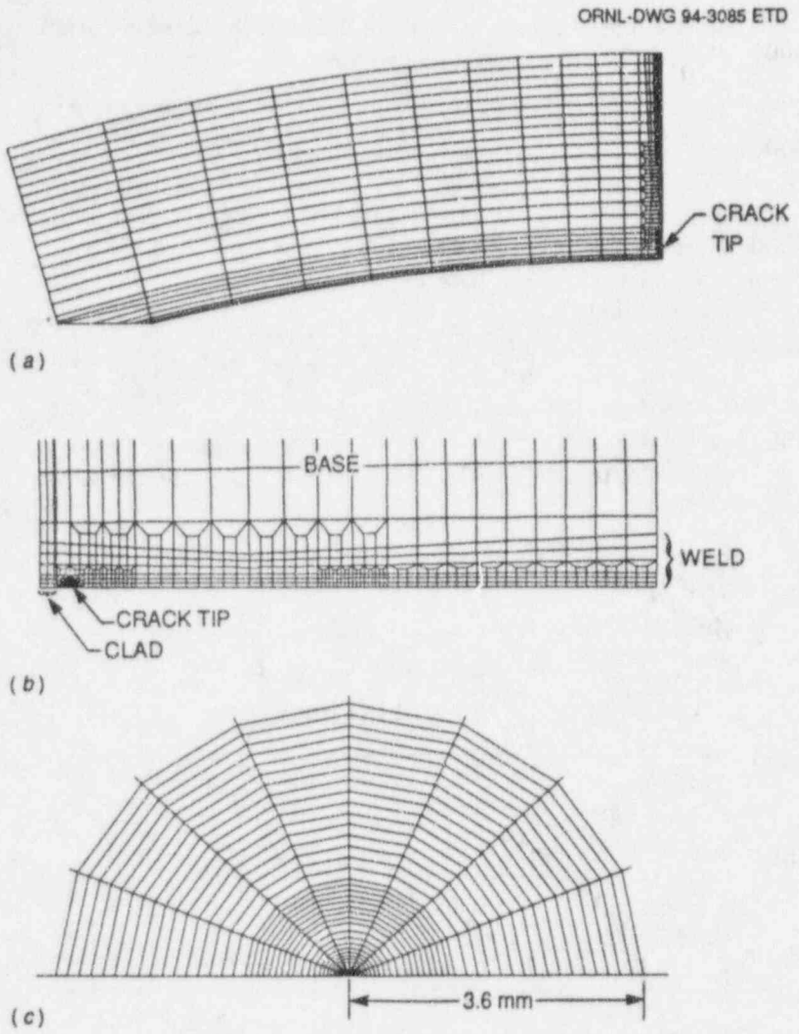

Figure 3.3 (*a*) Finite-element mesh of clad beam specimen with a/W = 0.05, (*b*) crack-plane region, and (*c*) crack-tip region

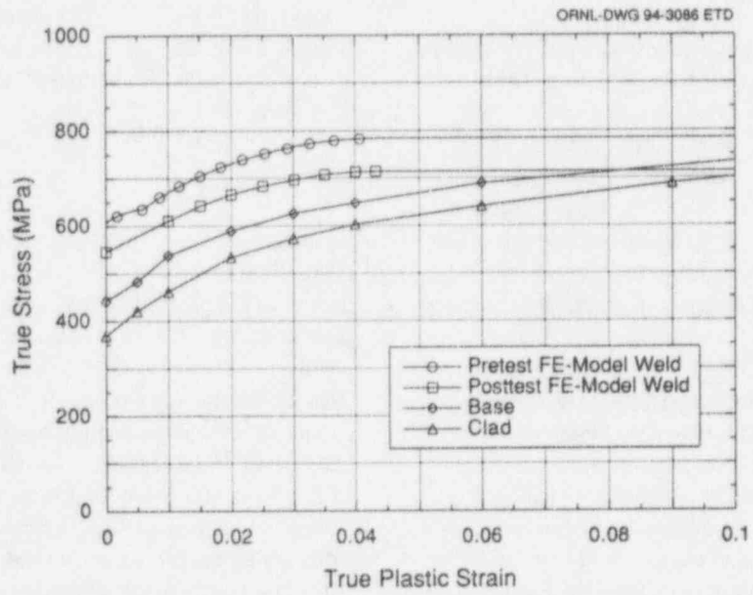

Figure 3.4 Material representation for clad beam at T = –25°C

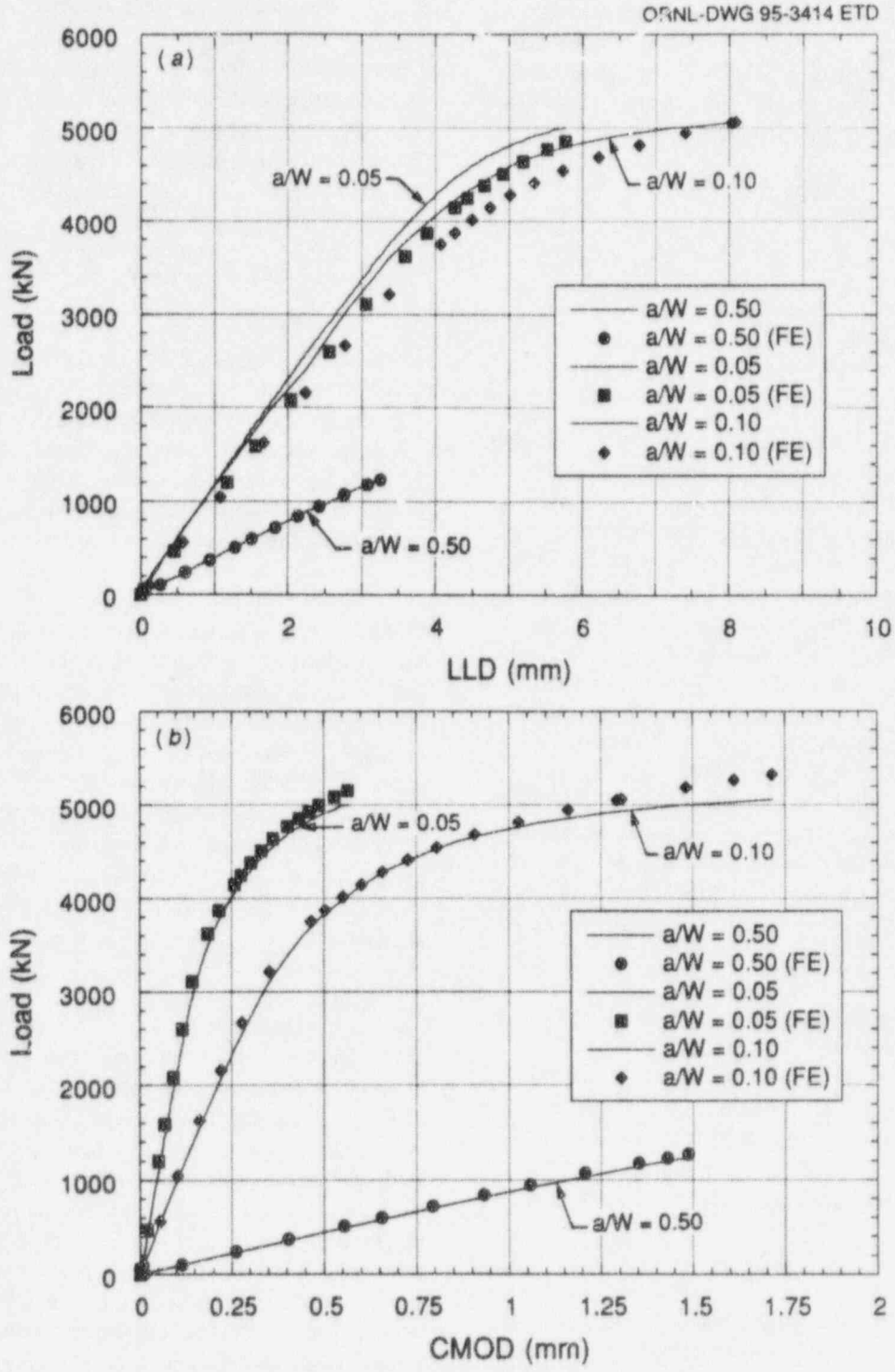

Figure 3.5 Comparison of calculated and measured displacements for clad beam specimens: (*a*) LLD and (*b*) CMOD

For the analyses presented herein, emphasis was placed on modeling the P vs CMOD response accurately for use in determining fracture toughness.

3.2.3.2 Toughness Estimation Techniques

For the clad beam tests, fracture toughness is estimated in terms of the critical J-integral and then converted into an elastic-plastic stress-intensity factor, K_{Jc}. The two techniques[4,14,15] used to determine the critical J are based on the "work" at the crack tip as measured by the area under the load–displacement (LLD or CMOD) curves. The methods require an η-factor, which relates work at the crack tip to the plastic portion of the crack-driving force. The η-factor is not affected by the value of σ_0 because the η-factor is evaluated from the ratio of J to the area under

the load-displacement curve and both parameters are equally affected by σ_0. The first method of estimating J is similar to the technique used in ASTM E 813 because the P vs LLD test record is used as input for the toughness estimate. The J-integral is divided into elastic and plastic terms given by

$$J = J_{el} + J_{pl} \quad , \tag{3.1}$$

where

$$J_{pl} = \left(\eta_{pl}^{\ell} U_{pl}\right) + Bb \quad , \tag{3.2}$$

and U_{pl} is the plastic component of the area under the P vs LLD curve, B is specimen thickness, b is the remaining ligament (W-a), and η_{pl}^{ℓ} is the dimensionless constant relating the area term (U_{pl}) to J_{pl}. Finite-element analysis provides values of η_{pl}^{ℓ} as a function of U_{pl} for each loading and specimen configuration. Analysis is also required to determine the relationship between J_{el} and P. The variations of η_{pl}^{ℓ} as a function of U_{pl} for tests CB-1.1, -1.2, and -1.3 are shown in Fig. 3.6(*a*–*c*). The U_{pl} value from the measured P vs LLD curve and the corresponding value of η_{pl}^{ℓ} for each test at cleavage initiation are included in Table 3.3. The value of η_{pl}^{ℓ} is expected to be ~2.0 for deep-crack bend specimens at initiation (ASTM E 813) but was determined to be 1.37 from the finite-element calculations. The low η_{pl}^{ℓ} value at initiation may be the result of overestimating the measured LLD, which would lead to a larger value of U_{pl} and ultimately a smaller value for η_{pl}^{ℓ}.

The second technique for determining the critical J-integral, first proposed by Kirk and Dodds,[17] uses the plastic component of the area under the P vs CMOD curve (A_{pl}) to calculate J_{pl}. Finite-element analyses provided the variations of η_{pl}^{c} as a function of A_{pl}, shown in Fig. 3.7(*a*)–(*c*) for tests CB-1.1, -1.2, and -1.3, respectively. The values of A_{pl} (from the measured P vs CMOD data) and η_{pl}^{c} for each test at initiation are listed in Table 3.3.

The values of J calculated from the two η-factor techniques are compared to J determined from finite-element analyses for the three specimens in Fig. 3.8(*a*)–(*c*). In Fig. 3.8(*a*), the P vs J curve for CB-1.1 from the finite-element analysis is above the curves generated from toughness estimation techniques. This may be related to the variation of η_{pl} with increasing plastic area for the CB-1.1 specimen, while a constant value of η_{pl} is used in the estimation techniques. The shallow-crack specimens did not have as large a variation in η_{pl} (or become asymptotic) and showed good agreement among the three methods of calculating J.

3.2.3.3 Constraint Analyses

One of the methods previously used to assess the effects of shallow-crack depths and biaxial loading on crack-tip stress triaxiality is the J-Q methodology.[4,14,15] The definition of Q employed here is given by O'Dowd and Shih[8] in the form

$$Q(\bar{r}) = \frac{\sigma_{\theta\theta}(\bar{r}) - [\sigma_{\theta\theta}(\bar{r})]_{SSY}}{\sigma_0} \quad , \tag{3.3}$$

where $\bar{r} = r/(J/\sigma_0)$ is a normalized distance measured in the crack plane ahead of the crack tip ($\theta = 0$), and the r, θ polar coordinate system is centered at the crack tip such that $\theta = 0$ corresponds to the crack plane ahead of the tip. In Eq. (3.3), Q measures the departure of the opening-mode stress $\sigma_{\theta\theta}$ from the reference plane-strain small-scale yielding (SSY) solution, normalized by σ_0.

Using a modified boundary layer formulation, O'Dowd and Shih[9] showed that Q characterizes the magnitude of a spatially uniform (approximately) hydrostatic stress state in a forward sector ($|\theta| \le \pi/2$ and $1 \le \bar{r} \le 5$) of the crack-tip region. The coefficient Q, although found to be independent of $\bar{r}$, was formally defined at $\bar{r} = 2$, which falls just outside the finite strain blunting zone. For conditions ahead of the crack that do not conform to a spatially uniform hydrostatic stress field, O'Dowd and Shih[8] introduced Eq. (3.3) to emphasize the explicit dependence of Q upon distance $\bar{r}$.

The J-Q methodology was used to assess crack-tip stress triaxiality in the clad beam specimens. In these analyses, results for the deep-crack specimen (CB-1.1) at a J value of 43.63 kN/m [J_c = 139.4 kN/m (in Table 3.3)] are employed as an approximation to the SSY reference solution. Earlier analyses[4] have shown that Q ≈ 0 for the deep-crack specimens under these loading conditions. This observation is supported by results shown in Fig. 3.9(*a*) for the normalized opening-mode stress (σ_{yy}/σ_0) distributions vs $\bar{r}$ for the deep-crack specimen CB-1.1. The opening-mode stresses ahead of the crack tip for the shallow-crack specimens (CB-1.2 and -1.3), shown in Fig. 3.9(*b*), exhibit an essentially uniform deviation from the SSY solution over a distance of $2 \le \bar{r} \le 10$ (i.e., spatially uniform). Both shallow-crack clad beam specimens were found to have Q values of about –0.78 at failure (for $\bar{r} = 2$), which represents a significant loss of constraint. The normalized stress distributions did not change for J values ranging from 200 to 240 kN/m for CB-1.2 (J_c = 235.3 kN/m) and from 522 to 750 kN/m for CB-1.3 (J_c = 716.5 kN/m). The Q value for

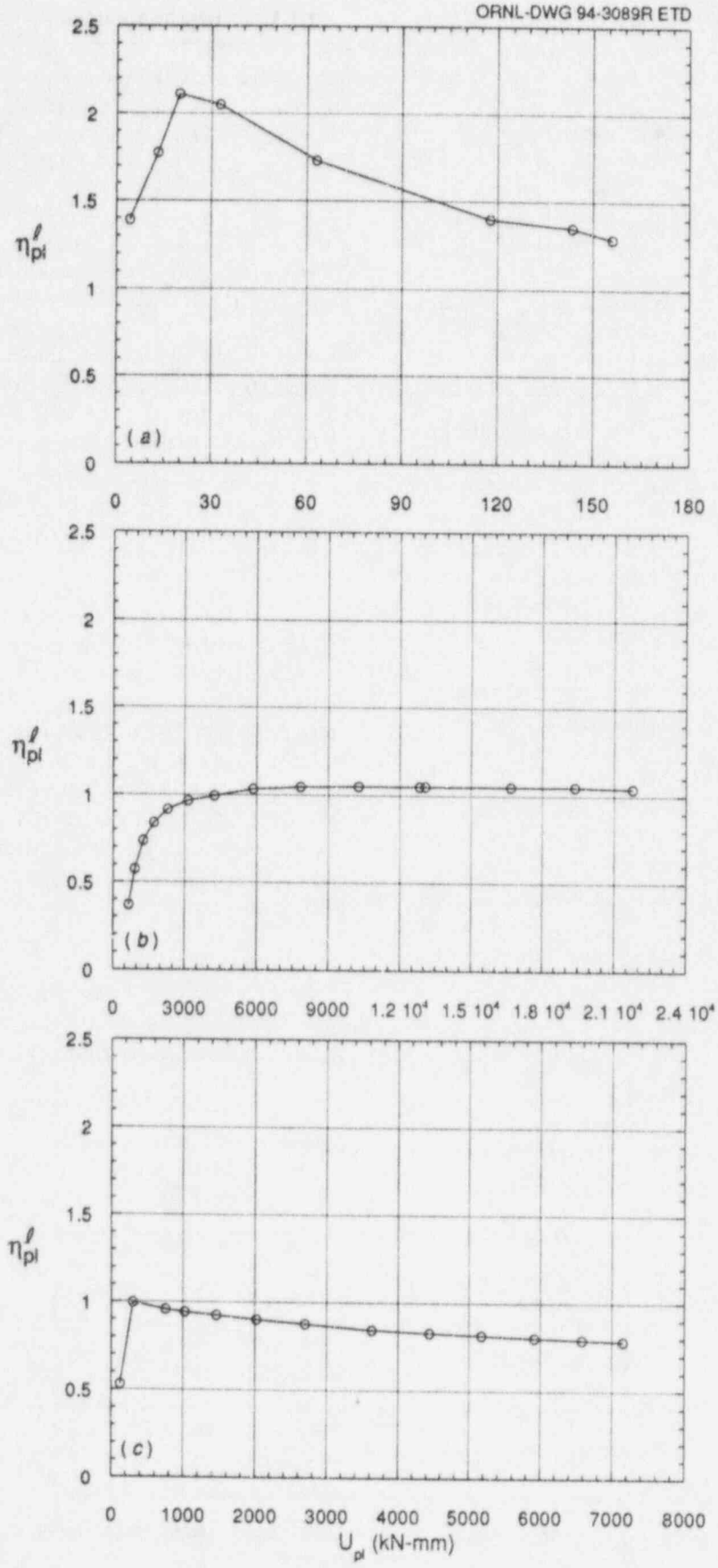

Figure 3.6 Variation of η^{ℓ}_{pl} with U_{pl} (based on LLD) for clad beam specimens: (*a*) a/W = 0.50, (*b*) a/W = 0.05, and (*c*) a/W = 0.10

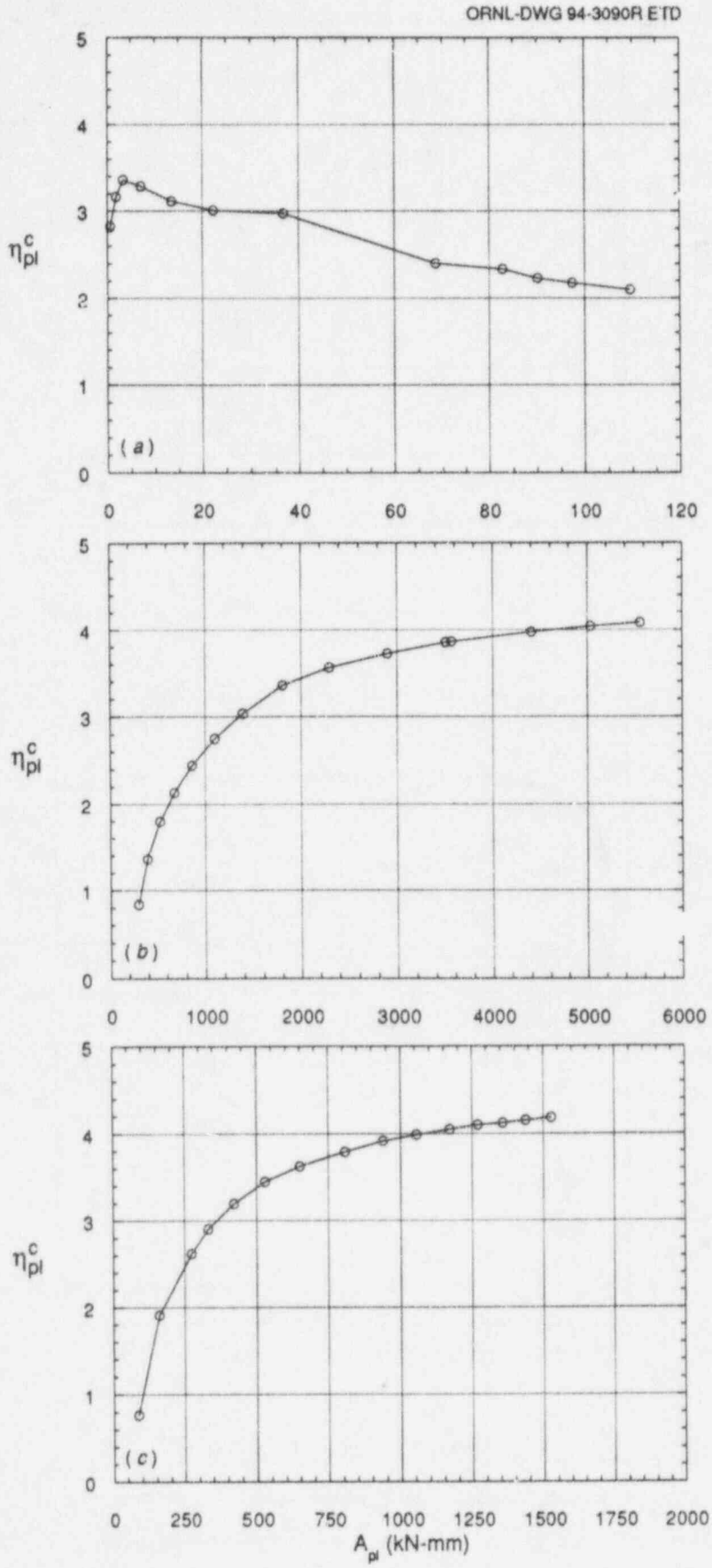

Figure 3.7 Variation of η^c_{pl} with A_{pl} (based on CMOD) for clad beam specimens: (*a*) a/W = 0.50, (*b*) a/W = 0.05, and (*c*) a/W = 0.10

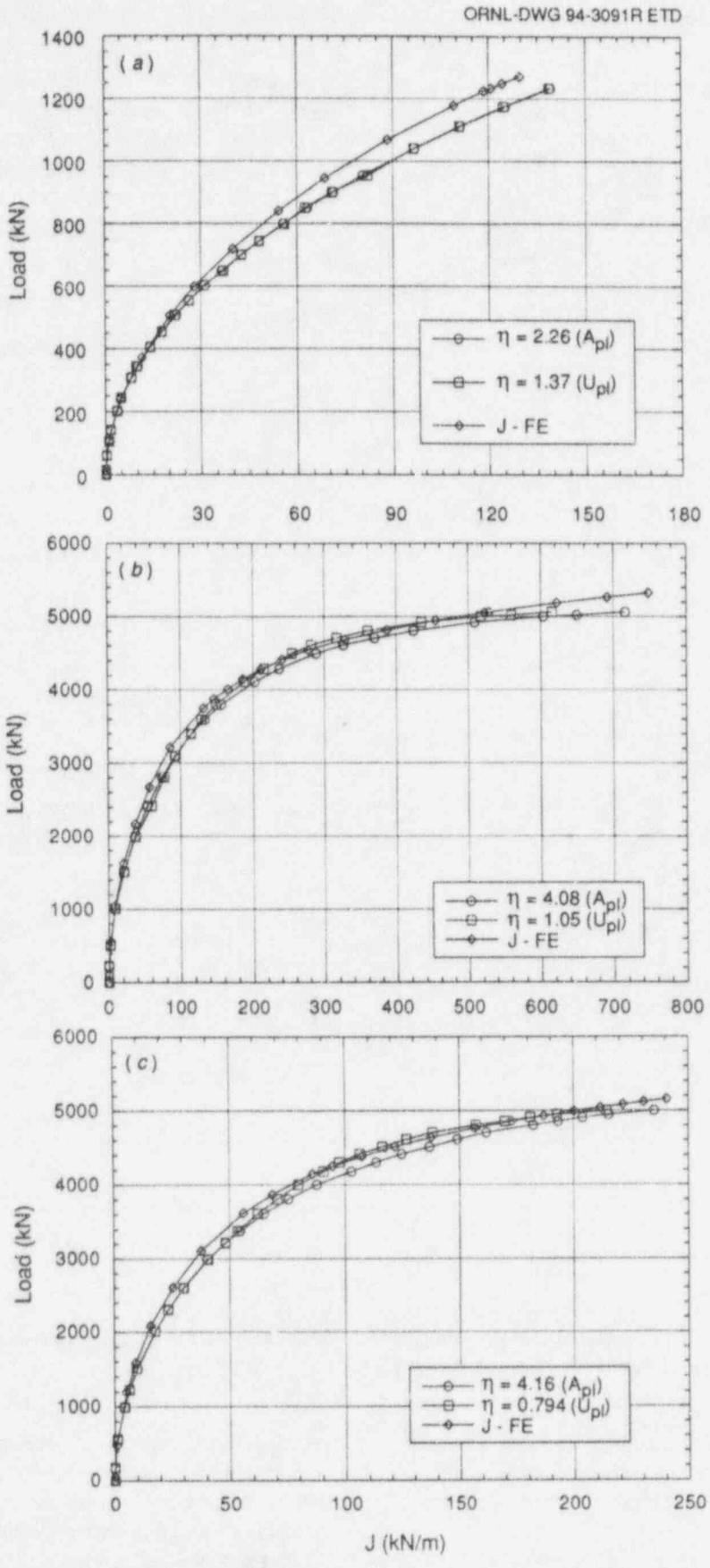

Figure 3.8 Comparison of calculated J values for clad beam specimens: (*a*) a/W = 0.50, (*b*) a/W = 0.05, and (*c*) a/W = 0.10

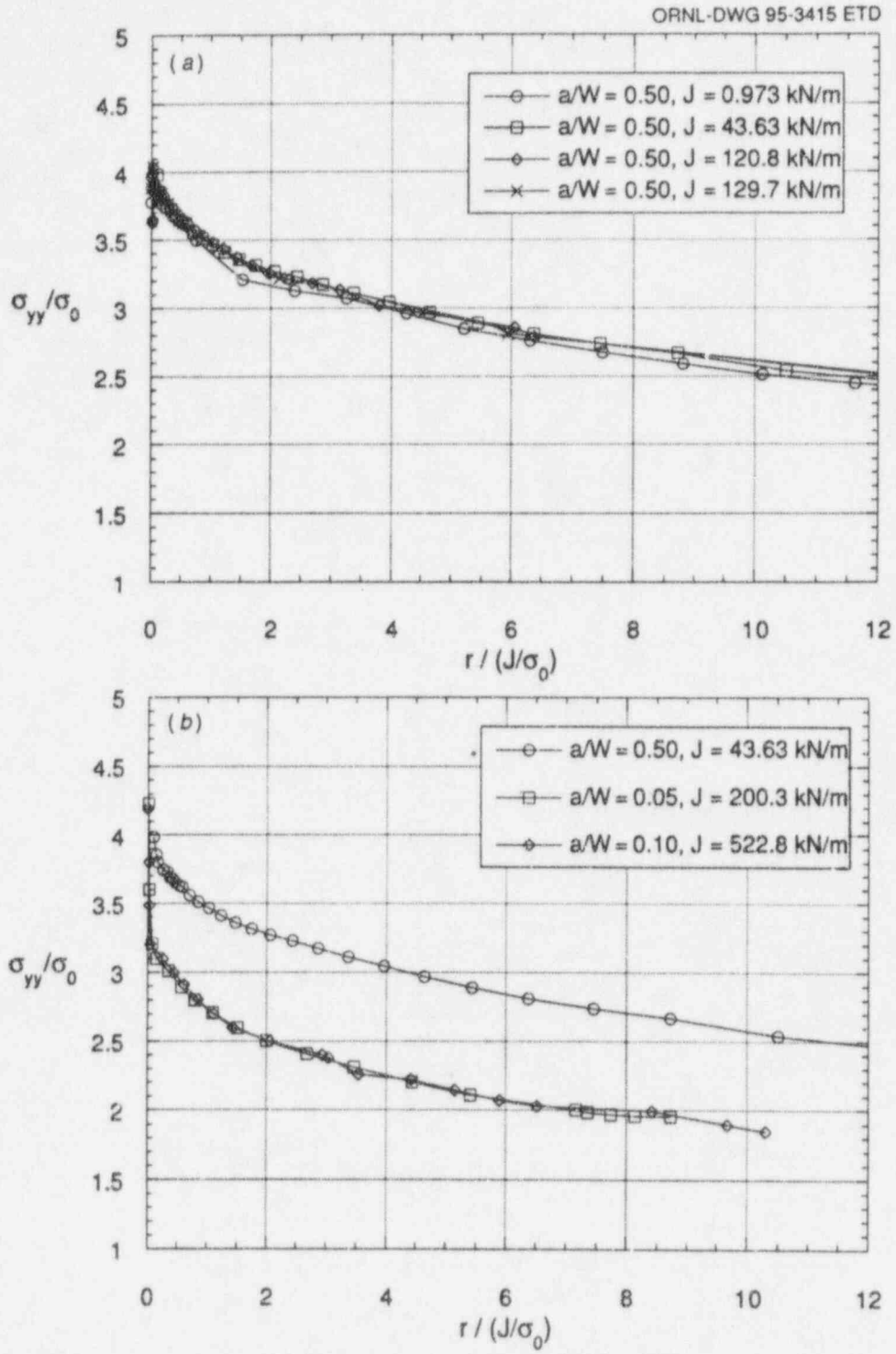

Figure 3.9 Distributions of normalized opening-mode stress for clad beam specimens as a function of applied J: (*a*) a/W = 0.50 and (*b*) at a/W of 0.50, 0.05, and 0.10

the shallow-crack clad beam specimens was very similar to the value for the shallow-crack SENB specimens previously tested at ORNL[4] ($Q \approx -0.70$).

3.2.3.4 Fracture Toughness Scaling Model

The D-A scaling model[11] analyzes constraint conditions by utilizing the area (or volume for 3-D geometries) within principal stress contours to correlate toughness values from finite-body geometries with SSY conditions. The SSY state is then considered to yield fracture toughness results independent of specimen size or loading mode and is comparable to a specimen of infinite size. The scaling model has been successfully applied to fracture toughness results exhibiting either a loss of in-plane constraint (i.e., shallow

cracks) or out-of-plane constraint (i.e., thickness effects).[11] The scaling model assumes that the volume of critically stressed material surrounding the crack tip is the same in different specimens with different constraint conditions. As a result, the SSY critical fracture toughness can be determined in a high-constraint geometry and then applied to a low-constraint geometry or vice versa.

The D-A scaling model was used to investigate in-plane constraint loss in the clad beam test specimens. Application of the model was based on information available in the literature[18] that obviates additional crack-tip analysis. Fracture toughness data from the clad beam, shallow-crack, and biaxial cruciform programs are shown in Fig. 3.10(*a*)

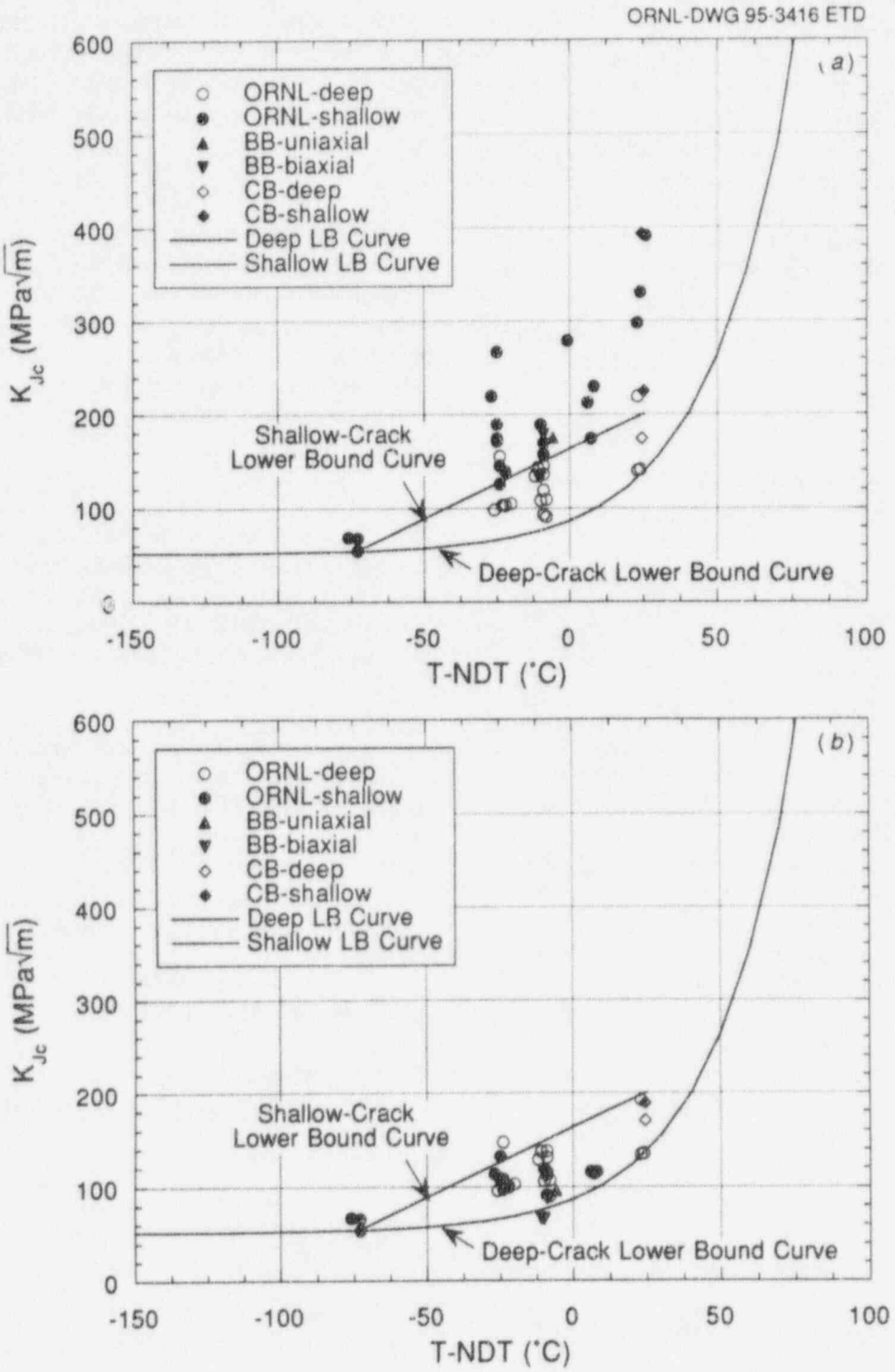

Figure 3.10 Fracture toughness as function of normalized temperature T – NDT: (*a*) fracture toughness and (*b*) SSY toughness (K_o)

as a function of normalized temperature (T – NDT). A lower bound curve to the uniaxial shallow-crack data is drawn as a straight line. Figure 3.10(*a*) indicates an increase in toughness and data scatter with decreased constraint.

The following criterion developed by Dodds and Anderson[11] determines dimensions in deep-crack (a/W ≥ 0.5) specimens necessary for SSY:

$$a, b, B \geq 200\, J_c/\sigma_f \quad . \tag{3.4}$$

In Eq. (3.4) a is the crack depth, b is the remaining ligament, B is the specimen thickness, J_c is the cleavage J-integral toughness, and σ_f is the material flow stress. Specimens not meeting the criterion are expected to exhibit a toughness increase due to the loss of constraint. The ratio $a\sigma_f/J_c$ was determined for each specimen and is listed in Table 3.4. As expected, the ratio exceeds 200 for the deep-crack specimen and is considerably less than 200 for the shallow-crack specimens.

Using the D-A analysis[11] results, Wallin[18] has quantified in-plane constraint loss by the following equation:

$$J_o \approx J_{FB}/\{1 + [A \cdot J_{FB}/(a \cdot \sigma_0)]^B\} \quad , \tag{3.5}$$

where

$$A = 38.1 \cdot \ln(N/3.14), \qquad 5 \leq N \leq 50$$
$$B = 1.27 + N/104.0, \qquad 5 \leq N \leq 50$$

and J_o is the SSY or reference value of J, J_{FB} is the value of J in the finite body geometry, and N is the hardening exponent. It is recommended in Ref. 11 that the scaling model not be used in situations in which $J_{FB}/J_o > 4$. The SSY value (J_o) was computed from Eq. (3.5) for each clad beam specimen using N = 10, and the results are listed in Table 3.4 as J_{FB}/J_o and K_o. The K_o results for the HSST clad beam, shallow-crack SENB,[15] and biaxial cruciform[15] programs are shown in Fig. 3.10(*b*) as a function of T – NDT. The K_o results show no toughness increase associated with the shallow-crack specimens. The K_o values evaluated for specimens that exhibited $J_{FB}/J_o > 4$ do not represent the SSY toughness value and were not included in Fig. 3.10(*b*). The scaling model appears to be effective in adjusting the test data to account for in-plane loss of constraint.

3.2.4 Additional Test Data

During August 1994, testing was completed on the fourth (CB-1.4) and fifth (CB-1.5) full-thickness clad beams at the NIST in Gaithersburg, Maryland. Test parameters and some preliminary fracture results reported by NIST for the two tests are compared in Table 3.5. It should be emphasized that these results could change after further evaluation of the data.

For test CB-1.4, the recorded load vs deflection curves indicated a relatively small amount of plasticity in the beam at failure. The fracture surface was fairly flat and appeared to be cleavage to the unaided eye. After about 40 mm of crack extension in weld metal, part of the crack deviated into the base metal. This occurred well after initiation of fracture and should not affect interpretation of initiation events.

For test CB-1.5, a violent failure of the beam resulted in one half of the specimen and two rollers being ejected from the test rig. The test rig was significantly damaged by this action. Based on load vs deflections data, substantial plasticity developed in the beam prior to failure.

Examination of the fracture surface revealed that the fatigue crack was followed by ~2.6 mm of ductile tearing and then by a fairly flat cleavage surface.

Analysis of the clad beam test data provided by NIST will be provided in the next reporting period.

3.2.5 Residual Stress Effects

Work was begun in estimating residual stress values for the first series of full-thickness clad-beam tests (CB-1.1, -1.2,

Table 3.4 Results of scaling model applied to CB data

HSST clad beam	a (mm)	K_{Jc} ($MPa\sqrt{m}$)	$a/(J/\sigma_f)$	J_{FB}/J_o	K_o ($MPa\sqrt{m}$)
CB-1.1	117.5	174	499	1.04	170
CB-1.2	10.84	225	27	3.12	128
CB-1.3	23.69	393	20	4.35	189

Table 3.5 Results from tests of CB-1.4 and -1.5 full-thickness clad beam

	CB-1.4 a/W = 0.1	CB-1.5 a/W = 0.05
Specimen geometry		
Load span (S), mm	1219	1219
Thickness (B), mm	229	231.6
Width (W), mm	229	225
Crack depth (a_o), mm	22.6	12.1
Fatigue precracking		
Precracking temperature, °C	20	20
Ratio P_{max}/P_{min}	10	10
Maximum K, MPa$\sqrt{m}$	36.6	42.7
Final K range, MPa$\sqrt{m}$	28	28
Fracture		
Test temperature, °C	–25	–25.9
Failure load (Pc), kN	3114	5783
K_J (from P vs CMOD curve), MPa$\sqrt{m}$	133	437

and -1.3). This work is being done in conjunction with Task H.7, which is to assess the inclusion of residual stresses in fracture-analysis methods used in current regulatory applications.

After the beams were machined to the final dimensions, the flaws were machined into the beams using the wire EDM process. The flaws extended from the shell inner surface (clad surface) to predetermined depths into the beam. Using the EDM process, flows with a very narrow width (~0.5 mm) and uniform depth can be machined into thick sections with a minimum impact on the surrounding material; heating and the associated potential for introduction of surface residual stresses is minimized, and only small amounts of material are removed. After the flaws were machined into the beams, and prior to fatiguing, the slot width did not remain constant but increased toward the inner surface due to the weld residual stresses. The measured slot widths are shown in Table 3.6.

Residual stresses in base metal (due to welding when vessels are fabricated) are generally tensile on the inside and outside surface and compressive in the midwall.[19] Finite-element analyses will be performed to produce residual stresses in the full-thickness clad beams by applying a fictitious temperature distribution through the beam width in the form of a cosine function. The vertical (opening) displacements will be compared with the measured slot-width values to determine the appropriate amplitude and period of the cosine function for residual-stress evaluation. Results of these studies will be described in the next reporting period.

Table 3.6 Measured EDM notch widths for the full-thickness clad beams

Distance from inner surface (cm)	EDM notch width (mm)
CB-1.1 (a/W = 0.50 and slot depth = 11.43 mm)[a]	
0.0000	0.54600
0.63000	0.53350
1.2700	0.52050
1.9000	0.50800
2.5400	0.49550
3.1700	0.48250
3.8100	0.47000
5.0800	0.45750
5.7100	0.44450
6.9900	0.43150
7.6200	0.41900
8.2600	0.40650
10.790	0.40650
CB-1.2 (a/W = 0.05 and slot depth = 0.762 mm)[b]	
0.0000	0.33020
0.38100	0.30480
CB-1.3 (a/W = 0.10 and slot depth = 2.032 mm)[b]	
0.0000	0.33020
1.0160	0.30480
2.0320	0.27940

[a] Slot width is an average of the front and back sides measured with feeler gages.
[b] Slot width is measured in the center (from beneath the specimen) with feeler gages.

3.3 Cleavage Fracture Analysis of French Clad Beams (J. A. Keeney)

3.3.1 Introduction

This section describes the detailed analyses performed under the HSST Program at ORNL for that portion of the Project FALSIRE II devoted to the French clad beam experiments, DSR3 and DD2 (Refs. 20–22). Project FALSIRE is organized by the Fracture Assessment Group (FAG) of the Organization for Economic Cooperation and Development/Nuclear Energy Agency's Committee on the Safety of Nuclear Installations Principal Working Group No. 3 (CSNI/PWG-3) to assess various fracture methodologies through interpretive analyses of selected large-scale fracture experiments.

Evaluation

These results are based on specimen geometry, material data, and experimental results described in the FALSIRE/Phase II Project problem statement, which is included in Appendix A of Ref. 23. The HSST/ORNL analysis results are reported in Appendix B of Ref. 23 using the format of special analysis forms provided by the CSNI/FAG to each participant in Project FALSIRE II. The following sections include a description of the experiments conducted by Electricité de France (EdF) and the local crack-tip field analyses carried out at ORNL.

3.3.2 Test Description

A series of clad beams containing subclad cracks is being tested in four-point bending in an experimental program at EdF. The central part of each beam is A 508 Class 3 steel with an RT_{NDT} of –40°C. The fabricated specimen DSR3 has dimensions of 120 × 145 × 1700 mm, with a 4.5-mm layer of cladding on the top surface produced by an automatic submerged-arc welding process. Specimen DD2 has dimensions of 119.2 × 145 × 1700 mm with a 6.0-mm layer of cladding. The cladding is applied in two layers, the first of which is 309L stainless steel followed by a second layer of 308L stainless steel. The beams contain a small subclad crack (approximately semielliptical) with a depth of 13 mm and length of 40 mm for DSR3 and a depth of 4.5 mm and length of 48 mm for DD2. The cracks were generated by fatigue-precracking. After the cladding process, a stress relief heat treatment was applied at 600°C for 8 h. The cladding layer had relatively low yield stresses and relatively high toughness. Data collected during the tests are load, load-point displacement, strains, and temperatures. Strains were measured with strain gages placed on the clad surface and on the opposite surface of the beam. Temperatures were measured with thermocouples placed on the surface and inside the specimen.

Before the mechanical test, the beam is cooled with LN_2 such that the temperature (≈ –170°C) is uniform inside the specimen after the cooling. The beam is insulated to avoid significant reheating during the test. The specimens are then loaded in four-point bending with a 1450-mm major span and 450-mm minor span. In the DSR3 test, the load on the beam at fracture was reported to be 695 kN. The cleavage fracture initiated in the ferritic base material, with no crack arrest. The temperature at the crack tip at the time of fracture was between –165 and –170°C. In the DD2 test, the beam fractured at a load of 870 kN with no crack arrest. The point of cleavage initiation was located about 1.5 to 2 mm from the clad/base interface in DD2; the corresponding location in DSR3 was about 2.5 mm from the interface.

Detailed information concerning the EdF clad beam testing program is given in Refs. 20–22 and Appendix A of Ref. 23.

3.3.3 Analysis Methods

The beams were analyzed with the ABAQUS finite-element program[16] [a nuclear quality assurance certified (NQA-1) code], which employs a domain integral method for the computation of the J-integral. The stress-intensity factor (K_I) was calculated from the J-integral using the following plane-strain relation:

$$K = \sqrt{JE/(1-\nu^2)} \quad , \tag{3.6}$$

where E = 210.0 GPa and ν = 0.3. The elastic-plastic small-strain analyses were performed using the material properties in Table 3.7 and the multilinear true stress–plastic strain curves depicted in Fig. 3.11.

Table 3.7 Material properties for clad beam analyses

Material property	Base A 508 Class 3	Stainless steel cladding 309L and 308L
Young's modulus (E), GPa	210.0	160.0
Poisson's ratio (ν)	0.30	0.30
Yield stress (σ_y), MPa	768.0	347.0

The 3-D finite-element models of the clad beams were generated with the ORMGEN mesh-generating program.[24] From symmetry conditions, only one-fourth of the beam is included in the model (DD2 is shown in Fig. 3.12). Both models consist of 16,178 nodes and 3,312 twenty-noded isoparametric elements. The measured crack front for each beam was modeled with a highly refined mesh in which the crack-tip element dimensions were on the order of 0.012 mm. Collapsed-prism elements surround the crack tip to allow for blunting and for an 1/r singularity in the strains at the crack front. Detailed plots of the crack-tip regions for both subclad cracks are shown in Fig. 3.13.

The finite-element model was subjected to four-point bending with boundary conditions shown in Fig. 3.12. A distributed pressure load was applied over the surface of a thin strip of elements (5 mm wide), and the beam was simply supported on the opposite surface by fixing nodes in the direction opposite to the applied load. In each load step of the analyses, iterations were performed to establish global equilibrium using a force equilibrium method. Integrations of the stiffness matrix were performed with a 2 × 2 × 2 Gauss point rule. The "stress-free" temperature was taken as the test temperature of the beam (residual stress and differential thermal strain effects were ignored).

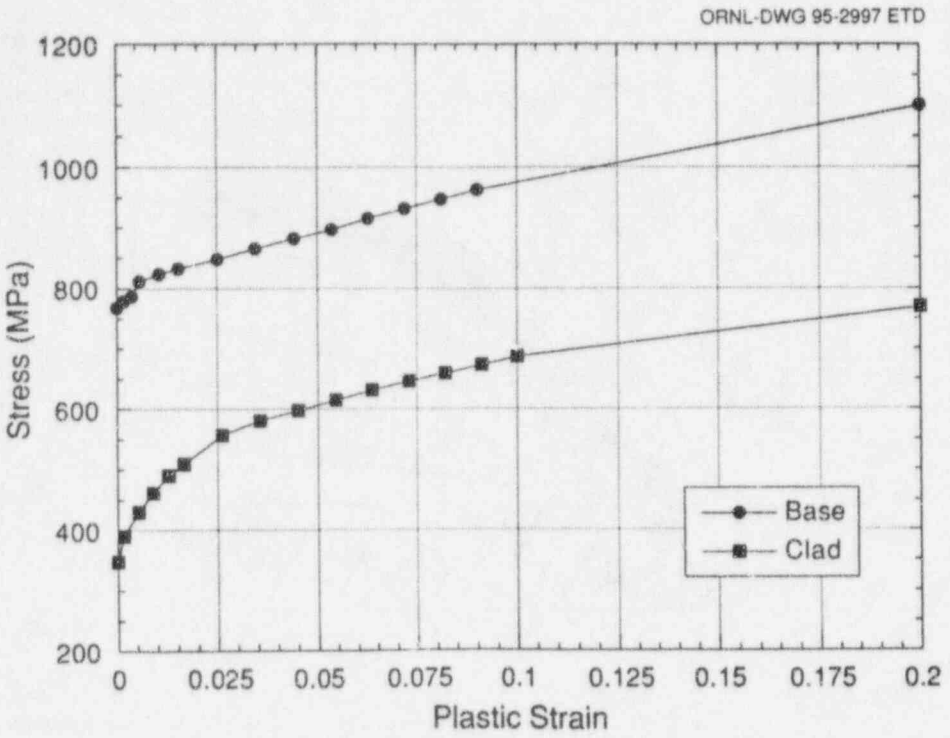

Figure 3.11 Young's modulus as a function of temperature as experimentally determined, compared to the dynamically measured value at room temperature and the other sources indicated

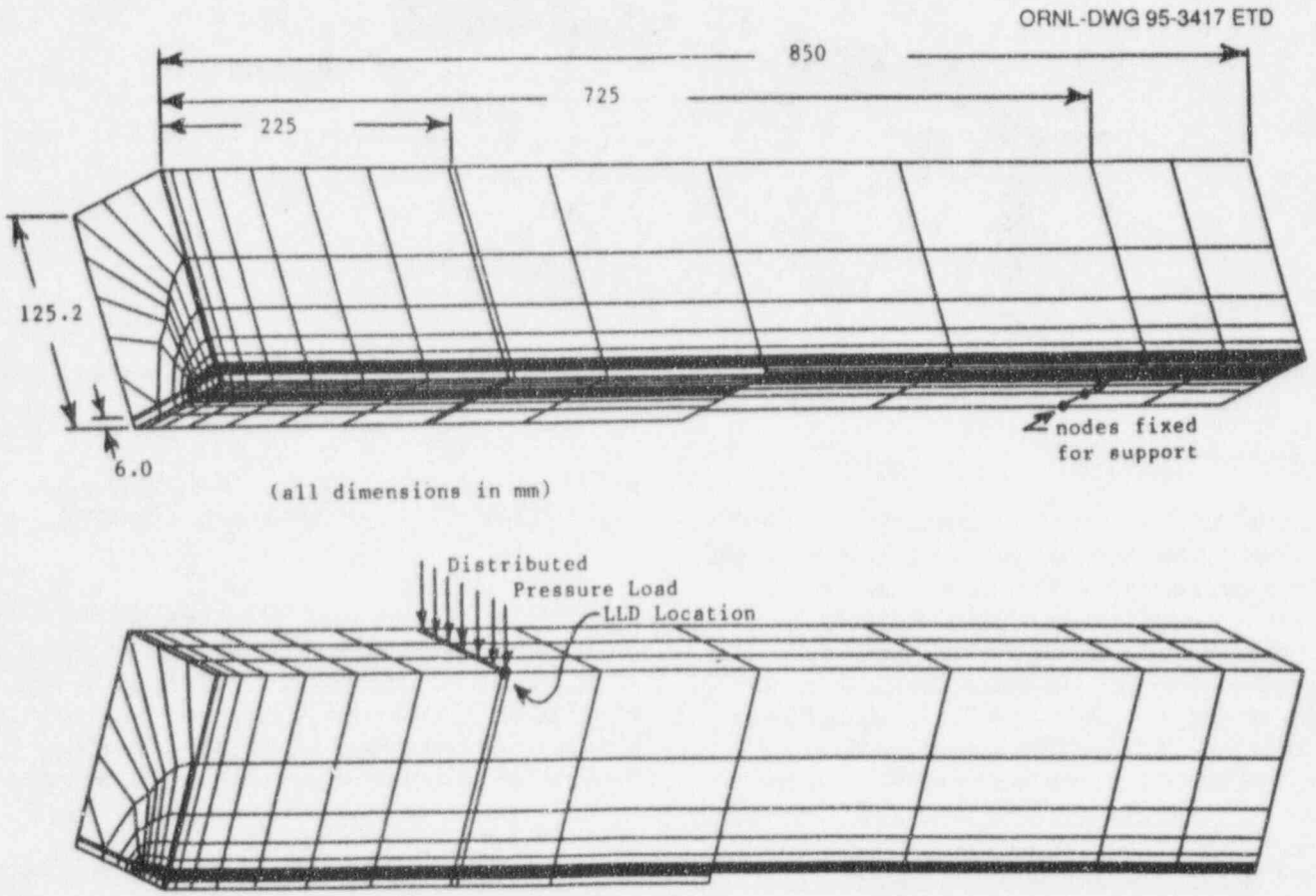

Figure 3.12 Finite-element model used in analysis of DD2 with dimensions and boundary conditions

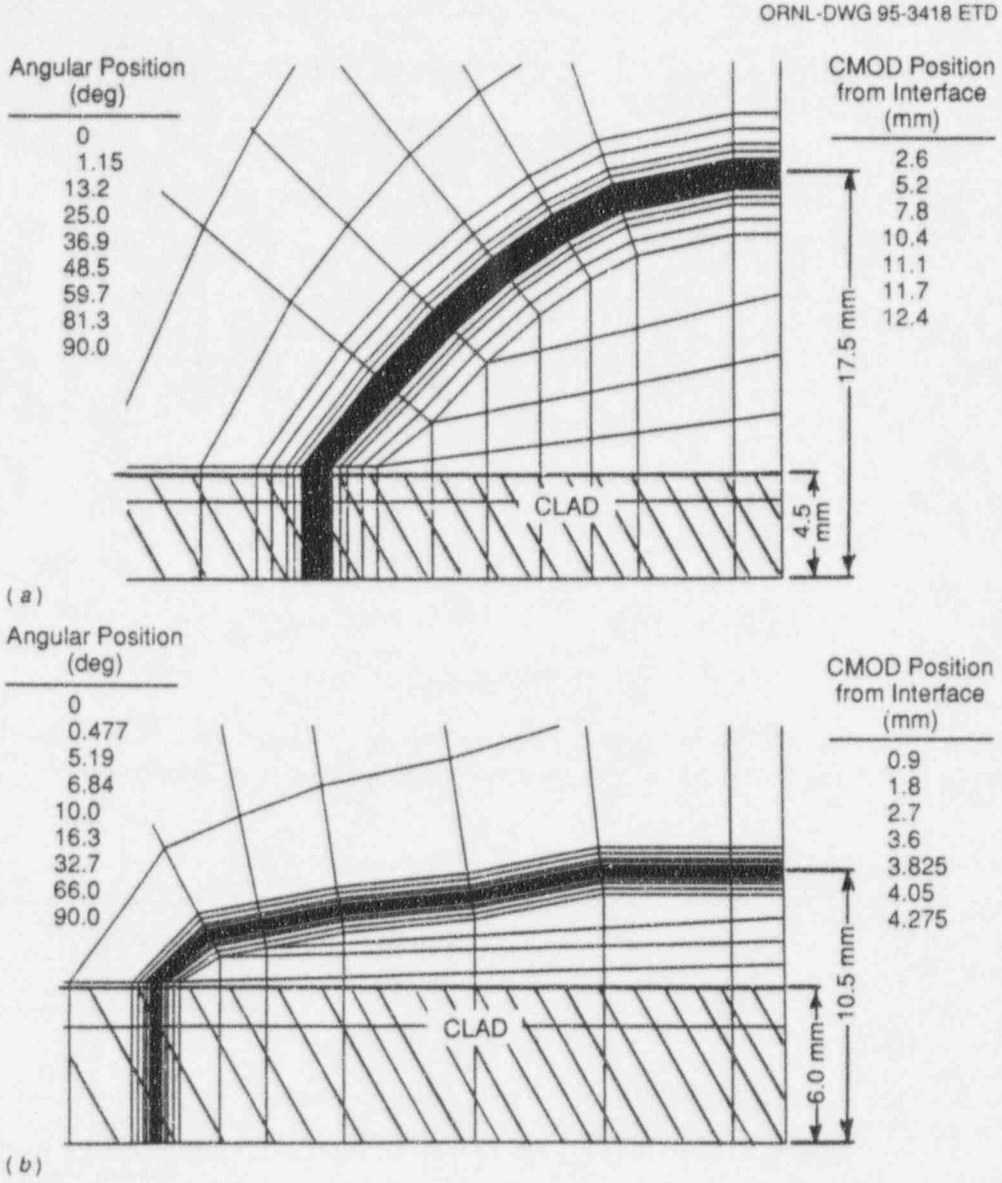

Figure 3.13 Detail of crack-tip region: (*a*) DSR3 with crack depth of 13 mm and (*b*) DD2 with crack depth of 4.5 mm

3.3.4 Analysis Results

Results from 3-D elastic-plastic analyses of the French clad beam experiments are summarized in Figs. 3.14–3.23. The deformation of the overall finite-element model and the crack-tip region are shown in Fig. 3.14 for DD2. The deformation indicates that the boundary conditions have been applied correctly. Calculated LLDs, CMODs, and strains were reported previously.[6] The calculated CMOD values for both DSR3 and DD2 indicate that the largest values of CMOD are located near the clad/base interface, which is due to the cladding layer stretching and allowing the crack to open more. The calculated and measured values of LLD and strain are compared for each test. The comparisons showed good agreement, which indicates that the overall structural response has been modeled appropriately. The opening-mode stress component and von Mises effective stress are given for DSR3 in Figs. 3.15 and 3.16 for loads of 300, 600, and 700 kN, and for DD2 in Figs. 3.17 and 3.18 for loads of 300, 600, and 900 kN.

The calculated K_I values for DSR3 and DD2 at the deepest point of the crack are shown as a function of load in Fig. 3.19 and as a function of crack-front angle in Figs. 3.20 and 3.21. The peak K_I values for DSR3 and DD2 at the initiation load are 49.7 and 50.5 MPa$\sqrt{m}$, respectively, and lie between the lower- and upper-bound small-specimen fracture toughness curves at the test temperature (40 and 53 MPa$\sqrt{m}$). The peak K_I values occur 9 mm from the interface for DSR3 and 4.5 mm from the interface (maximum crack depth) for DD2. The test results indicate that in DSR3 the crack initiated 2.5 mm from the clad/base interface, which has a calculated K_I value of

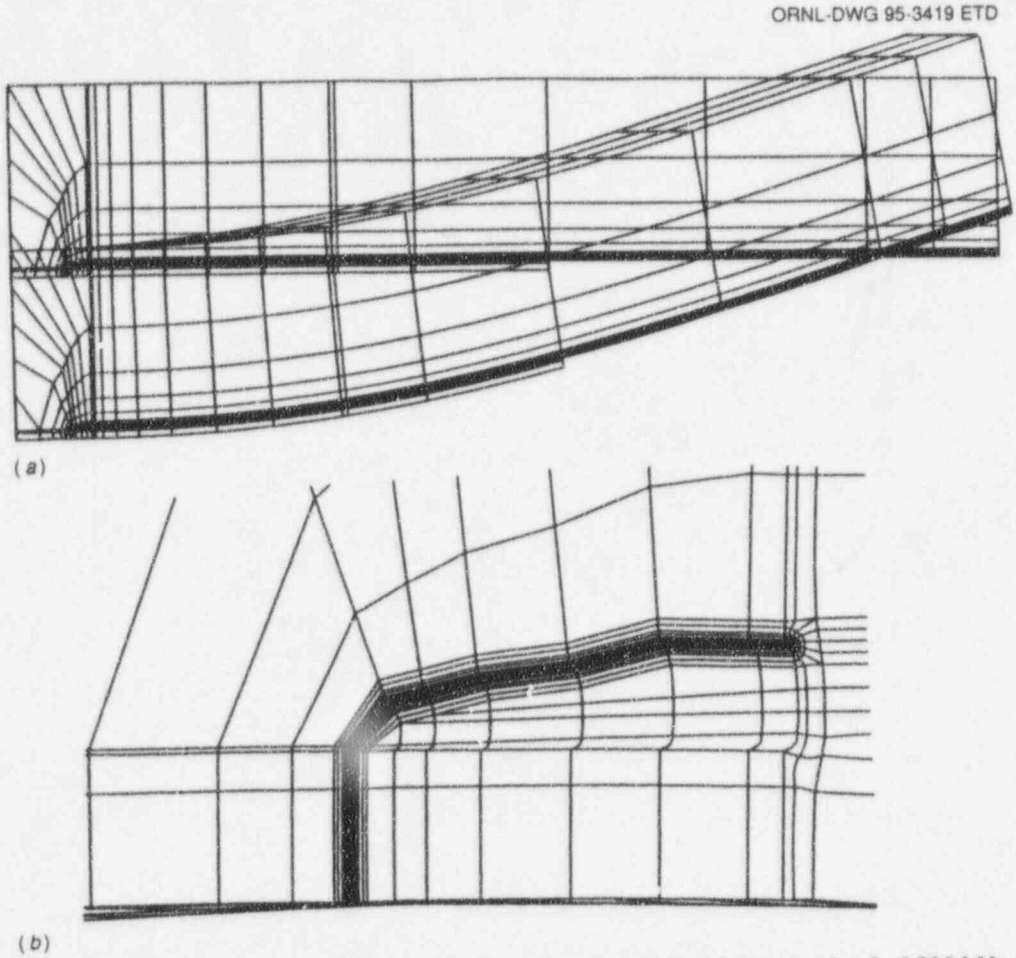

Figure 3.14 Deformation of finite-element model (DD2) under applied initiation load of 890 kN: (*a*) 3-D model (displacement magnification factor = 10) and (*b*) crack-tip region (displacement magnification factor = 50)

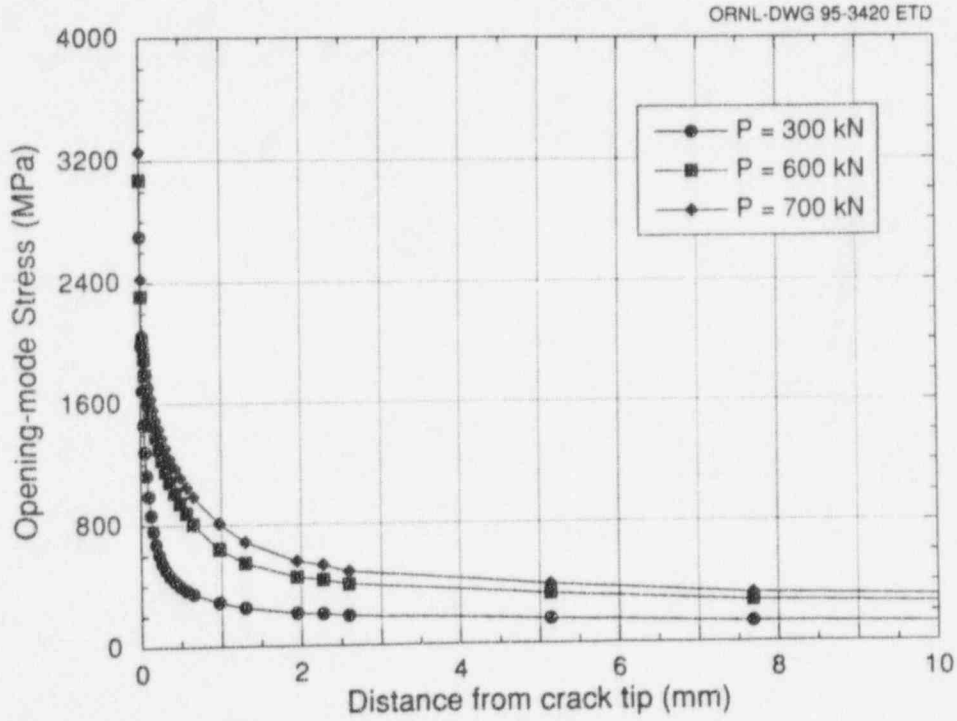

Figure 3.15 Opening-mode stress vs distance from crack tip for DSR3

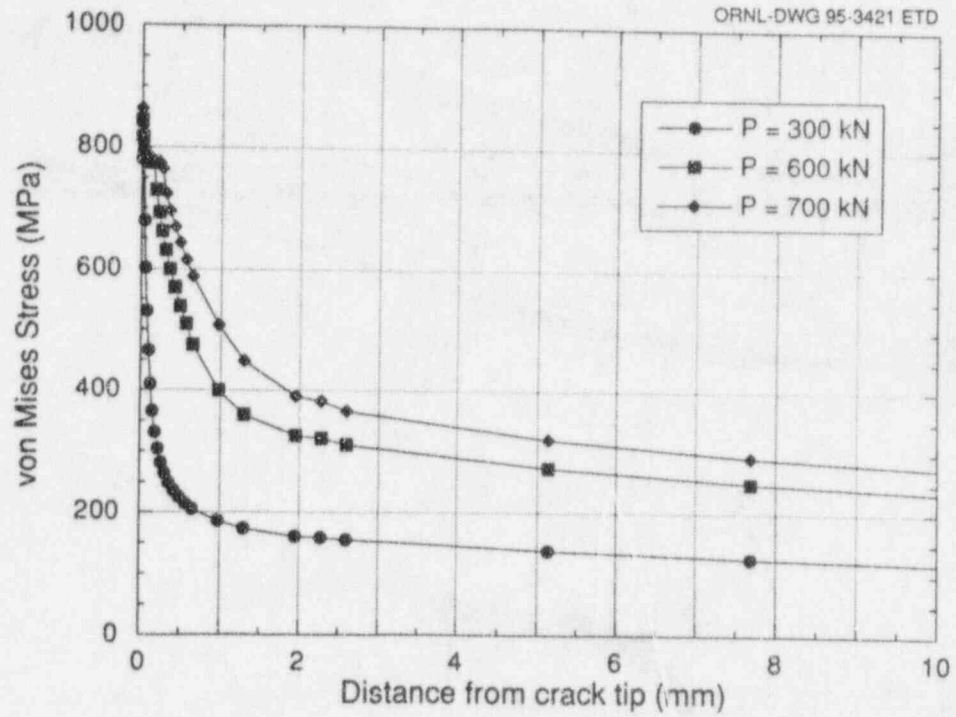

Figure 3.16 Von Mises stress vs distance from crack tip for DSR3

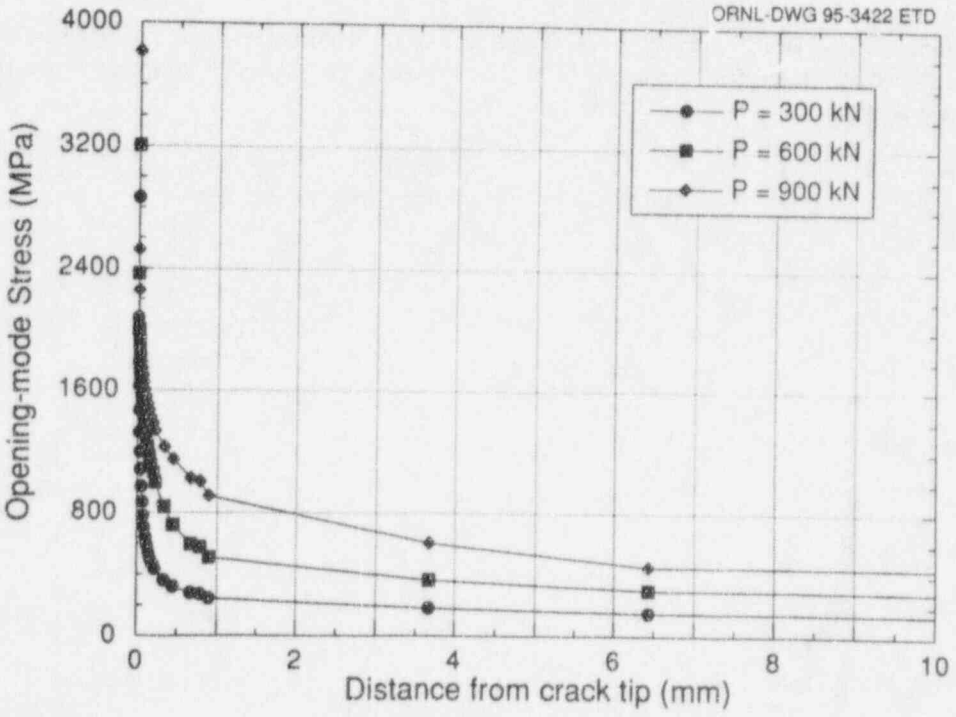

Figure 3.17 Opening-mode stress vs distance from crack tip for DD2

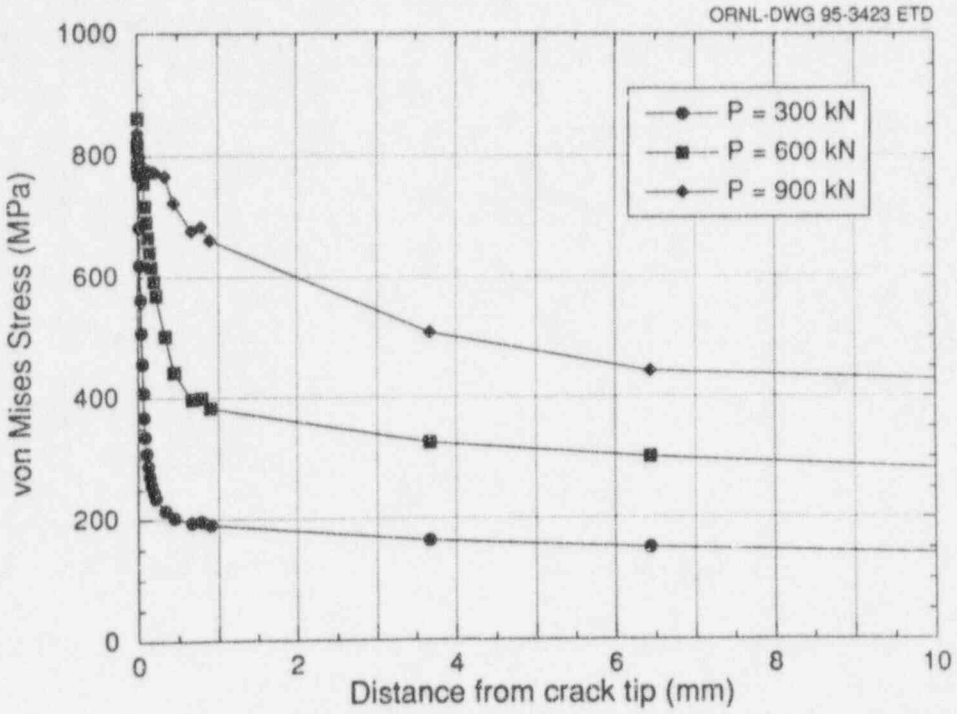

Figure 3.18 Von Mises stress vs distance from crack tip for DD2

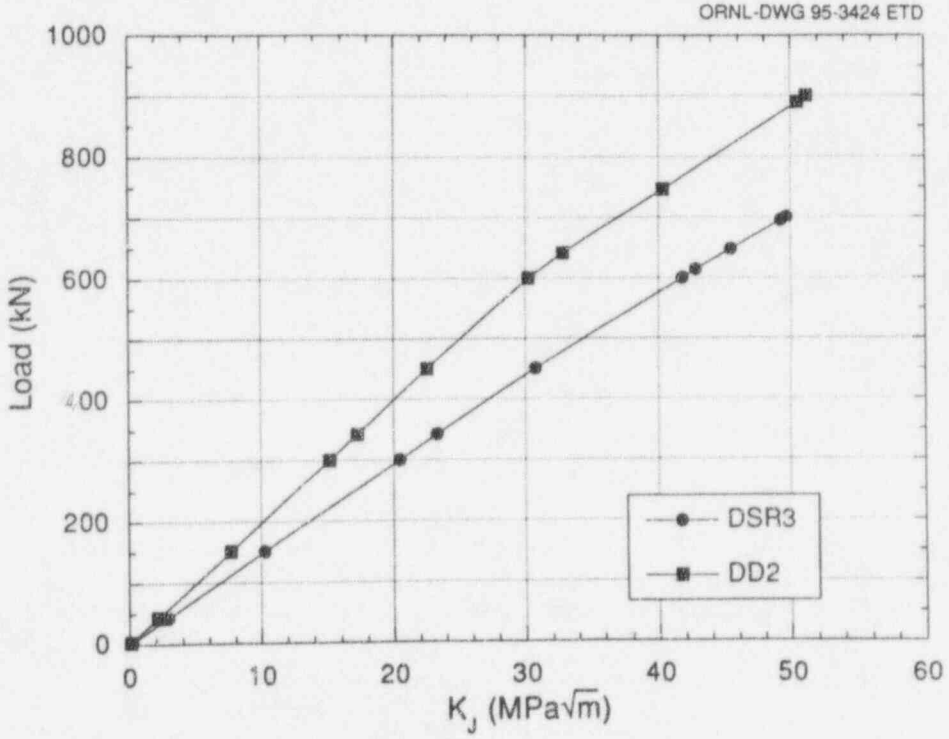

Figure 3.19 Comparison of load vs K for DSR3 and DD2

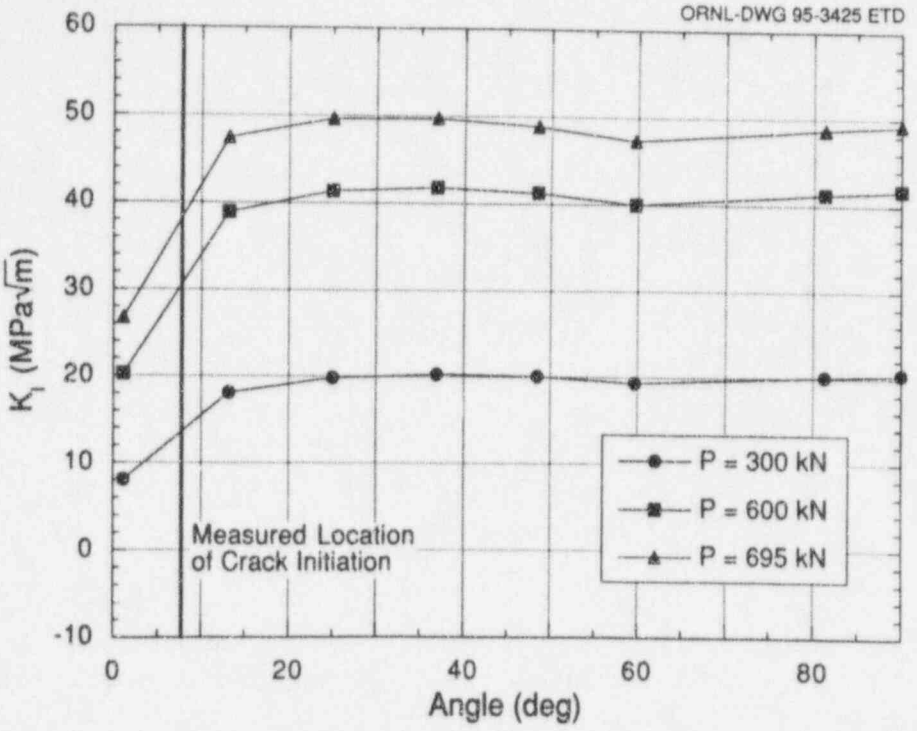

Figure 3.20 Calculated K vs angle for DSR3

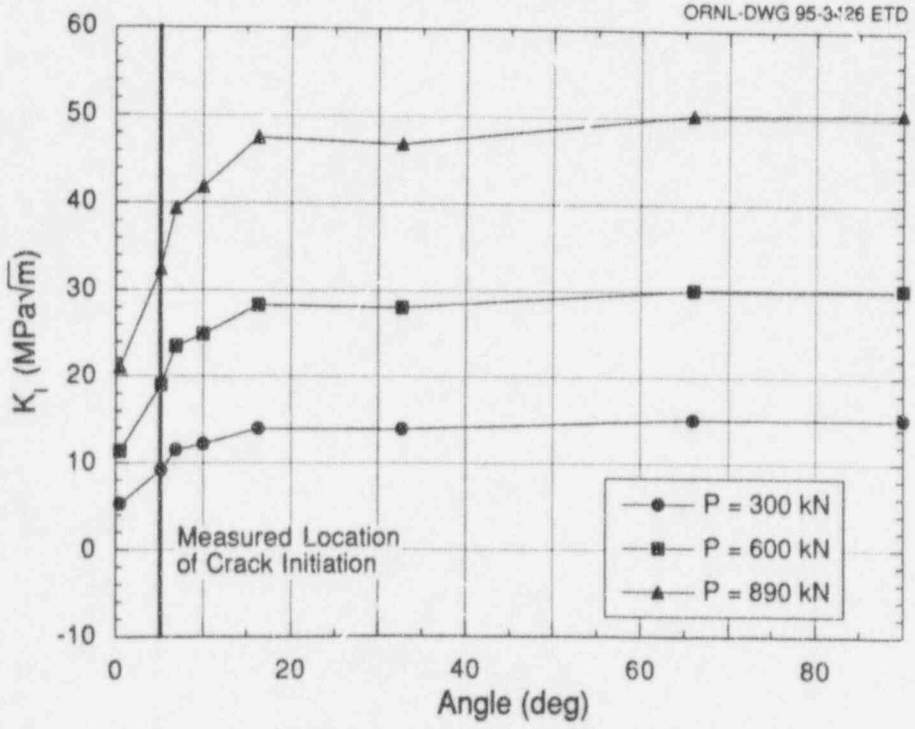

Figure 3.21 Calculated K vs angle for DD2

38.8 MPa$\sqrt{m}$. In DD2, the crack initiated 1.5 to 2.0 mm from the interface and has a corresponding calculated K_I range of 29.2 to 32.4 MPa$\sqrt{m}$. The calculated K_I values for the initiation locations fall below the lower-bound fracture toughness of the base-metal small-scale specimens at the test temperature.

Two different constraint parameters were used to assess the crack-tip stress triaxiality conditions in the clad beams. In Fig. 3.22, the h parameter (hydrostatic stress divided by the effective stress) is plotted over a normalized distance measured in the crack plane ahead of the crack tip [$r/(J/\sigma_0)$ or $\tilde{r}$, as measured from the deepest point of the crack] for DSR3, DD2, and the SSY solution. The h parameter for both specimens exhibits an essentially uniform negative deviation (loss of constraint) from the SSY solution over a distance of $2 \le \tilde{r} \le 10$ (i.e., spatially uniform). The comparable loss of constraint is also shown using J-Q methodology as given by O'Dowd and Shih,[8] where Q measures the departure of the opening-mode stress (σ_y) from the reference SSY solution, normalized by σ_0. The normalized opening-mode stresses (σ_y/σ_0) ahead of the crack tip ($\tilde{r}$) for the clad beams are shown in Fig. 3.23. The clad beams (DSR3 and DD2) were found to have Q values of about –0.38 and –0.61, respectively, at failure (for $\tilde{r} = 2$). The Q values for the French clad beams (subclad cracks) were less negative than the Q values evaluated in the HSST full-thickness clad-beam[25] and shallow-crack[4] testing programs (approximately –0.78 and –0.70, respectively).

The cracks in the clad beams are shallow (near the clad/base interface) and may be influenced by the cladding heat-affected zone (HAZ). The potential influence of the HAZ adjacent to the cladding has also been observed in the HSST full-thickness clad-beam testing program,[25] that is, reducing the toughness below the small-specimen fracture toughness values due to an embrittled region. The characterization of the HAZ is currently in progress at EdF.[22] Also, the values of the coefficients for thermal expansion for cladding and base material were not included in the FALSIRE/Phase II Project problem statement. Assuming the "stress-free" temperature is the test temperature of –170°C does not fully reflect the effects of residual stress and differential thermal strains. If another "stress-free" temperature were used in the analyses, the generated thermal strains might have a substantial effect on the K_I values near the clad/base interface.

Another potential influence on crack initiation is locally intensified strain-aging effects currently being studied by TWI.[25] Localized strain aging of material occurs at the tips of preexisting cracks, which are located adjacent to areas where further welding operations are in progress (i.e., cracks in areas influenced by the cladding process). Thermal stresses produced by the transient temperature distribution cause high opening-mode tensile stresses to be generated at the crack tip. This occurs at a time when local temperatures are sufficiently high for thermally activated carbon and nitrogen atoms to be available to diffuse to

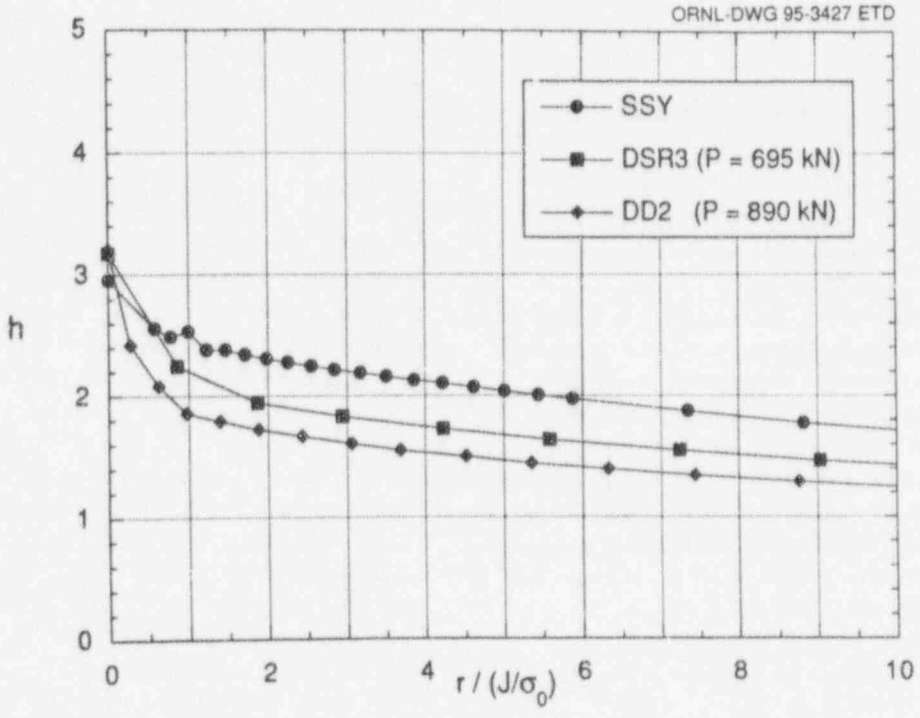

Figure 3.22 Comparison of h from SSY solution with DSR3 and DD2 indicates loss of constraint (r measured from deepest point of crack)

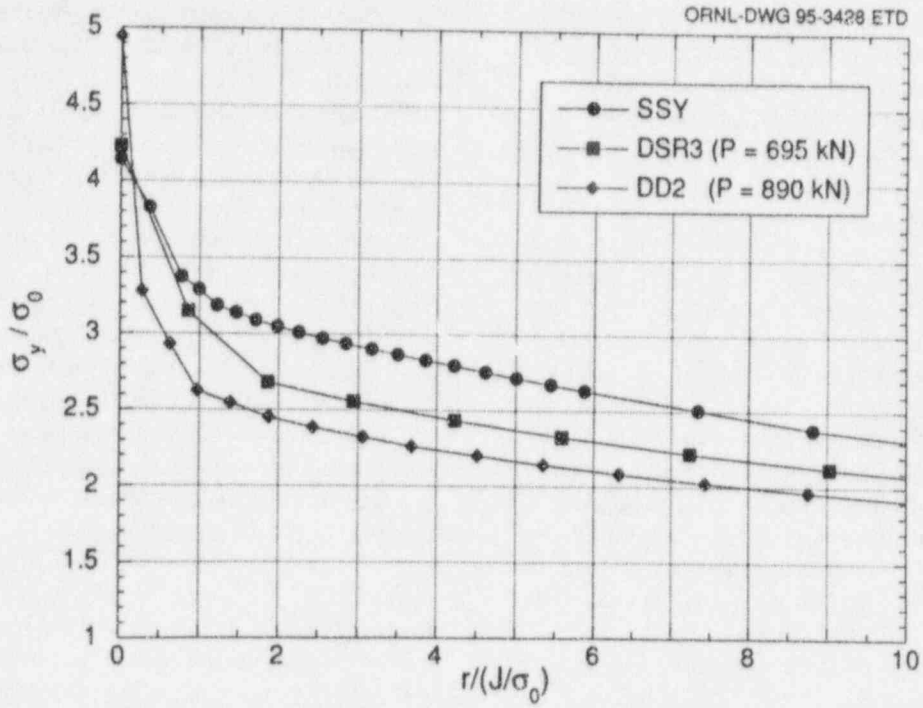

Figure 3.23 Comparison of σ_y/σ_0 from SSY solution with DSR3 and DD2 indicates loss of constraint [Q = –0.38 for DSR3 and Q = –0.61 for DD2 at $r/(J/\sigma_0) = 2$, with r measured from deepest point of crack]

dislocations and effectively lock them. The net effect is to restrict further plastic deformation of the crack-tip material and, thereby, reduce the transition-range fracture toughness of material at the crack tip by reducing its ability to yield and produce blunting. This effect could impact the material fracture toughness associated with preexisting subclad cracks.

3.4 Clad Methods Development

Modifications were made to the specifications for development of a cladding process to meet requirements for testing of clad/base-metal cruciform specimens under subtasks H.3.4 and H.3.5. Specifically, requirements for low ductile-tearing toughness of the cladding were deleted. The original specification for the cladding toughness properties was interpreted to require target values of J_{Ic} and tearing modulus at room temperature of 50 to 100 kJ/m^2 and 180 kJ/m^2, respectively. The most recent test of a heat-treated austenitic stainless-steel 1/2T C(T) compact specimen at ORNL yielded substantially higher J_{Ic} and tearing modulus values at room temperature of 804 and 271 kJ/m^2, respectively. Previous testing of the material subjected to a different heat treatment resulted in failure by unstable fracture. This material, in the absence of heat treatment, is AL 6XN austenitic stainless steel with a room temperature CVN impact energy greater than 300 J.

Because of difficulties associated with achieving the target toughness properties using heat treatment, deterministic analyses were performed with the FAVOR code[26] to investigate whether the tearing toughness of irradiated cladding should be considered an issue in meeting the goals of the clad testing program. Thus, the objective was to determine from the FAVOR analysis whether irradiated cladding is predicted to experience ductile tearing in a prototypic vessel subjected to a severe PTS transient.

For the analysis, a K_{Ic} curve was derived from a temperature-dependent ductile tearing initiation toughness curve (J_{Ic}) for 3-wire stainless steel cladding that had been irradiated to 2.41 neutrons/cm^2 (data from Ref. 27). The resulting K_{Ic} curve was incorporated into the FAVOR code assuming that both the clad region and the base metal were governed by this K_{Ic} toughness curve.

A prototypic PWR geometry (R_i = 86 in., t_{wall} = 8.5 in.) was subjected to a severe PTS event defined by the reference calculational model used in the NRC/Electric Power Research Institute (EPRI) PTS benchmarking exercise. This is a stylized thermal transient with initial and final coolant temperatures of 288°C (550°F) and 60°C (150°F), respectively, with an exponential decay constant of 0.15. Pressure was maintained constant at 1.0 ksi.

The FAVOR code was then used to generate critical crack depth curves for axially oriented flaws with aspect ratios (i.e., total flaw length to flaw depth) of 2, 6, 10, and infinity. Analyses were performed for clad thicknesses of 0.156 and 0.25 in. The minimum flax depth predicted to initiate in cleavage ($K_I = K_{Ic}$) was ~0.7 in. Therefore, the stainless steel cladding is predicted *not* to experience tearing during the experiment. Note that these results are derived from a deterministic analysis utilizing a mean fracture toughness curve. If the scatter in toughness is not large, then it can be concluded that a relatively high tearing toughness of the cladding should not be an issue in achieving the objectives of the clad cruciform testing program. Remaining specifications for the cladding process under development focus on properties of the cladding near the NDT of the heat-treated base metal. Specifically, in the temperature interval NDT ± 25°C, the cladding should be in the ductile regime with a yield stress in the range of 300 to 400 MPa (based on data from Ref. 27).

Cladding properties and the cladding deposition process required for the clad cruciform testing program in Subtask 3.4 were reviewed further. It was concluded that use of the SNUPPS shell material would be the most desirable approach to an evaluation of cladding effects on fracture toughness of shallow flaws. This conclusion is based on several factors: (1) there is an ample supply of this material for execution of a definitive matrix of tests, (2) the material fabrication processes are prototypic of RPVs currently in service, and (3) use of this material removes the necessity for development of both clad material and process(es) for specimen fabrication.

3.5 Clad Cruciform Specimen Testing

Analysis and testing of clad cruciform specimens containing finite-length shallow surface cracks will be performed under this task. These clad-specimen tests are needed to generate significant amounts of test data to understand the behavior of flaws in RPVs with test conditions as close to prototypic as possible. Ductile deformation and failure processes are known to be sensitive to the biaxial stress fields (i.e., axial/circumferential in a cylindrical vessel) that are imposed on an RPV wall by pressure and thermal loading conditions. Testing of clad cruciform specimens under biaxial loading provides a mechanism for approximating the effects of those stress fields on shallow through-clad surface cracks.

Clad cruciform specimens will be fabricated for clad-plate SNUPPS material taken from the broken halves of uniaxial beams and from the remaining portion of the SNUPPS wall section at ORNL. The weld-overlay cladding from the SNUPPS wall segment will be retained in the test section of the cruciform specimens. The fabricated specimens will be heat-treated to simulate appropriate properties (mechanical and fracture toughness) for the plate material near NDT. Following heat treatment, the cladding must exhibit ductile behavior at the test temperature, but tearing toughness of the cladding is not regarded as an issue in achieving the objectives of the testing program.

3.5.1 Medium-Scale Specimens

Initially, six development clad cruciform specimens will be fabricated from SNUPPS material and heat-treated concurrently with the unclad cruciform specimens described under Subtask H.2.1. The development clad specimens will contain finite-length surface cracks with the same dimensions as the unclad specimens of Subtask H.2.1 (a = 0.6 in.; 2c = 1.5 in.). Testing will take place at the NDT of the heat-treated plate material. These specimens will be tested in uniaxial and biaxial loading (three) to develop test procedures and to identify critical test parameters and instrumentation requirements (e.g., required instrumentation for measuring CMOD for through-clad cracks).

Following completion of the development phase, a series of clad cruciform specimens will be tested from a verification test matrix. The series of clad cruciform specimens will provide a data set that can serve as a reference in the transition temperature region for a particular set of conditions. These results should provide guidance for further investigation of variables associated with cladding effects on crack initiation and propagation. These variables include crack geometry (depth and length), cladding thickness, cladding residual stresses, cladding deposition direction, HAZ, as well as material and fracture toughness properties associated with the various regions.

3.5.2 Large-Scale Clad Cruciform Specimen

The objective of this series of tests is to study the most prototypic specimen, less than a clad cylinder, to assess cladding effects. Using limited laboratory-scale specimens, it has been shown both experimentally and analytically that a tensile, out-of-plane, biaxial stress reduces fracture toughness below the value in uniaxial loading of the same specimen. Large-scale clad cruciform-specimen tests were performed to investigate the influence of cladding, flaw depths, and biaxial-loading ratios on fracture toughness. Large-scale cruciform specimens allow these factors to be studied under prototypic biaxial conditions while circumventing some difficulties associated with transfer of fracture toughness data from smaller laboratory-scale specimens to full-scale structures.

Evaluation

Clad cruciform specimens will be fabricated from clad-plate SNUPPS material. Once the specimens have been prepared, a readiness review will be conducted prior to any testing. Posttest finite-element, near-crack-tip analyses of the specimens and correlations will be performed with the selected-constraint effects model (from Subtask H.2.2).

3.5.3 Upgrade of Servo-Hydraulic Test Machine

The servo-hydraulic test machine employed by the HSST program at ORNL will be modified to increase both the total load capacity of the test fixture and the size of the beam specimen that can be tested. The modification will involve replacement of the control system and servo valve, as well as recalibration of the loading system, to increase overall machine capacity from 550 to 700 kips maximum. Modification of the system will be performed in connection with Subtask H.2.1; also, a fitness demonstration will be completed for the test facility and test procedures using a dummy full-thickness cruciform specimen.

3.6 Clad Yielding Model

Influence-coefficient methodology based on linear-elastic fracture-mechanics (LEFM) concepts is generally used to perform deterministic and probabilistic RPV assessments. As a near-term refinement in the assessment methodology, a generic model is being developed that incorporates the clad yield stress into the calculations, while permitting the LEFM influence coefficient approach to be retained in the presence of the clad nonlinear response. An empirical approach utilizing a matrix of clad vessel solutions is being employed to construct the model. Validation of the model predictions will be done using available test data and analyses.

Thermo-elastic (TE) and thermo-elastic-plastic (TEP) analyses will be performed with ABAQUS to provide clad vessel solutions for use in a generic model based on an empirical approach. This will facilitate the development of an empirical correlation that has sufficient generality to correct LEFM K_I solutions for the effect of clad plasticity as would be required for prototypical PTS scenarios. This correlation will be incorporated into the FAVOR code.

A matrix of flaw geometries has been developed to carry out the clad yielding model development. There will be three different aspect ratios (2:1, 6:1, and 10:1) and three different a/t (crack depth/vessel thickness) ratios (0.0294, 0.05, and 0.075) that correspond to crack depths of 0.25, 0.425, and 0.6375 in. A total of nine finite-element models will be required. Initially, one cladding thickness will be utilized (0.156 in.). A set of four different thermal transients will be used. The first transient analyzed will be the PTS benchmarking transient. The other three transients will be selected from the workscope currently being implemented in Task H.5 to develop a technical basis for potential revisions to Regulatory Guide 1.154. The workscope includes the generation of thermal-hydraulic boundary conditions for a prototypical plant-specific case. Initially, TE and TEP analyses will be performed for a number of flaw geometries and thermal transients so ABAQUS and FAVOR can be benchmarked elastically. Ultimately, more than 36 analyses will be performed.

3.7 Effect of Mesh Refinement on Structural Response of a Beam in Four-Point Bending (J. W. Bryson)

Additional 2-D mesh refinement studies have been completed for a beam in four-point bending having the same dimensions as the longitudinal cross-section of the biaxial bend specimen. These studies were undertaken to try to explain the discrepancies between measured and calculated structural response of certain ORNL biaxial bend tests where the calculated response is somewhat stiffer than the measured response. Previous 3-D mesh refinement studies indicated that the finite-element model used in the ORNL analyses was a converged model and that additional mesh refinement did not improve the structural response in the sense that a more "flexible" response was obtained. These earlier 3-D analyses were not thoroughly documented, however; and a decision was made to revisit the mesh refinement issue.

Figure 3.24 shows a 2-D model having identical mesh refinement as the longitudinal cross-section of the 3-D finite-element model used in the earlier analyses. This model will subsequently be referred to as the "regular" 2-D model. It has been conjectured that the "regular" model might have modeling that is too coarse in the compressive region of the specimen and that this could be inhibiting the bending response. Figure 3.25 shows a mesh with increased refinement through the thickness of the beam and will be referred to as the "refined" model. Both 2-D models employ eight-noded isoparametric elements with reduced 2×2 integration. These 2-D elements have the identical shape functions in 2-D space as the 20-node isoparametric bricks in 3-D space; hence, any improvements in the structural response (i.e., increased flexibility) that may be observed in the 2-D calculations can also be expected to apply to the 3-D finite-element models. Likewise, if there is no increased flexibility in the refined 2-D calculations, then it can be assumed that additional refinement of the 2-D

ORNL-DWG 95-3429 ETD

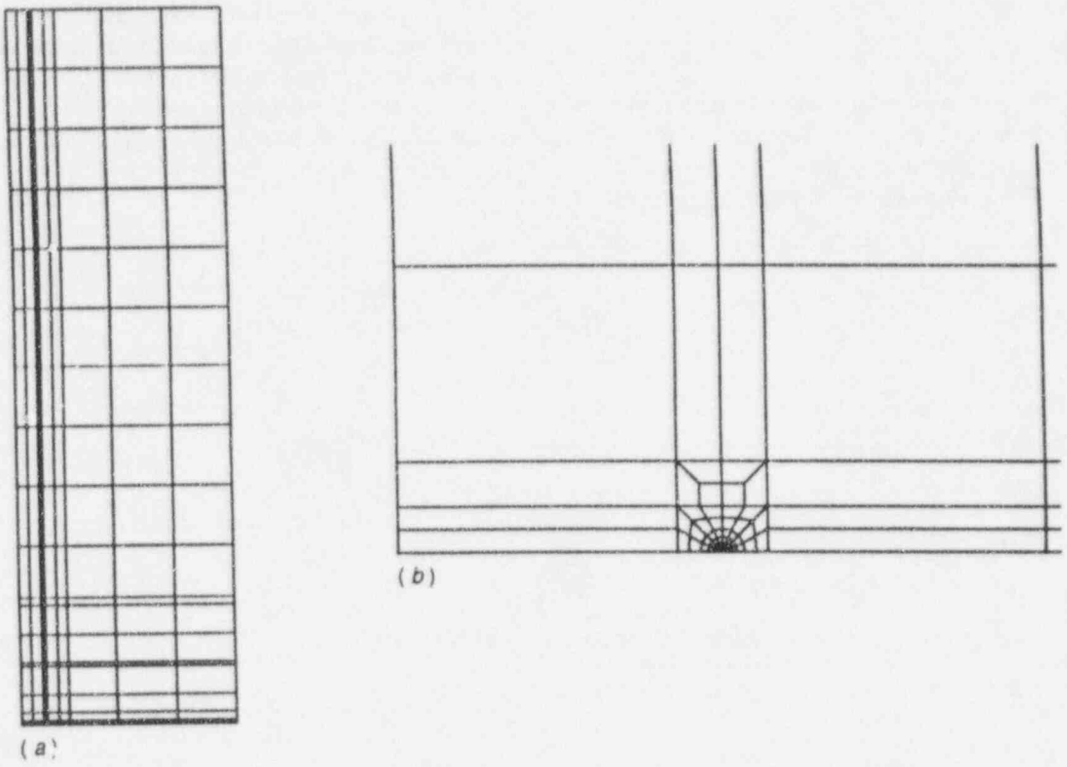

Figure 3.24 Finite element model for beam in four-point bending, "regular" mesh (*a*) full model and (*b*) crack-tip region

ORNL-DWG 95-3430 ETD

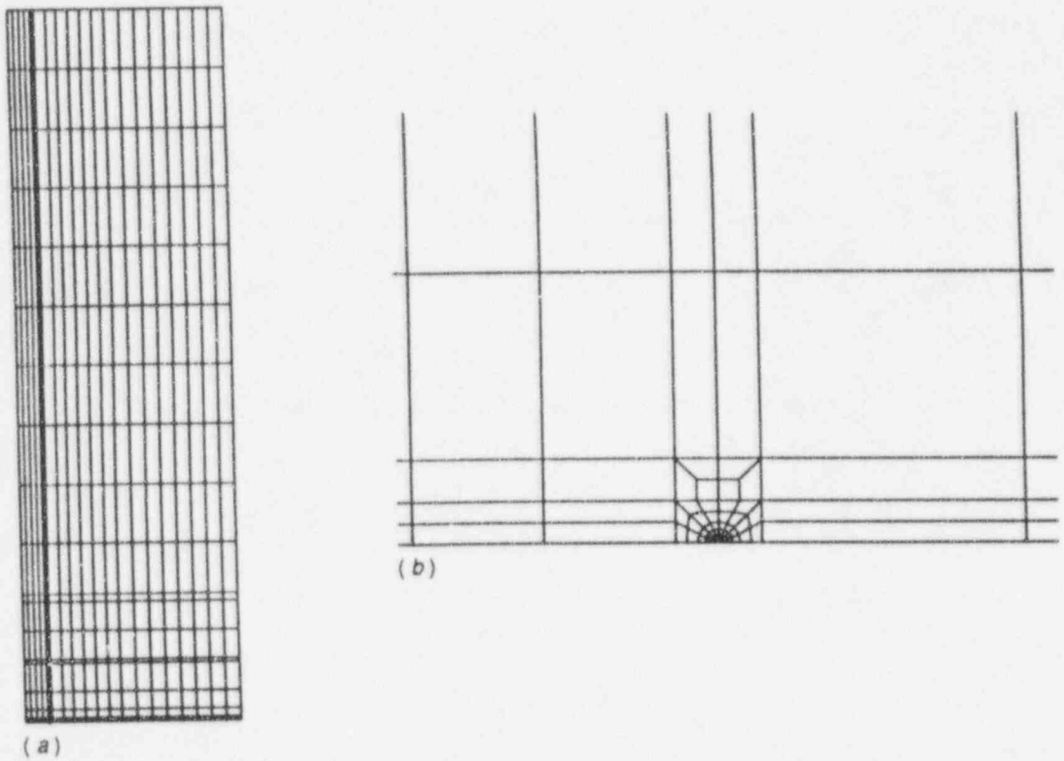

Figure 3.25 Finite element model for beam in four-point bending, "refined" mesh (*a*) full model and (*b*) crack-tip region

models will not yield an improvement in the structural response.

Figures 3.26–3.29 show the results of the 2-D mesh refinement study. As can be seen, there are essentially no differences in the calculated structural responses for the "regular" and "refined" finite-element models. This implies that additional refinement in the compressive region of the 3-D model of the biaxial bend specimen will not improve the structural response, leaving boundary conditions and material property representation as candidates for further consideration with regard to explaining the observed differences between measured and calculated structural response.

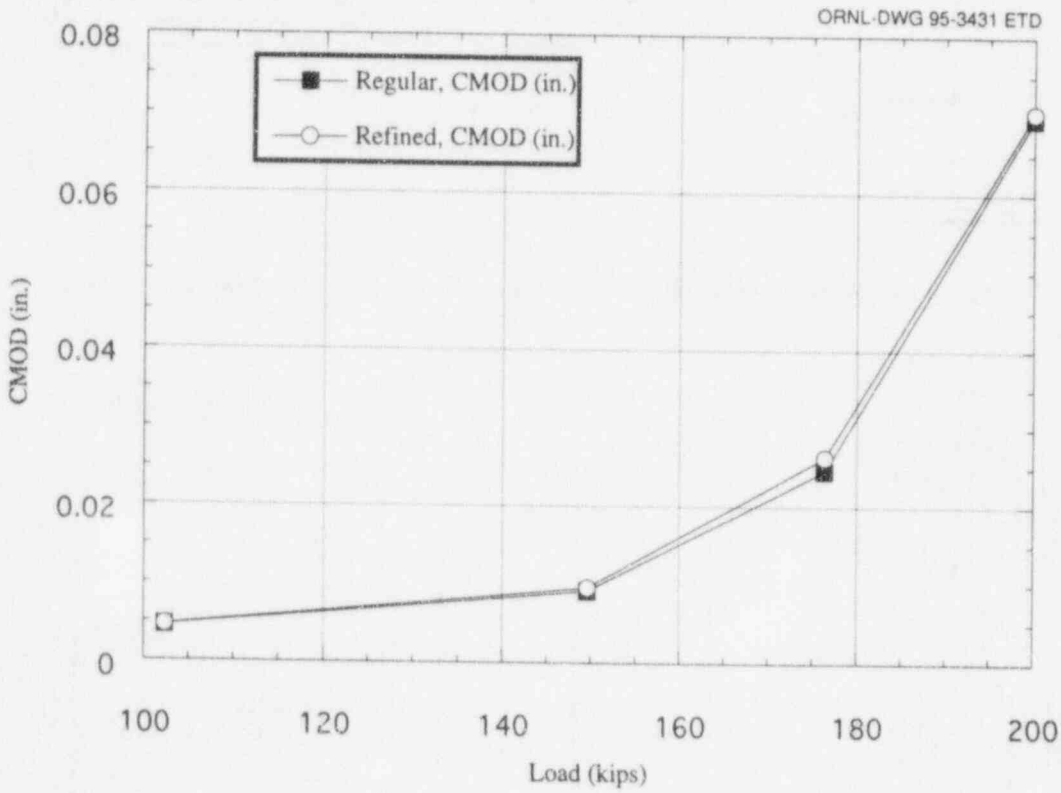

Figure 3.26 Effect of mesh refinement on CMOD

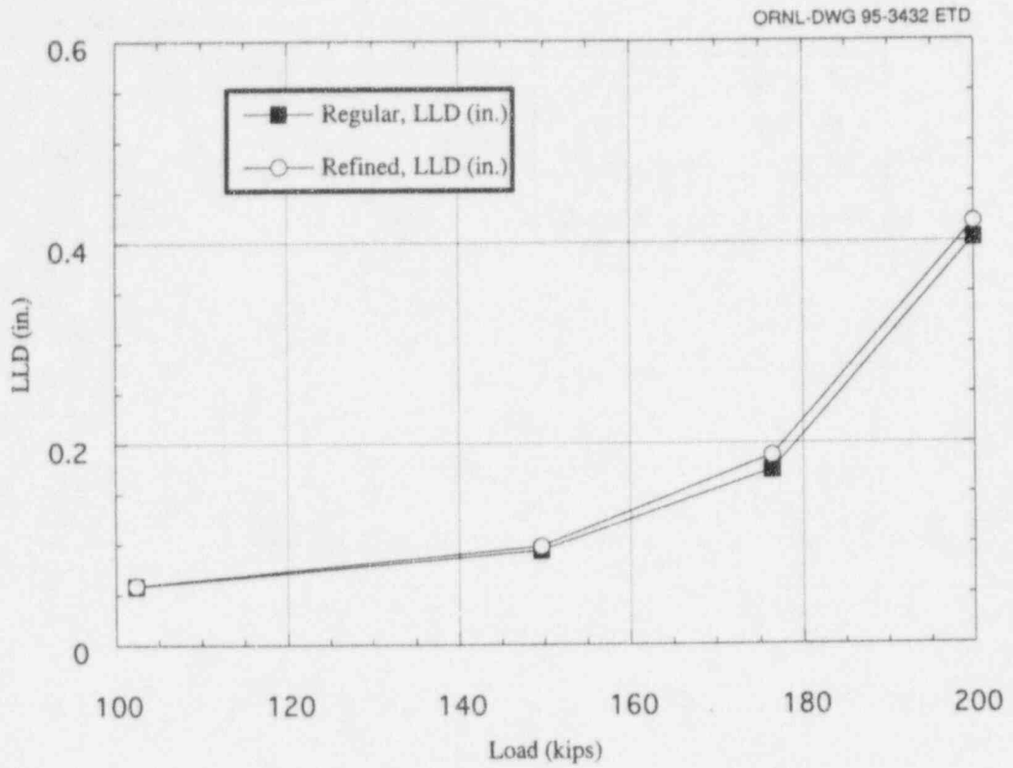

Figure 3.27 Effect of mesh refinement on LLD

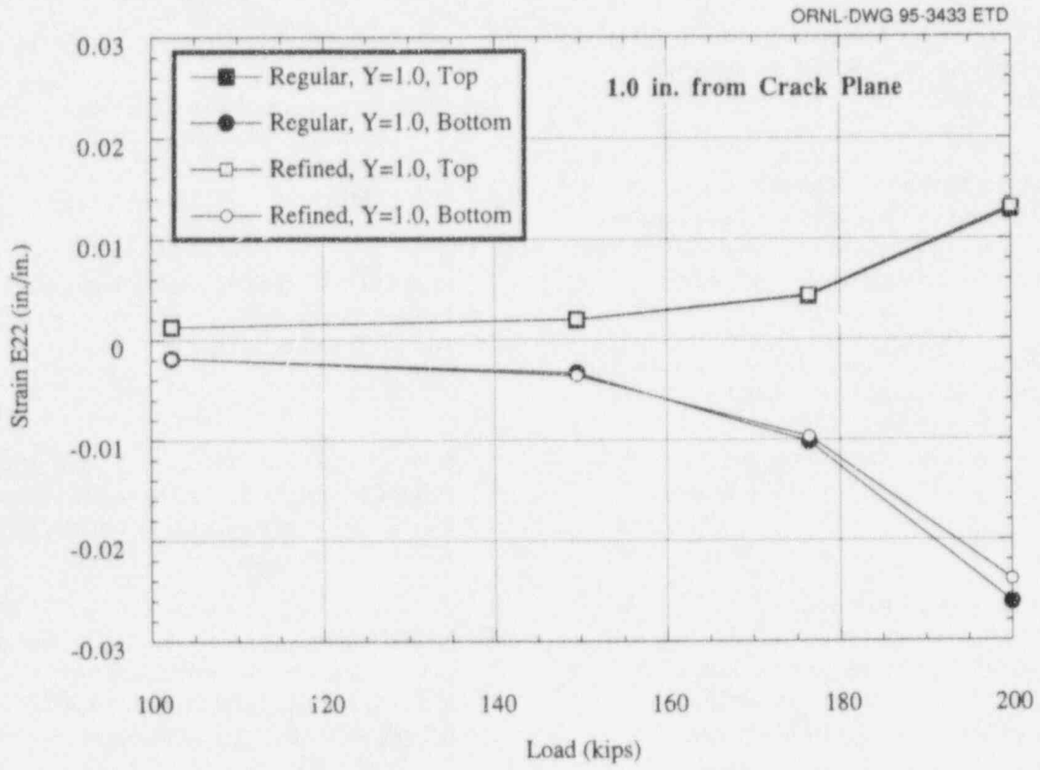

Figure 3.28 Effect of mesh refinement on longitudinal strain at distance of 1.0 in. from crack plane

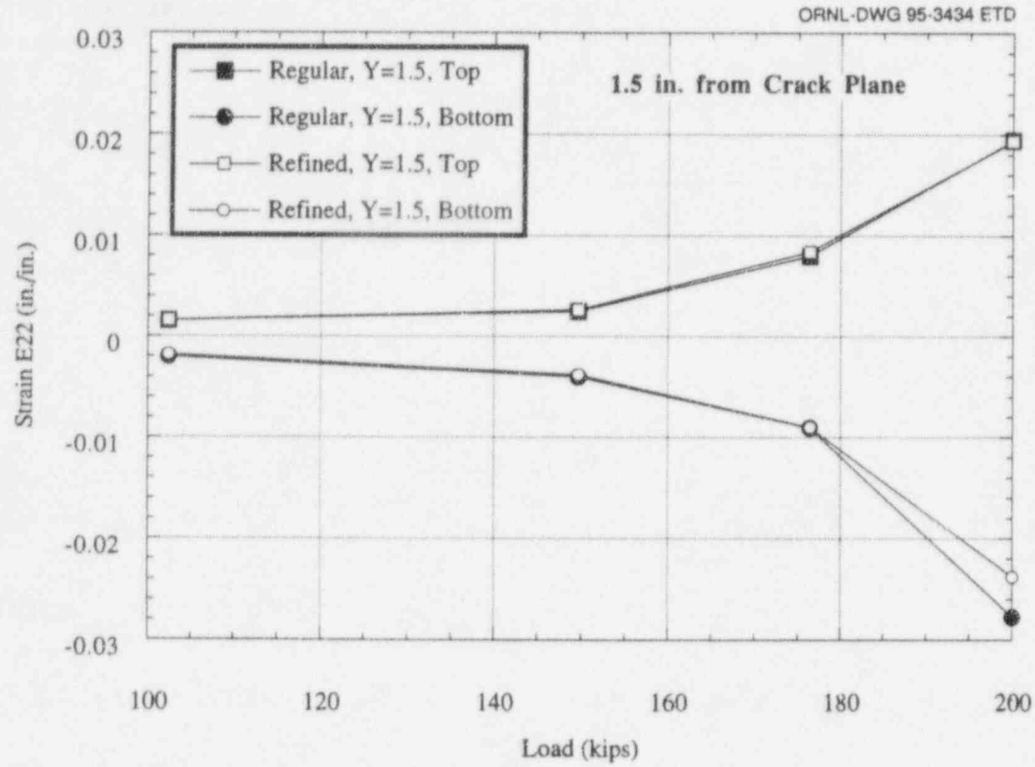

Figure 3.29 Effect of mesh refinement on longitudinal strain at distance of 1.5 in. from crack plane

References

1. W. Marshall et al., "An Assessment of the Integrity of PWR Pressure Vessels," UKAEA Study Group Reports, March 1982.

2. U S. Nuclear Regulatory Commission Regulatory Guide 1.154, "Format and Content of Plant-Specific Pressurized Thermal Shock Safety Analysis Reports for Pressurized Water Reactors," January 1987.*

3. R. D. Cheverton and D. G. Ball, Martin Marietta Energy Systems, Inc., Oak Ridge Natl. Lab., "Pressurized-Thermal-Shock Evaluation of the Calvert Cliffs Nuclear Power Plant," pp. 201–244, NUREG/CR-4022 (ORNL/TM-9408), September 1985.†

4. T. J. Theiss, D. K. M. Shum, and S. T. Rolfe, Martin Marietta Energy Systems, Inc., Oak Ridge Natl. Lab., "Experimental and Analytical Investigation of the Shallow-Flaw Effect in Reactor Pressure Vessels," NUREG/CR-5886 (ORNL/TM-12115), July 1992.†

5. G. R. Irwin and X. J. Zhang, University of Maryland for Oak Ridge Natl. Lab., "Gradient Study of a Large Weld Joining Two Forged A 508 Shells of the Midland Reactor Vessel," NUREG/CR-5867 (ORNL/Sub/79-7778/10), June 1992.†

6. W. E. Pennell et al, Martin Marietta Energy Systems, Inc., Oak Ridge Natl. Lab., "HSST Semiannual Progress Report for October 1993–March 1994," NUREG/CR-4219 (ORNL/TM/V11&N1), July 1995.†

7. N. P. O'Dowd and C. F. Shih, "Family of Crack-Tip Fields Characterized by a Triaxiality Parameter: Part I—Structure of Fields," *J. Mech. Phys. Solids* 39, 989–1015 (1991).‡

8. N. P. O'Dowd and C. F. Shih, "Family of Crack-tip Fields Characterized by a Triaxiality Parameter: Part II—Fracture Applications," *J. Mech. Phys. Solids* 40, 939–963 (1992).‡

9. N. P. O'Dowd and C. F. Shih, Naval Surface Warfare Center, "Two Parameter Fracture Mechanics: Theory and Applications," USNRC Report NUREG/CR-5958 (CDNSWC/SME-CR-16-92), February 1993.†

10. R. H. Dodds, T. L. Anderson, and M. T. Kirk, "A Framework to Correlate a/W Ratio Effects on Elastic-

Plastic Fracture Toughness (J_c)," *Int. J. Frac.* 48, 1–22 (1991).‡

11. T. L. Anderson and R. H. Dodds, "Specimen Size Requirements for Fracture Toughness Testing in the Ductile-Brittle Transition Region," *J. Test. Eval.* 19, 123–134 (1991).‡

12. R. H. Dodds, C. F. Shih, and T. L. Anderson, University of Illinois, "Continuum and Micromechanics Treatment of Constraint in Fracture," Report UILU-ENG-92-2014, November 1992.

13. "Rules for Construction of Nuclear Power Plant Components," Section III, *American Society of Mechanical Engineers Boiler and Pressure Vessel Code*, American Society of Mechanical Engineers, New York, 1989.

14. T. J. Theiss et al., Martin Marietta Energy Systems, Inc., Oak Ridge Natl. Lab., "Initial Results of the Influence of Biaxial Loading on Fracture Toughness," NUREG/CR-6036 (ORNL/TM-12349), June 1993.†

15. B. R. Bass et al., Martin Marietta Energy Systems, Inc., Oak Ridge Natl. Lab., "Biaxial Loading and Shallow-Flaw Effects on Crack-Tip Constraint and Fracture Toughness," NUREG/CR-6132 (ORNL/TM-12498), January 1994.†

16. *ABAQUS Theory Manual*, Version 5–3, Hibbit, Karlson, and Sorensen, Inc., Providence, RI, 1992.

17. M. T. Kirk and R. H. Dodds, Jr., University of Illinois, "J and CTOD Estimation Equations for Shallow Cracks in Single Edge Notch Bend Specimens," USNRC Report NUREG/CR-5969 (CDNSWC/SME-CR-17-92), July 1993.†

18. K. Wallin, "Statistical Aspects of Constraint with Emphasis on Testing and Analysis of Laboratory Specimens in the Transition Region," in *Constraint Effect in Fracture, ASTM STP 1171*, E. M. Hackett, K. H. Schwalbe, and R. H. Dodds, Eds. (American Society for Testing and Materials, 1993), pp. 264–288.‡

19. E. F. Rybicki and J. R. Shadley, University of Tulsa, "Residual Stress Evaluation of a K-Bevel Weld," ORNL/NRC/LTR-90/27, October 31, 1990.*

20. D. Moinereau et al., "Cleavage Fracture of Plates with Small Underclad Crack: Elements Presentation and Interpretation by Fracture Mechanics," PVP-Vol. 213/MPC-Vol. 32, *Pressure Vessel Integrity* (American Society for Mechanical Engineers, 1991).‡

21. D. Moinereau et al., "Cleavage Fracture of Specimens Containing an Underclad Crack," PVP-Vol. 223, *Pressure Vessel Fracture, Fatigue, and Life Management* (American Society for Mechanical Engineers, 1992).‡

22. D. Moinereau et al., "Behavior of Underclad Cracks in Reactor Pressure Vessels: Evaluation of Mechanical Analyses Used in French RPV Integrity Assessment by Cleavage Fracture Tests on Large Scale Plates," PVP-Vol. 250, *Pressure Vessel Integrity* (American Society for Mechanical Engineers, 1993).‡

23. J. A. Keeney, "French Clad Beam Analysis," Martin Marietta Energy Systems, Inc., Oak Ridge Natl. Lab., letter report, October 31, 1994.

24. B. R. Bass and J. W. Bryson, Martin Marietta Energy Systems, Inc., Oak Ridge Natl. Lab., "Applications of Energy Release Rate Techniques to Part-Through Cracks in Plates and Cylinders, Volume 1, ORMGEN-3D: A Finite Element Mesh Generator for 3-Dimensional Crack Geometries," USNRC Report NUREG/CR-2997/V1 (ORNL/TM-8527), December 1982.‡

25. W. E. Pennell, Martin Marietta Energy Systems, Inc., Oak Ridge Natl. Lab., "Report of Foreign Travel of W. E. Pennell, Engineering Technology Division," ORNL Foreign Trip Report ORNL/FTR-5102, August 24, 1994.

26. T. L. Dickson, Martin Marietta Energy Systems, Inc. Oak Ridge Natl. Lab., FAVOR: A Fracture Analysis Code for Nuclear Reactor Pressure Vessels, Release 9401, ORNL/NRC/LTR-94/01, February 1994.

27. F. M. Haggag, W. R. Corwin, and R. K. Nanstad, Martin Marietta Energy Systems, Inc., Oak Ridge Natl. Lab., "Irradiation Effects on Strength and Toughness of Three-Wire Series-Arc Stainless Steel Weld Overlay Cladding," NUREG/CR-5511 (ORNL/TM-11439), 1990.

---

*Copies are available from U.S. Government Printing Office, Washington, D.C. 20402. ATTN: Regulatory Guide Account.

†Available for purchase from the National Technical Information Service, Springfield, VA 22161.

‡Available from public technical libraries.

**Available in NRC PDR for inspection and copying for a fee.

4 Ductile to Cleavage Fracture-Mode Conversion

J. A. Keeney

4.1 Introduction

In the lower-to-upper transition regions of fracture toughness vs temperature behavior, RPV materials can exhibit considerable ductile flaw growth followed by a fracture-mode conversion to cleavage. The material failure by cleavage after some amount of ductile tearing can be regarded as a combined effect of a deterministic stable-tearing process (J-R curve) and a probabilistic cleavage process. Ignoring the presence of significant amounts of precleavage ductile tearing may lead to reduced accuracy in predicting cleavage initiation and resulting margins of safety. The fracture-mode conversion model is needed to provide a comprehensive fracture prediction methodology for RPVs.

During this report period, work continues on the characterization of precleavage tearing behavior and development of a fracture-mode conversion model to take into account any precleavage ductile tearing in fracture predictions.

4.2 Metallurgical Investigations

(R. K. Nanstad, D. J. Alexander, M. C. Rao)

Metallurgical investigations are being carried out based on existing test results to describe the behavior of precleavage ductile tearing and mode conversion to cleavage. The physical factors involved in this phenomenon have to be taken into account in the development of a fracture-mode conversion model. Also, different fractographic features are important depending on the model that is used (i.e., void and inclusion volume fraction for void formation and coalescence models). The steps of this investigation will include (1) identifying potential sources of fracture surfaces relevant to precleavage ductile tearing (i.e., ORNL); (2) securing the fracture surfaces that are from other sources besides ORNL; and (3) conducting examinations of the fracture surfaces. The initial metallurgical examination will (1) characterize the extent of crack-tip blunting prior to crack growth; (2) identify and characterize the microstructural features associated with microvoid formation and growth; (3) identify and characterize the microstructural features responsible for the mode conversion to cleavage; and (4) describe the relationship between the ductile crack morphology and the trigger points at mode conversion. The results from these investigations will be used in the development of the fracture-mode conversion model.

In preparation for detailed metallurgical examinations of previously tested materials, a review of the test results and scanning electron microscope (SEM) fractography results was conducted. The initial material to be studied is HSST Plate 13B, which was used for the shallow-flaw test program.[1] Several of shallow-flaw beam fracture surfaces have been examined fractographically to identify the amount of precleavage ductile tearing and the location of the cleavage origin. Pieces of this material have been retrieved and submitted for metallographic preparation. Moreover, the SEM photographs are being examined to determine void size and spacing on the fracture surfaces. The metallographic samples will be examined to characterize the nonmetallic inclusion population. Other materials, such as weld material from the full-thickness clad beams test program,[2] A 508 Class 2 forging steel (specially heat treated),[3] the low upper-shelf (LUS) weld from the Midland reactor vessel,[4] HSSI weld 73W,[5] and an A 508 class 3 forging steel used in an Metal Properties Council (MPC) round-robin program,[6] have also been retrieved for metallographic and fractographic examination.

Preliminary experiments were conducted with the University of California, Santa Barbara, to determine the feasibility of conducting fracture surface reconstruction on replicas of fracture toughness specimens (a 1T compact specimen from HSST Plate 13 was used). These tests indicated that the replicas can be imaged satisfactorily, and the calculated fracture toughness parameters determined from the fracture surface reconstruction (K_{Jc} values of 74 and 80 MPa$\sqrt{m}$) agreed very well with the value measured during the actual test (76 MPa$\sqrt{m}$).

4.3 Fracture-Mode Conversion Model Development (J. A. Keeney, B. R. Bass, J. G. Merkle)

4.3.1 Fracture Models

A fracture prediction model applicable to the transition toughness region is being developed that includes the effects of precleavage ductile tearing, as well as those due to large-scale yielding. During this report period, work continued on a letter report* that summarizes the fracture

*B. R. Bass et al., Martin Marietta Energy Systems, Inc., Oak Ridge Natl. Lab., "Development of Ductile Tearing-to-Cleavage Fracture-Mode-Conversion Models for Reactor Pressure Vessel Steels," ORNL/NRC/LTR-94/30, to be published.

models available in the technical literature and the additional developments that may be required to model ductile tearing-cleavage interaction in the transition temperature region.

Fracture toughness testing of ferritic steels in the ductile-to-brittle transition temperature region is characterized by complex interactions of several effects that complicate the interpretation of fracture toughness data for applications to engineering structures. Dodds, Tang, and Anderson[7] have provided a concise summary of these factors that occur on macrostructural and microstructural levels in the material. Specimens tested in the transition region consistently show large scatter in measured fracture toughness data and frequently exhibit varying amounts of stable ductile tearing prior to cleavage fracture. This scatter of toughness data in the transition region is usually associated with interactions between the mechanistic effects associated with crack-tip constraint and the statistical variability of microstructural features that promote cleavage fracture. Loss-of-constraint occurs with departure from SSY conditions and development of crack-tip plastic zones that interact with free boundaries and gross plasticity in the specimen or structure. Under these circumstances, crack-tip conditions cannot be characterized uniquely by a single-parameter model such as that represented by the intensity parameter J [or stress-intensity factor (K)].

Recent studies (described in the report) indicate that the onset of stable ductile tearing leads to stress fields ahead of the growing crack and crack-tip profiles that differ from those of a stationary crack. Also, stable ductile tearing exposes additional volumes of material to high stresses as the crack tip advances, which alters the sampling of potential cleavage initiation sites on the microstructural level. Measured fracture toughness values for specimens with prior stable crack growth can be significantly larger than those from specimens with no prior growth.

The strategy employed within the HSST Program to develop and validate a fracture model for predicting mode conversion in the transition temperature region is depicted in the logic diagram of Fig. 4.1. Five areas of investigation that contribute to the overall objective of achieving a validated model are detailed in the diagram:

- fracture and tearing toughness data
- cleavage-initiation models
- ductile-tearing models
- fractography and micromechanical features
- fracture-mode-conversion models

A brief discussion of each area of investigation is provided in the following sections.

4.3.1.1 Fracture and Tearing Toughness Data (Column 1—Logic Diagram)

Analyses of postulated PTS events in RPVs have demonstrated that the majority of predicted crack initiations originate from shallow flaws located on the inner surface of the vessel. Fracture-mechanics tests of SENB specimens,[1] coupled with detailed elastic-plastic finite-element analyses, have shown that shallow surface flaws exhibit an elevation of mean fracture toughness due partly to effects of constraint relaxation at the crack tip.[8] A limited biaxial toughness data base developed at ORNL[9] provides evidence of a significant out-of-plane biaxial loading effect on the cleavage fracture toughness of shallow flaws. These data show a decrease in the lower-bound shallow-flaw fracture toughness with increasing biaxiality (i.e., out-of-plane to in-plane) ratios. Both the SENB and biaxial toughness data play an important role in development and validation of dual-parameter correlations for predicting the mechanistic effects of constraint on fracture toughness. In particular, the ORNL-developed cruciform test specimen provides an effective mechanism for varying crack-tip constraint conditions to reveal cause and effect relationships between constraint and fracture toughness under multiaxial loading. It is anticipated that development of an associated cruciform testing technology for producing shallow-flaw J_R-curve data with variable crack-tip constraint will provide a similar contribution to performance assessments of ductile-tearing models.

4.3.1.2 Cleavage Initiation Model (Column 2—Logic Diagram)

A key element in the development of a fracture model to describe mode conversion in the transition temperature region is a viable model of cleavage initiation for stationary cracks (i.e., no stable tearing). Several dual-parameter methodologies have been introduced to quantify the effects of specimen geometry and loading conditions on crack-tip constraint. The existing dual-parameter methodologies include both stress-based and stress-strain-based characterizations of cleavage fracture. Both options are pursued in the logic diagram (Fig. 4.1) to ensure success in achieving a validated fracture model. Initial emphasis was placed on evaluating stress-based models through applications to uniaxial and biaxial shallow-flaw data. These applications demonstrated that the stress-based models cannot predict the effects of biaxial loading on shallow-flaw fracture toughness. This evaluation process will be repeated for (1) a strain-based fracture-toughness correlation[10,*]

*W. E. Pennell, B. R. Bass, J. W. Bryson, and W. J. McAfee, "An Interim Report on Shallow-Flaw Fracture Technology Development," 1995 ASME Pressure Vessel & Piping Conference, to be published.

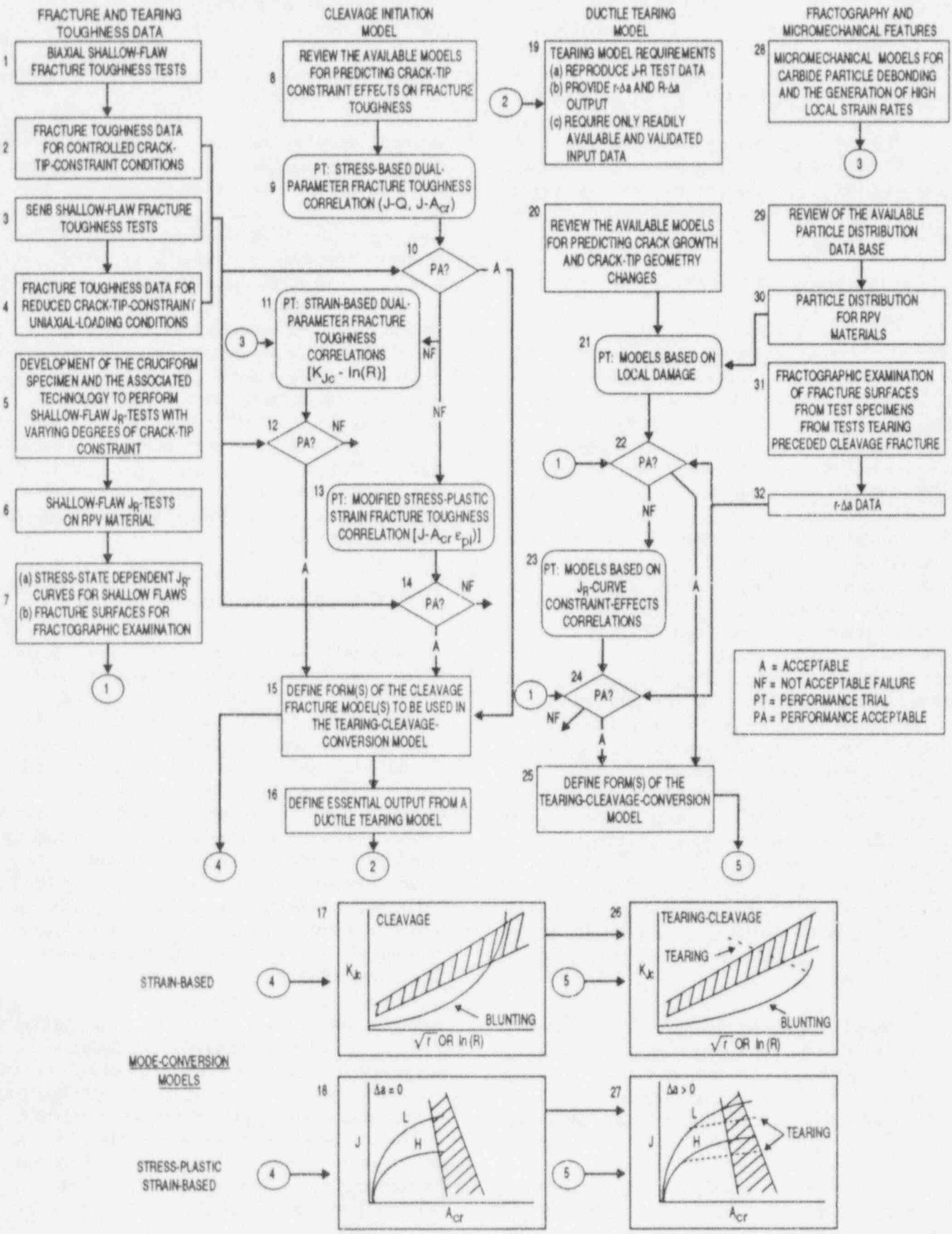

Figure 4.1 Logic diagram for development and validation of fracture model for mode conversion in transition temperature region

developed by ORNL and (2) a modified stress-plastic strain correlation that represents a generalization of the D-A stress-based scaling model.[11,12] A validated model for cleavage fracture must successfully predict the effects of both uniaxial and biaxial loading on shallow-flaw fracture toughness in the transition region of RPV steels. The outcome of these evaluations (to be conducted concurrently) will be the selection of a validated model for initiation of cleavage fracture. The verification process for the selected cleavage model will (1) demonstrate the practicality of the model and (2) identify the parameter(s) controlling cleavage initiation.

4.3.1.3 Ductile-Tearing Model (Column 3—Logic Diagram)

The ductile-tearing model provides output data that represent essential input to the selected cleavage model for predicting fracture initiation. Functional requirements for candidate ductile-tearing models include the following: (1) reproduce J_R-curve test data; (2) require only input data that are validated and readily available; and (3) provide output that includes crack-tip radius and crack plane plastic zone width as a function of crack growth. For the candidate ductile-tearing model, a clear understanding must be developed concerning the tearing mechanism that acts to trigger cleavage fracture. This understanding is crucial to the validation process indicated in the logic diagram of Fig. 4.1 for the tearing model. Initial evaluations will focus on constitutive formulations that describe progressive damage and material softening of the local crack-tip region. Validation studies of the local damage models will utilize (1) stress-state-dependent J_R-curve data obtained from biaxially loaded shallow-flaw cruciform specimens and (2) fractographic data from fracture surfaces of test specimens that exhibited ductile tearing prior to cleavage fracture. Should the local damage approach not prove to be viable, emphasis will shift to a model based on a parametric correlation of J_R-curve data with controlled changes in crack-tip constraint. These data will be obtained from cruciform specimen tests performed with varying biaxial load ratios. Output from these performance evaluations will be used to define the form of the ductile tearing-to-cleavage mode conversion model.

4.3.1.4 Fractography and Micromechanical Features (Column 4—Logic Diagram)

Determinations will be made concerning the availability of required data for the calibration and practical application of the ductile-tearing models. This includes relevant information concerning distributions of void nucleating particles in RPV steels. Fractographic examinations will be conducted on fracture surfaces of test specimens for which ductile tearing preceded initiation of cleavage fracture. These examinations will provide essential data for performance evaluations of candidate ductile tearing models and final validation checks on the proposed fracture-mode-conversion model.

4.3.1.5 Fracture-Mode Conversion Models (Bottom—Logic Diagram)

Performance assessments based on applications of the candidate cleavage and ductile tearing models to measured data from RPV steels will provide necessary input for defining the tearing-to-cleavage mode conversion model. One possible form of a model derived from an ORNL-developed strain-based correlation[10,*] of fracture toughness (K_{Jc}) vs natural logarithm of plastic zone width (R) is depicted at the bottom of Fig. 4.1. The plot illustrates schematically how the progression from crack-tip blunting to stable ductile tearing would affect predictions of mode conversion to cleavage for that particular correlation. A possible alternative fracture mode conversion model derived from a modified D-A stress-based methodology[11,12] is also depicted in Fig. 4.1. In this model, stable ductile tearing alters the path by which a critical area (A_{cr}) within a contour of critical maximum stress is achieved to predict fracture initiation in high- and low-constraint geometries.

4.3.2 Computer Program Development

The development and verification of the WARP-3D finite-element code[13] continues during this report period. This research code analyzes very large 3-D solid models encountered in fracture mechanics studies of crack-tip fields and ductile crack growth. Static and dynamic solution capabilities are constructed on the framework of a linear-preconditioned solver implemented in an element-by-element format. This software architecture dramatically reduces both the memory requirements and CPU time for very large, nonlinear solid models because formation of the assembled stiffness matrix is avoided. Models with 30,000 elements are routinely analyzed on supercomputers. Models with 10,000 eight-node brick elements are analyzed in-memory on desktop workstations. A robust kinematic formulation including finite strains and large displacements is adopted. Element technology is built around eight-node isoparametric solids with B-bar to prevent locking. Nonlinear constitutive material models include rate-independent and rate-dependent Mises plasticity with various isotropic/kinematic hardening rules and a fully implicit implementation of the Gurson hole growth model (with optional void nucleation and matrix viscoplasticity). An element death option facilitates removal of heavily damaged elements during crack growth analyses. J-integrals along crack fronts are evaluated using a domain-integral methodology.

New work focuses on verification of the crack growth procedures through comparisons with available plane-strain solutions and experimental J-R curves for A 533 B. Predictions of experimental J-R curves are very encouraging. Near-term plans include a port of the software to IBM Risc 6000 workstations/servers and to DEC-Alpha workstation/servers. A "discrete" crack growth capability based on growth at a critical CTOA at points along surface and through cracks is planned for later this year. A draft of the user guide will be available in November.

Discussions were held with R. Dodds regarding the material parameters needed for the WARP-3D finite-element program. In the simplified version of the model, the evolution equation for void nucleation is neglected, leaving only the void growth rate term $\dot{f}$, which is proportional to the triaxiality [i.e., $\dot{f} = (1 - f)\,\dot{\varepsilon}_p$]. To overcome the lack of an internal length scale in Gurson's model, an explicit length scale is introduced through a finite-width process zone defined ahead of the extending crack. The width of the zone (D) is the average void spacings of the major particles (to be determined by metallurgical examination). The specified parameters for the model include the flow properties of the material, the initial void volume fraction (porosity) f_o, and a porosity at microscopic rupture f_c.

References

1. T. J. Theiss, D. K. M. Shum, and S. T. Rolfe, Martin Marietta Energy Systems, Inc., Oak Ridge Natl. Lab., "Experimental and Analytical Investigation of the Shallow-Flaw Effect in Reactor Pressure Vessels," USNRC Report NUREG/CR-5886 (ORNL/TM-12115), July 1992.*

2. J. A. Keeney, B. R. Bass, W. J. McAfee, and S. K. Iskander, Martin Marietta Energy Systems, Inc., Oak Ridge Natl. Lab., "Preliminary Assessment of the Fracture Behavior of Weld Material in Full-Thickness Clad Beams," USNRC Report NUREG/CR-6228 (ORNL/TM-12735), October 1994.*

3. R. D. Cheverton et al., "Pressure Vessel Fracture Studies Pertaining to the PWR Thermal-Shock Issue: Experiments TSE-5, TSE-5A, and TSE-6," USNRC Report NUREG/CR-4249 (ORNL/TM-6163), June 1985.*

4. R. K. Nanstad, D. E. McCabe, R. L. Swain, and M. K. Miller, Martin Marietta Energy Systems, Inc., Oak Ridge Natl. Lab., "Chemical Composition and RT_{NDT}, Determinations for Midland Weld WF-70," USNRC Report NUREG/CR-5914 (ORNL/TM-12157), December 1992.*

5. R. K. Nanstad, F. M. Haggag, D. E. McCabe, S. K. Iskander, K. O. Bowman, and B. H. Menke, "Irradiation Effects on Fracture Toughness of Two High-Copper Submerged-Arc Welds, HSSI Series 5," USNRC Report NUREG/CR-5913 (ORNL/TM-12156/V1) October 1992.*

6. A. Van Der Sluys and M. Miglin, "Results of MPC/JSPS Cooperative Testing Program In the Brittle to Ductile Transition Region," in *Fracture Mechanics: Twenty-Fourth Symposium*, ASTM STP 1207, L. D. Landes, D. E. McCabe, and J. A. M. Boulet, Eds. (American Society for Testing and Materials Philadelphia, 1994).†

7. R. H. Dodds, Jr., M. Tang, and T. L. Anderson, Naval Surface Warfare Center, Carderock Division, "Numerical Modeling of Ductile Tearing Effects on Cleavage Fracture Toughness," USNRC Report NUREG/CR-6162 (UILU-ENG-93-2014, CARDIVNSWC-TR-61-CR-93/04), June 1994.*

8. T. J. Theiss et al., Martin Marietta Energy Systems, Inc., Oak Ridge Natl. Lab., "Initial Results of the Influence of Biaxial Loading on Fracture Toughness," USNRC Report NUREG/CR-6036 (ORNL/TM-12498), June 1993.*

9. B. R. Bass, J. W. Bryson, T. J. Theiss, and M C. Rao, Martin Marietta Energy Systems, Inc., Oak Ridge Natl. Lab., "Biaxial Loading and Shallow-Flaw Effects on Crack-Tip Constraint and Fracture Toughness," USNRC Report NUREG/CR-6132 (ORNL/TM-12498), January 1994.*

10. W. E. Pennell and T. L. Dickson, Martin Marietta Energy Systems Inc., Oak Ridge Natl. Lab., "Preliminary Assessment of the Effects of Biaxial Loading on Reactor Pressure Vessel Structural Integrity Assessment Technology," ORNL/NRC/LTR-95/3, January 1995.‡

11. T. L. Anderson and R. H. Dodds, "Specimen Size Requirements for Fracture Toughness Testing in the Ductile-Brittle Transition Region," *J. Test. Eval.* 19, 123–134 (1991).

12. R. H. Dodds, Jr., M. Tang, and T. L. Anderson, "Effects of Ductile Tearing on Cleavage Fracture Toughness in the Transition Region," in ASTM STP 1244, M. Kirk and A. Bakker, Eds., *Constraint Effects in Fracture: Theory and Applications* (American Society for Testing and Materials, Philadelphia, 1994).†

13. K. C. Koppenhoefer et al., "WARP-3D: Dynamic Nonlinear Analysis of Solids using a Preconditioned Conjugate Gradient Software Architecture," UILU-ENG-94-2017, University of Illinois at Urbana-Champaign, November 1994.

---

*Available for purchase from the National Technical Information Service, Springfield, VA 22161.
†Available from public technical libraries.
‡Available in NRC PDR for inspection and copying for a fee.

5 Fracture Analysis Methods Development and Applications

T. L. Dickson and J. W. Bryson

5.1 Stress-Intensity Factor Influence Coefficients

A continuing objective in this subtask is the development of a comprehensive data base of accurate validated stress-intensity influence coefficients (SIFICs). The SIFICs shall be generated for various inner-surface flaw geometries over the range of clad RPV geometries that envelopes the commercial PWR and boiling-water reactor (BWR) vessel geometries in the United States. The requirement for this SIFIC data base is to have the capability to produce SIFICs for any vessel geometry with an internal radius (R_i) to wall thickness (t) ratio such that $7 \leq (R_i/t) \leq 20$. The incorporation of this SIFIC data base into predictive fracture-mechanics codes, such as FAVOR, will facilitate the generation of accurate fracture-mechanics solutions for the range of flaw geometries as may be required in structural integrity assessments of any commercial U.S. PWR or BWR geometry.

During a previous reporting period, a data base of SIFICs was generated for infinite length axial and continuous 360° circumferential flaws that reside on the inner surface of an RPV.[1] These SIFICs were implemented into the initial release of FAVOR.[2] Also, during a previous reporting period, a data base of SIFICs was generated for axially oriented finite-length semielliptical inner-surface flaws with aspect ratios of 2, 6, and 10 (Ref. 3).

During the current reporting period, a letter report[4] was completed that presents a data base of SIFICs for circumferentially oriented finite-length semielliptical inner-surface flaws.[4] In Ref. 4, SIFICs are presented for circumferentially oriented finite-length semielliptical inner-surface flaws with aspect ratios [total crack length (2c) to crack depth (a)] of 2, 6, and 10. The SIFICs were computed for flaw depths in the range of $0.01 < a/t < 0.5$ with particular emphasis on shallow flaws ($a/t < 0.1$). SIFICs were also computed for two cladding thicknesses [t_{clad} = 3.96 mm (0.156 in.) and t_{clad} = 6.35 mm (0.25 in.)]. Reference 4 makes the recommendation that SIFICs for axially oriented finite-length semielliptical flaws may also be used for circumferential flaws for flaw depths up to 30% of the wall thickness without an appreciable loss of accuracy.

ABAQUS (Ref. 5), a nuclear quality assurance certified (NQA-1) multidimensional finite element code with fracture-mechanics capabilities, was used to generate the SIFICs. All of the SIFICs generated thus far have been for RPVs with an internal radius to wall thickness ratio (R_i/t) of 10. This geometry is prototypical of a large percentage of the commercial PWRs in the United States.[6] All of the SIFICS generated thus far have been implemented into FAVOR. The current development version of FAVOR has the capability to perform deterministic and probabilistic fracture analyses of RPVs (with $(R_i/t) = 10$), containing axially and/or circumferentially oriented inner-surface flaws with aspect ratios of 2, 6, 10, and infinity. FAVOR, which uses SIFICs and superposition, has been verified to produce K_I solutions that are within 1 to 2% of those obtained by direct ABAQUS 3-D finite element solutions.

The ABAQUS-generated SIFICs for circumferentially oriented semielliptical inner-surface flaw geometries were compared with similar results generated by other independent investigators. References 7 and 8 provide normalized K-solutions for inner surface circumferential surface flaws in cylindrical vessels subjected to remote tension loading. Direct comparisons of these solutions with the HSST-generated SIFICs can be obtained by multiplying the HSST values for uniform pressure loading by $\sqrt{Q}$ where the shape factor Q is the square of the complete elliptical integral of the second kind. The shape factor for an elliptical crack is approximated by $Q = 1 + 1.464\,(a/c)^{1.65}$, where a is the crack depth and 2c is the crack length.

Figure 5.1 compares the HSST-generated SIFICs to those generated by Raju and Newman[7] at various positions around the crack front of circumferentially oriented 2:1 semielliptical flaws of depth (a/W) = 0.2 and 0.5. Raju and Newman provide SIFICs for remote tension loading at the free surface and maximum depth locations only, that is, angular positions of 0 and 90°, respectively.

Figure 5.2 compares the HSST-generated SIFICs to those generated by Kumar et al., in Ref. 8, which employed a line spring model implemented in the ADINA[9] finite-element code. The results shown are for a circumferentially oriented flaw 1.7 in. in depth with an aspect ratio of 6:1.

As illustrated, the HSST-generated SIFICs were in very good agreement with those previously generated by other investigators, thus providing mutual validation.

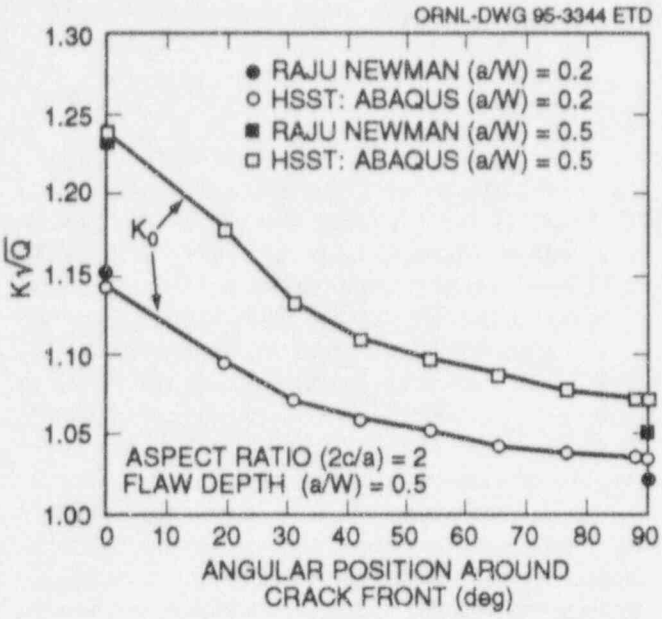

Figure 5.1 Comparison of HSST-generated SIFICs with those of Raju-Newman for circumferentially oriented semielliptical 2:1 flaws of depth (a/W) = 0.2 and 0.5

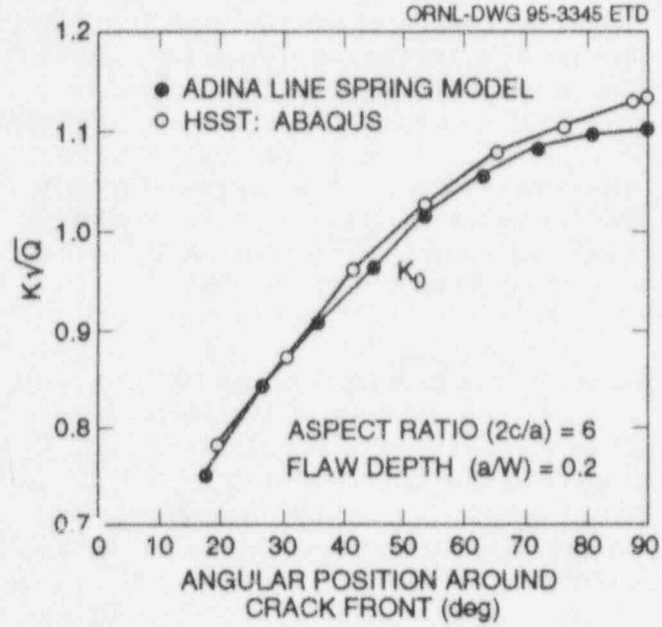

Figure 5.2 Comparison of HSST-generated SIFICs with those of an ADINA line-spring model for circumferentially oriented semielliptical 6:1 flaw of depth (a/W) = 0.2

In future reporting periods, SIFICs will be generated for axially and circumferentially oriented finite-length semielliptical inner-surface flaw geometries for a clad RPV geometry with an (R_i/t) ratio of 20. This geometry is prototypical of a large percentage of the commercial BWRs in the United States.[6] SIFICs will also be generated for a sufficient number of other (R_i/t) ratios such that accurate interpolating functions can be derived to generate accurate K_I solutions for vessel geometries with $7 < (R_i/t) < 20$.

5.2 FAVOR

Two documents were completed to satisfy quality assurance (QA) requirements of the FAVOR computer code. These documents satisfy requirements specified in the ASME NQA-2a-1990 Addenda to ASME NQA-2-1989 Edition, Quality Assurance Requirements for Nuclear Facility Applications, Part 2.7, Quality Assurance Requirements of Computer Software for Nuclear Facility Applications. These two documents and their objectives are as follows:

Software Configuration Control and Problem Reporting/ Corrective Action Plan for the FAVOR Computer Program—This document specifies the procedures implemented to control future modifications, releases, and distribution of FAVOR.

FAVOR—Verification and Validation Documentation—This document specifies a set of benchmark validation problems to verify the correctness of the various mathematical models (thermal analysis, stress analysis, and K_I analysis) as implemented into FAVOR. Validation is accomplished by comparing various FAVOR-generated thermal, stress, and K_I solutions to direct ABAQUS 3-D solutions. Prior to the establishment of a new baseline configuration (future releases of FAVOR), these validation problems will be executed to check the previously established benchmarks. This ensures that no errors are introduced into the code during modification(s).

The Computing Applications Division at ORNL conducted a QA surveillance of FAVOR. A surveillance is an act of monitoring or observing whether an activity conforms to specified requirements. The scope of the QA surveillance assessed the implementation of the QA plan primarily in three specific areas: (1) configuration control, (2) user documentation, and (3) verification and validation. The findings of the QA surveillance were satisfactory in 24 out of 25 categories examined. Remedial action has been taken to correct the noted deficiency.

5.3 PTS Applications

The NRC plans to revise Regulatory Guide 1.154 (Ref. 10). The objective is to publish a revised Regulatory Guide 1.154 that reflects the fracture technology developed in the

last decade and lessons learned from the analysis of the Yankee Rowe nuclear plant. Technical bases must be developed to support this revision. Specific aspects of the PTS problem that are being revisited include thermal-hydraulics, human factors, probabilistic risk assessment, and fracture-mechanics analyses. This effort involves interaction between personnel from Idaho (thermal-hydraulics), Sandia (probabilistic risk assessment), and Oak Ridge (fracture mechanics) national laboratories. The work scope is divided into two phases: Phase I is the development of technical bases and methodologies; and Phase II will be a demonstration analysis, i.e., a coordinated effort between the various laboratories to integrate and apply the revised technical bases and methodologies on a plant-specific test case(s).

During this reporting period, PFM sensitivity analyses were performed to determine the potential impact of various modifications to the fracture-mechanics model currently specified in Regulatory Guide 1.154. Specific fracture-mechanics model assumptions examined included flaw geometry, the effect of clad, flaw density, fracture initiation, and arrest toughness. The current development version of FAVOR was used to perform these fracture analyses. A draft of an NRC letter report (ORNL/NRC/LTR-94/31) entitled "Potential Modifications to the Fracture Mechanics Model in Regulatory Guide 1.154" was submitted to the NRC. This report summarizes the assumptions, results, and conclusions of the fracture-mechanics model scoping analyses. This document is currently undergoing prepublication review.

Based on previous experience, PFM sensitivity analysis results are dependent, to some extent, on the severity and characteristics of the transient. PFM analysis results are also dependent on the degree of vessel embrittlement (RT_{NDT}). Therefore, PFM sensitivity analyses were performed for three transients of varying severity and characteristic, each over a range of embrittlement. The results are reported at the PTS screening criteria; that is, $RT_{NDTs} + 2\sigma = 270°F$ for axially oriented welds and plates and 300°F for circumferentially oriented flaws. RT_{NDTs} is the best estimate value of RT_{NDT} at the inner surface of the vessel; 2σ was assumed to be 59°F in these analyses. Two of the transients (transients 1 and 2) are characterized by a stylized exponentially decaying coolant temperature and a constant pressure, analogous to the transient definitions utilized in the NRC/EPRI cosponsored PTS benchmarking exercise.* The following formulation is used for the exponentially decaying thermal transient:

$$T(t) = T_f + (T_i - T_f) \exp(-\beta t) \qquad (5.1)$$

where

$T(t)$ = coolant temperature at time t,
T_i = coolant temperature at time = 0,
T_f = final coolant temperature,
β = exponential decay constant (min^{-1}).

The final coolant temperatures were 150 and 200°F, respectively, for transients 1 and 2. β, the exponential decay constant, was 0.15 min^{-1} for transients 1 and 2. The pressure was constant and equal to 1 ksi for transients 1 and 2. The third transient analyzed in this scoping analysis was a transient characterized by repressurization. The initial temperature was 550°F for all three transients. The heat transfer coefficient was assumed to be constant and equal to 500 $Btu/h \cdot ft^2 \cdot °F$ for all transients.

The range of sensitivity, analyzed for all three transients, evaluated at the applicable PTS screening criterion for axially and circumferentially oriented flaws are tabulated in Tables 5.1 and 5.2, respectively. Sensitivity is measured as the ratio of the P(FIE) for the current Regulatory Guide 1.154 fracture-mechanics model to P(FIE) for the modified model.

There was a continuing interaction with personnel from Idaho (thermal-hydraulics) and Sandia (probabilistic risk assessment) National Laboratories regarding the development of a methodology for performing a detailed PFM uncertainty analysis.

*B. A. Bishop, Draft for Review: Benchmarking of Probabilistic Fracture Mechanics Analyses of Reactor Vessels Subjected to Pressurized Thermal Shock (PTS) Loading, EPRI Research Project 2975-5, March 1993.

Table 5.1 Ranked PTS sensitivities for axial flaws at $RT_{NDTs} + 2\sigma = 270°F$

	Range of sensitivity, base model/modified model
Flaw density	= N for N < 50; < N for N > 50 (where N = flaw density)
Expanded K_{Ic} data base	5.9–7.5[a]
Clad plasticity	
Clad yield = 50 ksi	1.1–5.9
Clad yield = 65 ksi	1.0–2.2
Flaw geometry (finite-length semielliptical flaws)	1.1–3.5
Ignoring clad as distinct thermoelastic region	1.1–3.6
Expanded K_{Ia} data base	1.1–1.3
Flaw (2-m-length) for arrest and reinitiation	1.03–1.08
Dynamic effects	~2[b]

[a]Ratio of conditional probability of initiation P(I|E); others are ratio of conditional probability of failure P(F|E).
[b]Based on results of previous study reported in Ref. 11.

Table 5.2 Ranked PTS sensitivities for circumferential flaws at $RT_{NDTs} + 2\sigma = 300°F$

	Range of sensitivity, base model/modified model
Flaw density	= N for N < 50; < N for N > 50 (where N = flaw density)
Expanded K_{Ic} data base	5.9–587[a]
Clad plasticity	
Clad yield = 50 ksi	1.1–7.1
Clad yield = 65 ksi	1.1–2.7
Flaw geometry (finite-length semielliptical flaws)	1.0–3.0
Ignoring clad as distinct thermoelastic region	1.1–2.6
Expanded K_{Ia} data base	1.2–2.0

[a]Ratio of conditional probability of initiation P(I|E); others are ratio of conditional probability of failure P(F|E).

References

1. J. W. Bryson and T. L. Dickson, Martin Marietta Energy Systems, Inc., Oak Ridge Natl. Lab., "Stress Intensity Factor Influence Coefficients for Axial and Circumferential Flaws In Reactor Pressure Vessels," *Pressure Vessel Integrity*, *PVP*-Vol. 250, pp. 77–88, ASME 1993.*

2. T. L. Dickson, Martin Marietta Energy Systems, Inc., Oak Ridge Natl. Lab., "FAVOR: A Fracture Analysis Code for Nuclear Reactor Pressure Vessels, Release 9401," ORNL/NRC/LTR/94/1, February 1994.

3. J. A. Keeney and T. L. Dickson, Martin Marietta Energy Systems, Inc., Oak Ridge Natl. Lab., "Stress-Intensity-Factor Influence Coefficients for Axially Oriented Semielliptical Inner-Surface Flaws in Clad Vessels ($R_i/t = 10$)," ORNL/NRC/LTR-93/33, April 1994.†

4. J. W. Bryson and T. L. Dickson, Martin Marietta Energy Systems, Inc., Oak Ridge Natl. Lab., "Stress-Intensity-Factor Influence Coefficients for Circumferentially Oriented Semielliptical Inner-Surface Flaws in Clad Vessels ($R_i/t = 10$)," ORNL/NRC/LTR-94/8, April 1994.†

5. *ABAQUS User Manual*, Hibbit, Karlsson & Sorenson, Inc., Providence, Rhode Island, 1991.

6. ASME Section XI, Task Group on Reactor Vessel Integrity Requirements, "White Paper on Reactor Vessel Integrity Requirements for Level A and B Conditions," EPRI Project 2975-13, January 1993.

7. I. S. Raju and J. C. Newman, "Stress Intensity Factors for Circumferential Surface Cracks in Pipes and Rods Under Tension and Bending Loads," *Fracture Mechanics: Seventeenth Volume*, ASTM STP 9056 (American Society for Testing and Materials, Philadelphia, 1986), pp. 789–805.*

8. V. Kumar, M. D. Germa, and B. I. Schumacher, "Elastic Surface Crack Analysis Using a Shell Line-Spring Model," Advances in Elastic-Plastic Fracture Analysis, EPRI NP-3607, Electric Power Research Institute, August 1984.

9. K. J. Bathe, "ADINA—A Finite Element Program for Automatic Dynamic Incremental; Nonlinear Analysis," Report 82448-1, Massachusetts Institute of Technology, December 1978.

10. U.S. Nuclear Regulatory Commission, Regulatory Guide 1.154, "Format and Content of Plant-Specific Pressurized Thermal Shock Safety Analysis Reports for Pressurized Water Reactors," 1987.‡

11. T. L. Dickson, Martin Marietta Energy Systems, Inc., Oak Ridge Natl. Lab., "Impact of Dynamic Crack Arrest on Fracture Analyses of Reactor Pressure Vessels Subjected to Pressurized-Thermal Shock," ORNL/NRC/LTR-93/35, May 1994.†

---

*Available from public technical libraries.
†Available in NRC PDR for inspection and copying for a fee.
‡Copies are available from U.S. Government Printing Office, Washington, D.C. 20402. ATTN: Regulatory Guide Account.

6 Material Property Data and Test Methods

D. E. McCabe and R. K. Nanstad

6.1 J-R Curve Evaluations of A 302 Grade B (Modified) Steel

(D. E. McCabe)

A previous study with one particular heat of A 302 grade B steel that had LUS energy in the transverse, TL, orientation showed decreasing J-R curve with increased specimen size. Compact specimens ranged in size from 1/2T to 6T, and the J-R curve fracture toughness decreased consistently with increased specimen size. The usual specimen size characteristic is to show increased J-R curve toughness with increased specimen size.

All the Charpy impact, tensile, drop-weight, and fracture toughness tests have been completed. This includes over 230 compact specimen tests for J-R curves on seven heats of modified A 302 grade B steel with three test temperatures, three test directions, and three specimen orientations. The material characterization included full chemistries, tensile tests, metallographic examinations, and Charpy transition temperature curves. A good portion of this information has been compiled in a letter report, "Presentation of Preliminary J-R Curve Fracture Toughness Data on Modified A 302 Grade B Steel."[1] For J-R curve evaluations, J_{Ic} was used as determined by ASTM test standard E813-81 and the J-R curve toughness at the point of crossing the second exclusion line. These values can be compared to representative J-R curve toughness for A 533 grade B or A 508 class 2 steels in Table 6.1. The typical J-R curve was calculated from the Eason et al. multivariable modeling work.[2] The two grades of material are compared at four selected levels of upper-shelf CVN toughness. It appears that the modified A 302 grade B steel is somewhat inferior compared to the more recently produced grades of pressure vessel steel.

A wealth of new information has been created by this project, and the ongoing work plan is to thoroughly evaluate this information for presentation in an NRC report.

6.2 Ductile Fracture Toughness Under Nonisothermal Conditions

(D. E. McCabe)

This project has been initiated to explain why J-R curves determined isothermally on the 2.25Cr-1Mo steel used for the PTSE-2 experiment did not correctly characterize the ductile tearing observed in the PTSE-2 test vessel. It has been hypothesized that the J-R curve under nonisothermal conditions cannot be accurately estimated from a set of J-R curves generated under isothermal conditions.

The experimental plan was developed to generate J-R curves in simulation of the thermal gradient experienced by the PTSE-2 vessel where there was a 100°C temperature drop over about 5 mm (0.2 in.) of slow-stable crack propagation. Consideration has been given to (1) the design of a specimen that would be tested with a stable temperature gradient in the ligament ahead of the crack tip and (2) the use of standard specimens in which the J-R curve would be obtained by loading the specimen incrementally at different isothermal temperatures (i.e., the temperature of the specimen would be changed at regular intervals during the test while the load is held constant). The latter technique is the most likely candidate, and the first phase of tests will be completed prior to the end of CY 1994.

6.3 Dynamic Fracture Toughness

(R. K. Nanstad)

A specification, "Dynamic Fracture Initiation Fracture Toughness Testing of a Reactor Pressure Vessel Steel," for conduct of dynamic fracture toughness testing was prepared under Task H.2. Recommendations regarding material characterization testing were prepared for inclusion in that specification. The material characterization testing will include Charpy impact, tensile, drop-weight, and quasi-static fracture toughness testing. Negotiations for placement of a subcontract for performance of the dynamic fracture toughness testing were completed. A subcontract was placed with the CDNSWC, Annapolis, Maryland. A preliminary specimen layout plan was developed by CDNSWC, and based on that plan, a section of HSST Plate 14 was identified for shipment to Annapolis.

Table 6.1 Comparison of J-R toughness values at 1.5-mm (0.06-in.) crack growth point (models for A 533 grade B versus experimental for A 302 grade B)

Upper-shelf energy [J(ft-lb)]	Test temperature [°C(°F)]	Multivariable model predictions for A 533 B base metal J-R [kJ/m^2(in.-lb/in.^{2})]	Selected A 302 grade B test data, J-R at 1.5 mm (0.06 in.) Δa_p			
			1/2T [kJ/m^2(in.-lb/in.^{2})]	1T [kJ/m^2(in.-lb/in.^{2})]	2T [kJ/m^2(in.-lb/in.^{2})]	4T [kJ/m^2(in.-lb/in.^{2})]
89 (65)	93 (180)	464 (2650)	236 (1350)	236 (1350)	236 (1350)	
	204 (400)	298 (1700)	184 (1050)			
	288 (550)	228 (1300)	140 (800)	148 (850)	131 (750)	
130 (95)	93 (180)	607 (3470)	385 (2200)	438 (2500)	508 (2900)	499 (2850)
	204 (400)	385 (2200)	236 (1350)	298 (1700)	341 (1950)	
	288 (550)	298 (1700)	192 (1100)	315 (1600)	324 (1850)	324 (1850)
171 (125)	93 (180)	718 (4100)	420 (2400)	560 (3200)	648 (3700)	455 (2600)
	204 (400)	472 (2700)	358 (2050)	315 (1800)	368 (2100)	
	288 (550)	385 (2200)	324 (1850)	298 (1700)	341 (1950)	
219 (160)	93 (180)	840 (4800)	674 (3850)	621 (3550)	612 (3500)	
	204 (400)	560 (3200)	525 (3000)	359 (2050)	455 (2600)	
	288 (550)	420 (2400)	306 (1750)	394 (2250)	464 (2650)	

References

1. D. E. McCabe, R. K. Nanstad, R. L. Swain, and E. T. Manneschmidt, Martin Marietta Energy Systems, Inc., Oak Ridge Natl. Lab., "Presentation of Preliminary J-R Curve Fracture Toughness Data on Modified A 302 Grade B Steel," ORNL/NRC/LTR-94/29, October 1994.*

2. E. D. Eason, J. E. Wright, and E. E. Nelson, Modeling and Computing Services, "Multivariable Modeling of Pressure Vessel and Piping J-R Data," USNRC Report NUREG/CR-5729 (MCS 910401), May 1991.†

*Available in NRC PDR for inspection and copying for a fee.
†Available for purchase from the National Technical Information Service, Springfield, VA 22161.

7 Integration of Results

J. G. Merkle

7.1 Technical Review and Comments on Russian Warm-Prestress Technical Basis Documents

This report responds to a request from the NRC* for a technical review of and comments on a translated Russian report[1] and accompanying documents concerning a proposed WPS procedure for increasing the effective fracture toughness of embrittled materials in Russian and East European PWR vessels. Related documents and an open literature paper[2] were received with Ref. 1. These additional documents contained valuable supplementary information, and they were also reviewed. These documents presume a general knowledge of the Russian civilian nuclear power program and its associated fracture safety regulations. Figure 7.1 shows the locations of nuclear power plants in Eastern Europe and the former Soviet Union.[3] A concise summary of the current Russian approach to RPV integrity is given in Appendix D to Ref. 4. The Russian procedures are similar in concept to those of the United States, but differ somewhat in detail. Their reference temperature, T_k, is based on Charpy impact energy data and room temperature yield stress. They use material-specific reference toughness curves, using only K_{Ic} and apparently not K_{IR} or K_{Ia}. Their reference flaw has a depth-to-length ratio of one-third instead of one-sixth, and their safety factor scheme is different from that used in the United States.[4]

The vessel embrittlement problem facing the Russians is worse than that of the United States. Supposedly because their vessels were designed to be transported through existing railroad tunnels, they have smaller diameters and less water between the core and the vessel wall than U.S. vessels. Consequently, their fluences are as much as ten times those of U.S. vessels.† Also, because of the phosphorous and copper contents, annealing is only partially effective in reducing embrittlement.† Consequently, the Russians are seeking additional ways of recovering lost safety margins, and in this context they are considering a combination of annealing and WPS.‡ In their efforts to develop a reliable toughness restoration scheme, the Russians are actively seeking technical and financial support, particularly in Germany and in the United Kingdom where both technical expertise and similar problems exist.

7.2 Nature of the Procedure

As a type of inducement, the Russians have patented their proposed procedure‡ and will disclose its details only in exchange for financial (or perhaps significant technical) support. However, it may be possible to surmise the nature of the procedure from the given information and the nature of the problem. To warm prestress relatively shallow inside surface flaws against the effects of thermal shock, stresses higher than would be produced by a thermal shock in service must be produced in the region of the flaws. These stresses will probably have to exceed the yield stress, and they will have to be of equal magnitude in both the axial and circumferential directions in order to match potential thermal stresses. However, permanent distortions of the vessel must be avoided. Therefore, a relatively steep thermal gradient near the vessel inside surface is likely to be the means for developing the required near-inside surface stress, because by this means gross distortion can be avoided. The thermal gradient would likely be produced at the beginning of cooling down from annealing to minimize the chances of inducing fractures. If this is the WPS procedure (the Russians use the acronym PTL for preliminary thermomechanical loading), then it may be an adaptation of the U.K. technique for spray cooling the inside surface of a warm precracked spinning test cylinder. WPS only provides protection against fracture due to flaws that exist at the time of its application. Thus, if there is a problem of delayed cracking due to any cause, such as stress corrosion cracking, WPS would not be a remedy.

7.3 Issues Identified

The following significant issues have been identified concerning the proposed annealing-WPS procedures.

A. Concepts

1. Understanding the fracture-mechanics concepts and empirical results involved

*Letter from S. N. Malik, NRC, to John G. Merkle, ORNL, April 14, 1994.

†V. V. Pokrovsky, "Warm Prestressing, A Promising Method for Justifying and Extending the Service Life Under Radiation Conditions, Also for Increasing the Safety of PWR Vessels," probable date, November 1993.

‡A. Hofler, J. Sievers, and V. Pokrovsky, minutes of a meeting on warm prestressing, held on November 3–5, 1993, at GRS in Köln, Germany.

Figure 7.1 Locations of nuclear power plants in Eastern Europe and the former Soviet Union

2. Method of WPS for small flaws
3. Size and geometry effects on fracture toughness

B. Physical mechanisms of WPS

1. Effects of unloading and reloading
2. Effects of crack-tip blunting
3. Effects of residual stresses

C. Limitations

1. Strain aging
2. Variability of toughness
3. Effect of crack growth

D. Regulatory applicability

7.4 Fracture-Mechanics Concepts

The WPS phenomenon is by no means completely understood. A general consensus probably exists that plastic strains near the crack tip must be increasing with increasing load point displacement at the instant of fracture. Beyond that, theories diverge, and the Russians are using two different theories that do not completely agree. The analysis procedure described in the first part of Ref. 1 was developed by Chell[5] at the U.K., Central Electricity Generating Board (CEGB). This analysis procedure is based on the strip yield model that represents the crack-tip plastic zone as a line of yielding of zero thickness ahead of the crack tip. Because the assumed plastic zone has no volume, all displacements are elastic, and incremental superposition is still valid.[6] The J-integral is used as the fracture criterion. For the ideally plastic (no strain hardening) strip yield plastic zone, the J-integral is path dependent. Its value around the active plastic zone at fracture is taken as the fracture criterion and equated in the usual way to $K_{Ic}^2(1-\nu^2)/E$. SSY (a plastic zone size small compared to the crack depth) is assumed. Residual stresses play an important role in this analysis method.[6] Regarding details, Ref. 1 appears to assume that complete reverse yielding occurs during each incremental load decrease following WPS. In fact, reverse yielding only occurs immediately for the first incremental load decrease and then for each subsequent load decrease only after the plastic zone for that load increment becomes longer than the plastic zone for the previous load decrease.

Using relatively small- and medium-sized specimens, the Russians performed WPS experiments[2] from which they concluded that fracture at a lower temperature occurs when the crack-tip opening displacement (CTOD) begins to exceed the maximum previous value developed at the warmer temperature of WPS. This conclusion implies that if a specimen is simply cooled without being unloaded, it will fail at the slightest load increase. Experimentally, this does not always appear to be the case. The equation for calculating CTOD when applying the Russian CTOD hypothesis is one developed by McMeeking.[7]

Given the incomplete understanding of the detailed WPS mechanisms, the HSST Program recently undertook a preliminary analytical investigation of the phenomenon using 2- and 3-D elastic-plastic finite-element analyses. The results are described in a draft report.* Analyses of inside surface cracks in RPVs subject to PTS loading patterns indicate minimal loss of constraint while K_I is initially increasing, but net degrees of constraint loss during unloading and reloading that increase as the time of reloading increases. Analyses of separately modeled crack-tip regions subject to PTS load patterns involving loading, unloading, and reloading indicate net degrees of constraint loss that tend to decrease as the amount of unloading increases. Due to cyclic loading and 3-D effects, constraint changes vary with distance from the crack tip, unlike the uniform constraint changes indicated by 2-D analyses for monotonically increasing loads. Consequently, 3-D analyses are expected to be required to properly model constraint losses that occur in laboratory specimens, especially under cyclic loading.* Such analyses can reasonably be expected to produce an improved understanding of WPS.

7.5 WPS Method

The incompleteness of information on the Russian-proposed WPS procedure has already been discussed. No additional information is presently available.

7.6 Size and Geometry Effects on Fracture Toughness

Size and geometry effects on fracture toughness measured with laboratory specimens for three different steels were investigated by the Russians and the results reported in Ref. 2. The effects of size were found to be material dependent as described in Ref. 2. These results may appear contrary to current theories, but they could be caused by differences in grain size,[8] the values of which were not reported in Ref. 2. The issue of size effects in this case is slightly complicated by the absence of information in Refs. 1 or 2 about how fracture toughness has been calculated from small specimen data. Therefore, we do not know definitely whether the observed size effects result from the

*D. K. M. Shum, Martin Marietta Energy Systems, Inc., Oak Ridge Natl. Lab., "Preliminary Investigation on the Inclusion of Warm Prestress Effects in Fracture-Margin Assessment of Reactor Pressure Vessels," NUREG/CR-5946 (ORNL/TM-12236), draft dated December 3, 1993.

method of calculation or are true material and geometry effects. The fundamental problem with using small specimens to represent cyclic loading effects on fracture toughness for large structures is that the remaining ligaments of the small specimens may be completely yielded, while the crack-tip plastic zone ahead of a crack in the structure at the same K_I or J level may be completely surrounded by unyielded material, with resulting differences in the degrees of constraint and effects of residual stresses. Preliminary investigations* focused on quantifying these differences and their effects. Discussions have taken place between the Russians and Gesellschaft für Anlagen–und Reaktorsicherheit (GRS) in Köln, Germany, regarding the possibiiity of analyses on the same problems being done at GRS. The HSST Program is pursuing issues of constraint experimentally and analytically, but not with regard to the effects of cyclic loading. Inclusion of load cycling effects would be a relatively straightforward and logical extension of current work.

7.7 Effects of Unloading and Reloading, Crack-Tip Blunting, and Residual Stresses

The effects of unloading and reloading, crack-tip blunting, and residual stresses are not separable. From their small- and medium-scale specimen test results, the Russians concluded that WPS effects are governed primarily by crack-tip blunting and are almost unaffected by the degree of intermediate unloading and residual stresses.[2] They therefore postulate that the CTOD is the fracture criterion and attempt to explain the absence of residual stress effects in their data, although observed by others, as resulting from material differences. They judge that residual stress effects are significant under SSY conditions, but not for fully plastic conditions. HSST Program experimental data for Intermediate Test Vessels ITV-7A and ITV-8, tested to failure under monotonically increasing loads,[9,10] support this hypothesis. As mentioned earlier, the translated document[1] uses two analytical representations of WPS: one (Chell's[5] theory), for assumed SSY, postulates the relevance of residual stresses, and the other, based on at least partially yielded small specimen data,† ignores residual stresses (see Ref. 1). The ORNL analyses previously mentioned* are the beginning of attempts to reconcile these partial viewpoints through comprehensive and detailed analyses of both laboratory specimens and structures. This approach will ultimately be required for understanding WPS.

7.8 Strain Aging

Strain aging was one of the three possible limitations on the WPS reliability identified by Yukawa in the first report published by the HSST Program.[11] Strain aging is described by Tetelman and McEvily[12] in terms of the formation of dislocations at the forward ends of Luder's lines during initial yielding, the time- and temperature-induced diffusion of impurity atoms to these dislocation sites during hold time at reduced load, the consequent immobility of the pinned dislocations, and finally the resulting increase in stress required for further yielding. Presuming cleavage to be caused by a critical stress above the yield stress, raising the near crack-tip stress for reyielding effectively reduces the fracture toughness. The Russians recognized this possible material-dependent limitation on WPS and conducted hold time tests on warm prestressed specimens to 10,000 h (more than 1 year), demonstrating no significant effects for the materials tested.[2] Confirmatory testing was discussed with GRS.‡ It was remarked† that the weld HAZ of A 533 steel used in U.S. vessels may be much more sensitive to thermal embrittlement than the base metal and that thermal and radiation embrittlement may be synergistic. The temperature of thermal embrittlement for A 533 HAZ material was not given, and a reference for the results was not cited. Some confirmatory testing of irradiated specimens of material proposed to be warm prestressed would seem a wise precaution.

7.9 Variability of Fracture Toughness

Variability of fracture toughness was the second factor identified as a limitation in Yukawa's report.[11] It was mentioned primarily with regard to the estimation of the flaw size range ruled out by periodic proof testing, in the sense that a proof test only protects against flaws that would be larger than those of critical size in the proof test. Considering the upper bound of a possible toughness scatter band during proof testing implies large critical flaw sizes. But considering the lower bound of a possible toughness scatter band and a lower temperature during service leads to smaller critical flaw sizes against which no protection is provided by the proof test without considering WPS. Providing the right type of stress distribution during proof testing is an additional consideration already discussed. In addition, protection against failure or even crack growth during the proof test requires setting the proof test stresses according to a lower-bound estimate of the toughness and

*D. K. M. Shum, Martin Marietta Energy Systems, Inc., Oak Ridge Natl. Lab., "Preliminary Investigation on the Inclusion of Warm Prestress Effects in Fracture-Margin Assessment of Reactor Pressure Vessels," NUREG/CR-5946 (ORNL/TM-12236), draft dated December 3, 1993.

†V. V. Pokrovsky, "Warm Prestressing, A Promising Method for Justifying and Extending the Service Life Under Radiation Conditions, Also for Increasing the Safety of PWR Vessels," probable date, November 1993.

‡A. Hofler, J. Sievers, and V. Pokrovsky, minutes of a meeting on warm prestressing, held on November 3–5, 1993, at GRS in Köln, Germany.

an upper-bound estimate of the possible undetected flaw size. But as previously stated, the estimation of the lower bound of the flaw size range ruled out must be based on an upper-bound estimate of the toughness. Toughness variability also needs to be considered with respect to WPS, to protect against crack growth during the procedure, and to avoid overestimating the resulting benefit. Both these criteria imply the use of conservative estimates of unprestressed toughness.

7.10 Crack Growth

The third factor identified by Yukawa[11] as a possible limitation on the WPS reliability was crack growth, during or after the application of the procedure. All causes of crack growth must be considered. A historic, spectacular, and fatal example of failure due to ignorance of the possible damaging effects of progressive crack growth under prior and current loads was the failure in February 1844 of Stockton's ill-designed experimental gun barrel aboard the "Princeton," fired under reduced charge with dignitaries aboard.[13] Progressive ductile crack growth was probably the cause of this failure. For highly irradiated pressure vessel steels containing significant amounts of copper, phosphorous, and sulfur, the possibility of ductile crack growth in LUS materials under PTS loading must be considered. Figure 7.2 shows J-T data for irradiated LUS weld metal.[14] The lower ends of the material J-T curves identify the J_{Ic} values, which lie between 56 and 88 kJ/m^2. The corresponding K_{JIc} values are 113 and 141 MPa$\sqrt{m}$. Plotting these values in Fig. 7.3, which shows typical applied K_I values for a U.S. PWR vessel under steam-line-break loading, indicates that some ductile crack growth is likely for inside surface cracks in LUS materials under PTS loads. Because, in ferritic pressure vessel steels, ductile tearing resistance decreases as temperature increases, the potential

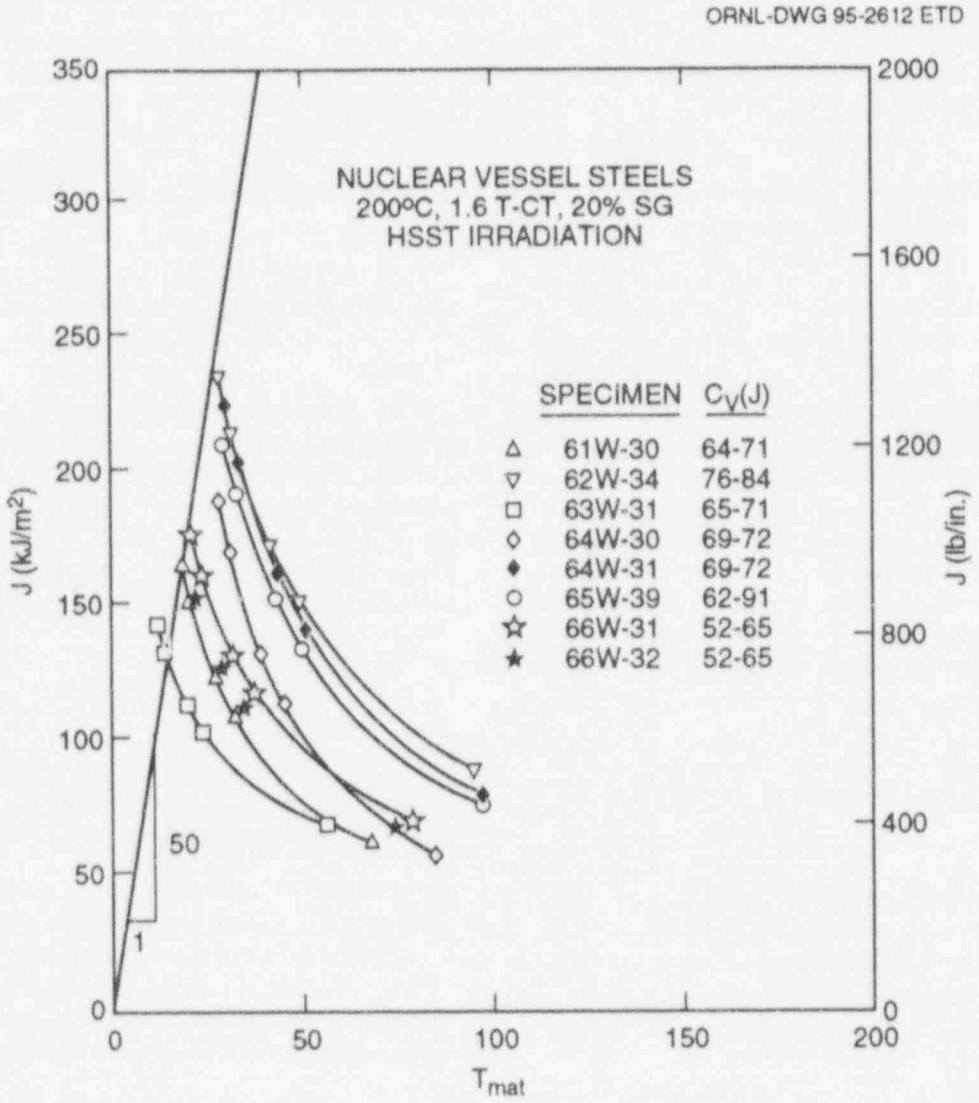

Figure 7.2 J-T data for irradiated LUS weld metal

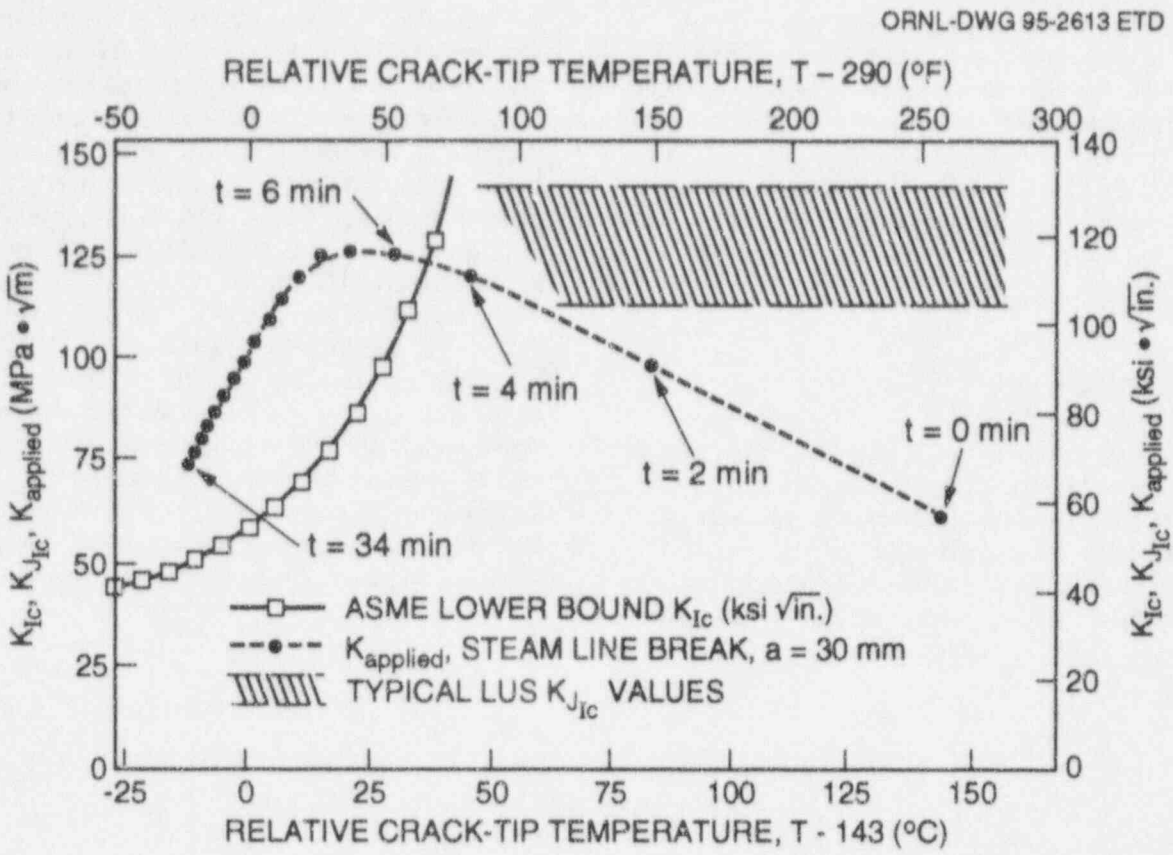

Figure 7.3 Typical applied K_I values for a 30-mm-deep (1.1-in.) inside surface crack in U.S. PWR vessel under steam-line-break loading and typical PWR toughness value range

for ductile tearing during the WPS procedure must also be considered. Avoidance is the most prudent criterion, although a modification of Chell's analysis[15] is available to deal with the problem, because the uncertainties associated with crack growth might well make the difference between a safe and an unsafe situation. To avoid the intervention of ductile tearing into a WPS procedure, it will be necessary to characterize the ductile tearing resistance as well as the cleavage fracture toughness of the materials involved. Reference 1 gives evidence that the Russians are aware of this problem. Fatigue crack growth and stress corrosion cracking originating in cladding are obvious but less likely additional modes of crack growth to be considered. Intergranular cracking in submerged arc welds due to phosphorous segregation was also mentioned by the British as a consideration in the case of their Magnox reactor vessels.*

7.11 Regulatory Applicability

Currently WPS is not allowed to be considered in PTS analyses for U.S. vessels according to Regulatory Guide 1.154.[16] The stated reason for this precaution is uncertainty concerning the degree of late repressurization in some transients. Nevertheless, the probabilistic fracture analysis code FAVOR[17] newly developed by the HSST Program at ORNL contains the option of applying WPS criteria to individual transients as they are collectively analyzed by the Monte Carlo technique to calculate a probability of failure. Therefore, a decision concerning the use of WPS for reactor vessels hinges not on probabilistic calculational capability, but on confidence in understanding the physical phenomenon and in the permanence and reliability of the effects of the procedure.

7.12 Conclusions

1. The Russians appear to be serious in their intent to pursue WPS as a partial remedy for RPV embrittlement.
2. The WPS phenomenon is still incompletely understood in physical and mathematical terms. However, its main mechanisms involving cyclic yielding, crack-tip blunting, and residual stresses, and major potential limitations including strain aging, variability of toughness, and crack growth, have been identified.
3. Laboratory specimens that undergo larger amounts of yielding than larger structures at equal K_I or J values

*J. Lacey, *Validity of Warm Prestressing Arguments for Magnox RPV's*, 1993.

may not behave in exactly the same way as the structures, under WPS conditions, because of the gradual disappearance of residual stresses as yielding progresses.

4. Ductile crack growth poses an important potential limitation to the WPS reliability. It must be understood and tightly controlled, or better yet eliminated, in the WPS context.

7.13 Recommendations

If the NRC would like to further evaluate Ukrainian WPS studies, a logical progression of experiments, with accompanying analyses, would be the following:

1. assessment of effects on standard laboratory specimens, initially unirradiated, eventually irradiated;
2. biaxial shallow-cracked beam experiments;
3. large-scale confirmatory thermal-shock cylinder tests;
4. demonstration application to an RPV; and
5. plant applications.

References

1. Anon., *Technique for Evaluating Impact of Preliminary Thermomechanical Loading on Resistance to Failure of Reactor Vessel Materials*, M-PTN-01-94, Moscow, 1994 (NRC Translation 2850, April 1994). (In related documents, the Russians refer to this document with a document number ending in "93." The translation shows "93" on p. 2 and "94" on pp. 1, 6, and 7. The correct number is probably "93.")

2. V. V. Pokrovsky et al., "A Promising Method for Enhancing Resistance of Pressure Vessels to Brittle Fracture," *Int. J. Pressure Vessel. & Piping* 58, 9–24 (1994).*

3. R. Havel, "IAEA Extrabudgetary Programme on the Safety of Nuclear Power Plants in Eastern Europe and Countries of the Former Soviet Union," IAEA, 1994.

4. ASME Section XI Task Group on Reactor Vessel Integrity Requirements, "White Paper on Reactor Vessel Integrity Requirements for Level A and B Conditions," EPRI TR-100251, Electric Power Research Institute, January 1993.

5. G. G. Chell, "Some Fracture Mechanics Applications of Warm Pre-Stressing to Pressure Vessels," pp. 117–124 in *Proceedings of the 4th Int. Conference on Pressure Vessel Technology* (Inst. Mech. Engineers, London, 1980).

6. J. G. Merkle, Martin Marietta Energy Systems, Inc., Oak Ridge Natl. Lab., Commentary on the CEGB Strip Yield Model for Analyzing the Effects of Warm Prestressing," pp. 18–32 and 47–48 in *HSST Program Progress Report*, ORNL/TM-9154/V2, December 1984.†

7. R. M. McMeeking, "Finite Deformation Analysis of Crack-Tip Opening in Elastic-Plastic Materials and Implications for Fracture," *J. Mech. Phys. Solids* 25, 357–381 (1977).*

8. G. R. Irwin, X. J. Zhang, and C. W. Schwartz, Martin Marietta Energy Systems, Inc., Oak Ridge Natl. Lab., "Small Scale Nonuniformities Related to Cleavage Initiation and Their Implications for Constraint Modeling," ORNL/NRC/LTR-94/18, August 1994.‡

9. R. H. Bryan et al., Union Carbide Corp. Nucl.. Div., Oak Ridge Natl. Lab., "Test of 6-in. Thick Pressure Vessels, Series 3: Intermediate Test Vessel V-7A Under Sustained Loading," USNRC Report ORNL/NUREG-9, February 1978.†

10. R. H. Bryan et al., Union Carbide Corp. Nucl. Div., Oak Ridge Natl. Lab., "Test of 6-in. Thick Pressure Vessels, Series 3: Intermediate Test Vessel V-8," USNRC Report NUREG/CR-0675 (ORNL/NUREG-58), December 1979.†

11. S. Yukawa, *Evaluation of Periodic Proof Testing and Warm Prestressing Procedures for Nuclear Reactor Vessels*, HSSTP-TR-1, General Electric Company, July 1, 1969.

12. A. S. Tetelman and A. J. McEvily, Jr., *Fracture of Structural Materials*, Wiley, New York, 1967.

13. E. L. Beach, *The United States Navy, 200 Years*, Holt, New York, 1986.

14. R. Johnson, "Resolution of the Task A-11 Reactor Vessel Materials Toughness Safety Issue," USNRC

Report NUREG-0744, Vols. 1 & 2, Rev. 1, October 1982.†

15. G. G. Chell, "The Effects of Sub-Critical Crack Growth on the Fracture Behavior of Cracked Ferritic Steels after Warm Prestress," *Fatigue and Fract. of Engineering Materials and Structures*, Vol. 9(4), 259–74 (1986).*

16. U.S. Nuclear Regulatory Commission, Regulatory Guide 1.154, "Format and Content of Plant-Specific Pressurized Thermal Shock Safety Analysis Reports for Pressurized Water Reactors," January 1987.**

17. T. L. Dickson, Martin Marietta Energy Systems, Inc., Oak Ridge Natl. Lab., "FAVOR: Fracture Analysis Vessels—Oak Ridge; Release 9401, A Fracture Analysis Code for Nuclear Reactor Pressure Vessels, Preliminary User Guide," ORNL/NRC/LTR-94-1, February 1994.‡

---

*Available from public technical libraries.
†Available for purchase from the National Technical Information Service, Springfield, VA 22161.
‡Available in NRC PDR for inspection and copying for a fee.
**Copies are available from U.S. Government Printing Office, Washington, D.C. 20402. ATTN: Regulatory Guide Account.

CONVERSION FACTORS[a]

SI unit	English unit	Factor
mm	in.	0.0393701
cm	in.	0.393701
m	ft	3.28084
m/s	ft/s	3.28084
kN	lb_f	224.809
kPa	psi	0.145038
MPa	ksi	0.145038
$MPa \cdot \sqrt{m}$	$ksi \cdot \sqrt{in.}$	0.910048
J	ft•lb	0.737562
K	°F or °R	1.8
kJ/m^2	$in.\text{-}lb/in.^2$	5.71015
$W \cdot m^{-2} \cdot K^{-1}$	$Btu/h \cdot ft^2 \cdot °F$	0.176110
kg	lb	2.20462
kg/m^3	$lb/in.^3$	3.61273×10^{-5}
mm/N	$in./lb_f$	0.175127
T(°F) = 1.8(°C) + 32		

[a]Multiply SI quantity by given factor to obtain English quantity.

Prior Heavy-Section Steel Technology Program Publications

The work reported here was performed at Oak Ridge National Laboratory under the Heavy-Section Steel Technology (HSST) Program, W. E. Pennell, Program Manager. The program is sponsored by the Office of Nuclear Regulatory Research of the U.S. Nuclear Regulatory Commission (NRC). The technical monitor for NRC is S. N. M. Malik. Prior and future reports in this series are listed below.

1. S. Yukawa, General Electric Company, Schenectady, N.Y., *Evaluation of Periodic Proof Testing and Warm Prestressing Procedures for Nuclear Reactor Vessels*, HSSTP-TR-1, July 1, 1969.

2. L. W. Loechel, Martin Marietta Corporation, Denver, Colo., *The Effect of Testing Variables on the Transition Temperature in Steel*, MCR-69-189, November 20, 1969.

3. P. N. Randall, TRW Systems Group, Redondo Beach, Calif., *Gross Strain Measure of Fracture Toughness of Steels*, HSSTP-TR-3, November 1, 1969.

4. C. Visser, S. E. Gabrielse, and W. VanBuren, Westinghouse Electric Corporation, PWR Systems Division, Pittsburgh, Pa., *A Two-Dimensional Elastic-Plastic Analysis of Fracture Test Specimens*, WCAP-7368, October 1969.

5. T. R. Mager and F. O. Thomas, Westinghouse Electric Corporation, PWR Systems Division, Pittsburgh, Pa., *Evaluation* by *Linear Elastic Fracture Mechanics of Radiation Damage to Pressure Vessel Steels*, WCAP-7328 (Rev.), October 1969.

6. W. O. Shabbits, W. H. Pryle, and E. T. Wessel, Westinghouse Electric Corporation, PWR Systems Division, Pittsburgh, Pa., *Heavy-Section Fracture Toughness Properties of A533 Grade B Class 1 Steel Plate and Submerged Arc Weldment*, WCAP-7414, December 1969.

7. F. J. Loss, Naval Research Laboratory, Washington, D.C., *Dynamic Tear Test Investigations of the Fracture Toughness of Thick-Section Steel*, NRL-7056, May 14, 1970.

8. P. B. Crosley and E. J. Ripling, Materials Research Laboratory, Inc., Glenwood, Ill., *Crack Arrest Fracture Toughness of A533 Grade B Class 1 Pressure Vessel Steel*, HSSTP-TR-8, March 1970.

9. T. R. Mager, Westinghouse Electric Corporation, PWR Systems Division, Pittsburgh, Pa., *Post-Irradiation Testing* of *2T Compact Tension Specimens*, WCAP-7561, August 1970.

10. T. R. Mager, Westinghouse Electric Corporation, PWR Systems Division, Pittsburgh, Pa., *Fracture Toughness Characterization Study of A533, Grade B, Class 1 Steel*, WCAP-7578, October 1970.

11. T. R. Mager, Westinghouse Electric Corporation, PWR Systems Division, Pittsburgh, Pa., *Notch Preparation in Compact Tension Specimens*, WCAP-7579, November 1970.

12. N. Levy and P. V. Marcal, Brown University, Providence, R.I., *Three-Dimensional Elastic-Plastic Stress and Strain Analysis for Fracture Mechanics, Phase I: Simple Flawed Specimens*, HSSTP-TR-12, December 1970.

13. W. O. Shabbits, Westinghouse Electric Corporation, PWR Systems Division, Pittsburgh, Pa., *Dynamic Fracture Toughness Properties of Heavy Section A533 Grade B Class 1 Steel Plate*, WCAP-7623, December 1970.

14. P. N. Randall, TRW Systems Group, Redondo Beach, Calif., *Gross Strain Crack Tolerance of A 533-B Steel*, HSSTP-TR-14, May 1, 1971.

15. H. T. Corten and R. H. Sailors, University of Illinois, Urbana, Ill., *Relationship Between Material Fracture Toughness Using Fracture Mechanics and Transition Temperature Tests*, T&AM Report 346, August 1, 1971.

16. T. R. Mager and V. J. McLaughlin, Westinghouse Electric Corporation, PWR Systems Division, Pittsburgh, Pa., *The Effect of an Environment of High Temperature Primary Grade Nuclear Reactor Water on the Fatigue Crack Growth Characteristics of A533 Grade B Class 1 Plate and Weldment Material*, WCAP-7776, October 1971.

17. N. Levy and P. V. Marcal, Brown University, Providence, R.I., *Three-Dimensional Elastic-Plastic Stress and Strain Analysis for Fracture Mechanics, Phase II: Improved Modelling*, HSSTP-TR-17, November 1971.

18. S. C. Grigory, Southwest Research Institute, San Antonio, Tex., *Tests of 6-in.-Thick Flawed Tensile Specimens, First Technical Summary Report, Longitudinal Specimens Numbers 1 through 7*, HSSTP-TR-18, June 1972.

19. P. N. Randall, TRW Systems Group, Redondo Beach, Calif., *Effects of Strain Gradients on the Gross Strain Crack Tolerance of A533-B Steel*, HSSTP-TR-19, June 15, 1972.

Prior

20. S. C. Grigory, Southwest Research Institute, San Antonio, Tex., *Tests of 6-Inch-Thick Flawed Tensile Specimens, Second Technical Summary Report, Transverse Specimens Numbers 8 through 10, Welded Specimens Numbers 11 through 13*, HSSTP-TR-20, June 1972.

21. L. A. James and J. A. Williams, Hanford Engineering Development Laboratory, Richland, Wash., Heavy Section Steel Technology Program Technical Report No. 21, *The Effect of Temperature and Neutron Irradiation Upon the Fatigue-Crack Propagation Behavior of ASTM A533 Grade B, Class 1 Steel*, HEDL-TME 72-132, September 1972.

22. S. C. Grigory, Southwest Research Institute, San Antonio, Tex., *Tests of 6-Inch-Thick Flawed Tensile Specimens, Third Technical Summary Report, Longitudinal Specimens Numbers 14 through 16, Unflawed Specimen Number 17*, HSSTP-TR-22, October 1972.

23. S. C. Grigory, Southwest Research Institute, San Antonio, Tex., *Tests of 6-Inch-Thick Tensile Specimens, Fourth Technical Summary Report, Tests of 1-Inch-Thick Flawed Tensile Specimens for Size Effect Evaluation*, HSSTP-TR-23, June 1973.

24. S. P. Ying and S. C. Grigory, Southwest Research Institute, San Antonio, Tex., *Tests of 6-Inch-Thick Tensile Specimens, Fifth Technical Summary Report, Acoustic Emission Monitoring of One-Inch and Six-Inch-Thick Tensile Specimens*, HSSTP-TR-24, November 1972.

25. R. W. Derby, J. G. Merkle, G. C. Robinson, G. D. Whitman, and F. J. Witt, Oak Ridge Natl. Lab., Oak Ridge, Tenn., *Test of 6-Inch-Thick Pressure Vessels. Series 1: Intermediate Test Vessels V-1 and V-2*, ORNL-4895, February 1974.

26. W. J. Stelzman and R. G. Berggren, Oak Ridge Natl. Lab., Oak Ridge, Tenn., *Radiation Strengthening and Embrittlement in Heavy Section Steel Plates and Welds*, ORNL-4871, June 1973.

27. P. B. Crosley and E. J. Ripling, Materials Research Laboratory, Inc., Glenwood, Ill., *Crack Arrest in an Increasing K-Field*, HSSTP-TR-27, January 1973.

28. P. V. Marcal, P. M. Stuart, and R. S. Bettes, Brown University, Providence, R.I., *Elastic Plastic Behavior of a Longitudinal Semi-Elliptic Crack in a Thick Pressure Vessel*, HSSTP-TR-28, June 1973.

29. W. J. Stelzman, R. G. Berggren, and T. N. Jones, Oak Ridge Natl. Lab., Oak Ridge, Tenn., *ORNL Characterization of Heavy-Section Steel Technology Program Plates 01, 02 and 03*, USNRC Report NUREG/CR-4092 (ORNL/TM-9491), April 1985.

30. Canceled.

31. J. A. Williams, Hanford Engineering Development Laboratory, Richland, Wash., *The Irradiation and Temperature Dependence of Tensile and Fracture Properties of ASTM A533, Grade B, Class 1 Steel Plate and Weldment*, HEDL-TME 73-75, August 1973.

32. J. M. Steichen and J. A. Williams, Hanford Engineering Development Laboratory, Richland, Wash., *High Strain Rate Tensile Properties of Irradiated ASTM A533 Grade B Class 1 Pressure Vessel Steel*, July 1973.

33. P. C. Riccardella and J. L. Swedlow, Westinghouse Electric Corporation, Pittsburgh, Pa., *A Combined Analytical-Experimental Fracture Study of the Two Leading Theories of Elastic-Plastic Fracture (J-Integral and Equivalent Energy)*, WCAP-8224, October 1973.

34. R. J. Podlasek and R. J. Eiber, Battelle Columbus Laboratories, Columbus, Ohio, *Final Report on Investigation of Mode III Crack Extension in Reactor Piping*, December 14, 1973.

35. T. R. Mager, J. D. Landes, D. M. Moon, and V. J. McLaughlin, Westinghouse Electric Corporation, Pittsburgh, Pa., *Interim Report on the Effect of Low Frequencies on the Fatigue Crack Growth Characteristics of A533 Grade B Class 1 Plate in an Environment of High-Temperature Primary Grade Nuclear Reactor Water*, WCAP-8256, December 1973.

36. J. A. Williams, Hanford Engineering Development Laboratory, Richland, Wash., *The Irradiated Fracture Toughness of ASTM A533, Grade B, Class 1 Steel Measured with a Four-Inch-Thick Compact Tension Specimen*, HEDL-TME 75-10, January 1975.

37. R. H. Bryan, J. G. Merkle, M. N. Raftenberg, G. C. Robinson, and J. E. Smith, Oak Ridge Natl. Lab., Oak Ridge, Tenn., *Test of 6-Inch-Thick Pressure Vessels. Series 2: Intermediate Test Vessels V-3, V-4, and V-6*, ORNL-5059, November 1975.

38. T. R. Mager, S. E. Yanichko, and L. R. Singer, Westinghouse Electric Corporation, Pittsburgh, Pa., *Fracture Toughness Characterization of HSST Intermediate Pressure Vessel Material*, WCAP-8456, December 1974.

39. J. G. Merkle, G. D. Whitman, and R. H. Bryan, Oak Ridge Natl. Lab., Oak Ridge, Tenn., *An Evaluation of the HSST Program Intermediate Pressure Vessel Tests in Terms of Light-Water-Reactor Pressure Vessel Safety*, ORNL/TM-5090, November 1975.

40. J. C. Merkle, G. C. Robinson, P. P. Holz, J. E. Smith, and R. H. Bryan, Oak Ridge Natl. Lab., Oak Ridge, Tenn., *Test of 6-In.-Thick Pressure Vessels. Series 3: Intermediate Test Vessel V-7,* USNRC Report ORNL/NUREG-1, August 1976.

41. J. A. Davidson, L. J. Ceschini, R. P. Shogan, and G. V. Rao, Westinghouse Electric Corporation, Pittsburgh, Pa., *The Irradiated Dynamic Fracture Toughness of ASTM A533, Grade B, Class 1 Steel Plate and Submerged Arc Weldment,* WCAP-8775, October 1976.

42. R. D. Cheverton, Oak Ridge Natl. Lab., Oak Ridge, Tenn., *Pressure Vessel Fracture Studies Pertaining to a PWR LOCA-ECC Thermal Shock: Experiments TSE-1 and TSE-2,* USNRC Report ORNL/NUREG/TM-31, September 1976.

43. J. G. Merkle, G. C. Robinson, P. P. Holz, and J. E. Smith, Oak Ridge Natl. Lab., Oak Ridge, Tenn., *Test of 6-In.-Thick Pressure Vessels. Series 4: Intermediate Test Vessels V-5 and V-9 with Inside Nozzle Corner Cracks,* USNRC Report ORNL/NUREG-7, August 1977.

44. J. A. Williams, Hanford Engineering Development Laboratory, Richland, Wash., *The Ductile Fracture Toughness of Heavy Section Steel Plate,* USNRC Report NUREG/CR-0859, September 1979.

45. R. H. Bryan, T. M. Cate, P. P. Holz, T. A. King, J. G. Merkle, G. C. Robinson, G. C. Smith, J. E. Smith, and G. D. Whitman, Oak Ridge Natl. Lab., Oak Ridge, Tenn., *Test of 6-in.-Thick Pressure Vessels. Series 3: Intermediate Test Vessel V-7A Under Sustained Loading,* USNRC Report ORNL/NUREG-9, February 1978.

46. R. D. Cheverton and S. E. Bolt, Oak Ridge Natl. Lab., Oak Ridge, Tenn., *Pressure Vessel Fracture Studies Pertaining to a PWR LOCA-ECC Thermal Shock: Experiments TSE-3 and TSE-4 and Update of TSE-1 and TSE-2 Analysis,* USNRC Report ORNL/NUREG-22, December 1977.

47. D. A. Canonico, Oak Ridge Natl. Lab., Oak Ridge, Tenn., *Significance of Reheat Cracks to the Integrity of Pressure Vessels for Light-Water Reactors,* USNRC Report ORNL/NUREG-15, July 1977.

48. G. C. Smith and P. P. Holz, Oak Ridge Natl. Lab., Oak Ridge, Tenn., *Repair Weld Induced Residual Stresses in Thick-Walled Steel Pressure Vessels,* USNRC Report NUREG/CR-0093 (ORNL/NUREG/TM-153), June 1978.

49. P. P. Holz and S. W. Wismer, Oak Ridge Natl. Lab., Oak Ridge, Tenn., *Half-Bead (Temper) Repair Welding for HSST Vessels,* USNRC Report NUREG/CR-0113 (ORNL/NUREG/TM-177), June 1978.

50. G. C. Smith, P. P. Holz, and W. J. Stelzman, Oak Ridge Natl. Lab., Oak Ridge, Tenn., *Crack Extension and Arrest Tests of Axially Flawed Steel Model Pressure Vessels,* USNRC Report NUREG/CR-0126 (ORNL/NUREG/TM-196), October 1978.

51. R. H. Bryan, P. P. Holz, J. G. Merkle, G. C. Smith, J. E. Smith, and W. J. Stelzman, Oak Ridge Natl. Lab., Oak Ridge, Tenn., *Test of 6-in.-Thick Pressure Vessels. Series 3: Intermediate Test Vessel V-7B,* USNRC Report NUREG/CR-0309 (ORNL/NUREG-38), October 1978.

52. R. D. Cheverton, S. K. Iskander, and S. E. Bolt, Oak Ridge Natl. Lab., Oak Ridge, Tenn., *Applicability of LEFM to the Analysis of PWR Vessels Under LOCA-ECC Thermal Shock Conditions,* USNRC Report NUREG/CR-0107 (ORNL/NUREG-40), October 1978.

53. R. H. Bryan, D. A. Canonico, P. P. Holz, S. K. Iskander, J. G. Merkle, J. E. Smith, and W. J. Stelzman, Oak Ridge Natl. Lab., Oak Ridge, Tenn., *Test of 6-in.-Thick Pressure Vessels, Series 3: Intermediate Test Vessel V-8,* USNRC Report NUREG/CR-0675 (ORNL/NUREG-58), December 1979.

54. R. D. Cheverton and S. K. Iskander, Oak Ridge Natl. Lab., Oak Ridge, Tenn., *Application of Static and Dynamic Crack Arrest Theory to TSE-4,* USNRC Report NUREG/CR-0767 (ORNL/NUREG-57), June 1979.

55. J. A. Williams, Hanford Engineering Development Laboratory, Richland, Wash., *Tensile Properties of Irradiated and Unirradiated Welds of A533 Steel Plate and A508 Forgings,* USNRC Report NUREG/CR-1158 (ORNL/Sub/79-50917/2), July 1979.

56. K. W. Carlson and J. A. Williams, Hanford Engineering Development Laboratory, Richland, Wash., *The Effect of Crack Length and Side Grooves on the Ductile Fracture Toughness Properties of ASTM A533 Steel,* USNRC Report NUREG/CR-1171 (ORNL/Sub/79-50917/3), October 1979.

57. P. P. Holz, Oak Ridge Natl. Lab., Oak Ridge, Tenn., *Flaw Preparations for HSST Program Vessel Fracture Mechanics Testing; Mechanical-Cyclic Pumping and Electron-Beam Weld-Hydrogen Charge Cracking Schemes,* USNRC Report NUREG/CR-1274 (ORNL/NUREG/TM-369), May 1980.

58. S. K. Iskander, Computer Sciences Div., Union Carbide Corp. Nuclear Div., Oak Ridge, Tenn., *Two Finite Element Techniques for Computing Mode I*

Stress Intensity Factors in Two- or Three-Dimensional Problems, USNRC Report NUREG/CR-1499 (ORNL/NUREG/CSD/TM-14), February 1981.

59. P. B. Crosley and E. J. Ripling, Materials Research Laboratory, Glenwood, Ill., *Development of a Standard Test for Measuring K_{Ia} with a Modified Compact Specimen,* USNRC Report NUREG/CR-2294 (ORNL/Sub/81-7755/1), August 1981.

60. S. N. Atluri, B. R. Bass, J. W. Bryson, and K. Kathiresan, Computer Sciences Div., Oak Ridge Gaseous Diffusion Plant, Oak Ridge, Tenn., *NOZ-FLAW: A Finite Element Program for Direct Evaluation of Stress Intensity Factors for Pressure Vessel Nozzle-Corner Flaws,* USNRC Report NUREG/CR-1843 (ORNL/NUREG/CSD/TM-18), March 1981.

61. A. Shukla, W. L. Fourney, and G. R. Irwin, University of Maryland, College Park, Md., *Study of Energy Loss and Its Mechanisms in Homalite 100 During Crack Propagation and Arrest,* USNRC Report NUREG/CR-2150 (ORNL/Sub/79-7778/1), August 1981.

62. S. K. Iskander, R. D. Cheverton, and D. G. Ball, Oak Ridge Natl. Lab., Oak Ridge, Tenn., *OCA-I, A Code for Calculating the Behavior of Flaws on the Inner Surface of a Pressure Vessel Subjected to Temperature and Pressure Transients,* USNRC Report NUREG/CR-2113 (ORNL/NUREG-84), August 1981.

63. R. J. Sanford, R. Chona, W. L. Fourney, and G. R. Irwin, University of Maryland, College Park, Md., *A Photoelastic Study of the Influence of Non-Singular Stresses in Fracture Test Specimens,* USNRC Report NUREG/CR-2179 (ORNL/Sub/79-7778/2), August 1981.

64. B. R. Bass, S. N. Atluri, J. W. Bryson, and K. Kathiresan, Oak Ridge Natl. Lab., Oak Ridge, Tenn., *OR-FLAW: A Finite Element Program for Direct Evaluation of K-Factors for User-Defined Flaws in Plate, Cylinders, and Pressure-Vessel Nozzle Corners,* USNRC Report NUREG/CR-2494 (ORNL/CSD/TM-165), April 1982.

65. B. R. Bass and J. W. Bryson, Oak Ridge Natl. Lab., Oak Ridge Tenn., *ORMGEN-3D: A Finite Element Mesh Generator for 3-Dimensional Crack Geometries,* USNRC Report NUREG/CR-2997, Vol. 1 (ORNL/TM-8527/V1), December 1982.

66. B. R. Bass and J. W. Bryson, Oak Ridge Natl. Lab., Oak Ridge, Tenn., *ORVIRT: A Finite Element Program for Energy Release Rate Calculations for 2-Dimensional and 3-Dimensional Crack Models,* USNRC Report NUREG/CR-2997, Vol. 2 (ORNL/TM-8527/V2), February 1983.

67. R. D. Cheverton, S. K. Iskander, and D. G. Ball, Oak Ridge Natl. Lab., Oak Ridge, Tenn., *PWR Pressure Vessel Integrity During Overcooling Accidents: A Parametric Analysis,* USNRC Report NUREG/CR-2895 (ORNL/TM-7931), February 1983.

68. D. G. Ball, R. D. Cheverton, J. B. Drake, and S. K. Iskander, Oak Ridge Natl. Lab., Oak Ridge, Tenn., *OCA-II, A Code for Calculating Behavior of 2-D and 3-D Surface Flaws in a Pressure Vessel Subjected to Temperature and Pressure Transients,* USNRC Report NUREG/CR-3491 (ORNL-5934), February 1984.

69. A. Sauter, R. D. Cheverton, and S. K. Iskander, Oak Ridge Natl. Lab., Oak Ridge, Tenn., *Modification of OCA-I for Application to a Reactor Pressure Vessel with Cladding on the Inner Surface,* USNRC Report NUREG/CR-3155 (ORNL/TM-8649), May 1983.

70. R. D. Cheverton and D. G. Ball, Martin Marietta Energy Systems, Inc., Oak Ridge Natl. Lab., Oak Ridge, Tenn., *OCA-P, A Deterministic and Probabilistic Fracture-Mechanics Code for Application to Pressure Vessels,* USNRC Report NUREG/CR-3618 (ORNL-5991), May 1984.

71. J. G. Merkle, Martin Marietta Energy Systems, Inc., Oak Ridge Natl. Lab., Oak Ridge, Tenn., *An Examination of the Size Effects and Data Scatter Observed in Small Specimen Cleavage Fracture Toughness Testing,* USNRC Report NUREG/CR-3672 (ORNL/TM-9088), April 1984.

72. C. E. Pugh et al., Martin Marietta Energy Systems, Inc., Oak Ridge Natl. Lab., Oak Ridge, Tenn., *Heavy-Section Steel Technology Program—Five-Year Plan FY 1983–1987,* USNRC Report NUREG/CR-3595 (ORNL/TM-9008), April 1984.

73. D. G. Ball, B. R. Bass, J. W. Bryson, R. D. Cheverton, and J. B. Drake, Martin Marietta Energy Systems, Inc., Oak Ridge Natl. Lab., Oak Ridge, Tenn., *Stress Intensity Factor Influence Coefficients for Surface Flaws in Pressure Vessels,* USNRC Report NUREG/CR-3723 (ORNL/CSD/TM-216), February 1985.

74. W. R. Corwin, R. G. Berggren, and R. K. Nanstad, Martin Marietta Energy Systems, Inc., Oak Ridge Natl. Lab., Oak Ridge, Tenn., *Charpy Toughness and Tensile Properties of Neutron Irradiated Stainless Steel Submerged-Arc Weld Cladding Overlay,* USNRC Report NUREG/CR-3927 (ORNL/TM-9309), September 1984.

75. C. W. Schwartz, R. Chona, W. L. Fourney, and G. R. Irwin, University of Maryland, College Park, Md., *SAMCR: A Two-Dimensional Dynamic Finite Element Code for the Stress Analysis of Moving CRacks,* USNRC Report NUREG/CR-3891 (ORNL/Sub/79-7778/3), November 1984.

76. W. R. Corwin, G. C. Robinson, R. K. Nanstad, J. G. Merkle, R. G. Berggren, G. M. Goodwin, R. L. Swain, and T. D. Owings, Martin Marietta Energy Systems, Inc., Oak Ridge Natl. Lab., Oak Ridge, Tenn., *Effects of Stainless Steel Weld Overlay Cladding on the Structural Integrity of Flawed Steel Plates in Bending, Series 1,* USNRC Report NUREG/CR-4015 (ORNL/TM-9390), April 1985.

77. R. H. Bryan, B. R. Bass, S. E. Bolt, J. W. Bryson, D. P. Edmonds, R. W. McCulloch, J. G. Merkle, R. K. Nanstad, G. C. Robinson, K. R. Thoms, and G. D. Whitman, Martin Marietta Energy Systems, Inc., Oak Ridge Natl. Lab., Oak Ridge, Tenn., *Pressurized-Thermal-Shock Test of 6-in.-Thick Pressure Vessels. PTSE-1: Investigation of Warm Prestressing and Upper-Shelf Arrest,* USNRC Report NUREG/CR-4106 (ORNL-6135), April 1985.

78. R. D. Cheverton, D. G. Ball, S. E. Bolt, S. K. Iskander, and R. K. Nanstad, Martin Marietta Energy Systems, Inc., Oak Ridge Natl. Lab., Oak Ridge, Tenn., *Pressure Vessel Fracture Studies Pertaining to the PWR Thermal-Shock Issue: Experiments TSE-5, TSE-5A, and TSE-6,* USNRC Report NUREG/CR-4249 (ORNL-6163), June 1985.

79. R. D. Cheverton, D. G. Ball, S. E. Bolt, S. K. Iskander, and R. K. Nanstad, Martin Marietta Energy Systems, Inc., Oak Ridge Natl. Lab., Oak Ridge, Tenn., *Pressure Vessel Fracture Studies Pertaining to the PWR Thermal-Shock Issue: Experiment TSE-7,* USNRC Report NUREG/CR-4304 (ORNL-6177), August 1985.

80. R. H. Bryan, B. R. Bass, S. E. Bolt, J. W. Bryson, J. G. Merkle, R. K. Nanstad, and G. C. Robinson, Martin Marietta Energy Systems, Inc., Oak Ridge Natl. Lab., Oak Ridge, Tenn., *Test of 6-in.-Thick Pressure Vessels. Series 3: Intermediate Test Vessel V-8A—Tearing Behavior of Low Upper-Shelf Material,* USNRC Report NUREG/CR-4760 (ORNL-6187), May 1987.

81. R. D. Cheverton and D. G. Ball, Martin Marietta Energy Systems, Inc., Oak Ridge Natl. Lab., Oak Ridge, Tenn., *A Parametric Study of PWR Pressure Vessel Integrity During Overcooling Accidents, Considering Both 2-D and 3-D Flaws,* USNRC Report NUREG/CR-4325 (ORNL/TM-9682), August 1985.

82. E. C. Rodabaugh, E. C. Rodabaugh Associates, Inc., Hilliard, Ohio, *Comments on the Leak-Before-Break Concept for Nuclear Power Plant Piping Systems,* USNRC Report NUREG/CR-4305 (ORNL/Sub/82-22252/3), August 1985.

83. J. W. Bryson, Martin Marietta Energy Systems, Inc., Oak Ridge Natl. Lab., Oak Ridge, Tenn., *ORVIRT.PC: A 2-D Finite Element Fracture Analysis Program for a Microcomputer,* USNRC Report NUREG/CR-4367 (ORNL-6208), October 1985.

84. D. G. Ball and R. D. Cheverton, Martin Marietta Energy Systems, Inc., Oak Ridge Natl. Lab., Oak Ridge, Tenn., *Adaptation of OCA-P, A Probabilistic Fracture-Mechanics Code, to a Personal Computer,* USNRC Report NUREG/CR-4468 (ORNL/CSD/TM-233), January 1986.

85. J. W. Bryson and B. R. Bass, Martin Marietta Energy Systems, Inc., Oak Ridge Natl. Lab., Oak Ridge, Tenn., *ORMGEN.PC: A Microcomputer Program for Automatic Mesh Generation of 2-D Crack Geometries,* USNRC Report NUREG/CR-4475 (ORNL-6250), March 1986.

86. G. D. Whitman, Martin Marietta Energy Systems, Inc., Oak Ridge Natl. Lab., Oak Ridge, Tenn., *Historical Summary of the Heavy-Section Steel Technology Program and Some Related Activities in Light-Water Reactor Pressure Vessel Safety Research,* USNRC Report NUREG/CR-4489 (ORNL-6259), March 1986.

87. C. Inversini and J. W. Bryson, Martin Marietta Energy Systems, Inc., Oak Ridge Natl. Lab., Oak Ridge, Tenn., *ORPLOT PC: A Graphic Utility for ORMGEN.PC and ORVIRT.PC,* USNRC Report NUREG/CR-4633 (ORNL-6291), June 1986.

88. J. J. McGowan, R. K. Nanstad, and K. R. Thoms, Martin Marietta Energy Systems, Inc., Oak Ridge Natl. Lab., Oak Ridge, Tenn., *Characterization of Irradiated Current-Practice Welds and A533 Grade B Class 1 Plate for Nuclear Pressure Vessel Service,* USNRC Report NUREG/CR-4880 (ORNL/TM-10387), July 1988.

89. K. V. Cook and R. W. McClung, Martin Marietta Energy Systems, Inc., Oak Ridge Natl. Lab., Oak Ridge, Tenn., *Flaw Density Examinations of a Clad Boiling Water Reactor Pressure Vessel Segment,* USNRC Report NUREG/CR-4860 (ORNL/TM-10364), April 1987.

90. D. J. Naus, B. R. Bass, C. E. Pugh, R. K. Nanstad, J. G. Merkle, W. R. Corwin, and G. C. Robinson, Martin Marietta Energy Systems, Inc., Oak Ridge Natl. Lab., Oak Ridge, Tenn., *Crack-Arrest Behavior*

in SEN Wide Plates of Quenched and Tempered A 533 Grade B Steel Tested Under Nonisothermal Conditions, USNRC Report NUREG/CR-4930 (ORNL-6388), August 1987.

91. D. B. Barker, R. Chona, W. L. Fourney, and G. R. Irwin, University of Maryland, College Park, Md., *A Report on the Round Robin Program Conducted to Evaluate the Proposed ASTM Standard Test Method for Determining the Plane Strain Crack Arrest Fracture Toughness, K_{Ia},* of Ferritic Materials, USNRC Report NUREG/CR-4966 (ORNL/Sub/79-7778/4), January 1988.

92. W. H. Bamford, Westinghouse Electric Corporation, Pittsburgh, Pa., *A Summary of Environmentally Assisted Crack-Growth Studies Performed at Westinghouse Electric Corporation Under Funding from the Heavy-Section Steel Technology Program,* USNRC Report NUREG/CR-5020 (ORNL/Sub/82-21598/1), May 1988.

93. R. H. Bryan, B. R. Bass, S. E. Bolt, J. W. Bryson, W. R. Corwin, J. G. Merkle, R. K. Nanstad, and G. C. Robinson, Martin Marietta Energy Systems, Inc., Oak Ridge Natl. Lab., Oak Ridge, Tenn., *Pressurized-Thermal-Shock Test of 6-in.-Thick Pressure Vessels. PTSE-2: Investigation of Low Tearing Resistance and Warm Prestressing*, USNRC Report NUREG/CR-4888 (ORNL-6377), December 1987.

94. J. H. Giovanola and R. W. Klopp, SRI International, Menlo Park, Calif., *Viscoplastic Stress-Strain Characterization of A533B Class 1 Steel,* USNRC Report NUREG/CR-5066 (ORNL/Sub/87-SA193/1), September 1989.

95. L. F. Miller et al., Martin Marietta Energy Systems, Inc., Oak Ridge Natl. Lab., Oak Ridge, Tenn., *Neutron Exposure Parameters for the Metallurgical Test Specimens in the Fifth Heavy-Section Steel Technology Irradiation Series Capsules,* USNRC Report NUREG/CR-5019 (ORNL/TM-10582), March 1988.

96. Canceled.

97. D. J. Naus, J. Keeney-Walker, and B. R. Bass, Martin Marietta Energy Systems, Inc., Oak Ridge Natl. Lab., Oak Ridge, Tenn., *High-Temperature Crack-Arrest Behavior in 152-mm-Thick SEN Wide Plates of Quenched and Tempered A 533 Grade B Steel,* USNRC Report NUREG/CR-5330 (ORNL/TM-11083), April 1989.

98. K. V. Cook, R. A. Cunningham, Jr., and R. W. McClung, Martin Marietta Energy Systems, Inc., Oak Ridge Natl. Lab., Oak Ridge, Tenn., *Detection and Characterization of Indications in Segments of Reactor Pressure Vessels,* USNRC Report NUREG/CR-5322 (ORNL/TM-11072), August 1989.

99. R. D. Cheverton, W. E. Pennell, G. C. Robinson, and R. K. Nanstad, Martin Marietta Energy Systems, Inc., Oak Ridge Natl. Lab., Oak Ridge, Tenn., *Impact of Radiation Embrittlement on Integrity of Pressure Vessel Supports for Two PWR Plants,* NUREG/CR-5320 (ORNL/TM-10966), February 1989.

100. D. J. Naus, J. Keeney-Walker, B. R. Bass, S. K. Iskander, R. J. Fields, R. deWitt, and S. R. Low III, Martin Marietta Energy Systems, Inc., Oak Ridge Natl. Lab., Oak Ridge, Tenn., *SEN Wide-Plate Crack-Arrest Tests* Utilizing *A 533 Grade B Class 1 Material: WP-CE Test Series,* USNRC Report NUREG/CR-5408 (ORNL/TM-11269), November 1989.

101. D. J. Naus, J. Keeney-Walker, B. R. Bass, S. K. Iskander, R. J. Fields, R. deWitt, and S. R. Low III, Martin Marietta Energy Systems, Inc., Oak Ridge Natl. Lab., Oak Ridge, Tenn., *High Temperature Crack-Arrest Tests Using 152-mm-Thick SEN Wide Plates of Low Upper-Shelf Base Material: Tests WP-2.2 and WP-2.6,* USNRC Report NUREG/CR-5450 (ORNL/TM-11352), February 1990.

102. Canceled.

103. D. J. Naus, J. Keeney-Walker, B. R. Bass, G. C. Robinson, S. K. Iskander, D. J. Alexander, R. J. Fields, R. deWitt, S. R. Low, C. W. Schwartz, and I.-B. Johansson, Martin Marietta Energy Systems, Inc., Oak Ridge Natl. Lab., Oak Ridge, Tenn., *Crack-Arrest Behavior in SEN Wide Plates of Low Upper-Shelf Base Metal Tested Under Non-isothermal Conditions: WP-2 Series,* USNRC Report NUREG/CR-5451 (ORNL-6584), August 1990.

104. T. L. Dickson, R. D. Cheverton, and D. K. Shum, Martin Marietta Energy Systems, Inc., Oak Ridge Natl. Lab., Oak Ridge, Tenn., *Inclusion of Unstable Ductile Tearing and Extrapolated Crack-Arrest Toughness Data in PWR Vessel Integrity Assessment,* USNRC Report NUREG/CR-5473 (ORNL/TM-11450), May 1990.

105. T. J. Theiss, Martin Marietta Energy Systems, Inc., Oak Ridge Natl. Lab., Oak Ridge, Tenn., *Recommendations for the Shallow-Crack Fracture Toughness Testing Task Within the HSST Program,* USNRC Report NUREG/CR-5554 (ORNL/TM-11509), September 1990.

106. J. G. Merkle, Martin Marietta Energy Systems, Inc., Oak Ridge Natl. Lab., Oak Ridge, Tenn., *An*

Overview of the Low Upper Shelf Toughness Safety Margin Issue, USNRC Report NUREG/CR-5552 (ORNL/TM-11314), August 6, 1990.

107. D. K. M. Shum, J. G. Merkle, J. Keeney-Walker, and B. R. Bass, Martin Marietta Energy Systems, Inc., Oak Ridge Natl. Lab., Oak Ridge, Tenn., *Analytical Studies of Transverse Strain Effects on Fracture Toughness for Circumferentially Oriented Cracks*, USNRC Report NUREG/CR-5592 (ORNL/TM-11581), April 1991.

108. J. D. Landes, The University of Tennessee for Martin Marietta Energy Systems, Inc., Oak Ridge natl. Lab., Oak Ridge, Tenn., *Extrapolation of the J-R Curve for Predicting Reactor Vessel Integrity*, USNRC Report NUREG/CR-5650 (ORNL/Sub/89-99732/1), January 1992.

109. J. Keeney-Walker, B. R. Bass, and J. D. Landes, (The University of Tennessee), Martin Marietta Energy Systems, Inc., Oak Ridge Natl. Lab., Oak Ridge, Tenn., *An Investigation of Crack-Tip Stress-Field Criteria for Predicting Cleavage-Crack Initiation*, USNRC Report NUREG/CR-5651 (ORNL/TM-11692), September 1991.

110. G. R. Irwin, University of Maryland, for Martin Marietta Energy Systems, Inc., Oak Ridge Natl. Lab., Oak Ridge, Tenn., *Use of Thickness Reduction to Estimate Values of K*, USNRC Report NUREG/CR-5697 (ORNL/Sub/79-7778/5), November 1991.

111. P. Albrecht and X. Chen, University of Maryland for Martin Marietta Energy Systems, Inc., Oak Ridge Natl. Lab., Oak Ridge, Tenn., *Limit Pressure Analysis of PTSE-2 Vessel*, USNRC Report NUREG/CR-5698 (ORNL/Sub/79-7778/6) (to be published).

112. J. W. Dally, W. L. Fourney, and G. R. Irwin, University of Maryland for Martin Marietta Energy Systems, Inc., Oak Ridge Natl. Lab., Oak Ridge, Tenn., *Lower-Bound Initiation Toughness with a Modified-Charpy Specimen*, USNRC Report NUREG/CR-5703 (ORNL/Sub/79-7778/7), November 1991.

113. S. K. Iskander, G. C. Robinson, W. R. Corwin, B. C. Oland, D. J. Alexander, and K. V. Cook, Martin Marietta Energy Systems, Inc., Oak Ridge Natl. Lab., Oak Ridge, Tenn., *Experimental Results of Tests to Investigate Flaw Behavior of Mechanically Loaded Stainless Steel Clad Plates*, USNRC Report NUREG/CR-5785 (ORNL/TM-11950), April 1992.

114. S. T. Rolfe, University of Kansas for Martin Marietta Energy Systems, Inc., Oak Ridge Natl. Lab., Oak Ridge, Tenn., *Interpretive Report on the Application of Shallow-Flaw CTOD Test Data to the Structural Margin Assessment of Reactor Pressure Vessels with Flaws*, USNRC Report NUREG/CR-5767 (ORNL/Sub/90-SH640/1), November 1991.

115. D. E. McCabe, Martin Marietta Energy Systems, Inc., Oak Ridge Natl. Lab., Oak Ridge, Tenn., *Comparison of Weibull and β_{Ic} Analysis of Transition Range Fracture Toughness Data*, USNRC Report NUREG/CR-5788 (ORNL/TM-11959), January 1992.

116. R. D. Cheverton, T. L. Dickson, J. G. Merkle, and R. K. Nanstad, Martin Marietta Energy Systems, Inc., Oak Ridge Natl. Lab., Oak Ridge, Tenn., *Review of Reactor Pressure Vessel Evaluation Report for Yankee Rowe Nuclear Power Station (YAEC No. 1735)*, USNRC Report NUREG/CR-5799 (ORNL/TM-11982), March 1992

117. T. L. Dickson, R. D. Cheverton, and J. W. Bryson, Martin Marietta Energy Systems, Inc., Oak Ridge Natl. Lab., Oak Ridge, Tenn., *Pressurized-Thermal-Shock Probabilistic Fracture Mechanics Sensitivity Analyses for Yankee Rowe Reactor Pressure Vessel*, USNRC Report NUREG/CR-5782 (ORNL/TM-11945) (to be published).

118. Canceled

119. J. W. Dally, G. R. Irwin, X-J. Zhang, and R. J. Bonenberger, University of Maryland for Martin Marietta Energy Systems, Inc., Oak Ridge Natl. Lab., Oak Ridge, Tenn., *The Influence of Precompression on the Lower-Bound Initiation Toughness of A 533 B Reactor Grade Steel*, USNRC Report NUREG/CR-5847 (ORNL/Sub/79-7778/8), May 1992.

120. Canceled

121. C. W. Schwartz, University of Maryland for Martin Marietta Energy Systems, Inc., Oak Ridge Natl. Lab., Oak Ridge, Tenn., *Crack Speed Relations Inferred from Large SEN Specimens of A 533 B Steel*, USNRC Report NUREG/CR-5861 (ORNL/Sub/79-7778/9) (to be published).

122. A. R. Rosenfield and C. W. Marschall, Battelle Columbus Division for Martin Marietta Energy Systems, Inc., Oak Ridge Natl. Lab., Oak Ridge, Tenn., *Fracture-Mechanics-Based Failure Analysis*, USNRC Report NUREG/CR-5860 (ORNL/Sub/82-17651/1), June 1992.

123. G. R. Irwin and X-J. Zhang, University of Maryland for Martin Marietta Energy Systems, Inc., Oak Ridge Natl. Lab., Oak Ridge, Tenn., *Gradient Study*

of a Large Weld Joining Two Forged A 508 Shells of the Midland Reactor Vessel, USNRC Report NUREG/CR-5867 (ORNL/Sub/79-7778/10), June 1992.

124. J. Keeney-Walker and B. R. Bass, Martin Marietta Energy Systems, Inc., Oak Ridge Natl. Lab., Oak Ridge, Tenn., *ORNOZL: A Finite-Element Mesh Generator for Nozzle-Cylinder Intersections Containing Inner-Corner Cracks*, USNRC Report NUREG/CR-5872 (ORNL/TM-11049), September 1992.

125. J. Keeney-Walker and B. R. Bass, Martin Marietta Energy Systems, Inc., Oak Ridge Natl. Lab., Oak Ridge, Tenn., *A Comparison of Analysis Methodologies for Predicting Cleavage Arrest of a Deep Crack in a Reactor Pressure Vessel Subjected to Pressurized-Thermal-Shock Loading Conditions*, USNRC Report NUREG/CR-5793 (ORNL/TM-11969), September 1992.

126. T. J. Theiss, D. K. M. Shum, and S. T. Rolfe (University of Kansas), Martin Marietta Energy Systems, Inc., Oak Ridge Natl. Lab., Oak Ridge, Tenn., *Experimental and Analytical Investigation of the Shallow-Flaw Effect in Reactor Pressure Vessels*, USNRC Report NUREG/CR-5886 (ORNL/TM-12115), July 1992.

127. B. R. Bass, D. K. M. Shum, and J. Keeney-Walker, Martin Marietta Energy Systems, Inc., Oak Ridge Natl. Lab., Oak Ridge, Tenn., *Constraint Effects on Fracture Toughness for Circumferentially Oriented Cracks in Reactor Pressure Vessels*, USNRC Report NUREG/CR-6008, (ORNL/TM-12131), August 1992.

128. R. E. Stoller, Martin Marietta Energy Systems, Inc., Oak Ridge Natl. Lab., Oak Ridge, Tenn., *Modeling the Influence of Irradiation Temperature and Displacement Rate on Radiation-Induced Hardening in Ferritic Steels*, USNRC Report NUREG/CR-5859 (ORNL/TM-12073), July 1992.

129. J. Keeney-Walker, J. G. Merkle, S. K. Iskander, and T. L. Dickson, Martin Marietta Energy Systems, Inc., Oak Ridge Natl. Lab., Oak Ridge, Tenn., *Recommendations for Thermal-Shock Testing of Clad Cylinders with Shallow Surface Cracks*, USNRC Report NUREG/CR-5915 (ORNL/TM-12166), November 1992.

130. W. E. Pennell, B. R. Bass, R. K. Nanstad, J. G. Merkle, T. L. Dickson, T. J. Theiss, J. Keeney-Walker, and D. K. Shum, *Heavy-Section Steel Technology Program Semiannual Progress Report for October 1991 through March 1992*, NUREG/CR-4219 (ORNL/TM-9593/V9&N1) June 30, 1992.

131. W. E. Pennell, Martin Marietta Energy Systems, Inc., Oak Ridge Natl. Lab., "Heavy-Section Steel Technology Program: Recent Developments in Crack Initiation and Arrest Research," *Nineteenth Water Reactor Safety Information Meeting*, NUREG/CP-0119, Vol. 1, pp. 29–51, October 1992.

132. W. E. Pennell, Martin Marietta Energy Systems, Inc., Oak Ridge Natl. Lab., "Aging Impact on the Safety and Operability of Nuclear Reactor Pressure Vessels," *Proceedings of the Aging Research Information Conference*, USNRC Conference Proceeding NUREG/CP-0122, Vol. 1, pp. 431–453, March 1992.

133. T. L. Dickson and F. A. Simonen, Martin Marietta Energy Systems, Inc., Oak Ridge Natl. Lab., "The Application of Probabilistic Fracture Analysis to Residual Life Evaluation of Embrittled Reactor Vessels," *Proceedings of the Aging Research Information Conference*, USNRC Conference Proceeding NUREG/CP-0122, Vol. 1, pp. 454-467, March 1992.

134. R. K. Nanstad, F. M. Haggag, D. E. McCabe, S. K. Iskander, K. O. Bowman, and B. H. Menke, Martin Marietta Energy Systems, Inc., Oak Ridge Natl. Lab., *Irradiation Effects on Fracture Toughness of Two High-Copper Submerged-Arc Welds, HSSI Series 5*, USNRC Report NUREG/CR-5913, Vol. 1 (ORNL/TM-12156/V1) October 1992.

135. D. E. McCabe, Martin Marietta Energy Systems, Inc., Oak Ridge Natl. Lab., *Evaluation of Crack Pop-ins and the Determination of Their Relevance to Design Consideration*, USNRC Report NUREG/CR-5952 (ORNL/TM-12247), February 1993.

136. Canceled

137. R. K. Nanstad, D. E. McCabe, R. L. Swain, and M. K. Miller, Martin Marietta Energy Systems, Inc., Oak Ridge Natl. Lab., *Chemical Composition and RT_{NDT} Determinations for Midland Weld WF-70*, USNRC Report NUREG/CR-5914 (ORNL-6740) December 1992.

138. T. J. Theiss, B. R. Bass, J. W. Bryson, W. J. McAfee , R. K. Nanstad, W. E. Pennell, and M. C. Rao, Martin Marietta Energy Systems, Inc., Oak Ridge Natl. Lab., *Initial Results of the Influence of Biaxial Loading on Fracture Toughness*, USNRC Report NUREG/CR-6036 (ORNL/TM-12349), June 1993.

139. D. K. Shum, J. W. Bryson, and J. G. Merkle, Martin Marietta Energy Systems, Inc., Oak Ridge Natl. Lab., *Potential Change in Flaw Geometry of an Initially Shallow Finite-Length Surface Flaw During a Pressurized Thermal Shock Transient*, NUREG/CR-5968 (ORNL/TM-12279), September 1993.

140. T. L. Dickson, Martin Marietta Energy Systems, Inc., Oak Ridge Natl. Lab., *Generic Analyses for Evaluation of Low Charpy Upper-Shelf Energy Effects on Safety Margins Against Fracture of Reactor Pressure Vessel Materials*, USNRC Report NUREG/CR-6023 (ORNL/TM-12340), July 1993.

141. C. W. Schwartz, Department of Civil Engineering, University of Maryland, *Crack-Speed Relations Inferred from Large Single-Edge-Notched Specimens of A 533 B Steel*, NUREG/CR-5861 (ORNL/Sub/79-7778/9), July 1994.

142. B. R. Bass, J. W. Bryson, W. J. McAfee, T. J. Theiss, and M. C. Rao, Martin Marietta Energy Systems, Inc., Oak Ridge Natl. Lab., *Biaxial Loading and Shallow-Flaw Effects on Crack-Tip Constraint and Fracture Toughness*, NUREG/CR-6132 (ORNL/TM-12498), January 1994.

143. J. A. Keeney, B. R. Bass, W. J. McAfee, S. K. Iskander, Martin Marietta Energy Systems, Inc., Oak Ridge Natl. Lab., *Preliminary Assessment of the Fracture Behavior of Weld Material in Full-Thickness Clad Beams*, NUREG/CR-6228 (ORNL/TM-12735), October 1994.

144–147. Canceled

148. Robert H. Dodds, Constraint Effects on Fracture Initiation Loads in HSST Wide-Plate Tests, NUREG/CR-6259 (ORNL/TM-12796), July 1994.

Internal Distribution

1. D. J. Alexander
2. B. R. Bass
3. J. W. Bryson
4. W. G. Craddick
5. W. R. Corwin
6. T. L. Dickson
7. R. G. Gilliland
8. W. F. Jackson
9. S. K. Iskander
10. J. A. Keeney
11. W. J. McAfee
12. D. E. McCabe
13. J. G. Merkle
14. R. K. Nanstad
15. D. J. Naus
16-19. W. E. Pennell
20. C. E. Pugh
21. C. C. Southmayd
22. Central Research Library
23. Document of Reference
24. Laboratory Records
25. Laboratory Records (RC)

External Distribution

26. R. D. Thompson, Office of Administration, Divison of Contracts and Properties, U. S. Nuclear Regulatory Commission, Mailstop T17/G-21, Mailstop T17/G21, Washington, DC. 20555-0001.
27. J. Strosnider, Division of Engineering, NRR, U.S. Nuclear Regulatory Commission, Mailstop O7-D4, Washington, DC 20555-0001
28. E. M. Hackett, Materials and Chemical Engineering Branch, Mailstop O7-D4, U.S. Nuclear Regulatory Commission, Washington, DC 20555-0001
29-31. S. N. M. Malik, EMMEB/DET/RES, U.S. Nuclear Regulatory Commission, Washington, DC 20555-001
32. M. E. Mayfield, EMMEB/DET/RES, U.S. Nuclear Regulatory Commission, Washington, DC 20555--0001
33. G. C. Millman, Division of Engineering, U.S. Nuclear Regulatory Commission, Washington, DC 20555-0001
34. M. Vassilaros, EMMEB/DET/RES, Mailstop T10-E10, U.S. Nuclear Regulatory Commission, Washington, DC 20555-0001
35. J. W. Dally, Department of Mechanical Engineering, University of Maryland, College Park, Maryland 20742
36. G. R. Irwin, Department of Mechanical Engineering, University of Maryland, College Park, Maryland 20742
37. L. James, Westinghouse Bettis Lab., P.O. Box 79, ZAP 13A, 814 Pittsburgh McKeesport Blvd., West Mifflin, Pennslyvania 15122
38. C. F. Shih, Box D, Division of Engineering, Brown University, Providence, Rhode Island, 02912
39. R. Dodds, 3140 Newmark Laboratory, 205 North Matthews, Urbana, Illinois 61801
40. R. Fields, National Inst. of Standards and Technology, Bldg. 223, B144, Gaithersburg, Maryland 20899
41. W. L. Fourney, Department of Mechanical Engineering, University of Maryland, College Park, Maryland 20742
42. J. D. Landes, The University of Tennessee, Knoxville, Tennessee 37996-2030
43. S. T. Rolfe, The University of Kansas, Lawrence, Kansas 66045-2235
44. A. R. Rosenfield, Battelle Columbus Division, Columbus, Ohio 43201
45. C. W. Schwartz, Department of Civil Engineering, University of Maryland, College Park, Maryland 20742
46. E. T. Wessel, 312 Wolverine, Haines City, Florida 33844
47. Office of Assistant Manager for Energy Research and Development, DOE–ORO, Oak Ridge, Tennessee 37831
48-49. Office of Scientific and Technical Information, P. O. Box 62, Oak Ridge, Tennessee 37831
50. R. L. Tregoning, Code-614, NSWC-CD, 3A Leggett Circle, Annapolis, Maryland 21402-5067

NRC FORM 335 (2-89) NRCM 1102, 3201, 3202

U.S. NUCLEAR REGULATORY COMMISSION

BIBLIOGRAPHIC DATA SHEET

(See instructions on the reverse)

1. REPORT NUMBER (Assigned by NRC. Add Vol., Supp., Rev., and Addendum Numbers, if any.)
NUREG/CR-4219
ORNL/TM-9593/V11&N2
Vol. 11, No. 2

2. TITLE AND SUBTITLE
Heavy-Section Steel Technology Program
Semiannual Progress Report for April-September 1994

3. DATE REPORT PUBLISHED
MONTH: April
YEAR: 1996

4. FIN OR GRANT NUMBER
B0119

5. AUTHOR(S)
W. E. Pennell

6. TYPE OF REPORT
Technical

7. PERIOD COVERED *(Inclusive Dates)*

8. PERFORMING ORGANIZATION – NAME AND ADDRESS *(If NRC, provide Division, Office or Region, U.S. Nuclear Regulatory Commission, and mailing address; if contractor, provide name and mailing address.)*
Oak Ridge National Laboratory
Oak Ridge, TN 37831-8056

9. SPONSORING ORGANIZATION – NAME AND ADDRESS *(If NRC, type "Same as above"; if contractor, provide NRC Division, Office or Region, U.S. Nuclear Regulatory Commission, and mailing address.)*
Division of Engineering Technology
Office Of Nuclear Regulatory Research
U.S. Nuclear Regulatory Commission
Washington, DC 20555-0001

10. SUPPLEMENTARY NOTES
S. N. Malik, NRC Project Manager

11. ABSTRACT *(200 words or less)*

The Heavy-Section Steel Technology (HSST) program is conducted for the Nuclear Regulatory Commission (NRC) by Oak Ridge National Laboratory (ORNL). The program focus is on the development and validation of technology for the assessment of fracture-prevention margins in commercial nuclear reactor pressure vessels. The HSST Program is organized in seven tasks: (1) program management, (2) constraint effects analytical development and validation, (3) evaluation of cladding effects, (4) ductile-to-cleavage fracture-mode conversion, (5) fracture analysis methods development and application, (6) material property data and test methods, and (7) integration of results. The program tasks have been structured to place emphasis on resolution fracture issues with near-term licensing significance. Resources to execute the research tasks are drawn from ORNL with sub-contract support from universities and other research laboratories. Close contact is maintained with the sister Heavy-Section Steel Irradiation (HSSI) Program at ORNL and with related research programs both in the United States and abroad. This report provides an overview of principal developments in each of the seven program tasks from April 1994 to September 1994.

12. KEY WORDS/DESCRIPTORS *(List words or phrases that will assist researchers in locating the report.)*
Analysis Methods
Cladding Effects
Constraint Effects
Data Interpretation
Fracture Toughness
Materials Testing
Probabilistic Analysis
Reactor Pressure Vessels
Structural Integrity
Tearing-Cleavage Mode Conversion

13. AVAILABILITY STATEMENT
Unlimited

14. SECURITY CLASSIFICATION
(This Page)
Unclassified
(This Report)
Unclassified

15. NUMBER OF PAGES

16. PRICE

Federal Recycling Program

UNITED STATES
NUCLEAR REGULATORY COMMISSION
WASHINGTON, DC 20555-0001

OFFICIAL BUSINESS
PENALTY FOR PRIVATE USE, $300

SPECIAL FOURTH-CLASS MAIL
POSTAGE AND FEES PAID
USNRC
PERMIT NO. G-67